

Scuola di Dottorato di Ricerca in

Scienze e Ingegneria dell'Ambiente, delle Costruzioni e dell'Energia - XXIX ciclo

ING-IND/26 TEORIA DELLO SVILUPPO DEI PROCESSI CHIMICI

Ph.D. Thesis

**Dynamic operation and control of cell culture environments
in bioreactors for bioartificial liver application**

Ph.D. Candidate

S. Danial Naghib

Supervisors

Dr. Alberto Di Renzo

Prof. Efrem Curcio

Prof. Francesco Paolo Di Maio

Dr. Loredana De Bartolo

Coordinator

Prof. Pietro Pantano

Rende, May 2017

Università della Calabria

Acknowledgements

This thesis was one of the most challenging accomplishments in my life thus far. It would not have been completed if it wasn't for the help of many different people, both from a professional and personal perspective. I am grateful for all of the help and support I received over the years. I'll never be able to name every single person who made a comment or helped guide me to graduation, but I would like to acknowledge some of the important people in my life who helped complete this work:

First of all, I am grateful to Prof. Alberto Di Renzo, Prof. Efrem Curcio and Prof. Francesco Paolo Di Maio for giving me the opportunity to work in their research group at University of Calabria (DIATIC), supporting me through the difficulties of my research work. I would especially like to thank Alberto, for his numerous edits on abstracts, reports, and the thesis itself, understanding, guidance, meetings upon meetings, and being a source of support and cheerleading to finish this degree. I could not have asked for someone better.

I would like to thank Dr. Loredana De Bartolo and her research group for guiding my research at Institute of membrane technology (ITM-CNR) as a collaboration in the frame of BIOART program, advising and encouraging me for my study. A special mention and thanks to Shervin Khakpour and Haysam Ahmed for their assistants in the whole project and lab works.

I wish to thank Prof. Cécile Legallais and her research team for guiding my research at University of Compiègne (my secondment in the frame of BIOART program) and providing insight and expertise that greatly assisted my research in the fluidized bed bioreactor field and also their supports during my stay in France. I would especially like to thank Vittoria Pandolfi, for her cooperation during the work in France and after that.

Thank you to Giacomo Rito, who provided a great deal of support during Fluidization Experiments. I also thank Mr. Virgilio Stellato for his help in DAQ box manufacturing.

I would like also to thank Prof. Augustinus Bader, Dr. Shibashish Giri and their research group at the University of Leipzig, Germany (my secondment in the frame of BIOART program), for helping me in developing my knowledge in iPS cell culturing field. Thank you to Aniela Skrzypczyk and Ilona Krystel, who provided a great deal of support during my stay in Germany.

Finally, I would like to acknowledge the financial support of the European Union through the Project FP7-PEOPLE-2012-ITN “Training network for developing innovative bioartificial devices for treatment of kidney and liver Disease (BIOART)” (G.A. no. 316690).

Now on to the more personal acknowledgements:

I wish to thank my family: I would especially like to thank my parents - Kamal and Rozi and also my awesome brother Navid. Without you, I would not have been able to experience the things that I have in the past few years which have brought so much happiness and light into my life. I thank you for all your love, support, and guidance throughout the years and for the future.

I would not be where I am today, graduated and much happier, if it wasn't for the support of my great friends, so I thank you: Shabnam Majidi, Babak Razdar, Parinaz Darvish, Soheil Shekarkar, Milad Mahour, Amir Zargahn, Mostafa Sheikhalishahi, Ali Hoseini, Morteza Alayi, Negin Nakhli, Sara Behnam, Sina Lesani, Behzad Azarhoushang, Maryam Janlou, Saeideh Riseh, Arash and Arya Bodaghi. Thanks for being who you are, each in your own respective way. I wish you nothing but success and happiness for the future.

To everyone I made a personal connection with, I love each and every one of you for what you have brought into my life, the moments we shared together, and what we did together. Thank you for enriching my time on this world and my life...

And for helping me finish this thesis.

Abstract

On the global scale, liver diseases are severe public health problems, with the incidences of end-stage liver disease (ESLD) rising annually. Isolated hepatocytes represent a good model of liver metabolism because they are able to perform the full range of functions. In recent years, biochemical and biotechnological engineering have been applied to the culture of human and animal hepatocyte cells, which requires the design, operation, and control of complex appropriate bioreactors. In this work, the predictable, stable and durable operation of two types of bioartificial reactors for cell cultures is investigated. The thesis is divided into the following two parts.

Part I: Fluidized bed bioreactor

Fluidized-bed-based biomedical devices acting as bioartificial liver, in which cells are trapped and encapsulated into appropriated fluidized beads, have proved effective solutions to many respects. However, the bioreactor performance is significantly affected by the hydrodynamics and mass transfer, not well characterized yet for most aspects. In the present work, the intrinsic and fluidization properties of alginate beads as encapsulation medium for hepatic cells are carefully analyzed experimentally using two rigs at different scales. Appropriate alginate beads were prepared and characterized in terms of size distribution and density. Expansion properties were evaluated for free alginate beads (i.e. without hepatic cells) using saline (Ringer) solutions as fluidization medium. Bed expansion tests over a wide range of voidage values have been conducted in a 1-cm diameter column, used for perfusion during *in vitro* experiments, as well as in a 10-cm diameter column close to human size bioreactor, in the latter case at two temperatures: ambient (20°C) and human body (37°C) conditions. Full fluid-dynamic characterization of the alginate beads is conducted, including expansion data, terminal velocity measurements, and velocity-voidage plots and their elaboration in terms of Richardson-Zaki parameters.

Part II: Hollow fiber membrane bioreactor

Due to their structure affine to the physiological environment *in vivo*, hollow fibre membrane bioreactors in crossed configuration can provide favourable conditions for the

cell behaviour and metabolism. Specific devices have been proposed in recent years with very promising potential for applications. To be able to develop bioartificial systems that operate effectively and for the long term, in addition to handling the biological complexities, fluid dynamics and transport phenomena require an advance model, careful control, and appropriate automation strategies. Tight control of the culturing environment and strategies for dealing with some inherently unsteady changes of conditions in a membrane bioreactor is investigated by developing and implementing a new hydrodynamic dual control system for an existing bioreactor prototype. The experimental implementation of the sensors-controllers-actuators system is complemented by the development of a transient mathematical model of the instrumented bioreactor, in which the membrane unit is treated as a three-compartment model. A four-input/seven-state transient model of the bioreactor is obtained, able to describe the time evolution of the flowrates, the extra-capillary space liquid level and the oxygen concentration across the system. The selection of appropriate sensors and the manipulated control variables is discussed. Bioreactor dynamic simulation and control is carried out within the Matlab/Simulink environment and Matlab is also used as a platform for the experimental data digital acquisition and control logic implementation (e.g. controller tuning), allowing both for flexibility with testing of different control schemes and for direct comparison of simulated and experimental values. Different experiments with selected input changes were carried out under idealized conditions and using water as perfusing medium. The applied stimuli served to mimick causes of previously observed bioreactor malfunctions (e.g. high sensitivity to liquid level variations during prolonged cell culturing experiments) and check the control system efficacy and efficiency. Finally, the developed control system is utilized during a prolonged experiment of multi-cell culture within the membrane bioreactor, demonstrating the reliable, continuous and successful cultivation for nearly one month time.

The set of results collected during the present work allows to achieve new insight into the operation and reliability of bioreactors for application as bioartificial devices, by improving the capacity to predict their behaviour and better design their structure as well as by enhancing the control over the cell culture environment conditions.

Sommario

Su scala globale, le malattie del fegato costituiscono un problema di salute pubblica molto grave, con un'incidenza di malattie in stadi terminali in continua crescita. Gli epatociti isolati rappresentano un buon modello di metabolismo del fegato poiché sono in grado di espletare l'intera gamma di funzioni tipiche. Negli ultimi anni l'ingegneria biochimica e biotecnologica è stata applicata alla coltura di cellule epatiche umane ed animali per la progettazione, l'esercizio ed il controllo di complessi bioreattori. In questo lavoro viene studiato il funzionamento attendibile, stabile e affidabile di due tipi di reattori bioartificiali per le colture cellulari. La tesi è divisa nelle seguenti due parti.

Parte I: Bioreattore a letto fluidizzato

I dispositivi biomedici a letto fluidizzato agenti da fegato bioartificiale si sono dimostrati per molti aspetti soluzioni efficaci. In questi le cellule sono intrappolate e incapsulate in sferette fluidizzate di natura appropriata. Le prestazioni del bioreattore sono notevolmente influenzate dalla fluido-dinamica e dal trasferimento di massa, attualmente non ancora ben caratterizzato per diversi aspetti. Nel presente lavoro si sono analizzate sperimentalmente le proprietà intrinseche e di fluidizzazione delle sferette di alginato, adottate come mezzo di incapsulamento per le cellule epatiche, utilizzando due impianti in scala diversa. Si è provveduto a preparare e caratterizzare sferette di alginato in termini di distribuzione di densità e di dimensione. Si sono quindi valutate le proprietà di espansione per le sferette di alginato libere (cioè senza cellule epatiche) utilizzando soluzioni saline (Ringer) come mezzo di fluidizzazione. I test di espansione del letto sono stati condotti su un'ampia gamma di valori di grado di vuoto in una colonna di diametro da 1-cm, utilizzata per l'espansione durante gli esperimenti in vitro, nonché in una colonna di diametro da 10-cm, prossima ai bioreattori utilizzabili su scala umana, in quest'ultimo caso a due diverse temperature: ambiente (20°C) e a condizioni corporee (37°C). E' stata condotta una completa caratterizzazione fluido-dinamica delle sferette di alginato, inclusi i dati di espansione, le misurazioni della velocità terminale ed i diagrammi velocità-grado di vuoto, con elaborazione in termini di parametri di Richardson-Zaki.

Parte II: Bioreattore a membrana a fibre cave

Grazie alla loro struttura affine all'ambiente fisiologico in vivo, i bioreattori a membrana a fibre cave in configurazione incrociata possono fornire condizioni favorevoli per il mantenimento ed il metabolismo di colture cellulari. Sono stati proposti dispositivi

specifici negli ultimi anni con un potenziale molto promettente per le applicazioni. Per essere in grado di sviluppare sistemi bioartificiali che operino in modo efficace ed a lungo termine, sono richiesti, al di là delle complessità biologiche, capacità di modellazione avanzata della fluidodinamica e dei fenomeni di trasporto ed un attento controllo attraverso strategie di automazione di processo efficaci. Oggetto di studio è stato un rigido controllo dell'ambiente colturale e le strategie per affrontare attraverso di esso modifiche di condizioni intrinsecamente instabili in un bioreattore a membrana, sviluppando ed implementando un nuovo sistema di controllo della fluidodinamica per un prototipo esistente di bioreattore. L'implementazione sperimentale del sistema di sensori-regolatori-attuatori è stata integrata dallo sviluppo di un modello matematico transitorio del bioreattore, in cui l'unità a membrana viene trattata come un modello a tre compartimenti. Si è ottenuto un modello transitorio a quattro ingressi / sette stati del bioreattore, in grado di descrivere l'evoluzione temporale dei flussi, del livello di liquido dello spazio extra-capillare e della concentrazione di ossigeno in tutto il sistema. Viene discussa la selezione dei sensori appropriati e delle variabili manipolabili per il controllo. La simulazione ed il controllo dinamico del bioreattore sono state realizzate in ambiente Matlab/Simulink e Matlab è anche stato utilizzato come piattaforma per l'acquisizione digitale dei dati sperimentali e l'implementazione di una logica di controllo (ad esempio, per il tuning dei controllori). Ciò ha consentito sia una certa flessibilità nello studio di diversi schemi di controllo sia di poter confrontare direttamente i valori simulati con quelli sperimentali. Sono stati condotti diversi esperimenti con selezionati variazioni delle variabili di input, assumendo condizioni idealizzate e utilizzando acqua come mezzo di perfusione. Gli stimoli applicati sono serviti a simulare le cause tipiche dei malfunzionamenti del bioreattore osservati in precedenza (ad esempio alta sensibilità alle variazioni del livello di liquido durante esperimenti di coltura prolungata) e controllare l'efficacia e l'efficienza del sistema di controllo. Infine, il sistema di controllo sviluppato è stato utilizzato durante un esperimento prolungato di coltura multi-cellulare all'interno del bioreattore a membrana, dimostrando nuovi livelli di affidabilità, continuità e successo nella coltura continuativa (quasi un mese di operatività).

L'insieme dei risultati raccolti durante il presente lavoro consente di ottenere una maggiore comprensione dell'esercizio e dell'affidabilità dei bioreattori per applicazioni come dispositivi bioartificiali, migliorando la capacità di prevedere il loro comportamento e di progettarne la struttura, nonché rafforzando le capacità di controllo delle condizioni dell'ambiente di coltura cellulare.

Table of Contents

Acknowledgements.....	ii
Abstract.....	iv
Sommario.....	vi
List of Figures.....	xii
List of Tables.....	xvi
List of Abbreviations and Symbols.....	xvii
Chapter 1.....	1
General introduction and background of study.....	1
1. General introduction and background of study.....	1
1.1 Liver failure.....	2
1.2 Liver support.....	3
1.3 Bioartificial liver.....	5
1.3.1 Cellular component of bioartificial liver devices.....	7
1.3.2 Bioreactors as bioartificial devices.....	8
1.4 A background of study on different type of bioreactors.....	9
1.4.1 Membrane-based bioreactors.....	9
1.4.2 Direct perfusion bioreactors.....	15
1.4.3 Entrapment-based bioreactors.....	17
1.5 Motivation and objectives.....	20
1.5.1 Fluidized bed bioreactor.....	21
1.5.2 Hollow fiber membrane bioreactor (HFMBR).....	22
Part I.....	29
Fluidized bed bioreactor.....	29
Chapter 2.....	30
The liquid-fluidized bed as bioartificial liver concept.....	30
2. Biological/biomedical applications of liquid-fluidized beds.....	30
2.1 The fluidized bed bioartificial liver principle.....	31
2.2 Improved conditions under fluidization conditions.....	32
Chapter 3.....	37
Materials and characterization methods.....	37

3.	Materials and characterization methods	37
3.1	Alginate beads characterization	38
3.1.1	Alginate preparation	38
3.1.2	Ringer solution	39
3.1.3	Characterization techniques: size	40
3.1.4	Characterization technique: density	40
3.1.5	Characterization technique: swelling	41
3.1.6	Characterization technique: settling velocity	42
3.1.7	Mass transfer into the beads	42
3.2	Expansion test and experimental rigs	44
3.2.1	Smaller (1-cm diameter) fluidization set-up	44
3.2.2	Bigger (10-cm diameter) fluidization set-up	45
3.2.3	Characterization of bed expansion	47
3.3	Effect of alginate beads on hepatocyte kinetic	48
Chapter 4		49
Results and discussion		49
4.	Results and discussion	49
4.1	Alginate bead size and density	50
4.2	Bead swelling properties	52
4.3	Terminal settling velocity	53
4.4	Mass transfer into the alginate beads	54
4.5	Expansion in the 1-cm and 10-cm columns	56
4.6	Effect of temperature	62
4.7	Albumin production (Effect of alginate bead encapsulation on kinetic of hepatocyte cell)	63
4.8	Conclusions	64
Part II		66
Hollow fiber membrane bioreactor		66
Chapter 5		67
Hollow fiber (HF) membrane bioreactor		67
5.	Hollow fiber membrane bioreactor	67
5.1	Membrane bioreactor for liver cell culturing	68

5.2	Typical set-up protocol and operational limitation.....	74
Chapter 6.....		75
Experimental setup		75
6. Experimental setup		75
6.1	Bioreactor configuration.....	76
6.1.1	Geometry.....	76
6.1.2	Fabrication.....	78
6.2	Instrumentation.....	78
6.2.1	Capillary level tank	80
6.2.2	Level sensor (contactless capacitive CLC)	85
6.2.3	Liquid flow meter	88
6.2.4	Peristaltic pumps	89
6.2.5	Data acquisition board.....	91
6.2.6	DAQ Box	92
6.3	Software (MATLAB)	94
6.3.1	Create DAQ session.....	95
6.3.2	MATLAB interface	99
6.3.3	Signal sending to the pumps	99
6.4	Hydrodynamic and control experiment setup	100
Chapter 7.....		102
Modeling and control system development.....		102
7. Modeling and control system development.....		102
7.1	Three-compartment dynamic modeling of bioreactor hydrodynamics	103
7.1.1	Mass balances	105
7.1.2	Geometrical description of the volume/height relationship.....	109
7.1.3	Linearization.....	112
7.1	Control system development	115
7.1.1	Scheme for controlled variables.....	115
7.1.2	Feedback multi-loop strategy with PID controllers	116
7.1.3	Input-output variable pairing and controller tuning	117
Chapter 8.....		120
Results and discussion.....		120

8. Results and discussion	120
8.1 Geometrical volume model validation	121
8.2 Level dynamics – comparison of the linear and non-linear model results with experiments	123
8.3 System response to step change in input variables – non-linear and linearized models	125
8.4 Control system and controller tuning	128
8.5 Level control	132
8.5.1 Level setpoint step-change	132
8.5.2 Inlet flowrate step-change	136
8.6 Flowrate control (full hydrodynamics control)	138
8.6.1 Inlet flowrate step-change	139
8.6.2 Automatic to manual switch (flowrate control disturbance)	142
8.6.3 Level setpoint step-change	145
8.7 Level control of bioreactor in actual cell culturing	146
8.8 Conclusion and outlook	150
References	152
Appendix A - MATLAB Scripts	161
Membrane bioreactor model	161
Control system	167
Appendix B – DAQ box manual	178
Appendix C – PLC level sensor manual	179
Appendix D – Flowmeter manual	182
Appendix E – Pump manual	186
Appendix F – DAQ manual	190
Appendix G – Linearized version of the three-compartment model	197

List of Figures

Fig. 1. Different steps of liver failure [8].	3
Fig. 2. Approaches to cellular therapies for the treatment of liver disease [9].	4
Fig. 3. Classification of the different artificial and bioartificial organs for temporary liver support [4].	5
Fig. 4. Schematic representation of hollow fiber based bioartificial livers relying on commercial cartridges. The cells (hepatocytes) may be located either in the lumen [49, 59] or in the extraluminal space [49, 50, 57]. Blood or plasma flows in the cell-free space. The membrane is employed as a barrier between the perfusion fluid and the hepatocytes.	13
Fig. 5. Schematic representation of the mat of fibers used in Berlin membrane-based bioartificial liver. □: open port; ■: closed port. (Adapted from [58]).	14
Fig. 6. Schematic description of Flendrig et al. [37] direct perfusion bioreactor (D). The hepatocytes aggregates (C) are anchored in the 3D matrix located between the spirally wound polyester film (B). The hollow fibers (A) provide the cells with oxygen.	16
Fig. 7. Fixed bed and fluidized bed configurations of bioreactors exploiting hepatocytes entrapment into spherical beads [4].	18
Fig. 8. The principle of the fluidized bed bioartificial liver.	32
Fig. 9. The time courses of VitB12 concentration in the tank under dynamic mass transfer conditions are shown for 4 different perfusion flow rates: (●): $Q = 29.4$ ml/min, (○): $Q = 40$ ml/min, (■): $Q = 55$ ml/min, and (□): $Q = 70.9$ ml/min [75].	33
Fig. 10. Shown is the time course of VitB12 concentration in the supernatant under static mass transfer conditions [75].	34
Fig. 11. The graph shows the influence of the superficial velocity u (divided by the terminal velocity u_t) on the fluidized bed porosity ε : (s) experimental data. The results are compared with different models: - - - Foscolo et al. [89], ... Richardson and Zaki [90], Hirata and Bulos [91], Ganguli [92], and Legallais et al. [79] — Equation 1.	35
Fig. 12. Alginate preparation setup actual (top) and schematic (bottom)	39
Fig. 13. Settling velocity measurement	42
Fig. 14. Fluidized bed bioreactor used to study the transport of vitamin B12 into the beads (dynamic system)	44
Fig. 15. Experimental setup of the bioreactor with 1-cm diameter column.	45
Fig. 16. Experimental setup of the bioreactor with 10-cm diameter column.	46
Fig. 17. Particle size distribution for the alginate beads (Malvern Mastersizer 2000) using the volume fraction density (blue solid line) and cumulative volume fraction (red dashed line) plots.	50
Fig. 18. Comparison between the densities of inert alginate beads and beads with hepatocyte spheroids during one week. Standard deviation $\sigma = 3$	52
Fig. 19. Sample microscope picture of inert alginate beads with the ruler scale (in mm units).	53
Fig. 20. Size change (swelling) properties of alginate bead. Standard deviation in William's E medium $\sigma = 0.04$ mm and in Ringer solution $\sigma = 0.02$ mm	53
Fig. 21. Alginate beads absorption trend in batch (static) condition.	55
Fig. 22. Alginate beads absorption trend in fluidized (dynamic) condition.	55

Fig. 23. Evaluation of the bed height in the 10-cm column with increasing Ringer solution flowrate.	56
Fig 24. Relative height h/h_0 vs. superficial velocity: comparison between 1 cm diameter and 10 cm diameter columns. $T = 20\text{ }^\circ\text{C}$	58
Fig. 25. Voidage vs. velocity: comparison between 1 cm diameter and 10 cm diameter columns (test No. 1 in Table 6). Fitted parameters for the Richardson-Zaki equation (R-Z) are reported in Table 6. Ambient temperature ($T = 20\text{ }^\circ\text{C}$).	58
Fig. 26. Comparison of alginate expansion in two different temperature (Two set of results are compared in case of $37\text{ }^\circ\text{C}$)	63
Fig. 27. Albumin kinetic comparison between hepatocyte spheroid and encapsulated hepatocyte spheroid in alginate bead.	64
Fig. 28. Crossed hollow fiber membrane bioreactor	70
Fig. 29. The rate of albumin and urea synthesis of human hepatocytes cultured in the crossed HF membrane bioreactor. The values are expressed as $\mu\text{g/h } 10^6 \text{ cells} \pm \text{s.e.m.}$ and are the mean of 6 experiments [6].	71
Fig. 30. a) Diazepam concentration in the inlet medium (\diamond) and in outlet medium from bioreactor loaded with cells (\circ) in presence of $10\text{ }\mu\text{M}$ diazepam added to the culture medium. b) Formation of diazepam metabolites: (full bar) oxazepam, (gray bar) temazepam and (white bar) N-desmethyl-diazepam. The values are expressed as $\text{ng/h } 10^6 \text{ cells} \pm \text{s.e.m.}$ and are the mean of 6 experiments [6].	73
Fig 31. Schematic vertical section of the crossed hollow fiber membrane bioreactor [6].	76
Fig 32. Bioreactor housing (left-a) and bioreactor assembled in-house, with 100 HFs (10×10 arrangement) in each bundle (right-b).	78
Fig 33. ITM-CNR membrane bioreactor set up before instrumentation.	79
Fig. 34. ITM-CNR membrane bioreactor set up with the multi input-multi output (MIMO) (2×2) control of hydrodynamics by two feedback loops on flowrate and liquid level.	80
Fig 35. Sketch of the capillary level tank (Side view).	82
Fig 36. Sketch of the capillary level tank (front and top view).	84
Fig 37. Capillary level tank.	85
Fig 38. CLC level sensor (a), CLC level sensor with a copper foil (b).	87
Fig. 39. A comparison of CLC level sensor accuracy measurement with and without copper foil	88
Fig 40. SENSIRION SLI 2000 flow meter.	89
Fig. 41. ISMATEC Peristaltic pump	90
Fig. 42. ISMATEC pump Analog interface details.	91
Fig 43. DAQ NI 6001.	92
Fig 44. DAQ box electrical circuit scheme.	93
Fig 45. Actual connections of the DAQ box.	94
Fig. 46. MATLAB software algorithm	95
Fig 47. Raw data vs. filtered data (Level).	97
Fig. 48. Raw data vs. filtered data (Flowrate).	98
Fig 49. MATLAB interface.	99
Fig 50. Experimental setup scheme.	101

Fig 51. Hollow-fibre membrane bioreactor scheme (a) showing the feed bundle (FB) zone through polyethersulphone, PES, membranes in red, the cell culture environment (extra capillary space, ECS) in yellow and the effluent bundle (EB) zone through the second, crossed set of membranes (also PES) in blue; the corresponding simplified three-compartment model of the bioreactor is also represented (b), also showing the model variable names for flowrates (F), volumes (V) and concentrations of species like oxygen (CA) and urea (CB).	105
Fig 52. A Simulink block diagram of the three-compartment non-linear model.	108
Fig 53. Assumed geometrical shape of the cell culturing environment with a variable liquid level within the bioreactor and level sensor range on the side.	110
Fig. 54. Volume to height conversion in Simulink	112
Fig 55. A Simulink block diagram of the linear model.	114
Fig 56. Block diagram of PID control system.	117
Fig 57. A Simulink simulation block diagram of the controlled MBR.	118
Fig 58. Comparison between the measured height and the model predictions during bioreactor filling at constant flowrate.	122
Fig 59. Step change from 1.03 to 0.73 ml/min in the outlet flowrate.	124
Fig 60. The response in the level height of the linear, Linear, and experimental data to a step change in outlet flowrate.	124
Fig. 61. Response of 4 variables: a) Level, b) Oxygen concentration in the inlet, c) Oxygen concentration in the outlet and d) Oxygen concentration in the outlet for an input step change (increasing 50% of Oxygen concentration in inlet).	126
Fig. 62. Response of 4 variables: a) Level, b) Oxygen concentration in the inlet, c) Oxygen concentration in the outlet and d) Oxygen concentration in the outlet for an input step change (decreasing 50% of Oxygen concentration in inlet and increasing 50% of inlet flowrate)	127
Fig. 63. Response of 4 variables: a) Level, b) Oxygen concentration in the inlet, c) Oxygen concentration in the outlet and d) Oxygen concentration in the outlet for an input step change (increasing 50% of Oxygen concentration in inlet and inlet flowrate)	127
Fig 64. A comparison of the simulated MBR model response with and without controller (response of ECS level to 10% increase of outlet flowrate).	129
Fig 65. Comparison of the system with and without tuning. a) Liquid level, b) Outlet flowrate (manipulated variable).	131
Fig 66. Measured flowrate variation (manipulated variable in the level control loop) as a result of step-changes in the level set-point in 10-by-10 mm steps from 80 to 50 mm.	133
Fig 67. Measured level evolution (controlled variable) as a result of step-changes in the level set-point in 10-by-10 mm steps from 80 to 50 mm.	134
Fig 68. Measured flowrate variation (manipulated variable in the level control loop) as a result of step-changes in the level set-point in 10-by-10 mm steps from 50 to 80 mm.	135
Fig 69. Measured level evolution (controlled variable) as a result of step-changes in the level set-point in 10-by-10 mm steps from 50 to 80 mm.	135
Fig 70. Measured outlet flowrate variation (manipulated variable in the level control loop) as a result of two (visible) step-changes in the inlet flowrate from 1.48 to 0.73 ml/min.	137
Fig 71. Measured level evolution (controlled variable) as a result of two (visible) step-changes in the inlet flowrate from 1.48 to 0.73 ml/min.	137

Fig. 72. Inlet flowrate set-point change (0.5 to 1.5 ml/min- by 0.25 ml/min step changes) - inlet flowrate (a), voltage sent to the pump 1 (flowrate controller) (b), bioreactor liquid level (c) and voltage sent to the pump 2 (level controller) (d).....	140
Fig. 73. Inlet flowrate set-point change (1.5 to 0.5 ml/min- by 0.25 ml/min step changes) - inlet flowrate (a), voltage sent to the pump 1 (flowrate controller) (b), bioreactor liquid level (c) and voltage sent to the pump 2 (level controller) (d).....	141
Fig. 74. Inlet flowrate set-point change (0.5 to 1.5 and 1.5 to 0.5 ml/min) - inlet flowrate (a), voltage sent to the pump 1 (flowrate controller) (b), bioreactor liquid level (c) and voltage sent to the pump 2 (level controller) (d).....	142
Fig. 75. Automatic control to manual as a flowrate control disturbance (0.5 to around 1.5 ml/min) - (a), voltage sent to the pump 1 (flowrate controller) (b), bioreactor liquid level (c) and voltage sent to the pump 2 (level controller) (d).....	143
Fig. 76. Automatic control to manual as a flowrate control disturbance (1.5 to around 0.5 ml/min) - (a), voltage sent to the pump 1 (flowrate controller) (b), bioreactor liquid level (c) and voltage sent to the pump 2 (level controller) (d).....	144
Fig. 77. Level set-point change from 50 to 80 mm (10 by 10 mm) - (a), voltage sent to the pump 1 (flowrate controller) (b), bioreactor liquid level (c) and voltage sent to the pump 2 (level controller) (d).....	145
Fig. 78. Level set-point change from 80 to 50 mm (10 by 10 mm) - inlet flowrate (a), voltage sent to pump 1 by flowrate controller (b), bioreactor medium level (c) and voltage sent to pump 2 by a level controller (d).....	146
Fig 79. 24-hour bioreactor level control results during cell culturing at day 18 (a) and evaluation of oxygen consumption rate of cells cultured into the bioreactor at day 27 (b).....	148

List of Tables

Table 1. Bioartificial liver support systems used in clinical trials [2].	7
Table 2. Bioreactor designs and comparison [9].	20
Table 3. Comparison of albumin production by human hepatoma C3A cells entrapped in alginate beads in static incubation compared with fluidized bed bioartificial liver experiment .	36
Table 4. Density measurements of inert alginate bead.	51
Table 5. Settling velocity of single alginate bead .	54
Table 6. Inert beads hydrodynamic data and Richardson-Zaki parameters .	59
Table 7. Dimensional properties of the bioreactor .	77
Table 8. Instrument and DAQ variables in order to convert voltage to actual units .	96
Table 9. Parameter definitions for the geometrical description of the height change with liquid volume.	111
Table 10. Geometrical Model validation parameter values.	121
Table 11. Without tuning and tuned controller parameters .	130
Table 12. Level control parameter values .	132
Table 13. Full hydrodynamics control parameters and variables .	139

List of Abbreviations and Symbols

μ	Viscosity
Ar	Archimede's number
C_A	Concentration component A
D	Column diameter
d	Particle size
D_{max}	Maximum of the instrument measurement limit
D_{min}	Minimum of the instrument measurement limit
g	Local acceleration
G	Transfer function
h	Height h of a liquid column
h_0	Height of difference between sensor and bioreactor
h_c	Height of cylinder
h_{cap}	Height of the small cap at sphere/cylinder interface
H_{vlt}	Height of vertical layer total
k	Correction factor
Kc	Proportional gain
K_m	Michaelis-Menten constants.
L_{fib}	Length of fiber
L_M	Level data
N_{row}	Number of rows (fiber)

N_{vlt}	Number of vertical layer total
Q_f	Flow rate
r	Radius of the tube
R	Raw data
r_c	Radius of cylinder
r_{fib}	Radius of fiber
r_s	Radius of sphere
Re	Reynolds' number
u	Superficial velocity
V_{cap}	Volume of the small cap at sphere/cylinder interface
V_{fib}	Volume of one fiber
V_{fibt}	Total volume of fiber
V_s	Volume of sphere
V_2	Liquid volume in the ECS
V_{max}	Michaelis-Menten constants
λ	Relative gain parameter
y_m	Measured variable
y_{sp}	Set-point variable
γ	Liquid-air surface tension
$\varepsilon(t)$	Error value
ε	Voidage
θ	Contact angle

ρ	Density
τ_d	Derivative time
τ_i	Integral time
<i>BAL</i>	Bioartificial liver devices
<i>DAQ</i>	Data acquisition board
<i>EB</i>	Effluent bundle
<i>ECS</i>	Extra-capillary space
<i>ELISA</i>	Enzyme-linked immunosorbent assay
<i>ESLD</i>	End-stage liver disease
<i>FB</i>	Feed bundle
<i>FBBAL</i>	Fluidized bed bioartificial liver
<i>GND</i>	Ground
<i>HEMA</i>	Hydroxyethyl methacrylate
<i>HF</i>	Hollow fibers
<i>HFMBR</i>	Hollow fiber membrane bioreactors
<i>HF_s</i>	Hollow fiber membranes
<i>ID</i>	Internal diameter
<i>IPA</i>	Isopropyl alcohol
<i>MA</i>	Moving average
<i>MBR</i>	Membrane bioreactor
<i>MIMO</i>	Multi input-multi output
<i>MW</i>	Molecular weight

<i>MWCO</i>	Molecular weight cut-off
<i>NI</i>	National instrument
<i>PEEK-WC</i>	Polyetheretherketone
<i>PERV</i>	Porcine endogenous retrovirus
<i>PES</i>	Polyethersulfone
<i>PID</i>	Proportional–integral–derivative
<i>PMMA</i>	Poly (methyl methacrylate)
<i>RGA</i>	Relative gain array
<i>RTD</i>	Residence time distribution
<i>SD</i>	Standard deviation
<i>TI</i>	Teach-

Chapter 1

General introduction and background of study

1. General introduction and background of study

In this chapter after a general introduction to liver failure and liver support, the technological aspects of the previously developed bioreactor devices like membrane-based devices, direct perfusion systems, and entrapment-based columns are reviewed. For each type, the technological requirements are theoretically addressed. At the end of the Chapter, the project motivations in relation to two important types of bioreactor such as fluidized bed bioreactor and hollow fiber membrane bioreactor are discussed.

1.1 Liver failure

The liver performs many important metabolic functions and is the only internal organ that has the capacity to regenerate itself with new healthy tissues. Loss of liver cell functions may result in the disruption of many essential metabolic functions, which could lead to death. On the global scale, liver diseases are severe public health problems, with the incidences of end-stage liver disease (ESLD) rising annually. The impairment of liver functions has also serious implications and it is responsible for high rates of patient morbidity and mortality. Progresses made within the last decades in surgical techniques, intensive care, immunosuppressive regimen, and organ preservation methods have made liver transplantation a form of well-established and successful therapy [1]. The 5-year survival rate in the United States was 70.5% for deceased donor transplants performed in 2007. However, the existing shortage in available donor organs allows no significant expansion of transplantation programs, and the number of patients on the waiting list for transplantation largely exceeds the number of donor organs available for transplantation [2, 3].

Presently, liver transplantation remains the treatment of choice for ESLD patients but it is limited by both the high costs and a severe shortage of donor organs. *Fig. 1* shows different steps of liver failure [4-7].

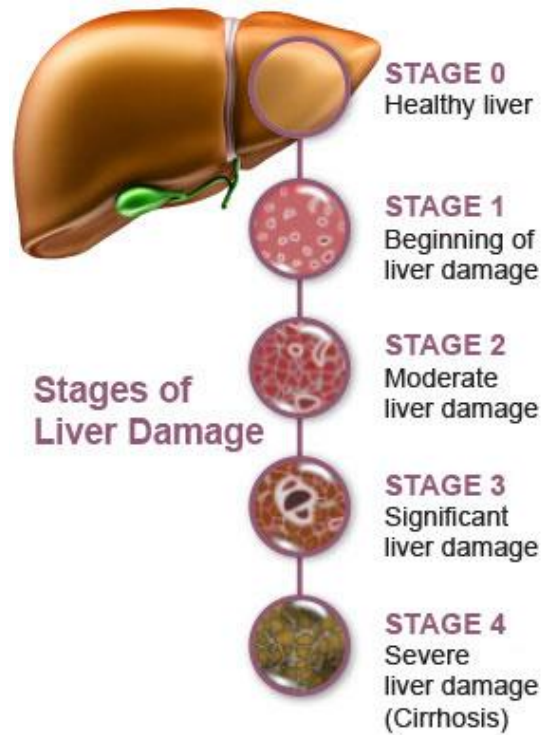


Fig. 1. Different steps of liver failure [8].

Throughout the years, survival after transplantation has enhanced with advances in both patient administration and surgical methods, yet the strategy is not generally accessible in a convenient manner, stimulating new surgical methodologies, for example, split-liver transplantation, acquisition from living donors, and assistant liver transplantation. The issue of organ lack is exacerbated by the difficulty in anticipating the result of liver failure. The King's College prognostic criteria have been embraced by most focuses, in spite of the fact that they neglect to distinguish patients at generally safe of dying [9-11].

1.2 Liver support

Since 20 years, the growing crevice between the number of patients on holding up rundown and the number of liver transplants has highlighted the necessity for a temporary liver support [4].

Other options to entire organ transplantation for liver dysfunction are under dynamic examination. *Fig. 2* schematically delineates the 4 fundamental cell approaches

that are presently being explored: isolated cell transplantation, tissue engineering of implantable constructs, transgenic xenotransplantation, and extracorporeal bioartificial liver devices (BAL). Extracorporeal bolster for patients experiencing liver failure has endeavored for more than 40 years. Transitory frameworks have been produced to endeavor to assist recuperation from intense decompensation, encourage recovery, or serve as a scaffold to liver transplantation [12-21].

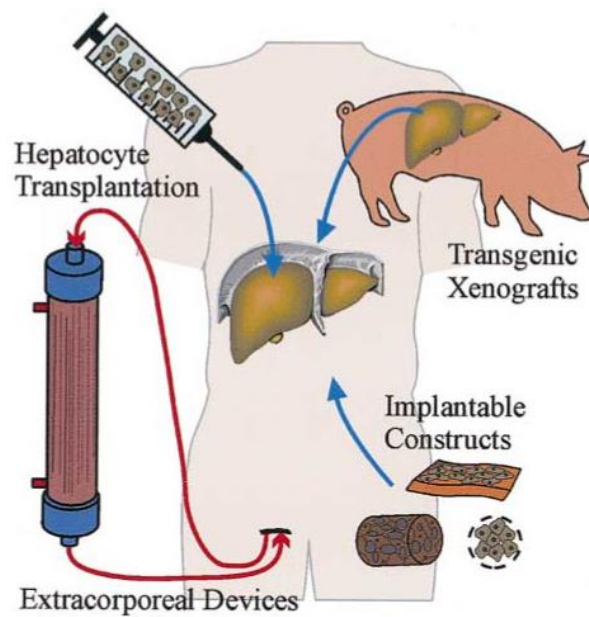


Fig. 2. Approaches to cellular therapies for the treatment of liver disease [9].

In the previous two decades, a few gadgets for liver support have been examined or created, which can be classified into two: purely artificial organs, in light of traditional strategies, for example, hemodialysis, plasmapheresis, specific or non-specific adsorption, and bioartificial organs (*Fig. 3*). As liver plays out numerous and complex functions (detoxification, transformation, synthesis), it has gotten to be apparent that mechanical or chemical forces cannot be adjusted to the treatment of intense liver diseases. In contrast, a bioartificial organ exploits a synthetic cartridge to host biological components such as liver cells (hepatocytes on account of a bioartificial liver). Such devices are presently being worked on and some have as of now achieved clinical trials. Apart from the functionality and efficacy of liver support systems, safety issues have to be considered. In particular, systems used for supporting the liver function in diseased liver need to be stable over the treatment period and show reproducible functions to

ensure a standardized quality. In addition, investigation of the biocompatibility of materials used and preventing infection of patients are demanded to ensure the clinical safety of treatments [2, 4, 22].

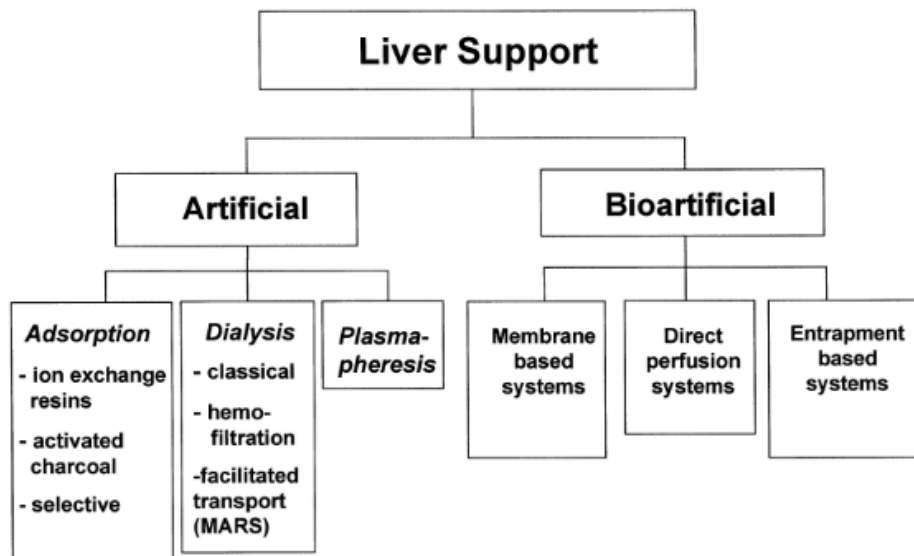


Fig. 3. Classification of the different artificial and bioartificial organs for temporary liver support [4].

Different non-biological methodologies have met with restricted achievement, probably in light of the part of the synthetic and metabolic functions of the liver that are deficiently supplanted in these frameworks. Haemodialysis, hemoperfusion over charcoal or resins or immobilized enzymes, plasmapheresis, and plasma exchange have all been investigated. Alternately, absolutely biological methodologies have demonstrated empowering brings about a few cases, however, have been difficult to execute in the clinical setting. Notwithstanding orthotropic liver transplantation, these incorporate entire organ perfusion, perfusion of liver slices, and cross hemodialysis [21].

1.3 Bioartificial liver

Bioartificial devices typically incorporate isolated cells into bioreactors to simultaneously promote cell survival and function as well as provide a level of transport seen in vivo [23]. In order to adequately compensate the metabolic and regulatory

performances of the failing organ in clinical application, bioartificial liver support systems have to:

- Provide differentiated, human-specific hepatic functions
- Procure sufficient cell quantities for efficient liver support in patients
- Ensure the stable maintenance of metabolic activities
- Enable a reproducible cell quality for standardized clinical applications
- Ensure the clinical safety of the system, in particular, with respect to the cell source used
- Allow the flow of blood and plasma with a mass exchange that can quantitatively address the required metabolism for the patient and the possible metabolism of the cells
- Ensure that problems of blood cell damage and coagulation during blood perfusion can be avoided
- Avoid negative interactions with the patients' coagulation system, while anticoagulation may be required [2].

An important challenge in engineering devices for culturing liver cells is the development of bioartificial systems that are able to favor the liver reconstruction and to modulate liver cell behaviour. Bioreactors allow the culture of cells under tissue specific mechanical forces (e.g. pressure, shear stress and interstitial flow), augmenting the gas and nutrient exchange under fluid dynamics control that ensures the long-term maintenance of cell viability and functions [6]. Table 1 gives an overview of bioartificial liver support systems that have been clinically used for extracorporeal liver support. Most of these systems represent two-compartment devices where the cells reside in the space between perfused hollow-fiber capillaries serving for plasma or blood perfusion [2].

Table 1. Bioartificial liver support systems used in clinical trials [2].

Bioreactor Technology	Cell type used	Clinical outcome
Hollow fiber-based bioartificial liver device perfused with plasma (ELAD)[24, 25]	Human hepatoblastoma cell line(C3A)	No significant difference in survival, improvement in galactose elimination and encephalopathy
Hollow fiber-based bioartificial liver device perfused with whole blood(BLSS)[26, 27]	Primary porcine hepatocytes	No serious adverse events; treatment well tolerated by patients
Hollow fiber-based bioartificial liver with hepatocytes attached to dextranmicro carriers (HepatAssist)[28]	Cryopreserved porcine hepatocytes	Tendency toward improved survival, yet not significant
Amsterdam Medical Centre Bioartificial Liver Device (AMC-BAL)[29]	Primary porcine hepatocytes	No severe adverse events, successful bridging to liver transplantation shown
Radial flow bioreactor perfused with plasma (RFB-BAL)[30]	Primary porcine hepatocytes	Improvement of encephalopathy level, decrease in ammonia and transaminases
Hollow fiber-based bioartificial liver with integral oxygenation (MELS)[31, 32]	Primary porcine or human liver cells	No severe adverse events; in some patients, clinical and/or biochemical improvement

1.3.1 Cellular component of bioartificial liver devices

The full supplement of cellular functions required in BAL devices to impact positive clinical results has not been resolved. To address this issue, surrogate markers of every class of liver-specific functions commonly are described including synthetic, metabolic, detoxification (stage I and II pathways), and biliary discharge [33, 34]. The certain suspicion is that hepatocytes fit for a wide cluster of known functions will likewise express those unmeasured (or obscure) functions that are integral to their metabolic part. Each of these primary hepatocytes, cell lines, and stem cells ought to be assessed on the

premise of accessibility, potential unfriendly connections, and efficacy in giving liver-specific function [9].

Primary porcine hepatocytes are most commonly used in devices undergoing preclinical and clinical evaluation. Primary hepatocytes, in particular, have a unique microenvironment *in vivo* and they notoriously lose their liver-specific functionality and/or viability *in vitro*. Additionally, the proliferation of mature human hepatocytes *in vitro* if present is very limited. Isolated hepatocytes represent a good model of liver metabolism because they are able to perform the full range of known *in vivo* biotransformation, synthetic and detoxification functions [35-38].

Although primary hepatocytes represent the most direct approach to replacing liver function in hepatic failure, they are anchorage-dependent cells and notoriously difficult to maintain *in vitro*. There is relatively limited information on the maintenance of liver-specific functions of hepatocytes. They rapidly lose their liver specific functions when maintained under the standard *in vitro* culture conditions. When enzymatically isolated from the liver and cultured in monolayer or suspension cultures, they rapidly lose adult liver morphology and differentiated functions. Many investigators have looked at the microstructure of the liver to provide inspiration for culture models that replace the lost cues from the hepatocyte microenvironment *in vivo* [9, 37, 38].

1.3.2 Bioreactors as bioartificial devices

This short-sighted approach comprises in considering such a device as a bioreactor in view of synthetic components ready to offer a satisfactory situation to the liver cells. This environment would thusly prompt to the support of efficient functions of the cells going for liver supply when putting in a bioreactor situated in an extracorporeal circuit [4].

The obligatory prerequisites for worthy cell viability and functions in a bioartificial liver (BAL) are likely recorded beneath, as indicated by a biotechnological perspective:

1. Anchorage to a support or a matrix.
2. Compelling exchanges with blood or plasma in order to
 - Receive satisfactory oxygen and supplements supply,

- Be in contact with the toxic substances and catabolites typically expelled from the blood by the liver (e.g. bilirubin),

- Release synthesized metabolites (e.g. urea, albumin, coagulation factors) to the blood stream.

3. Assurance from host immunological reaction.

Likewise, the synthetic segments of the bioreactors should themselves be biocompatible. A few bioreactor designs have been proposed to fulfill the vast majority of the above conditions [4].

1.4 A background of study on different type of bioreactors

1.4.1 Membrane-based bioreactors

Once the requirement for the incorporation of cellular compounds into an extracorporeal bioreactor got to be obvious, a few research groups exploited the membrane modules effectively produced for pure artificial organs. The flat sheet or hollow fiber hemodialysers, and additionally plasmafilters had effectively demonstrated their ability for solute and oxygen transport and their relative biocompatibility towards the patient's blood or plasma. Membranes were what's more ready to give an immune barrier between the hepatocytes and the perfusion fluid, and could likewise be utilized for cell anchorage [4].

In the accompanying, we first introduced how membranes and membrane reactors may hypothetically address the prerequisites beforehand drawn for an efficient BAL. From this investigation, we along these lines introduced and talked about the BAL under development [4].

1.4.1.1 Cell anchorage

There is an extensive variety of membrane materials utilized in extracorporeal circuits. They all demonstrated their relative biocompatibility with either blood or plasma,

yet before their application to bioartificial organs and particularly BAL, they had never been investigated in term of cell adhesion and development. Hence, a few parameters, for example, the type of polymer, the hydrophobicity or wettability, and the surface roughness were explored [39-45].

A few conclusions may be drawn from the gathered information: would cell attachment on membrane surface be looked for, the material ought to be hydrophilic and electrically charged (either emphatically or adversely) [40-42, 44].

The charge density appeared to essentially influence the cell adhesion, and thus the cellular integrity. From this point of view, polysulfone membranes appeared as the best material and gave the best yield as far as metabolic exercises. Cellulose-based membranes were substantially less appealing. The membrane roughness did not influence cell adhesion, and thus cell activities, for example, oxygen consumption or ammonium elimination kinetics [45]. In fact, the best cell adhesion, integrity, and prolonged viability were acquired after the membrane polymer coating with collagen or fibronectin [43]. These perceptions were in concurrence with information from Biagini et al. [46] demonstrating an improved fibroblasts adhesion and expansion on utilized dialysis membranes, i.e. materials on which a protein layer was stored.

This sort of coating offered a more appropriate environment for hepatocytes and was generally utilized with even non-porous materials. In any case, the direct attachment of hepatocytes to one membrane side could avoid efficient trade between both membrane sides. Along these lines, cell attachment could ideally be accomplished on different sorts of the matrix, for example, Collagen [47-49], Agarose [50] or Matrigel [51], set either in the lumen or the extraluminal part of the membrane. In these cases, the membrane would just be utilized as an exchanger and immunological barrier.

1.4.1.2 Sieving properties

Two types of membranes have been utilized as a part of present extracorporeal circuits. The first is an ultrafiltration membrane with a maximum molecular weight cut-off (MWCO) of around 70 kDa (molecular weight of albumin). The basis for utilizing

this kind of membrane as a part of BAL was the related immune barrier: such a membrane prevented xenogenic hepatocytes from immune rejection and conversely the patient from the dangers of hypersensitivity reactions and xenozoonosis. Subsequently, the evacuation of albumin-bound toxins or the discharge into the perfusion fluid of the novo-synthesized proteins was frustrated or even counteracted [52, 53].

The second is a microporous membrane with a mean pore size of around 0.2 μm which permits the exchange of even high molecular weight proteins which could prompt to the immunological hazard said above. However, a later in vitro study from Mullon [54] showed that a 0.15 μm pore size polysulfone membrane decreased the danger of porcine endogenous retrovirus (PERV) transmission by an element of 100,000.

1.4.1.3 Bioreactor geometry

Because of compactness and efficiency imperatives, hollow fiber membranes appeared to be a great deal more sufficient than flat sheet membranes. The solute mass transfer from the blood or plasma compartment to the cell compartment and the other way around in a membrane-based bioreactor did rely on upon the membrane type, as well as on the bioreactor geometry and the area of both compartments. As portrayed in detail by Catapano [55], mass transport experienced constraints in three unique areas: perfusion fluid (blood or plasma), membrane structure and cell compartment. Contingent on the bioreactor design, the solute mass transfer inside these three zones could be significantly distinctive. Inside these compartments, phenomena in charge of mass transport could be diffusion, convection, or both.

In the perfusion fluid side, mass transport was unequivocally influenced by the fluid velocity and viscosity. By relationship with hemodialysis, the flow of the perfusion fluid on the shell side (hepatocytes on the lumen side) could bring about zones where fluid was practically stagnant, and thus exceptionally poor diffusive transfer may happen. As highlighted by Catapano [55], the higher the velocity the better the mass transport. In term of viscosity, the utilization of plasma rather than blood, other than encouraging biocompatibility to the detriment of system complexity, resulted in a significant viscosity decrease for the perfusion fluid which on a basic level favored mass transport. In any case, Zydney et al. [56] depicted the impact of the presence of rotating red blood cells on solute effective diffusion in blood. These hypothetical contemplations contended for the

nearness of the hepatocytes on the shell side, yet don't take into consideration conclusion on the choice of fluid [4].

Membrane permeability for a solute decreases with the increase of its molecular size. It additionally relies on upon the solute shape and size. Other than the immunological measure, the membrane MWCO may speak to the key purpose of exchanges between perfusion fluid and hepatocyte [4].

In the cell compartment, mass transport unequivocally relied on compactness and density. The distinctive procedures utilized to give the cells with an adequate anchorage might here assume a critical part. In spite of a 3-D arrangement, the hepatocytes situated in the fiber lumen experienced a low contact region and additionally starvation for those situated a long way from the membrane. On the shell side, the cell viability emphatically depended on its accessibility. The collagen matrix offered an efficient anchorage but was in charge of low diffusion coefficients. The attachment to microcarrier could allow the presentation of every cell to the medium, additionally relied on upon the level of filling for the bioreactor [4].

Taking everything into account, hypothetical contemplations may be useful to maintain a strategic distance from a few mix-ups in the origination of a membrane-based BAL. In any case, they didn't prompt to the definition of the ideal design, since many inquiries were not completely replied [4].

1.4.1.4 Choice of membrane material

In the vast majority of frameworks, a polysulfone-based membrane was favored in concurrence with its better connections with the hepatocytes, despite the fact that cells were not attached directly to it [49, 50, 57]. Gerlach [58] has built up a bioreactor with three separate capillary membrane systems, according to the functions dedicated to each membrane (nutrient/plasma input or output, gas exchange).

1.4.1.5 Bioreactor design

Bioreactor designs differed from classical (hemodialysers) to more entangled geometry. In traditional membrane modules, the fluid flowed either inside or outside the fiber lumen, the hepatocytes being situated on the opposite side (*Fig. 4*). Filling the

bioreactor with hepatocytes on the membrane shell side appeared to be favored for practical reasons. Gerlach et al. [51] proposed a more intricate geometry including a mat of three diverse fibers offering a 3D environment to the cells seeded at the external surface and among the capillaries.

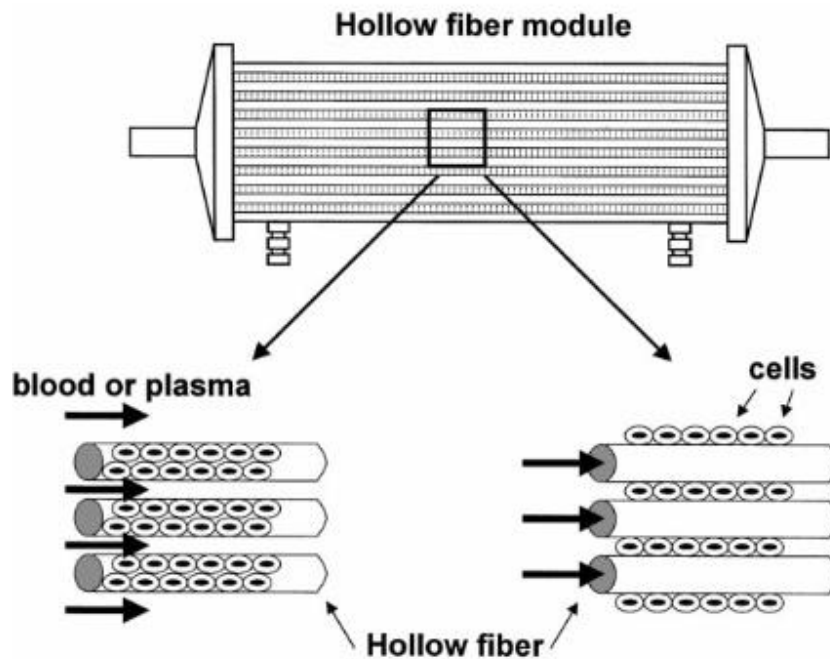


Fig. 4. Schematic representation of hollow fiber based bioartificial livers relying on commercial cartridges. The cells (hepatocytes) may be located either in the lumen [49, 59] or in the extraluminal space [49, 50, 57]. Blood or plasma flows in the cell-free space. The membrane is employed as a barrier between the perfusion fluid and the hepatocytes.

As shown in *Fig. 5*, each fiber type was perfused with various fluids (oxygen, nutrients during the culture period, plasma under powerful BAL function). Plasma or culture medium entered the bioreactor by means of a fiber bundle under dead end filtration conditions, and left by means of another bundle, resulting in adequate exchanges with the hepatocytes [58].

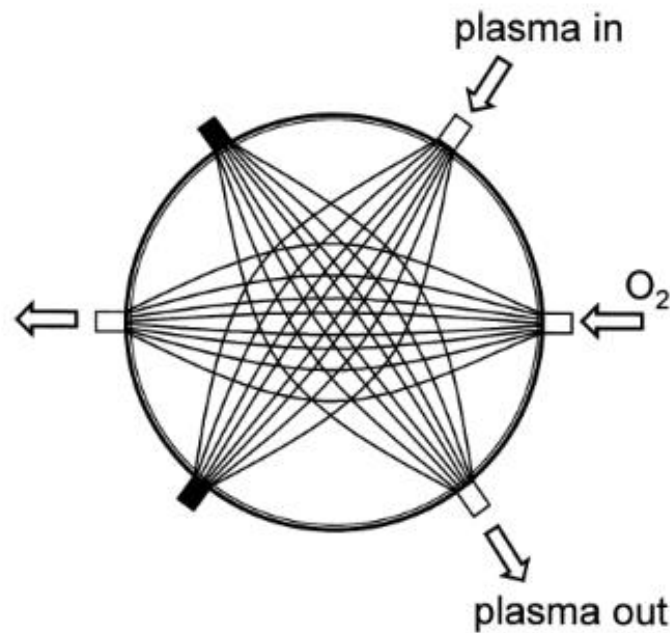


Fig. 5. Schematic representation of the mat of fibers used in Berlin membrane-based bioartificial liver. □: open port; ■: closed port. (Adapted from [58]).

Since no randomized tests have been defined yet, it appeared difficult to separate the distinctive bioreactors' efficiency. In any case, bioreactors using upgraded convective mass transfer seemed more efficient than those depending on pure diffusion. In the Circe bioreactor, the high perfusion flow rate (400 ml/min achieved by plasma recirculation) associated with a long plasmapheresis membrane (500 mm length) yielded high inside filtration flow rate took after by back filtration which enhanced transfers in both the directions [60]. Albeit other authors [40] recommended that pure diffusion techniques could be beneficial on account of the low concentration gradient produced on both sides of the membrane, no clinical information managed this approach.

1.4.1.6 Summary

The experience of the distinctive groups required in the origination of a membrane-based BAL demonstrated that some preparatory limitations could be kept away from with no malicious impact on the BAL functions. The efficient mass transfer of toxins and metabolites, furthermore most likely of oxygen, as opposed to the regard of

a tight immunological barrier, showed up as a key point for a reliable short-term BAL use.

It is in certainty extremely difficult to dissect the genuine efficiency of every framework and still many inquiries are opened. Particularly, the optimal amount of hepatocytes to be utilized has not been defined yet. Would it be bigger than that typically utilized for the occasion, the membrane bioreactors, even exceptionally appealing, could suffer from scaling-up difficulties [55]: expanding the number of hepatocytes into a similar cartridge could bring about a significant loss of mass transport and hence viability. Likewise, the impact of membrane fouling under high filtration flow rate has not been explored as such and could be a restricting component in future utilizations of such BAL [61].

1.4.2 Direct perfusion bioreactors

The direct perfusion of connected cells by plasma or blood into a bioreactor appears an encouraging and basic idea, which was taken up by a few research groups.

Two principle methodologies were under scrutiny. The first one endeavored at making a 3D environment for the liver cells, looking like the native organ [61-63]. The cells could form small aggregates, or be specifically appended to a porous support. They were in this way independently perfused, under a low dispersion slope as in a typical liver [61]. The other approach depended on more conventional cell culture as monolayers between two collagen-coated plates [64-66]. The restricting sinusoidal surfaces of the hepatocytes were joined to the extracellular matrix, duplicating the in situ configuration of the intact liver. Non-parenchymal cells could be deliberately added to enhance the hepatocyte functions [64].

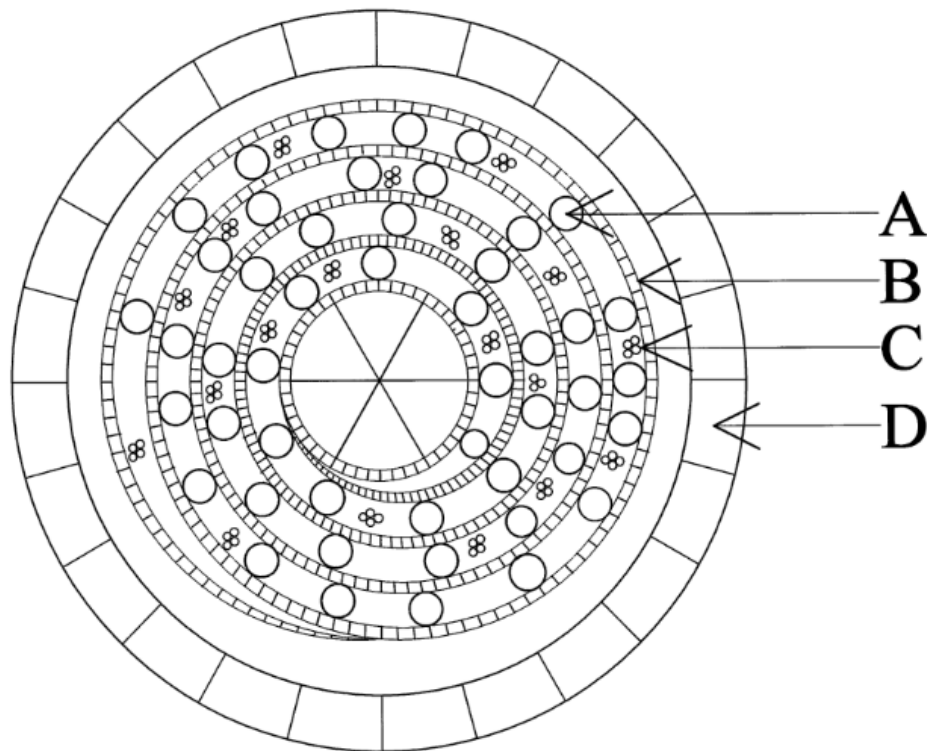


Fig. 6. Schematic description of Flendrig et al. [37] direct perfusion bioreactor (D). The hepatocytes aggregates (C) are anchored in the 3D matrix located between the spirally wound polyester film (B). The hollow fibers (A) provide the cells with oxygen.

A portion of the above bioreactors additionally utilized a few sections of membrane technology. Flendrig et al. [62] utilized hydrophobic polypropylene hollow fiber membranes for oxygen supply and Carbon Monoxide evacuation. The homogenous dispersion of the fibers went about as a spacer for the spirally twisted polyester film, reinforcing the 3D environment offered to the hepatocytes (*Fig. 6*). The idea of this type of bioreactor ought to encourage the scaling-up. Bader et al. [65] developed the hepatocytes on collagen-coated microporous membrane but, as Flendrig, did not use this membrane as a barrier between the cells and the perfusion fluid.

For the occasion, none of the displayed frameworks have achieved the clinical trials. Despite the fact that the mass exchanges ought to be streamlined, the scaling up of a few frameworks (particularly the plates) appeared difficult to perform. Likewise, hepatocytes could be subjected to high shear in some configurations, prompting to cell harm or conceivable discharge to the circulation system. With respect to most layer based frameworks, just constant culture permitted the capacity of such BAL [4].

1.4.3 Entrapment-based bioreactors

Another option to the above configurations was the incorporation of hepatocytes inside a semi-permeable spherical structure more often than not called “bead” or “capsule” [67]. The polymer bead matrix offered anchorage facilities to hepatocytes and its porous structure could go about as an immunological barrier.

The hepatocytes containing beads were first created by Tompkins et al. [68] and Dixit [19] for their direct implantation. Hepatocytes viability was observed to be kept up in such a tridimensional structure [69], even after cryopreservation [70]. The beads may even shield the cells from shear stress damage in an extracorporeal bioreactor. Since cell encapsulation is a broadly utilized instrument as a part of biotechnology, a few materials have been examined to fulfill the prerequisites of a bioartificial liver. A few groups tried the properties of Hydroxyethyl methacrylate-methyl methacrylate (HEMA-MMA) copolymer [71], chitosan-dextrose [72]. Calcium alginate was up to now the most famous material [8, 73] in view of its porosity, its mechanical properties, and its biocompatibility. The alginate bead external structure may be reinforced by the expansion of chelating segments (lysine for instance). The bead diameter ranged from 1 mm or less, taking into account sufficient mass transfer and oxygenation of all the hepatocytes. This size was appeared to be greatest by Sardonini et al. [74] whose findings demonstrated an ideal cell to a medium distance of 370 mm to keep up high cell viability. What's more, hepatocytes into alginate bead may be easily stored by cryopreservation [70].

A large portion of the bioreactors intended for beads perfusion relied on fixed bed configuration (*Fig. 7*), where the beads were densely packed into a column. Reactors intended for small animal trials worked appropriately [73]. Their significant restriction for scaling-up was the perfusion velocity profile into the column: the arrangement of preferential channels resulted in poor perfusion for a lot of beads and subsequently constrained mass transport outside the beads.

Furthermore, high shear stresses on the successfully perfused beads could prompt to conceivable harm on the beads structure, and as an impact to alginate and cells discharge to the blood stream. Nonetheless, the hepatocytes entrapment into alginate beads still seemed promising since the various criteria fixed for an operational BAL appeared to be fulfilled. Thus, it was proposed to make use of the possibility of hepatocytes entrapped in alginate beads in a more efficient bioreactor. In this novel

geometry, beads were subjected to a fluidized bed movement, prompting to the definition of a fluidized bed bioartificial liver (FBBAL) [75].

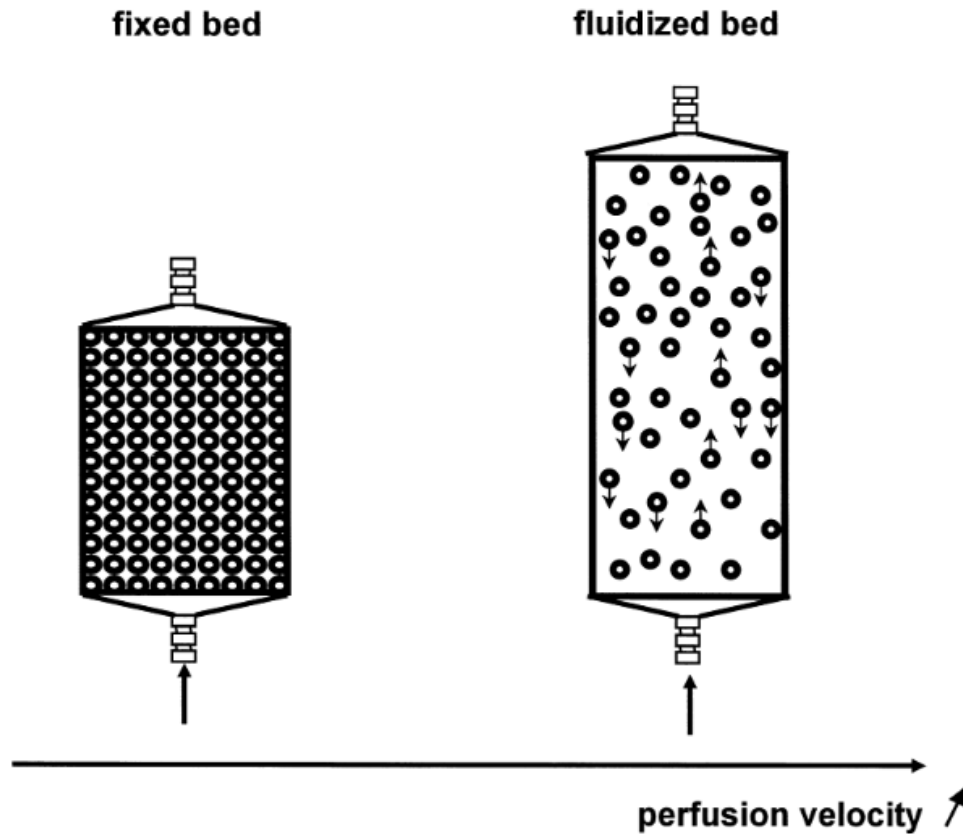


Fig. 7. Fixed bed and fluidized bed configurations of bioreactors exploiting hepatocytes entrapment into spherical beads [4].

The utilization of fluidized bed reactors was generally spread in chemical or biochemical engineering when a diphasic blend was available [76]. In the mix with cells entrapped into beads, it has likewise found a few biotechnological applications [77]. Thus we recommended to apply this innovation to a vast scale extracorporeal BAL, committed to in vivo applications on pigs [78] and as an extension of the past work of Fremont et al. [73] with a small-scale bioreactor. The in vivo application required the utilization of 300–400 ml of alginate beads (diameter 1 mm) containing porcine hepatocytes. The perfusion plasma flow rate ought to run 20–30 ml/min and the dead volume minimized. The framework created was depicted in detail somewhere else [75] and first approved with saline solution at 20 °C rather than plasma at 37 °C (same viscosity) and empty beads

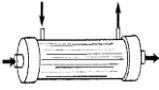
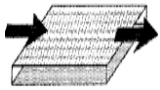
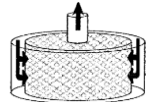

(supposed to be lighter than the cells containing ones) [79]. The fluidization was gotten from the fixed bed status by increasing the superficial velocity (*Fig. 7*).

The bed expansion suggested utilizing a column with a smaller diameter (to work at the same flow rate) and a larger height than a fixed bed column. Under optimized hydrodynamic conditions, bed expansion was steady and brought about a homogenous mixing [4].

The outcomes obtained with this kind of bioreactor and empty beads are extremely reassuring. In vivo animal trials were performed in Rennes, demonstrating an alternate conduct with hepatocytes containing beads. The following stride in the bioreactor advancement comprises of in vitro experimental trials with plasma and entrapped hepatocytes [4].

Table 2 summarizes the bioreactor designs that have been proposed and studied.

Table 2. Bioreactor designs and comparison [9]

 Hollow fiber	 Flat plate and monolayer	 Perfused beds/Scaffolds	 Encapsulation and suspension
Pros: attachment surface, potential for immunization , well characterized, cells protected from shear	Pros: uniform cell distribution and microenvironment	Pros: ease of scale-up, promotes 3-dimensional architecture, minimal transport barrier	Pros: ease of scale-up, uniform microenvironment
Cons: non-uniform cell distribution, transport barrier with membranes or gels	Cons: complex scale-up, potential large dead volume, cells exposed to shear, low surface area-to-volume ratio	Cons: non-uniform perfusion, clogging, cells exposed to shear forces	Cons: poor cell stability in suspension, transport barrier due to encapsulation, degradation of microcapsules over time, cells exposed to shear forces

1.5 Motivation and objectives

The fluidized bed and hollow fiber bioreactors are the most promising technologies. In their operation, several issues arise because of the complex hydrodynamics and mass transport; so, there is a need to characterize the dynamics (in the sense of dynamical operation of the fluidized bed vs. packed/static configurations) and possibly apply instrumentation for automatic control. The details about problems and issues related to these two type of bioreactors and the most important objectives of present work are discussed in the two further sections.

1.5.1 Fluidized bed bioreactor

Hepatic cells in the form of spheroids immobilized within alginate beads in fluidized bed devices have been recently subjected to tests and successfully validated in preclinical trials with respect to biological functions and metabolic activity [80]. The effect of alginate preparation and beads size on the mass transfer and metabolic activity has been investigated by Gautier et al. [81] and other groups [82]. Generally, it has been shown that the overall performance of the fluidized bed bioartificial liver strongly relies on the effective hydrodynamics and mass transfer in the bioreactor. Unfortunately, in real applications, the expansion of the beads is not clearly visible even in transparent bioreactors, as the fluidization medium may be opaque. As it is well known, measures of the pressure drop are also of little use to characterize expansion once the minimum fluidization velocity is overcome. Mass transport between the fluid and the cell encapsulating alginate beads is also connected to the expansion in a complicated way, as an increase in velocity tends to overcome transport limitations on the exterior of the cells but also increase the voidage, i.e. decreasing the contact surface area per unit volume. Therefore, the ability to accurately predict the expansion properties of the beads' bed is very important to the efficient use of the bioreactor.

The investigation related to fluidized bed bioreactor was carried out in a cooperation with the University of Compiegne. The main objective of the first part of this work is to provide data and analysis useful to the selection of the optimal hydrodynamic regime in the design and scale-up of bioartificial devices based on the fluidized bed of alginate beads. This is achieved first by preparing relatively monodisperse alginate beads, followed by a careful evaluation of their properties with specific respect to the characteristics influencing fluidization, including density (pure alginate and/or presence of hepatocytes), average size and size distribution, swelling characteristics in different culture media. It shall be emphasized that such properties of alginate are rather peculiar in comparison with more traditional particulate materials in fluidized beds (e.g. sand, fuel particles, and catalysts). For example, the density of alginate is very similar to that of water, also affected by possible swelling, making its correct determination crucial.

Fluidization properties are then investigated using Ringer solution as fluidization medium. A comparative hydrodynamic analysis is carried out of the expansion rate of the prepared beads up to very high voidage values in a 1-cm *vs.* 10-cm internal diameter

columns. Terminal velocity conditions are also investigated to compare values with extrapolated expansion properties. Measurements of the expansion properties at human body temperature are also attempted.

In summary the objectives of part I are:

- Alginate beads for the fluidized bed bioartificial liver characterization
- Size distribution, density, swelling, settling velocity and mass transfer properties evaluation
- Expansion/fluidization properties measurement at two rig scales
- Discussion and representation in terms of Richardson-Zaki parameters
- Investigation on the effects of temperature in the fluidization

1.5.2 Hollow fiber membrane bioreactor (HFMBR)

Hollow fiber membrane bioreactors (HFMBR) are commonly used in tissue engineering applications for cell-based therapies and are among promising types of extracorporeal bioartificial liver (BAL) devices. Depending on the application and the cell type used, different configurations are considered to serve different functions. Generally speaking, the cells can be attached to the outer wall of the hollow fibers (HF) with the medium flowing in the lumen of the fibers in order to protect the cells from shear stress. Alternatively, if shear stress is required as an external mechanical stimulus, the cells may be seeded in the lumen of the HF [6, 37, 83].

The research in this section is conducted in collaboration with the Institute of Membrane Technology of the Italian National Research Council (ITM-CNR) where an HFMBR test-rig with different facilities are available. The mentioned bioreactor include an HF cross-membrane system used in the inflow and outflow medium. In order to constitute three different compartments, the fibers were potted at each end, yielding two intraluminal compartments within the polyethersulfone (PES) fibers and an extra capillary compartment or shell outside the fibers. The inflow and outflow compartments communicate through the pores in the fiber wall. The human hepatocytes were seeded in the extra capillary compartment of the bioreactor on the outer surface of and between the HF membranes. After the liver cells adhered, the bioreactor was perfused with the oxygenated medium.

However, the increasing complexity of fluid dynamics and transport phenomena in present and future bioreactors requires advanced steady-state models and control strategies for the transient operations, since a well-controlled environment with respect to transfer processes and metabolic kinetics is necessary for activation of specific cellular response and long-time viability. From a methodological point of view, it is necessary to develop a complete system model, containing all the relevant elementary processes at sufficient level of detail, in order to build an input-output reactor representation and advice suitable control actions to maintain the desired set points [84, 85].

On the other hand, Several factors may limit the survival of hepatocyte cultures in an artificial environment including nutrient transport, oxygen diffusion as well as removal of catabolites. According to these factors, keeping the medium level constant in the bioreactor is vital. In hydrodynamics, the inlet and outlet regions were assumed of fixed volume, while the cell culturing environment is fixed pressure, in order to limit fluid stresses on the cells.

In addition, such an arrangement can lead to operational problems in keeping the desired liquid volume in the compartment. In terms of reaction engineering, the problem can be formulated as liquid level dynamics, for which a simulation study for level control purpose is proposed.

In summary, the objectives of part II are:

- HFMBR set-up and the operational issues identification
- Dynamic analysis and modeling of the bioreactor
- Develop a computer-based control system for the most important variables such as medium level
- The necessary instrumentation in order to synthesize control system
- Test the controlled system on a model bioreactor with inert fluid (water) and finally test it under cell culturing condition

Part I

Fluidized bed bioreactor

Chapter 2

The liquid-fluidized bed as bioartificial liver concept

2. Biological/biomedical applications of liquid-fluidized beds

In this Chapter, the concept of fluidized bed bioreactor as the bioartificial liver device is discussed and the biological/biomedical applications of liquid-fluidized beds are illustrated and summarized.

2.1 The fluidized bed bioartificial liver principle

The homogeneous expansion behaviour of liquid-fluidized beds is exploited in various fields such as minerals engineering and biotechnology [86, 87]. Innovative fluidized bed bioreactor concepts have been also explored for applications as bioartificial organs, particularly the bioartificial liver [5]. Due to the high cost and shortage of organ donors, liver transplantation suffers from severe limitations. Liver tissue constructs consisting of functional cells and artificial materials are being greatly studied for their applications in the field for organ replacement and for *in vitro* studies on drug development and metabolic diseases [6]. The concept of a two-phase bioreactor with a fluidized bed of alginate beads containing immobilized hepatocytes was initially proposed by Doré and Legallais [75, 79] although similar devices could be found in earlier patents [88].

The use of alginate beads in which hepatocytes are entrapped seems very promising because this spherical configuration offers, in addition to the hepatocyte anchorage, the largest surface area to volume ratio for optimal solute and oxygen transfer between the hepatocytes and the perfusion fluid (either blood or plasma) in both directions [81].

Application of the fluidized bed bioartificial liver requires a conceptually simple loop [81] (*Fig. 8*). The patient's blood is withdrawn and separated into plasma and blood cells. Plasma treatment is carried out by perfusion through a fluidization column hosting the hepatocytes. Plasma and blood cells are eventually mixed again and returned to the patient.

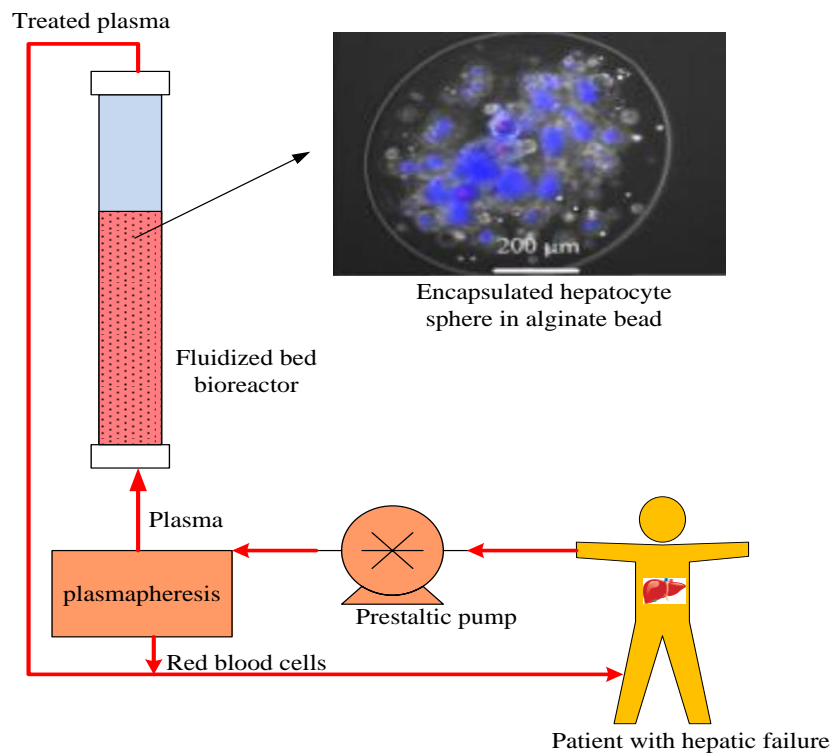


Fig. 8. The principle of the fluidized bed bioartificial liver.

2.2 Improved conditions under fluidization conditions

Several attempts have been made to develop fluidized bed bioartificial support for the treatment of patients with liver failure. In this part, the technological aspects of the previously developed fluidized bed bioreactor are reviewed.

Doré et al. [75] introduced an idea of a bioartificial liver in view of the fluidized bed movement of hepatocytes entrapped in alginate beads. The bioreactor was intended to offer stable behaviour. The maximum fluid perfusion velocity was estimated based on the intention to avoid bead elutriation from the bioreactor. This design criterion appeared simple to handle and to scale up once the number of beads to guarantee a productive supply was fixed. The fluidized bed height was verified to depend only on the total bead volume and the perfusion velocity. Also, mass transfers between the perfusion fluid and the alginate beads improved in the fluidized bed arrangement in comparison with the

fixed bed (static) condition. The fluidized bed concept should enhance the mass transfer velocity between the plasma and the hepatocytes entrapped in the beads. The solute concentration decrease was thus followed in the tank when the beads were in fluidized bed motion *Fig. 9*. *Fig. 10* shows the kinetics for VitB12 obtained under different perfusion flow rates in a fluidized condition in comparison with fixed bed condition respectively. Equilibrium was reached in as few as 10 min, compared to the 2 h observed under static condition. This result clearly shows the benefit of using an FBBAL and suggests the real efficiency of the process in term of mass transfer [75].

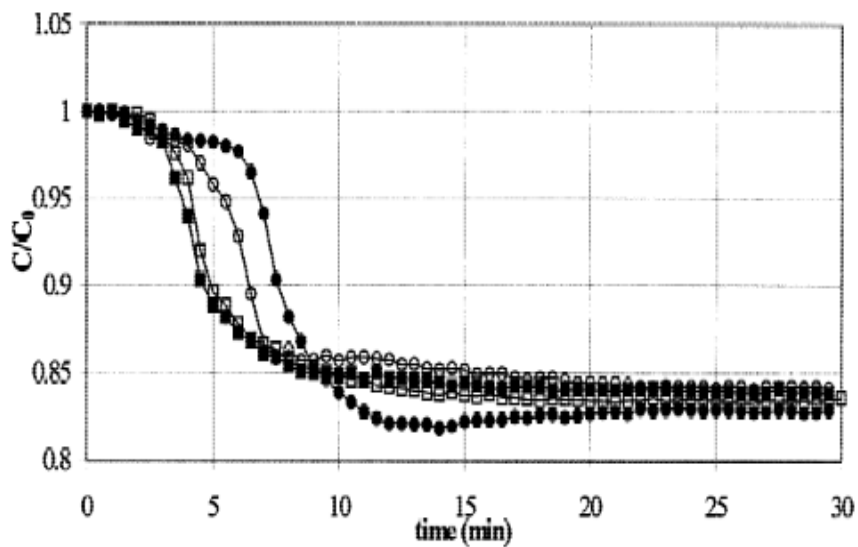


Fig. 9. The time courses of VitB12 concentration in the tank under dynamic mass transfer conditions are shown for 4 different perfusion flow rates: (●): $Q = 29.4$ ml/min, (○): $Q = 40$ ml/min, (■): $Q = 55$ ml/min, and (□): $Q = 70.9$ ml/min [75].

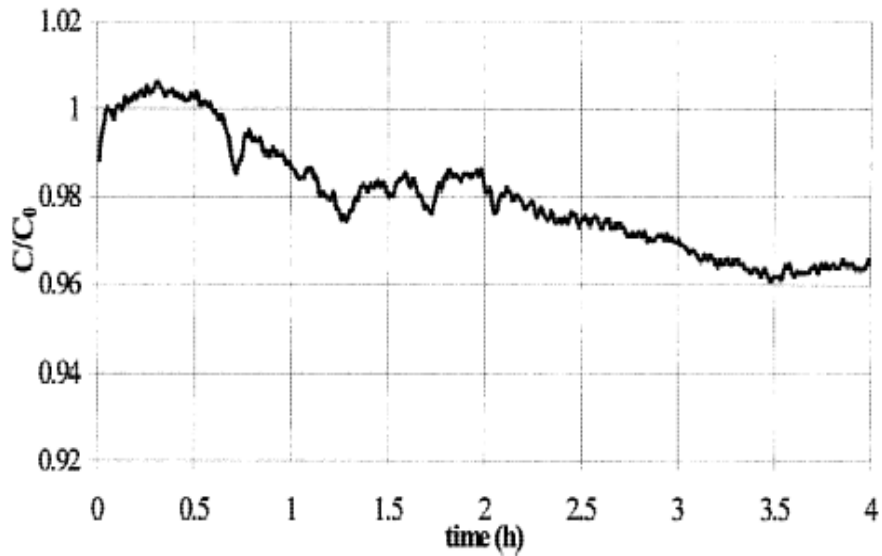


Fig. 10. Shown is the time course of VitB12 concentration in the supernatant under static mass transfer conditions [75].

Legallais et al. [79] focused on the design of a bioreactor for extracorporeal liver supply containing alginate beads in a fluidized bed regime. Their goal was to accomplish a satisfactory mixing into the bioreactor to improve the potential exchange and mass transfer. In the first place, they checked whether both present phases (solid: alginate beads; liquid: saline solution at 20°C) might allow for this fluidization. At that point the optimal design was characterized as a function of the required working conditions, bead volume, and perfusion flow rate; the column cross-section and initial height especially needed to be adjusted. The efficient fluidization, under enhanced conditions, was demonstrated through the measurement of the head losses created by the fluidized bed. Criteria for scaling up were likewise proposed.

Legallais et al. [79] compared the evolution of the bioreactor expansion with the values predicted by the well-known expansion models available in the literature (*Fig. 11*). They have gained, none of them could predict the observed trends sufficiently well. Only Ganguli's model results were close to the experimental data. As the porosity linearly changed with the superficial velocity, the following correlation was proposed:

$$\varepsilon = 30 + 17.456 \times 10^3 \times u \quad (1)$$

With ε in % and u in ms^{-1} [79]. The tests proved that the expansion properties of alginate beads can be different from conventional particulate materials.

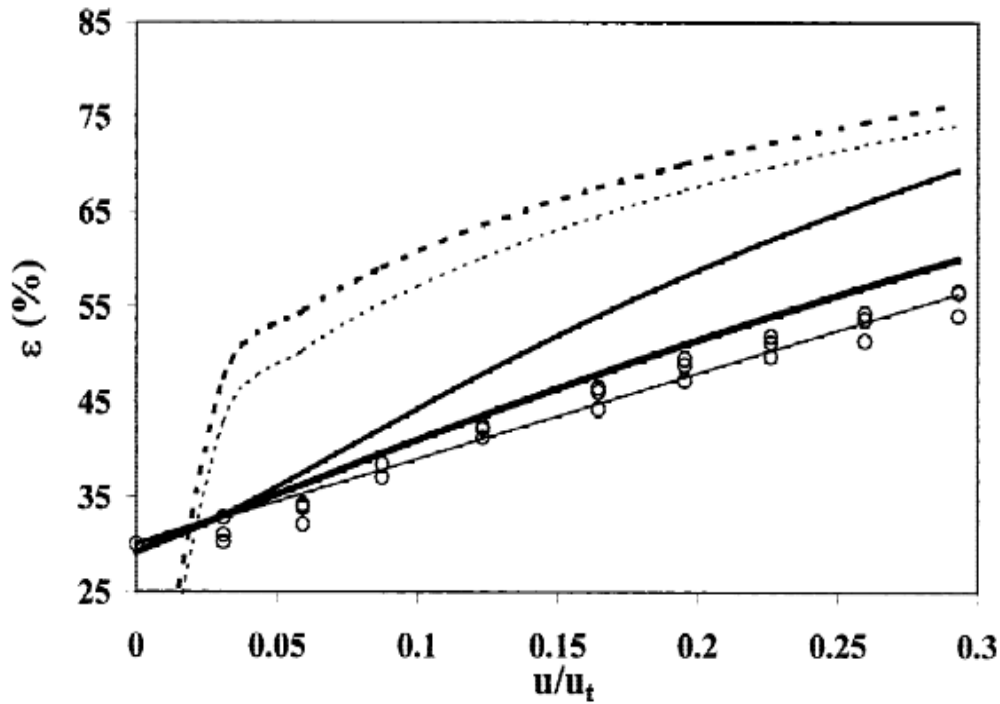


Fig. 11. The graph shows the influence of the superficial velocity u (divided by the terminal velocity u_t) on the fluidized bed porosity ε : (s) experimental data. The results are compared with different models: - - - Foscolo et al. [89], ... Richardson and Zaki [90], Hirata and Bulos [91], Ganguli [92], and Legallais et al. [79] — Equation 1.

Kinasiewicz et al. examined the influence of C3A cell culture in alginate beads on the synthetic function in a fluidized bed, bioartificial liver. Cells in alginate beads were prepared to utilize an electrostatic droplet generator of their own design utilizing low-viscosity alginate. Beads were cultured for 24 hours, then 7 days in static conditions and after that 24 hours of fluidization in the bioreactor to assess albumin production. They observed significantly increased albumin production by C3A cells entrapped in alginate

beads during static culture. Fluidization increased albumin production compared with static culture. Fluidization performed following 7 days of static culture brought about a significant increase in albumin synthesis. Their tests demonstrated that hepatic cells proliferated with expanded metabolic function after some time. *Table 3* reports a comparison of albumin production by human hepatoma C3A cells entrapped in alginate beads in static incubation with fluidized bed bioartificial liver experiment [93].

Table 3. Comparison of albumin production by human hepatoma C3A cells entrapped in alginate beads in static incubation compared with fluidized bed bioartificial liver experiment

	Fluidized bioreactor	Static incubation
	(ng/h per initial 10⁶ of cells)	(ng/h per initial 10⁶ of cells)
Albumin production after 24 hours of cultivation	72.9 ± 31.4	63.8 ± 9.6
Albumin production after 7 days of cultivation	743.3 ± 181.5	250.8 ± 58.5

Eventually, as it was discussed, liquid fluidization offers the advantage of the homogeneous and controllable expansion of suspended particles with limited pressure drop and favorable heat and mass transfer conditions. Bioreactors can exploit such potential and fluidized-bed-based biomedical devices acting as bioartificial liver have proved an effective alternative to other solutions. In such a systems, bioreactor performance significantly was affected by the hydrodynamics and mass transfer. It seems necessary to investigate about hydrodynamics of fluidized bed bioreactor due to a very low pressure drop to measure and an opaque fluidized system to predict the system behaviour. In the present work, the intrinsic and fluidization properties of alginate beads are carefully analyzed using two rigs at different scales.

Chapter 3

Materials and characterization methods

3. Materials and characterization methods

The planned tests required the laboratory preparation of alginate beads, use of the appropriate saline solution to store and fluidize the beads and an extensive set of characterization methods, as described in chapter 3.

3.1 Alginate beads characterization

3.1.1 Alginate preparation

The alginate beads are prepared by the process of alginate drops polymerization in calcium chloride, a careful procedure known to produce relatively monodisperse particles. To prepare the alginate solutions, alginate powder (MANUCOL® LKX 50DR, FMC BioPolyme) is dissolved in a sterile saline solution (154 mM NaCl solution buffered with 10 mM HEPES, pH 7.4). The mixture is then filtered using a 0.2 µm membrane. Alginate suspension solution is extruded as droplets through a gauge system. Droplets are size-controlled using co-axial air flow. The alginate droplets are collected in a calcium chloride gelation bath (154 mM NaCl, 10 mM Hepes, 115 mM CaCl₂) wherein they are immersed and reticulated for 15 min. Afterward, the beads are rinsed twice with sterile saline solution. The inert beads are then stored in the Ringer solution before use, whereas the hepatocytes-containing beads are placed in a culture vessel containing William's E medium (PAN Biotech). A picture and a schematic sketch are shown in *Fig. 12*.

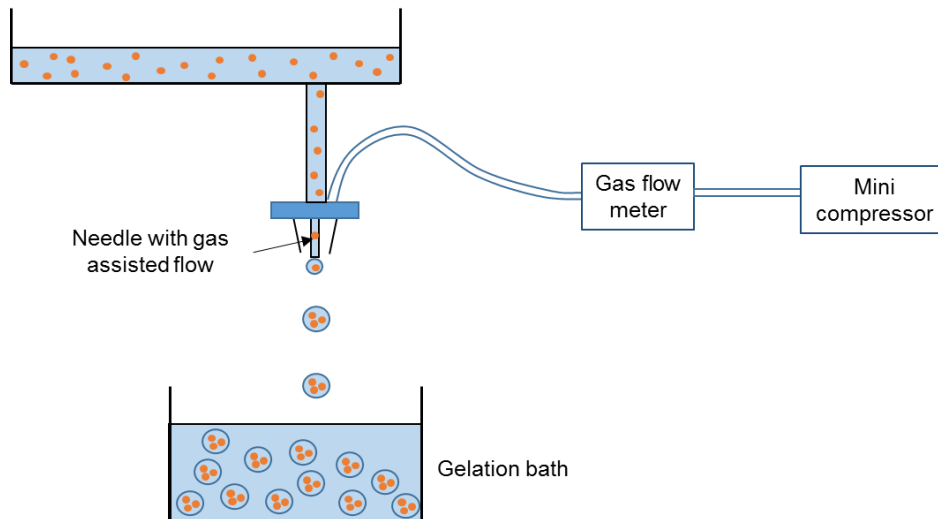


Fig. 12. Alginate preparation setup actual (top) and schematic (bottom)

3.1.2 Ringer solution

Alginate beads, even not encapsulating cells, have been shown to exhibit structural instability unless stored in appropriate solutions. Expansion tests have therefore

been carried out using the simplest solution known to ensure stability to the material, i.e. the Ringer solution (6.5 g NaCl, 0.42 g KCl, 0.25 g CaCl₂ and 0.29 g NaHCO₃ per liter of water). For the 10-cm diameter set-up, 200 liters of solution based on purified water (Milli-Q Merck Millipore) have been prepared.

3.1.3 Characterization techniques: size

The particle size distribution of the alginate beads is measured by laser diffraction using the Malvern Mastersizer 2000, with Ringer solution as the dispersion medium. Sauter's average (volume-to-surface, or $d_{3,2}$) diameter is calculated according to the distribution. Distributions are measured for two samples, each one subjected to three evaluations, and the average values are reported.

3.1.4 Characterization technique: density

As shown below, the hydrodynamic characteristics of the fluidized bed bioreactor are very sensitive to density. Therefore, density measurements are separately carried out for inert beads and beads encapsulating hepatocyte spheroids.

3.1.4.1 Inert beads

The density of inert alginate beads is calculated by separate measures of the mass and volume of approx. 8 ml (bulk) of beads. The same sample is weighted by laboratory balance (± 0.01 mg accuracy); the net bead volume is then precisely evaluated by helium

pycnometry (Quantachrome Ultrapycnometer 1000). The volume measurements were repeated five times and the average value and standard deviation calculated.

In addition, four samples of alginate beads are prepared for a simpler evaluation of inert bead density to compare with the beads filled with hepatocyte spheroids. To this purpose, the density is calculated by separate measures of mass and volume using laboratory balance and graded cylinder. In this case, a bulk volume of 3 ml of weighed alginate beads in 20 ml of solution (Ringer and William's E medium) is used.

3.1.4.2 Beads with cellular spheroids

For density measurements of alginate beads with spheroids, a set of alginate beads is synthesized with encapsulated spheroids under sterile conditions. The number of alginates beads is divided into three parts (each containing about 2 million cells) for three different tests at day 0, day 5 and day 7. The density is measured by the same technique as for inert beads.

3.1.5 Characterization technique: swelling

Transient swelling characterization of inert alginate beads, important for its effect on density and the related hydrodynamic implications, is investigated after storage in Ringer solution and William's E medium. Rather than statistical distributions of many particles, bead swelling requires observation of the same particles over time. Thus, the evolution of the beads size is analyzed under an inverted light microscope equipped with phase contrast (Leica DMI 6000B, Leica, Wetzlar, Germany). For each average datum, the diameter of 20 alginate beads is measured with the help of an image analysis and processing software (LAS AF software). Two batches, one per medium, are prepared. The size of beads in the batch is analyzed under the microscope every 2 hours for 6 hours and then every 24 hours until steady state conditions are achieved.

3.1.6 Characterization technique: settling velocity

The settling velocity of single inert alginate beads is measured by video recording and post-processing of falling beads in a 5-cm internal diameter (ID) graduated cylinder (Fig. 13). Due to high transparency of the beads and the very little difference of refraction index with respect to water, off-line digital processing of images turned out to be more effective than live visual observation. The processed video allows obtaining the precise passage time of the beads between two defined points after the bead acceleration phase. The experiment is repeated 4 times.

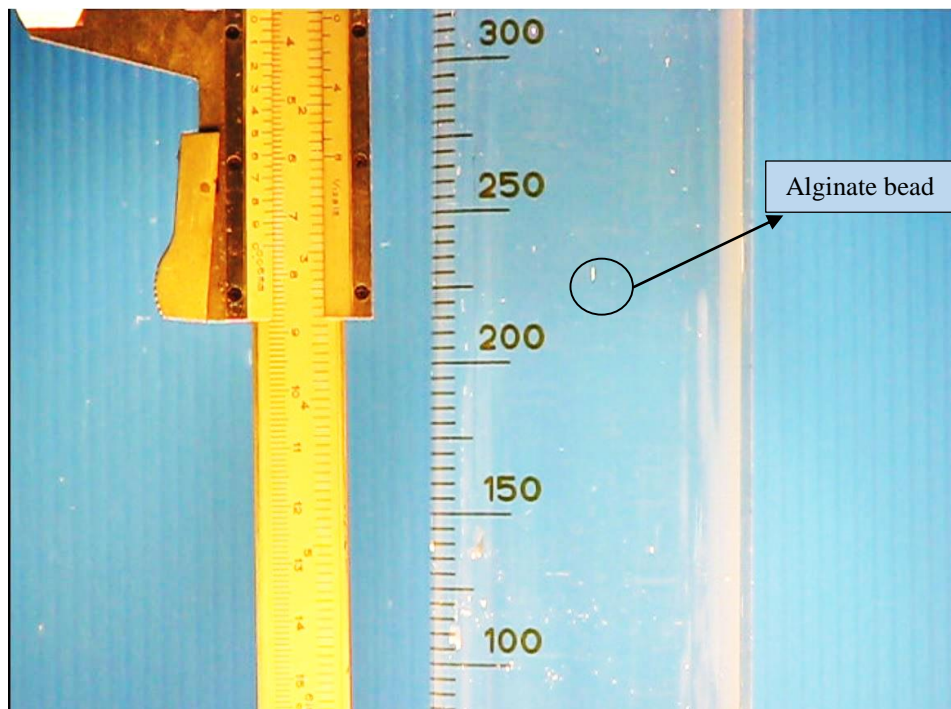


Fig. 13. Settling velocity measurement

3.1.7 Mass transfer into the beads

Mass transfer dynamics into the inert beads was studied using vitamin B12. The beads were exposed to 0.2 g/L vitamin B12 in Ringer solution in both batch (static) and

fluidized (dynamic) setups and the changes in the concentrations were monitored using spectrophotometry (at wavelength 550nm). This experiment can also be very valuable in validating the numerical analysis of the mathematical models as well as bead's properties.

3.1.7.1 Batch (static)

Alginate beads were carefully placed at the bottom of a cuvette so that the optical beam is not obstructed. 2ml of vitamin B12 (0.2 g/L) solution was added to top and the cuvette was placed in the spectrophotometer. The decrease in absorbance due to diffusion of the molecules into the beads was recorded until it reached steady-state.

3.1.7.2 Fluidized (dynamic)

5.5 ml of Inert, fresh beads was seeded into the bioreactor and upon starting the pump, were exposed to vitamin B12 solution (25ml total volume, 0.2 g/L). 100 μ L samples were taken over time for absorbance measurement as before. The fluidized bed bioreactor used to study the transport of vitamin B12 into the beads (dynamic system) is shown in *Fig. 14*.



Fig. 14. Fluidized bed bioreactor used to study the transport of vitamin B12 into the beads (dynamic system)

3.2 Expansion test and experimental rigs

3.2.1 Smaller (1-cm diameter) fluidization set-up

The bioreactor is composed of a glass column (internal diameter 1 cm, height 12 cm) sealed with top and bottom water-tight perforated caps through which the inlet and outlet channels, respectively, penetrate. A fine mesh tissue blocked between two sealing rings within the bottom cap acts as a liquid distributor. The column size is designed for a perfusion solution flowrate from 1 to 4 ml/min and beads' volumes not exceeding 5 ml. A peristaltic pump ensures the desired recirculation flowrate. A simple scheme of the bioreactor set-up is shown in *Fig. 15*.

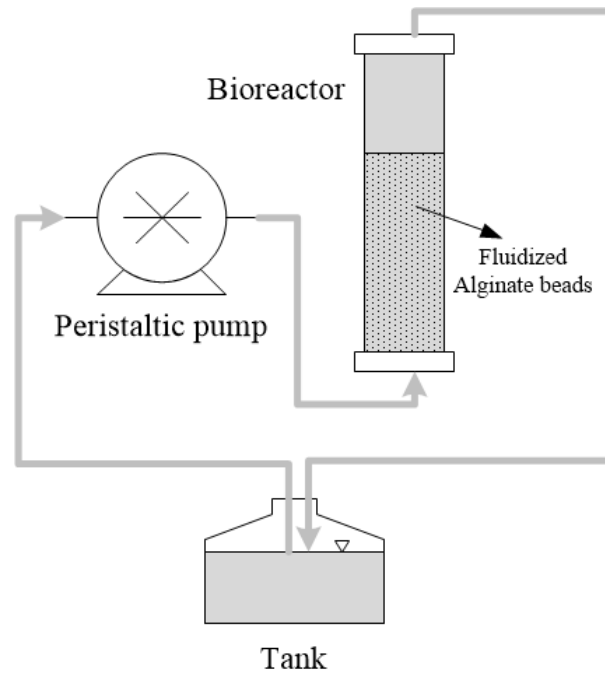


Fig. 15. Experimental setup of the bioreactor with 1-cm diameter column.

The alginate beads with a mass of 1 g are loaded into the bioreactor. Expansion tests are carried out by increasing the perfusion liquid flowrate step by step until the bed height reaches the whole length of the bioreactor. In each step, a ruler attached to the column walls precisely measures the height of the alginate beads interface.

3.2.2 Bigger (10-cm diameter) fluidization set-up

The larger set-up is based on a 10-cm diameter Poly(methyl methacrylate) (PMMA) column. The system is composed of a 175-cm high vertical tube with an internal diameter of 10 cm. A 25-cm long tube with internal diameter of 10 cm is positioned below the distributor, acting as a plenum. The distribution section includes three parts, namely: an upper flange, a perforated plate, and a lower flange. The perforated plate is a metal sheet disc with 400 μm diameter holes regularly arranged in a 1.5 mm pitch triangular mesh. In the plenum, a 10-cm-high packed bed of big glass beads (about 10 mm diameter)

is used to ensure uniform flow below the distributor. In *Fig. 16*, the fluidization column lab set-up is shown schematically.

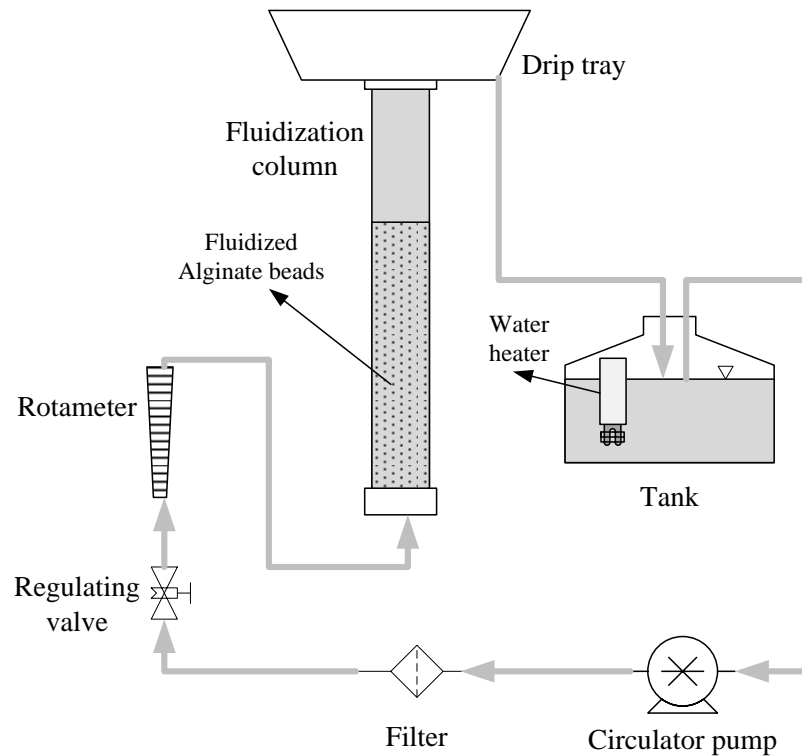


Fig. 16. Experimental setup of the bioreactor with 10-cm diameter column.

The circulator pump, with the help of a regulation valve and a bypass (not shown in *Fig. 16*), provides the desired flowrate to the fluidization column. The accumulation tank stores the 200 l of Ringer solution. In order to analyze the effect of temperature, a device consisting of three electrical heater cartridges (each one 1.2 kW), acted upon by an on-off temperature controller, is used inside the accumulation tank. Two temperature sensors are located inside the column, at its base and its top, readings from the former being used as bed temperature.

Sample preparation for the expansion test requires a weighed amount of the alginate beads (about 500 g) to be immersed in the solution and loaded into the column. Maximum care is paid to avoid the presence of air bubbles everywhere inside the column, as the

presence of gas-liquid interfaces entrapping particles would strongly affect the measurements.

The test is performed in small steps by increasing the Ringer solution flow until the superficial velocity of the fluid exceeds the minimum fluidization, with a consequent progressive increase in the fluidized bed voidage. The experimental procedure is carried out both with increasing and decreasing flow rates and at each step measurements of the flowrate values and the bed height is taken. Flowrate measurements through the rotameters are cross-checked for accuracy with a measure of the liquid volume collected in a cylinder in a given time. Although somewhat more tedious, this method ensures the flowrate data are reliable and stable in time. The alginate beads appear highly transparent (more than glass beads for example) since their refractive index is very similar to that of water; hence to accurately measure the bed height by rulers externally attached to the column an appropriate illumination system is used.

3.2.3 Characterization of bed expansion

Homogeneous expansion in fluidized beds is traditionally investigated using the Richardson-Zaki expression relating the superficial liquid velocity to the bed voidage, an extended version of which [94] is:

$$\frac{U}{U_0} = k \varepsilon^n \quad (2)$$

where k is a correction factor and $\frac{U_0}{k}$ and n are the intercept and the slope, respectively, of the linear relationship in a log-log plot of the velocity vs. voidage. The introduction of the k factor is due to the fact that the theoretical value of the intercept should be the logarithm of the free-settling velocity U_0 , but it typically turns out to be a lower value, possibly due to wall effects [94]. Well-established empirical equations for the parameters are

$$k = 1 - 1.15 \left(\frac{d}{D} \right)^{0.6} \quad (3)$$

$$\frac{4.8-n}{n-2.4} = 0.043 \text{ Ar}^{0.57} \quad (4)$$

$$U_0 = \frac{\mu}{\rho d} \text{ Ar}^{\frac{1}{3}} \left[\left(\frac{18}{\text{Ar}^{\frac{2}{3}}} \right)^{0.824} + \left(\frac{0.321}{\text{Ar}^{\frac{1}{3}}} \right)^{0.412} \right]^{-1.214} \quad (5)$$

where d is the particle size and D is the column diameter, Archimede's number is defined as $\text{Ar} = \frac{d^3 \rho (\rho_p - \rho) g}{\mu^2}$ and free-settling Reynolds' number is $\text{Re}_0 = \frac{\rho d U_0}{\mu}$, ρ and μ are the fluid density and viscosity, respectively, and ρ_p is the particle density. Eqs. (3,4) are due to Khan and Richardson [95] and Eq. (5) to Turton and Clark [96] and their validity in the present range of Archimede's and free-settling Reynolds' numbers has been verified.

3.3 Effect of alginate beads on hepatocyte kinetic

A kinetic comparison between hepatocyte spheroid and encapsulated hepatocyte spheroid is done by means of measuring albumin production. For this purpose, 2 million /condition rat hepatocyte cell from male Sprague-Dawley rats (Janvier Labs, France) is cultured in 7 ml/condition HCM (Hepatocyte Basal Media, HBMTM, Lonza) medium. The 12-hours spent medium was collected on days 3, 4, 7, 8 and 10 from all conditions, and separately stored at -20°C. Albumin synthesis was quantified by Enzyme-linked immunosorbent assay (ELISA) test (Bethyl Laboratories, Inc.). Tests were carried out according to manufacturer's instructions. For each independent experiment (n=3), results were presented as the mean \pm standard deviation (SD) [97].

Chapter 4

Results and discussion

4. Results and discussion

In the present Chapter, the intrinsic and fluidization properties of alginate beads are carefully analyzed using two rigs at different scales. Bed expansion tests over a wide range of voidage values have been conducted in a 1-cm diameter column used for perfusion during in vitro experiments as well as in a 10-cm diameter column close to human size bioreactor at two temperatures: ambient (20°C) and human body (37°C) conditions. The full characterization of the individual beads and their collective expansion behavior at ambient and higher temperature constitutes a unique set of data for expanding the application opportunities of this promising technology.

4.1 Alginate bead size and density

The average particle size distribution as obtained by the laser diffraction method is shown in *Fig. 17*. The alginate beads Sauter's average size is 813 μm with a coefficient of variation $COV = \frac{d_{90}-d_{10}}{d_{50}} = 86\%$. The size distribution essentially confirms the capacity of the method to produce relatively monodisperse beads within the desired size range (600-1000 μm).

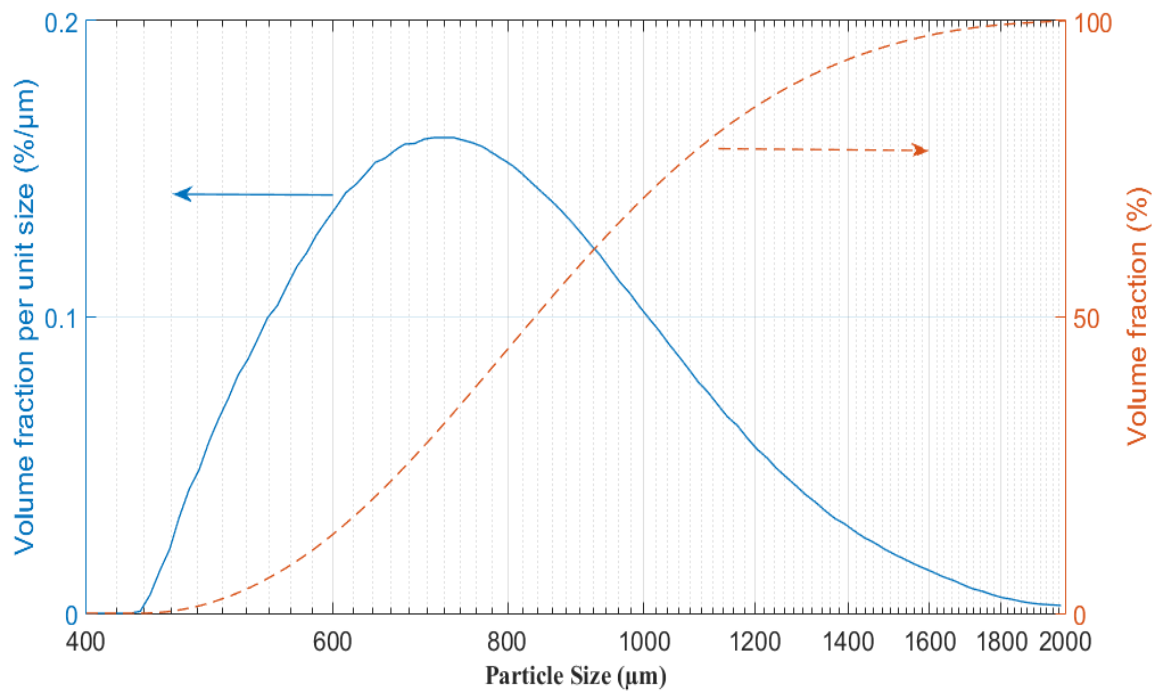


Fig. 17. Particle size distribution for the alginate beads (Malvern Mastersizer 2000) using the volume fraction density (blue solid line) and cumulative volume fraction (red dashed line) plots.

Density measurements are carried out by separate measurements of mass and volume of given sample quantities. Data for inert beads, for which volume is precisely evaluated using helium pycnometry, is reported in

Table 4. The value of inert bead density ρ_p is very similar to that of water ρ . Therefore, the need to use the relative density $\rho_p - \rho$ in the calculations requires a very careful evaluation of the absolute value of the bead density. As mentioned before the expansion properties are highly sensitive to the density of particles. Because of the small density, fluidization occurs at very low value of the liquid velocity, which can be insufficient for the volumes to treat in the intended applications. However, as it will be shown below, the addition of cells increases the density of the beads. In the same direction, it has been proposed that encapsulation of small inert particles (e.g. glass) within the bead could help increase their absolute density [88]. The density of Ringer solution was measured to be 1005 kg/m³.

Table 4. Density measurements of inert alginate bead

Property	Value
Alginate beads mass	5.187 g
Alginate beads average volume (5 runs)	5.087 ml
Standard deviation on volume (5 runs)	0.0012 %
Average density	1020 kg/m³

A comparison of the density of inert beads and beads with encapsulated hepatocyte spheroids is shown in *Fig. 18*. The presence of the cell spheroids increases the density of the beads. Although it is a small percent increase over the absolute value, the change in the density relative to water is important, reaching increases as high as 140% of the original value. It is remarkable that the activity of the cells also affects the density in time, probably due to cell proliferation within the beads. This is expected to have implications in the bioreactor, where the expansion properties of the beads can vary from day to day of operation.

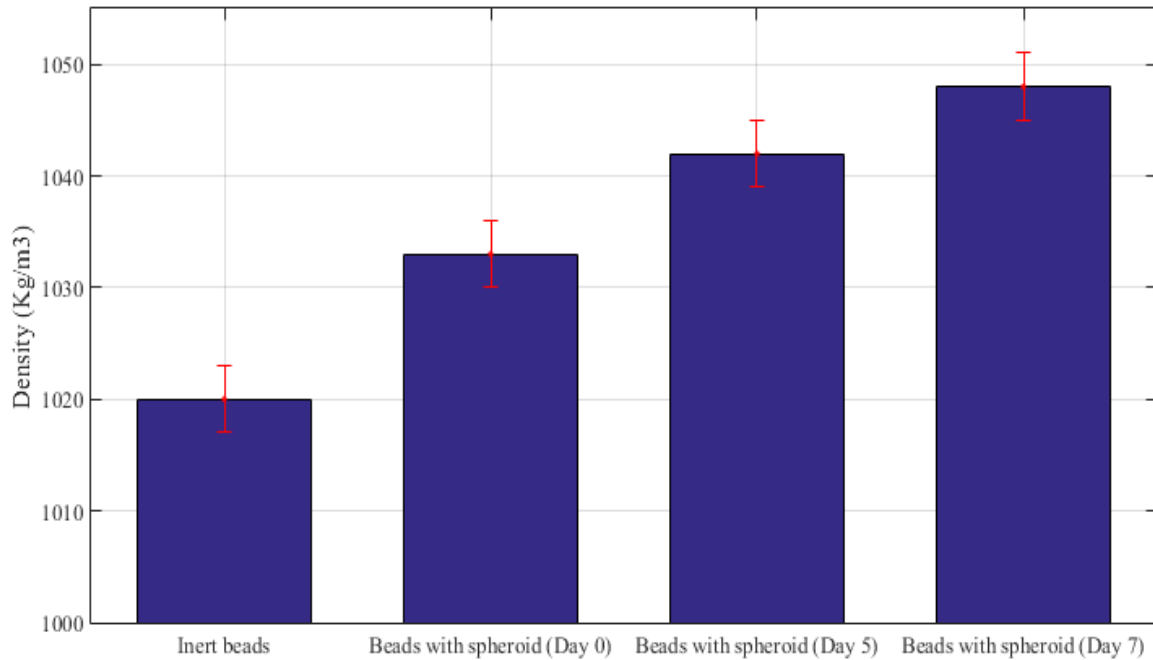


Fig. 18. Comparison between the densities of inert alginate beads and beads with hepatocyte spheroids during one week. Standard deviation $\sigma = 3$

4.2 Bead swelling properties

The presence of size change during operation could also affect the expansion properties of the bed. A typical microscope picture of inert alginate beads in the Ringer solution is shown in *Fig. 19*. The level of transparency is evident as it is the nearly perfect sphericity. Inert bead size evolution in time can be analyzed in terms of the data plotted in *Fig. 20*. Freshly immersed beads in the solution show an increase in size in both Ringer solution and William's E medium. The increase was proved statistically by measuring a reasonable number of beads. The increase in size is small but appreciable, with values of about 8% and 4% in the Ringer solution and William's E medium, respectively, on the first day. Size is found not to change appreciably later on. So, for a smooth operation, it can be recommended that beads are stored in the actual medium for one day before use.

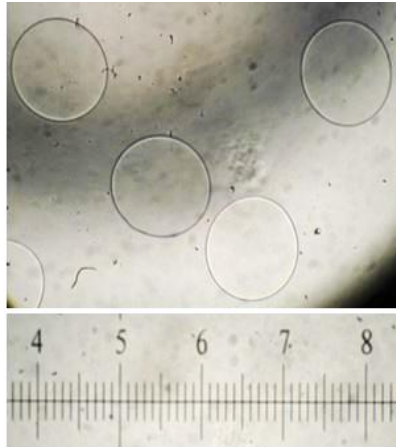


Fig. 19. Sample microscope picture of inert alginate beads with the ruler scale (in mm units).

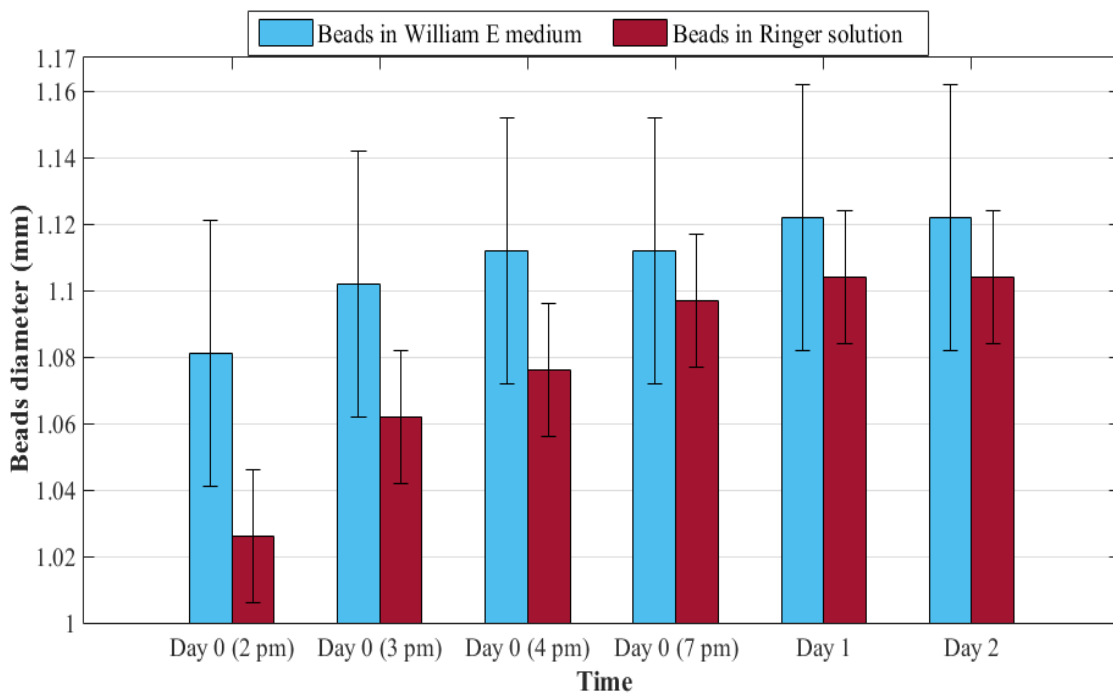


Fig. 20. Size change (swelling) properties of alginate bead. Standard deviation in William's E medium $\sigma = 0.04$ mm and in Ringer solution $\sigma = 0.02$ mm

4.3 Terminal settling velocity

Terminal settling conditions are significant as they can be thought of as the expansion properties of the particles under extreme dilution. The settling velocity of the several individual alginate beads is measured. The average value of four tests as obtained in a cylinder with 5 cm diameter is 1.69 mm/s. *Table 5* shows individual measurements as well as the mean value and its standard deviation. Considering the finite size of the column, also in analogy with the subsequent elaborations on expansion data, a reference settling velocity under infinite conditions can be calculated by dividing the experimental value by the correction factor k as calculated from Eq. 3, obtaining $U_0 = 2.03$ mm/s.

Table 5. Settling velocity of single alginate bead

Experiment No.	Settling velocity (mm/s)
Test 1	1.54
Test 2	1.87
Test 3	1.61
Test 4	1.73
Average	1.69 ± 0.13

4.4 Mass transfer into the alginate beads

All mass transfer experiments were carried out with empty beads in vitamin B12 solution. In order to evaluate the effect of fluidization on mass transfer, two configurations were examined: batch experiments under pure diffusion and dynamic experiments under fluidization condition. Vitamin B12 was used as a middle molecular weight marker (1.335 Da) to assess mass transfer phenomena within alginate beads. Absorption trend in batch (static) and fluidized (dynamic) condition are shown in *Fig. 21* and *Fig. 22* respectively. As it is clear from the figures, the steady-state concentration was reached in fluidized condition as few as 15 min, compared to the 160 min observed

under batch condition. This results clearly show the benefit of fluidization rather than fixed bed system.

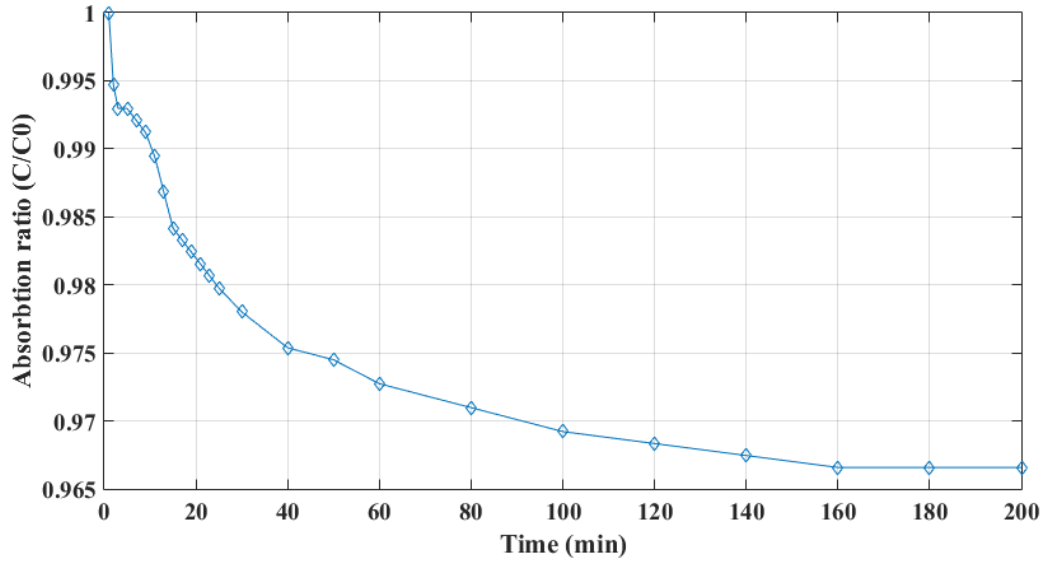


Fig. 21. Alginate beads absorption trend in batch (static) condition

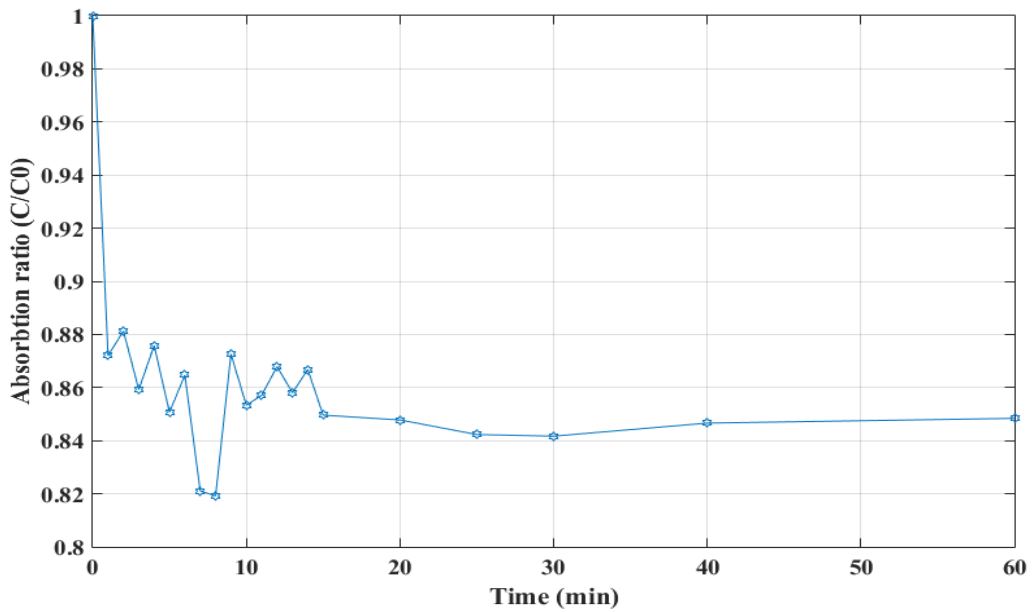


Fig. 22. Alginate beads absorption trend in fluidized (dynamic) condition

4.5 Expansion in the 1-cm and 10-cm columns

Expansion properties are evaluated for inert alginate beads using Ringer solutions as fluidization medium. Bed expansions have been conducted in a 1-cm diameter column used for perfusion during *in vitro* experiments as well as in a 10-cm diameter column similar to human size bioreactors. The expansion is clearly visible using appropriate illumination (*Fig. 23*). It is worth remarking that the height of the 10-cm diameter column (175 cm) proved particularly useful to explore high expansion degrees: bed height increased up to nearly nine times the packed bed value and voidage values of the order of $\varepsilon > 0.92$ could be attained.

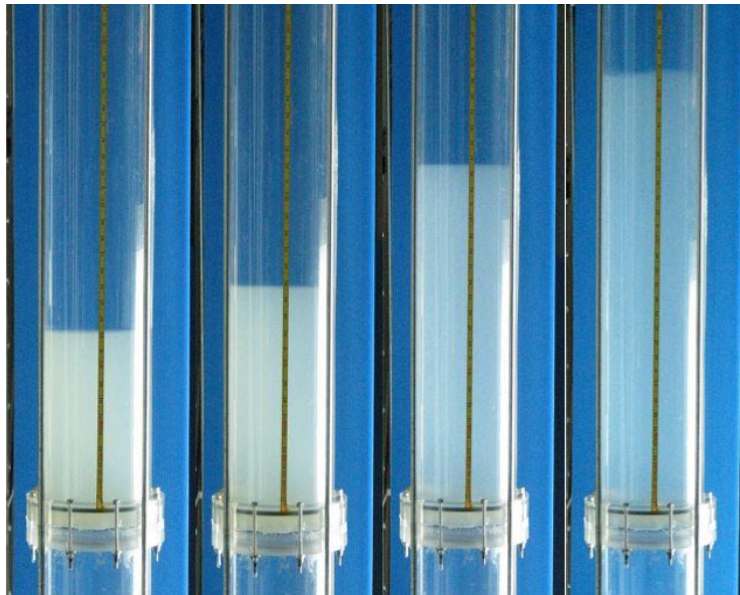


Fig. 23. Evaluation of the bed height in the 10-cm column with increasing Ringer solution flowrate.

Expansion measurements at ambient conditions ($T = 20^{\circ}\text{C}$) are plotted in *Fig 24* as steady-state particle bed height ratio h/h_0 (actual to packed bed value, $h_0 = 119$ mm) as a function of the fluidization velocity. In the smaller diameter set-up height ratio up to about 4 could be reached, whereas in the bigger column height ratios up to about 9 have

been obtained. The data obtained in the 10-cm column shows a steeper increase in the height ratio for the same superficial velocity. The flow regime during expansion belongs mostly to the viscous-dominated range, with values of $Re = 0.04$ to 1. This is due essentially to the very low density of the particle, which require a low velocity for suspension. Due to the difference in the particle to column size ratio, wall effects in the 1-cm set-up are more important. The higher influence of flow inhomogeneity near the walls could explain the smaller expansion rate.

Data are also converted and plotted as velocity vs. voidage log-log plot (*Fig. 25*) in order to observe the typical linear behaviour of homogeneously expanding fluidized beds. It can be observed that the data show a reasonable linear dependence, although some scatter is evident, probably due to the imperfect evaluation of bed height at the largest expansion degrees. At the highest velocities, both decreased bead visibility due to dilution and the variability of the interface levels (e.g. oscillations) yielded readings affected by a larger uncertainty. The two trends appear distinct, showing that the column size has an appreciable effect on the expansion. This confirms that the fluidization behaviour cannot be predicted by the simple adoption of the Richardson-Zaki equation without any correction term. On the other hand, from *Fig. 25* a similar expansion rate can be observed for most of the investigated velocities, as the two lines resulting from the fit appear quite parallel.

Richardson-Zaki (R-Z) parameters n and U_0 , as they appear in Eq. (2), have been extracted by data fitting for the datasets shown in *Fig. 25*. The curve fitting toolbox in MATLAB is used as an advance tool for fitting procedure. The parameters n and U_0 are calculated with 95 % confidence bounds and the determination coefficient R^2 for fitted line is 0.99. Note that the correction factor k which is dependent to alginate bead and column diameter, has been calculated using Eq. (3) and used in the R-Z model before the parameter estimation procedure; the U_0 so obtained should be corresponding to the value in an infinite fluid, i.e. independent of the column size. So, its value should be comparable for the big and small scale setups.

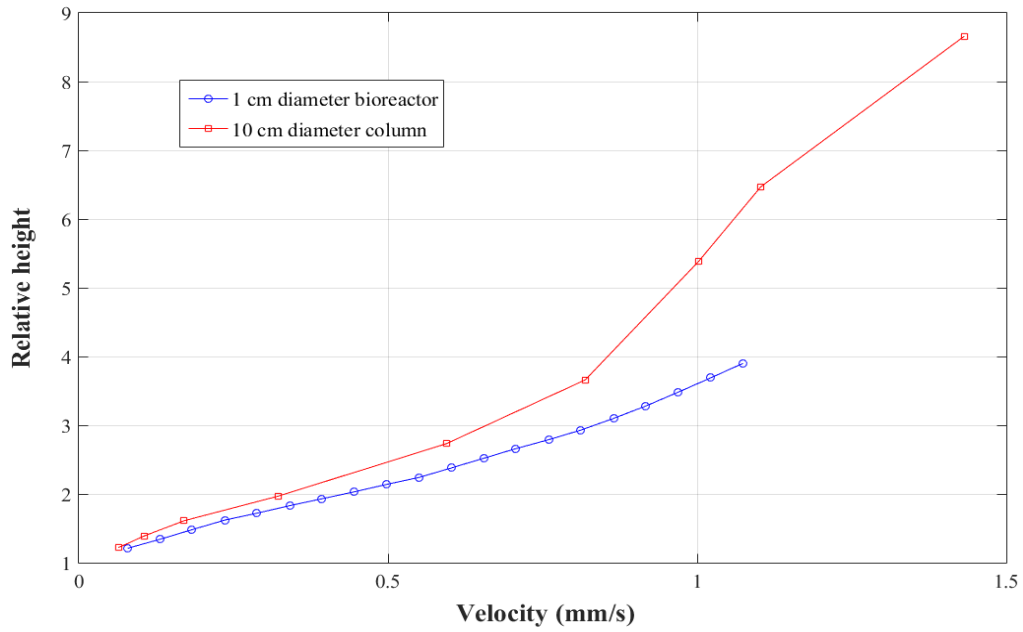


Fig 24. Relative height h/h_0 vs. superficial velocity: comparison between 1 cm diameter and 10 cm diameter columns. $T = 20\text{ }^\circ\text{C}$.

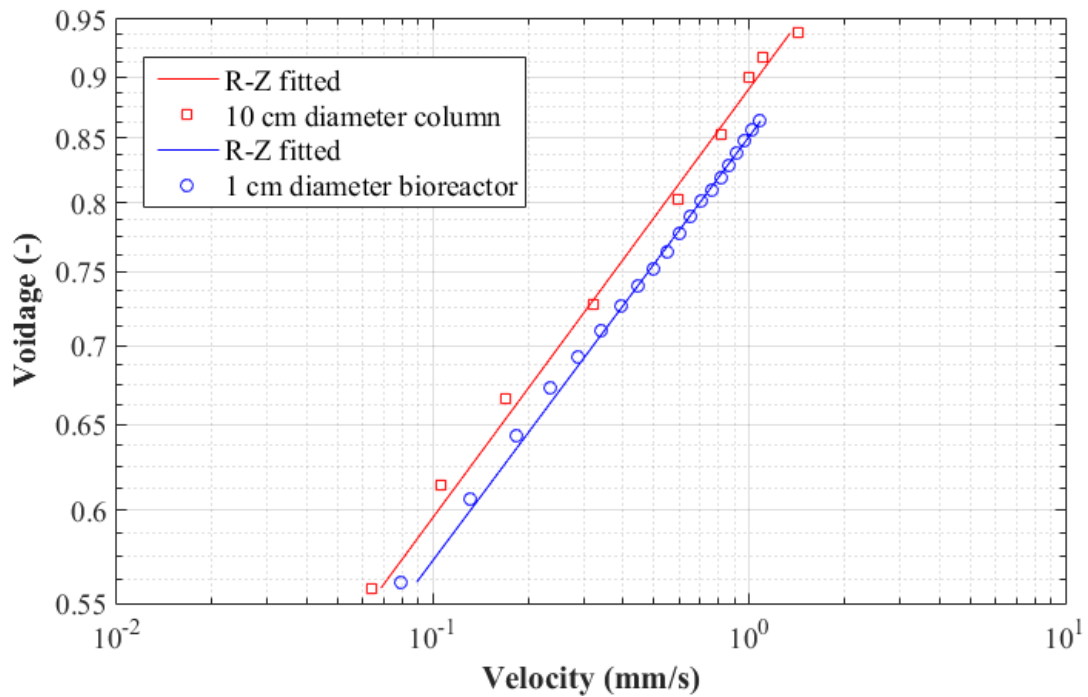


Fig. 25. Voidage vs. velocity: comparison between 1 cm diameter and 10 cm diameter columns (test No. 1 in Table 6). Fitted parameters for the Richardson-Zaki equation (R-Z) are reported in Table 6. Ambient temperature ($T = 20\text{ }^\circ\text{C}$).

To improve reliability and examine the level of variability of data collected under different runs, in the 10-cm setup, four separate tests have been carried out and analyzed. Individual and collective results are reported in *Table 6*, together with the corresponding predictions using Eq. (4) and (5).

Table 6. Inert beads hydrodynamic data and Richardson-Zaki parameters

	Ar (-)	Re₀ (-)	k (-) Eq. (2)	n (-) Eq. (3)	U₀ (mm/s) Eq. (4)	n (-) fitting ± 95% confidence	U₀ (mm/s) fitting ± 95% confidence
1-cm column	79	3.1	0.74	3.98	3.75	5.75 ± 0.20	3.35 ± 0.14
10-cm column (1)	79	3.1	0.94	3.98	3.75	5.62 ± 0.96	2.03 ± 0.24
10-cm column (2)	79	3.1	0.94	3.98	3.75	5.16 ± 0.48	1.93 ± 0.19
10-cm column (3)	79	3.1	0.94	3.98	3.75	6.18 ± 1.54	2.61 ± 0.54
10-cm column (4)	79	3.1	0.94	3.98	3.75	5.97 ± 2.06	2.13 ± 0.57
Overall Fit						5.72 ± 0.67	2.18 ± 0.20
10-cm column 37 °C (1)	167	5.8	0.94	3.74	4.88	6.34 ± 0.61	5.50 ± 0.70
10-cm column 37 °C (2)	167	5.8	0.94	3.74	4.88	3.58 ± 1.33	1.26 ± 0.29
10-cm column 37 °C (3)	167	5.8	0.94	3.74	4.88	1.53 ± 0.67	1.08 ± 0.24
10-cm column 37 °C (4)	167	5.8	0.94	3.74	4.88	2.46 ± 0.68	2.05 ± 0.56
Overall Fit						2.60 ± 1.15	1.85 ± 0.56

The R-Z exponent and settling velocity for the smaller column set-up are 5.75 and 3.35 mm/s, respectively, with a relatively narrow uncertainty range (see *Table 6*). Individual tests in the 10-cm column show some appreciable variation in the slope n with ranges of variation that can be relatively high, particularly when the data are collected at decreasing velocity. Overall, the average values (from the global fit) for the 10-cm column are 5.72 and 2.18 mm/s for n and U_0 , respectively, with a relatively narrow uncertainty range, although larger than that of the 1-cm column.

Moving from the 1-cm column to the 10-cm column, it can be noticed that there is practically no change in the expansion rate, as represented by the exponent n , which is a significant result. On the other hand, the terminal velocity appears noticeably different, with smaller values in the larger column. The two velocities can be confronted with the direct measurement of the terminal velocity in the graduated cylinder. The measured infinite medium velocity (2.03 mm/s) seems to support the validity of the data obtained in the bigger column, being very well within the range of variability of the extrapolated velocity of each of the four tests listed in *Table 6*.

A comparison of the fitted parameters and empirical predictions reveals that there is discrepancy between both the predicted values for U_0 and n and the ones extracted by the fitted lines. Concerning U_0 , it should be considered that predictions for the terminal velocity are extremely sensitive to the values of the apparent density and size of the beads, the former being peculiarly small for alginate beads. As an example, if we consider an absolute bead density of 1013 kg/m³ instead of 1020 kg/m³ the terminal velocity changes from 3.8 to around 2 mm/s. With a particle density of 1025 kg/m³ the terminal-settling velocity would be 4.8 mm/s. Clearly, predictions of U_0 are affected by any small change (in absolute terms) in density, with factors such as particle-to-particle density variations that may play a non-negligible role. This should be carefully taken into account in the real application with alginate particles encapsulating cells or cellular spheroids, particularly in consideration of both the absolute variation in density and its time evolution (*Fig. 18*).

In comparison with the predictions using Eq. (4), the fitted slope obtained from all experimental datasets turns out to be significantly higher. This is also due to the fact that the predicted values are limited to the value $n = 4.8$ under viscous-dominated flows. The Richardson-Zaki model with the fitted parameters indicates a dependence of voidage on velocity that is weaker (the higher slope is in the u vs. ε , i.e. inverted, plot) than predictable using empirical equations like Eq. (4). This unusually high value, however, comes as no particular surprise, as similar observations on alginate beads strongly deviating from conventional empirical equations have already been reported in the literature [79]. Also with other materials, values of the slope as high as 6.3 have been obtained from experimental data (see e.g. [98]).

Data of the slope values n in *Table 6* confirm that the expansion rate of alginate beads in the two columns is similar. If the model accounted correctly for all the effects of scaling up from 1 to 10 cm also the fitted free-settling velocity values would be the same. Hence, the difference in the values of U_0 in *Table 6* is a measure of residual influence that the correction factor is not able to represent. By taking into account the ratio of the particle to column size ratio (Eq. (3)), the corrective term k is supposed to take the effect of the use of different scale of the fluidized bed. It can be argued that part of the responsibility might be attributed to the different distributor section (tissue in the smaller scale vs. a perforated plate in the bigger set-up). In order to perform a check on the distribution system, two ways have been conceived: visual observation of the fluidized bed surface flatness and comparison of the pressure drop with the apparent weight of the particles divided by the column cross section. The first one, especially just above minimum fluidization conditions and together with a check of full bed mobilization, is a qualitative indication of uniform inflow of liquid through the distributor. Under all but the highest velocities (at which the surface appeared randomly irregular) the surface of the fluidized bed in the larger column was horizontal and very flat (see e.g. *Fig. 23*). Unfortunately, the definitive quantitative confirmation from pressure drop measurement could not have been achieved, due to practical difficulties related to the extremely low dissipative fluid pressure drop. A simple calculation for the big column tests yields a total weight per unit cross section as low as 10.8 Pa. Similar measured pressure drop values would indicate

full bed suspension, i.e. uniform inflow. Pressure transducers, however, would measure *absolute* values of differential pressures, which are of the order of 10 kPa (the column is 1.75 m tall). To achieve that, a sensor with unrealistic accuracy would be necessary (i.e. error ≈ 0.1 Pa out of 10000 Pa of measured value).

4.6 Effect of temperature

As a final remark on the experimental characteristics of fluidized alginate beads, the experience with tests executed using the slightly heated fluidizing medium (e.g. 37°C), in order to mimic treatment of human body blood/plasma fluids is mentioned. Measurement of the bead size distribution and bead density at 37°C revealed no appreciable effects of temperature on these two properties. Fluidization medium density was checked to be insensitive to a temperature in the range considered. The dependence of viscosity on temperature for pure water has been used for the solution.

Due to the slow expansion dynamics (characteristic times of 10-15 minutes) and the need to keep a uniform non-ambient temperature along a column where the heated fluid flowed at velocities below 1 mm/s eventually led to the impossibility to guarantee repeatable measurements. It is extremely complicated to keep the temperature uniform along the column and constant in time. Different tests under comparable conditions yielded discrepant results (variable U_0 and large SD for n), making them insufficiently reliable (*Table 6*).

Fig. 26 shows a comparison of the measurements carried out at the two temperatures. There is an evident effect of the increased temperature on the expansion properties of inert alginate beads. Quantification of the difference is best carried out in terms of the fitted Richardson-Zaki parameters, as reported in (*Table 6*).

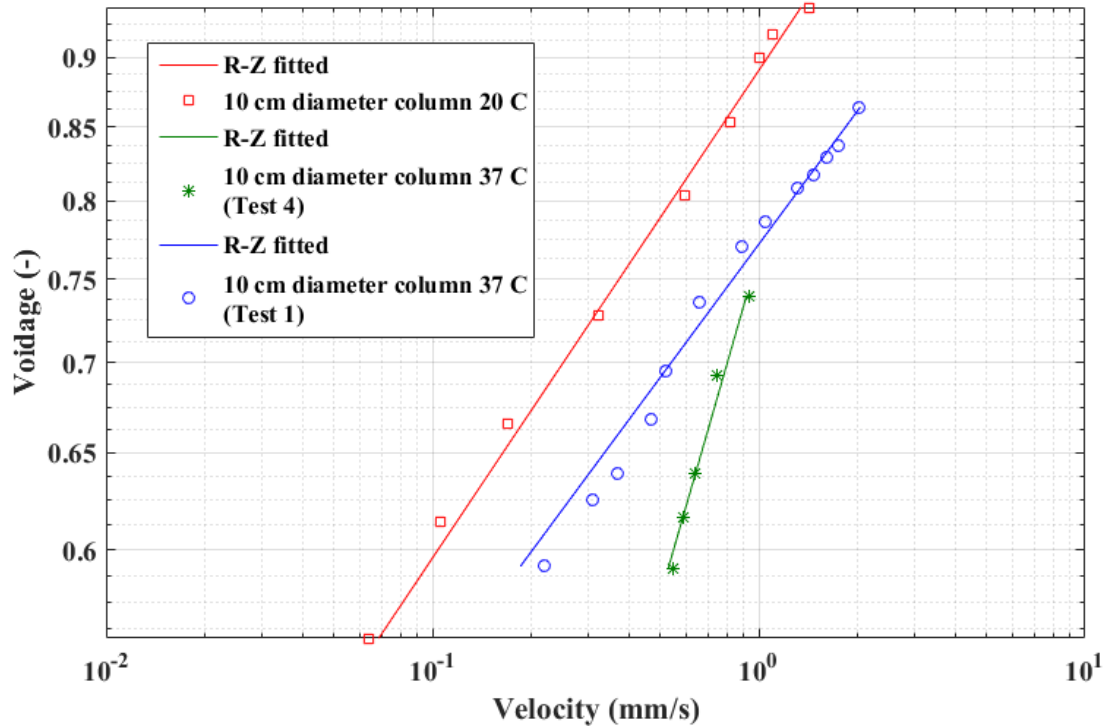


Fig. 26. Comparison of alginate expansion in two different temperature (Two set of results are compared in case of 37 ° C)

4.7 Albumin production (Effect of alginate bead encapsulation on kinetic of hepatocyte cell)

Albumin productions are highly differentiated and well-characterized functions of the hepatocyte. It was thus considered here to be indications of kinetic of hepatocyte cells and identifying the impact of encapsulation of hepatocyte spheroid. The evaluation was carried out at defined time-points (days 3, 4, 7, 8 and 9) and the corresponding results are shown below in *Fig. 27*. The effect of alginate beads encapsulation in kinetic is clear especially after day 7. The albumin production of the spheroid is higher than encapsulated one in the days 3 and 4, but as it was mentioned in the days 7, 8 and 9 the trend is reversed. As it can be seen from the *Fig. 27* the decrease of albumin production of hepatocyte spheroid in a comparison between days 4 and 7 at the same hours (P14 and P20) is highly

significant and around 380 % in the event that for the encapsulated spheroid the decrease is just around 10%.

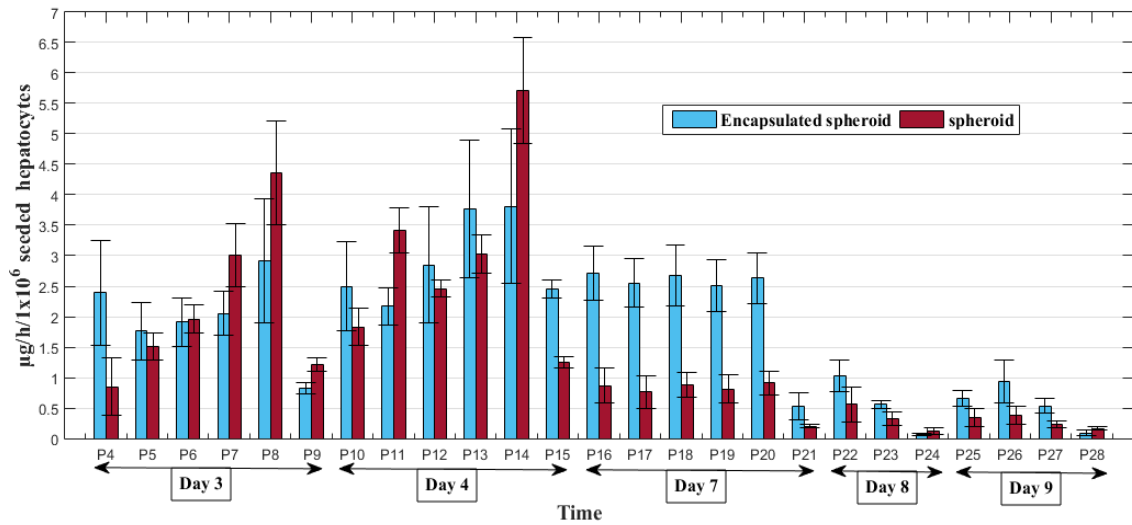


Fig. 27. Albumin kinetic comparison between hepatocyte spheroid and encapsulated hepatocyte spheroid in alginate bead.

4.8 Conclusions

The use of innovative bioartificial devices based on the fluidized bed bioreactor requires the capability to accurately characterize hydrodynamics and mass transfer, as they must act in perfect efficiency and synergy with the cell biology and metabolism to ensure effective applicability in medical treatments. The suspended bed is composed of alginate beads with encapsulated hepatocytes. The present work reports useful data on the characterization of suitably prepared inert alginate beads in terms of size distribution and density when stored in appropriate solutions. Density, which exhibits sensitivity to the degree of accuracy, has been evaluated also for beads containing the hepatocytes. Data on the swelling properties of alginate in two different media are also presented. Expansion test results using Ringer solution as fluidization medium are reported in the comparison between a smaller scale (1-cm diameter) and a bigger (10-cm diameter) column. The

bigger column allows quantifying the wall effects observed in the smaller scale set-up. The analysis is conducted by evaluating the Richardson-Zaki (R-Z) parameters resulting by fitting the various datasets. Overall, in consideration that applications as bioreactors and bioartificial/biomedical devices require operations with opaque fluids, the collected data provide a substantial basis regarding alginate beads expansion properties that will help to design fluidized-bed-based bioreactors.

Part II

Hollow fiber membrane bioreactor

Chapter 5

Hollow fiber (HF) membrane bioreactor

5. Hollow fiber membrane bioreactor

Application of hollow fiber membrane bioreactor for hepatocyte cultures will be cited in this chapter. The interest towards biotechnological and biomedical devices for the life sciences is very high and intense research efforts are being devoted to the development of new process/technologies or improvement of existing ones such as hollow fiber membrane bioreactor. In addition, the typical set-up protocol and operational limitation of hollow fiber membrane bioreactor for cell culturing are mentioned here highlighting operational difficulties that have hindered the possibility to cultivate cells within tightly controlled conditions.

5.1 Membrane bioreactor for liver cell culturing

Semipermeable membranes provide selectivity for the size of biological molecules that will be exchanged between the patient and the device. They are inherent in hollow fiber devices but have been used also in flat-plate and perfusion systems. In many hollow fiber devices, the membrane must simultaneously function as a permselective barrier and as a scaffold for cell attachment. As noted earlier, the interaction of the hepatocyte with its microenvironment dramatically affects stability and function. Therefore, this design may not allow for optimization of both function and transport. Conversely, hollow fiber designs provide a larger surface area to volume ratio than flat plate designs, thus improving metabolite transport and minimizing dead volume [9].

The membrane in a BAL device is typically characterized by its molecular weight cut-off, which is selected both to prevent the exposure of bioreactor cells to components of the immune system and to block the transport of larger xenogeneic substances into the circulation. Membranes also prevent the migration of cells into the patient's circulation, although case reports of cellular translocation exist. While transport in BAL devices is a combination of convective and diffusional phenomena, mass transfer limitations of key nutrients to and from the cellular compartment often arise because of diffusion resistances [9].

Among the bioreactors, hollow fiber membrane bioreactors meet the main requirements for cell culture: a wide area for cell adhesion, oxygen and nutrient transfer, removal of catabolites and protection from shear stress. Furthermore, hollow fiber membranes may serve as scaffolding material guiding the spatial organization and microarchitecture of the liver tissue. Critical issues in the hollow fiber membrane bioreactors are the configuration of the bioreactor, the fluid dynamics and the membrane properties which depend on the cell adhesion and mass transport [6].

De Bartolo et al. [6] evaluated the cytocompatibility of polyetheretherketone (PEEK-WC) membranes by culturing hepatocytes isolated from rat liver. Morelli et al.

[99] reported on the performance of galactosylated polyethersulphone (PES) membrane bioreactor that enables the long-term maintenance of liver-specific functions of human hepatocytes under continuous perfusion. Cell adhesion and metabolic behaviour in terms of ammonia elimination, urea synthesis, and protein synthesis were evaluated during the first days of culture.

Curcio et al. [100] carried out experiments and calculations aimed at discerning the simultaneous influence of both diffusive and convective mechanisms to the transport of metabolites.

Mass transfer across the membrane occurs by diffusion and/or convection in response to existing trans- membrane concentration or pressure gradients. Both mechanisms of transport should be taken into account in the design of HF membrane bioreactors. In the case of hepatocytes, which are anchorage-dependent cells, the membrane properties are critical not only for the transport but also for their interaction with cells.

De Bartolo et al. [6] developed a crossed hollow fiber membrane bioreactor to support the long-term maintenance and differentiation of human hepatocytes. The bioreactor consisted of two types of hollow fiber (HF) membranes with different molecular weight cut-off (MWCO) and physicochemical properties cross-assembled in an alternating manner: modified polyetheretherketone (PEEK-WC) and polyethersulfone (PES), used for the medium inflow and outflow, respectively. The combination of these two fiber sets produces an extra capillary network for the adhesion of cells and a high mass exchange through the cross-flow of culture medium (*Fig. 28*).



Fig. 28. Crossed hollow fiber membrane bioreactor

In their study, they describe the morphological and functional maintenance of human hepatocytes in a crossed HF bioreactor whose configuration and fluid dynamics were optimized in order to ensure an adequate mass transfer of nutrients and drug to the cell compartment and a removal of specific products and catabolites from the cell compartment. The two-fiber system with different morphological and physico-chemical properties has a constant distance of 250 μm inside the bioreactor. This geometry allows achieving a homogeneous and small size cell aggregates, which facilitate mass transfer and therefore the perfusion of cells cultured inside the network of the fibers and the necessary turnover of the medium in the cell compartment. Both for nutrient supply and waste elimination, mass transfer to and from cells is a critical issue in any bioreactor design especially when cells are cultured in three-dimensional multicellular aggregates where mass transfer limitation of oxygen and metabolism may occur in the core of aggregates. In the case of the design of bioartificial liver besides the catabolites (e.g., lactate, ammonium, carbon dioxide) removal, the accumulation of toxins and toxic metabolites produced by drug biotransformation must be avoided in order to maintain

viable and functional cells inside the bioreactor environment. Furthermore, the delivery of plasma proteins, as well as large molecular weight (MW) proteins (e.g., clotting factors) and drug metabolites, must be ensured in both clinical and in vitro devices.

The efficient mass transfer of nutrients, metabolites, and toxins appear to be a key point in all bioreactor designs varied from classical (hemodialyzers) to more complicated geometry. Here the transport phenomena related to diffusion and reaction of liver metabolites such as albumin and urea and of diazepam are mathematically described and experimentally verified.

The rate of albumin and urea synthesis of human hepatocytes cultured in the crossed HF membrane bioreactor in 18 days is shown in *Fig. 29*. In particular, the good performance of the reactor in terms of detoxification functions is confirmed by the high urea synthesis rate that reaches the maximum value of 28.7 $\mu\text{g/h } 10^6$ cells at day 15, remarkably higher with respect to the values reported in the literature.

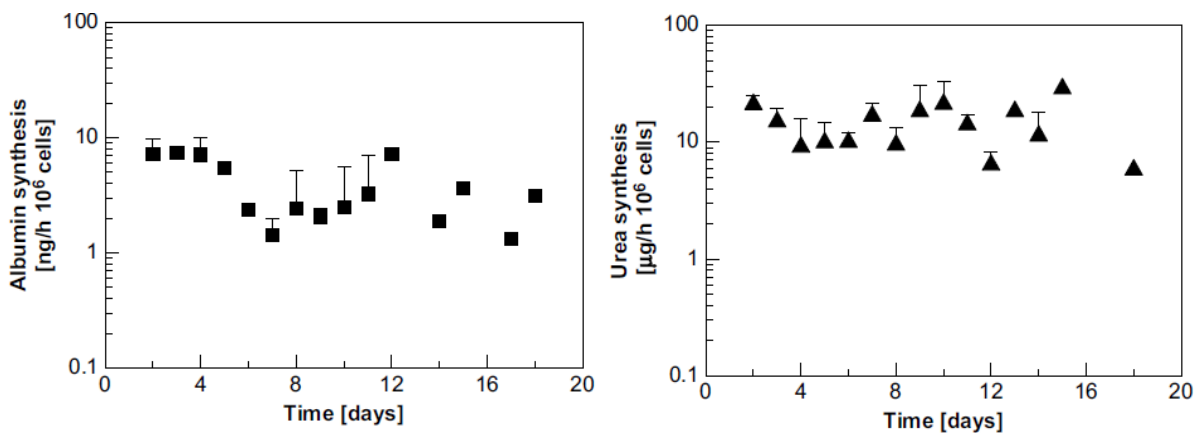


Fig. 29. The rate of albumin and urea synthesis of human hepatocytes cultured in the crossed HF membrane bioreactor. The values are expressed as $\mu\text{g/h } 10^6$ cells \pm s.e.m. and are the mean of 6 experiments [6].

Also, the biotransformation functions were performed by cells in the bioreactor for all culture time. Diazepam is metabolized by cytochrome P450 activities. In the bioreactor, about 87% of the administered diazepam was metabolized during the first days of culture.

According to *Fig. 30a* the agreement between the theoretical concentration of diazepam at day 2 (1.80 $\mu\text{g/ml}$) and the experimentally observed one (1.56 ± 0.33 mg/ml) is satisfactory. Moreover, the model results can be extended over the first 5 days of culture with reasonable accuracy, thus representing a powerful predictive tool for evaluating the performance of the crossed fibers membrane bioreactor. The metabolic pathway of diazepam includes the metabolites temazepam, oxazepam and N-desmethyl-diazepam; all these metabolites were generated in the bioreactor, as shown in *Fig. 30b*.

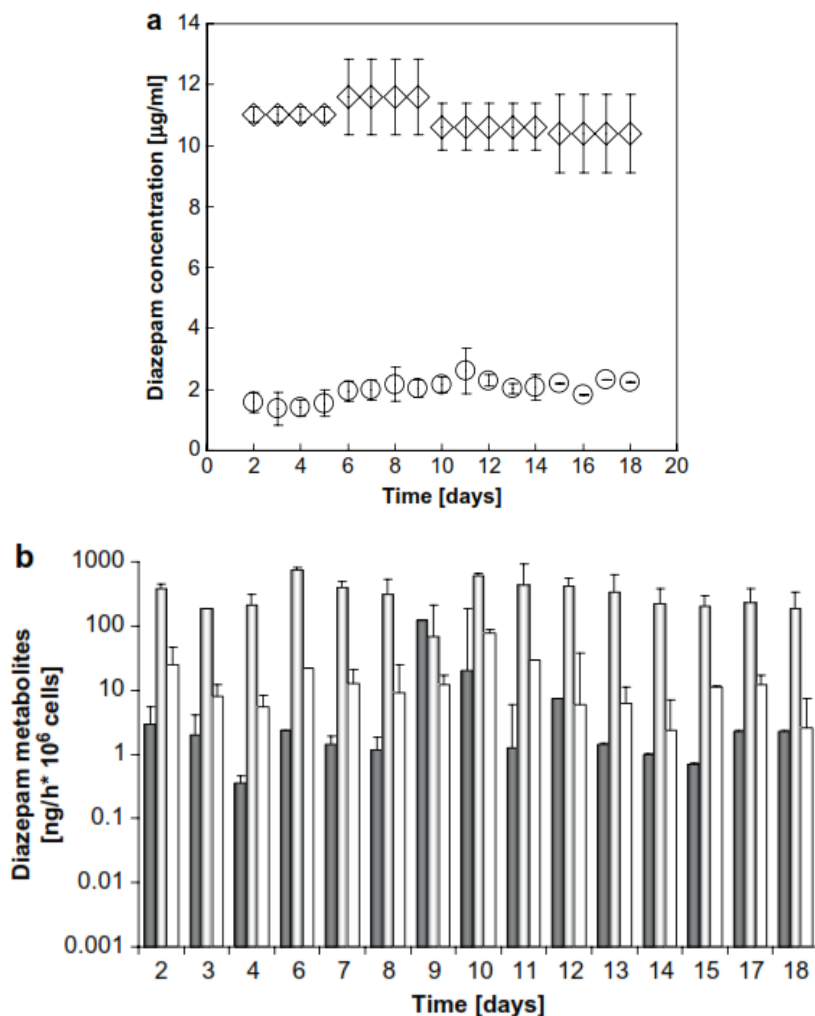


Fig. 30. a) Diazepam concentration in the inlet medium (◇) and in outlet medium from bioreactor loaded with cells (○) in presence of 10 µM diazepam added to the culture medium. b) Formation of diazepam metabolites: (full bar) oxazepam, (gray bar) temazepam and (white bar) N-desmethyl-diazepam. The values are expressed as ng/h 10⁶ cells ± s.e.m. and are the mean of 6 experiments [6].

The results are shown in *Fig. 30* demonstrate that the diazepam is completely metabolized as occur in humans where each of metabolites is finally converted to oxazepam. In the bioreactor, the human hepatocytes expressed at high levels the individual CYP isoforms involved in the diazepam biotransformation. These enzymes are

among the most sensitive and fragile found in hepatocytes, responding quickly to loss of activities to unfavorable culture conditions.

The high cell specific activity found in their study demonstrates the good performance of the bioreactor to maintain the viable and functional integrity of human hepatocytes. The crossed HF membrane bioreactor can potentially be used to address the mass transfer limitations currently seen in liver tissue engineered constructs.

5.2 Typical set-up protocol and operational limitation

Cryopreserved primary human hepatocytes (Life Technologies, California, US), isolated from human tissue were thawed in a 37° C water bath with gentle shaking. Cell suspension was slowly transferred into pre-heated 25 ml of Williams' medium E supplemented with dexamethasone 1 µM, HEPES 15 mM, recombinant human insulin 4 µg/ml, GlutaMAX™ 2 mM and penicillin/streptomycin (10,000 U/mL/10,000 µg/mL) and 10% fetal bovine serum, and centrifuged at 50g at room temperature for 5 min. The viability of the hepatocytes (assessed by Trypan blue exclusion) ranged between 80 and 90%. The human hepatocytes were then seeded at a density of 105 cells/cm² on the outer surface of HF membranes previously sterilized and conditioned with medium containing 5% fetal calf serum. After 24 hours, the medium was removed and replaced with serum-free medium. Cells were incubated at 37° C in 5% CO₂ with 95% relative humidity for the duration of the experiments. During the experiment, the medium was changed every 3-4 days with a fresh one.

In the whole experiment, the level and flowrate were adjusted to desired value appropriate for cell culturing, manually with valves. The manual way of the level and flowrate adjustment has a significant risk of overflow (bad transport) or dry-up of the cell culturing environment (cell death). In addition, the continuous need for sterilization to avoid any type of contamination, make additional problems related to all manual interventions on the plant.

Chapter 6

Experimental setup

6. Experimental setup

The point of departure of the present chapter is an existing crossed hollow fiber membrane bioreactor developed originally by the Institute on Membrane Technology (ITM-CNR) to support the long-term maintenance and differentiation of human hepatocytes. In this Chapter, the simple scheme of operation of the bioreactor is extended to include additional instrumentation, a control box with a digital acquisition board and a flexible and extensible PC-based control system within the MATLAB/Simulink interface.

6.1 Bioreactor configuration

6.1.1 Geometry

The perfusion system in the prototype bioreactor under investigation consists of one types of hollow fiber membranes (HFs) arranged in a crossed configuration, mimicking the blood capillary network. This type of HF is employed to serve a distinguished function: polyethersulfone (PES) for supplying the cells with nutrients and metabolites and PEEK – WC for removing the catabolites [5, 6].

Depending on the cell type and the intended structure in the cellular compartment of the bioreactor, other materials could also be employed as hollow fiber membranes to promote or inhibit desired characteristics such as cellular adhesion, biodegradability, etc.

In the ongoing research in ITM-CNR, PEEK-WC – PES bioreactor is used when cells are seeded in suspension, while PES – PES bioreactor is employed for hepatocyte spheroids. In the latter case, the spheroids are believed not to disintegrate due to limited interaction with PES HF, which in turn promotes fusion of the spheroids instead [6].

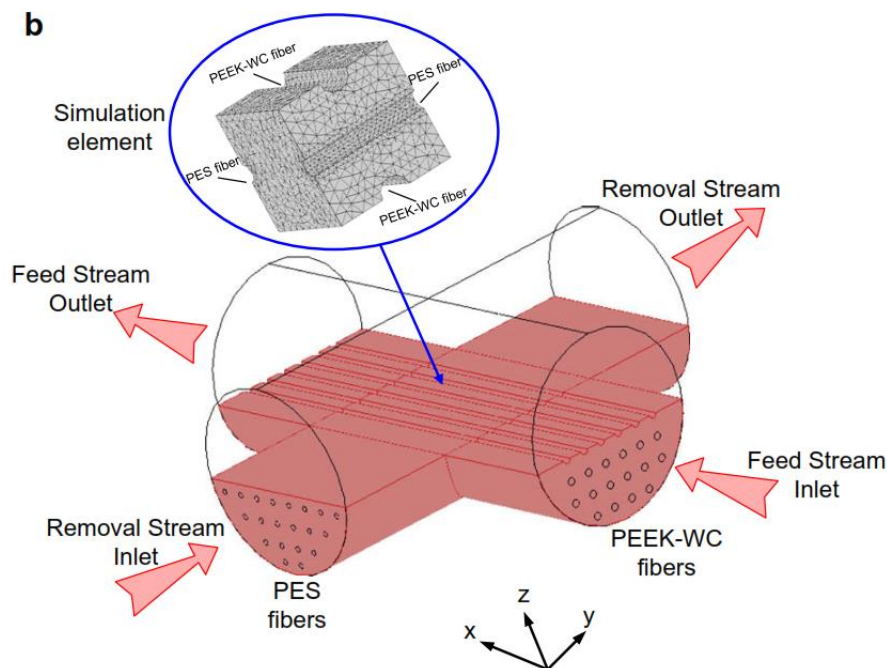


Fig 31. Schematic vertical section of the crossed hollow fiber membrane bioreactor [6].

The internal structure of the bioreactor is schematically depicted in *Fig 31*. The system is investigated in each of its distinguished compartments: two intraluminal compartments which are feed bundle (FB) and effluent bundle (EB), the membrane walls and the extra-capillary space (ECS) in which the cells will be seeded. The oxygenated medium from the reservoir enters the membrane bioreactor with a flow rate (Q_f) of 1 ml/min. The flowrate is optimized and limited between 0 to 2 ml/min in order to decrease shear stress to cells. Fresh medium was perfused in single-pass and the stream leaving the bioreactor Q_{out} was collected as waste until approaching the steady state. When the system reached the steady state, the stream leaving the bioreactor was recycled (Q_r) in order to obtain the accumulation of products.

Table 7. Dimensional properties of the bioreactor

PES diameter	300±40µm ID, 100±25µm thickness
HF active length	~4cm
Number of HFs	>100 /bundle
Bioreactor Volume	Housing (total): 42ml ECS (assembled bioreactor): 25ml

Note that the peculiar configuration is based on two dead-ends (i.e. fixed volume, variable pressure) crossed fiber bundles (FB and EB).

Extra capillary space volume is open to atmospheric pressure (i.e. fixed pressure, variable volume). The mild pressure condition in the ECS allows maintaining the shear stress to a very low level but it is subjected to liquid level variations. With this configuration, over 100 fibers can be used in each bundle. *Table 7* lists the dimensional properties of the bioreactor.

6.1.2 Fabrication

The bioreactor is assembled in-house using commercial PES fibers (Membrana, Germany). The glass housing of the bioreactor is designed in ITM-CNR and manufactured by Microglass, Italy. Stagnant regions at the connections were eliminated by minimizing connection length and having additional potting compound during bioreactor assembly so that in the end the active section of the hollow fibers is confined in a spherical frame. Polyurethane potting compound (BASF, Germany) was used as a non-toxic sealing material to tightly hold the HF bundles (*Fig 32*).



Fig 32. Bioreactor housing (left-a) and bioreactor assembled in-house, with 100 HFs (10x10 arrangement) in each bundle (right-b).

6.2 Instrumentation

This part includes a description of the instrumentation required in order to set-up and implements the level control system on the ITM-CNR membrane bioreactor and the detailed specifications available for each element. Schematic sketches of ITM-CNR membrane bioreactor set up before and after instrumentation are shown in *Fig 33* and *Fig. 34*. As it is clear from figures below, it is necessary to change the current ITM-CNR set-up in order to system variables online monitoring and a digital controlling.

Instrumentation has been acquired including level and flow sensors and a National instrument (NI) data acquisition board (DAQ) board for real-time digital acquisition of sensor signals as well as manipulation of the pump rotational speed. Another peristaltic pump was added in order to measure and manipulate inlet and outlet flowrate separately. An auxiliary small tank (capillary-tank), required for non-intrusive level measurement, was manufactured. In order to connect the DAQ board to the sensors and the pump, a Command Box has been manufactured. Obviously, the previous set-up doesn't have the capability of installing control system without instrumentation.

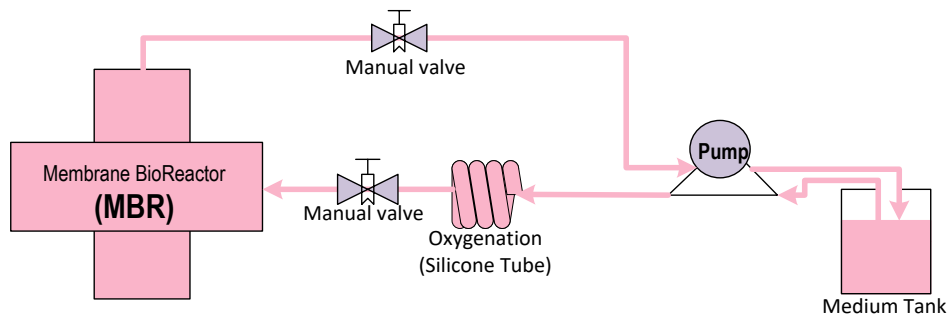


Fig 33. ITM-CNR membrane bioreactor set up before instrumentation.

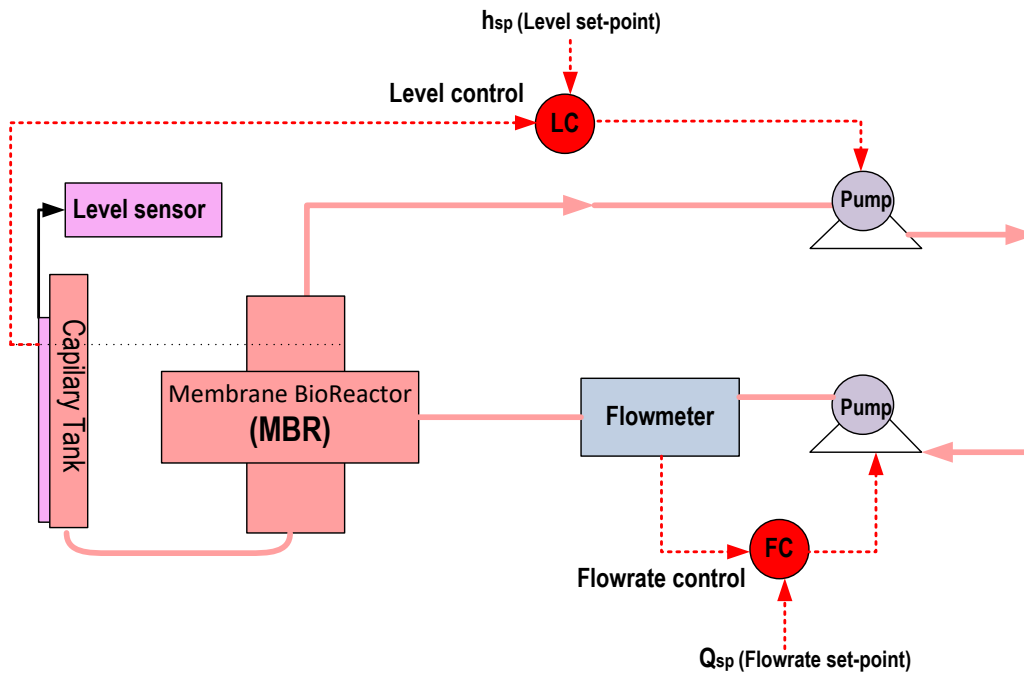


Fig. 34. ITM-CNR membrane bioreactor set up with the multi input-multi output (MIMO) (2×2) control of hydrodynamics by two feedback loops on flowrate and liquid level.

Below is a short description of each required instruments:

6.2.1 Capillary level tank

A capillary-tank (Microglass, Italy) that has a same liquid level as membrane bioreactor (MBR) was designed and installed in the experimental set-up. The level measurement of bioreactor must be contact-less because of the contamination problem. As the bioreactor system, especially during the cell culturing procedure, is super sensitive to contamination, using a sensor inside the bioreactor is impossible. In the other hand the level sensor could not be attached to the complex-shape of MBR bioreactor, so a capillary-tank was designed in order to connect to the bioreactor. As it was mentioned before it works on the same level with a bioreactor and the level sensor could easily attach

on the surface of the tank. Same as another part of bioreactor the capillary-tank is autoclavable and it can make a contact-less level measurement without contamination.

As the medium used in cell culturing system is expensive, in the design procedure, an optimum volume has been selected, also considering the capillary effect of the liquid in the thin tube. The height h of a liquid column is given by:

$$h = \frac{2\gamma \cos(\theta)}{\rho g r} \quad (6)$$

where γ is the liquid-air surface tension (force/unit length), θ is the contact angle, ρ is the density of the liquid (mass/volume), g is local acceleration due to gravity (length/square of time), and r is the radius of the tube (length). Thus the thinner the space in which the water can move, the further up it goes for a given pressure conditions. For a water-filled glass tube in air at standard laboratory conditions, the parameters are $\gamma = 0.0728$ N/m at 20 °C, $\theta = 0^\circ$ ($\cos(0) = 1$), $\rho = 1000$ kg/m³, and $g = 9.81$ m/s². For these values, the height of the water column is:

$$h \approx \frac{1.48 \times 10^{-5}}{r} \text{ m [101]} \quad (7)$$

Thus for a 8 mm diameter glass tube in lab conditions given above (radius 4 mm), the water would rise around 3 mm. *Fig 35*, *Fig 36* and *Fig 37* show a draft sketch and actual capillary level tank respectively. A design is provided below in order to guide the manufacturing.

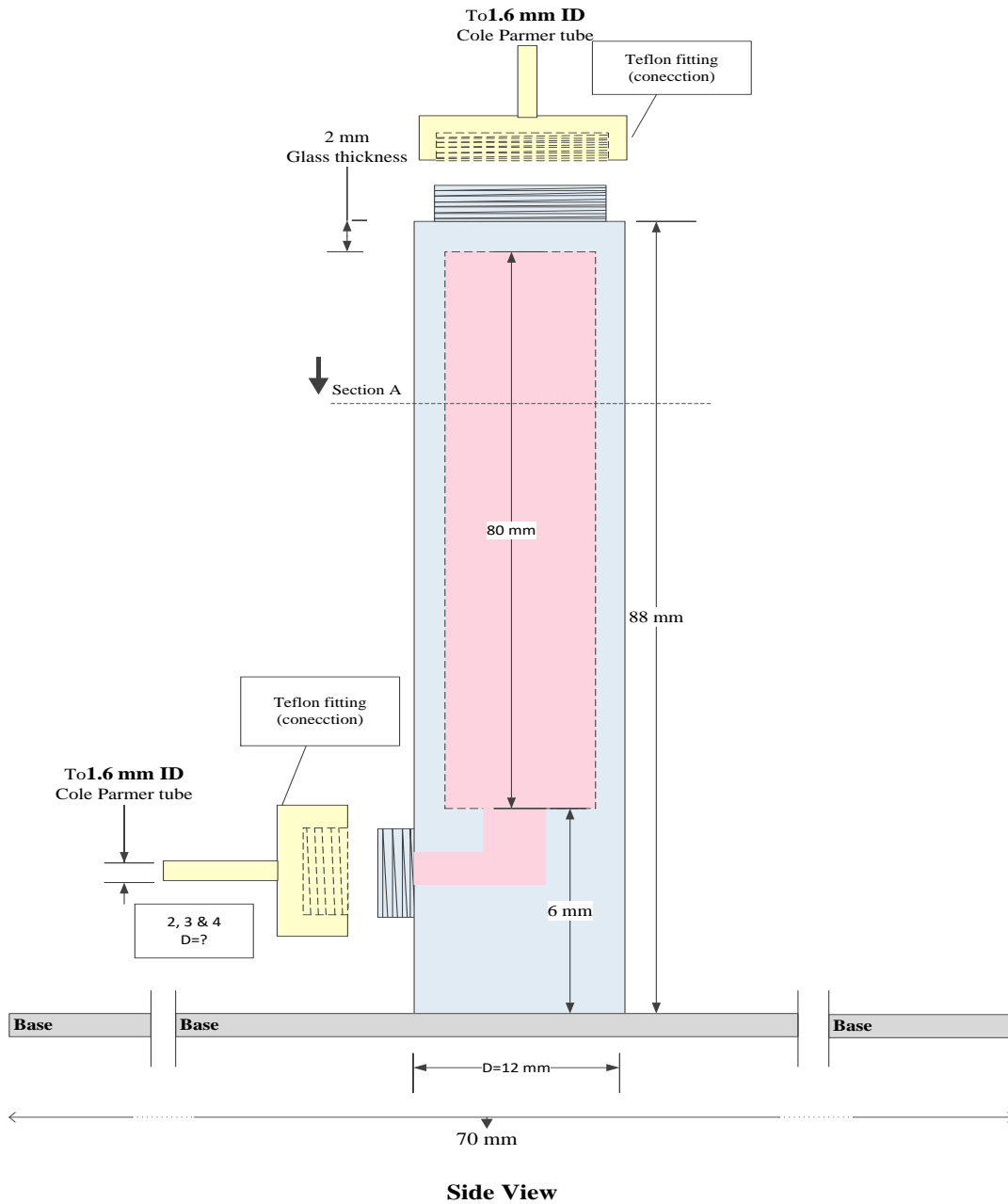


Fig 35. Sketch of the capillary level tank (Side view).

As it can be seen from the *Fig 35*, the tank was designed with a glass thickness of 2 mm in order to increase level sensor accuracy. Two Teflon caps were designed for the top (connect to air with the filter in atmospheric pressure) and bottom (for connecting to

the bioreactor). The connection part in the caps was designed based on Cole-Parmer tube size.

Fig 36 shows a sketch of the front and top view of capillary-tank. A base was designed in the same quality (glass) in order to keep the tank stable. The base and the tank was manufactured in as a uniform instrument that was called capillary-tank. In a preliminary step, the tank was designed as a cube with rectangular base in order to mount easily the sensor on the surface of capillary-tank but at the end, it was changed to cylindrical shape because of limitation in manufacturing.

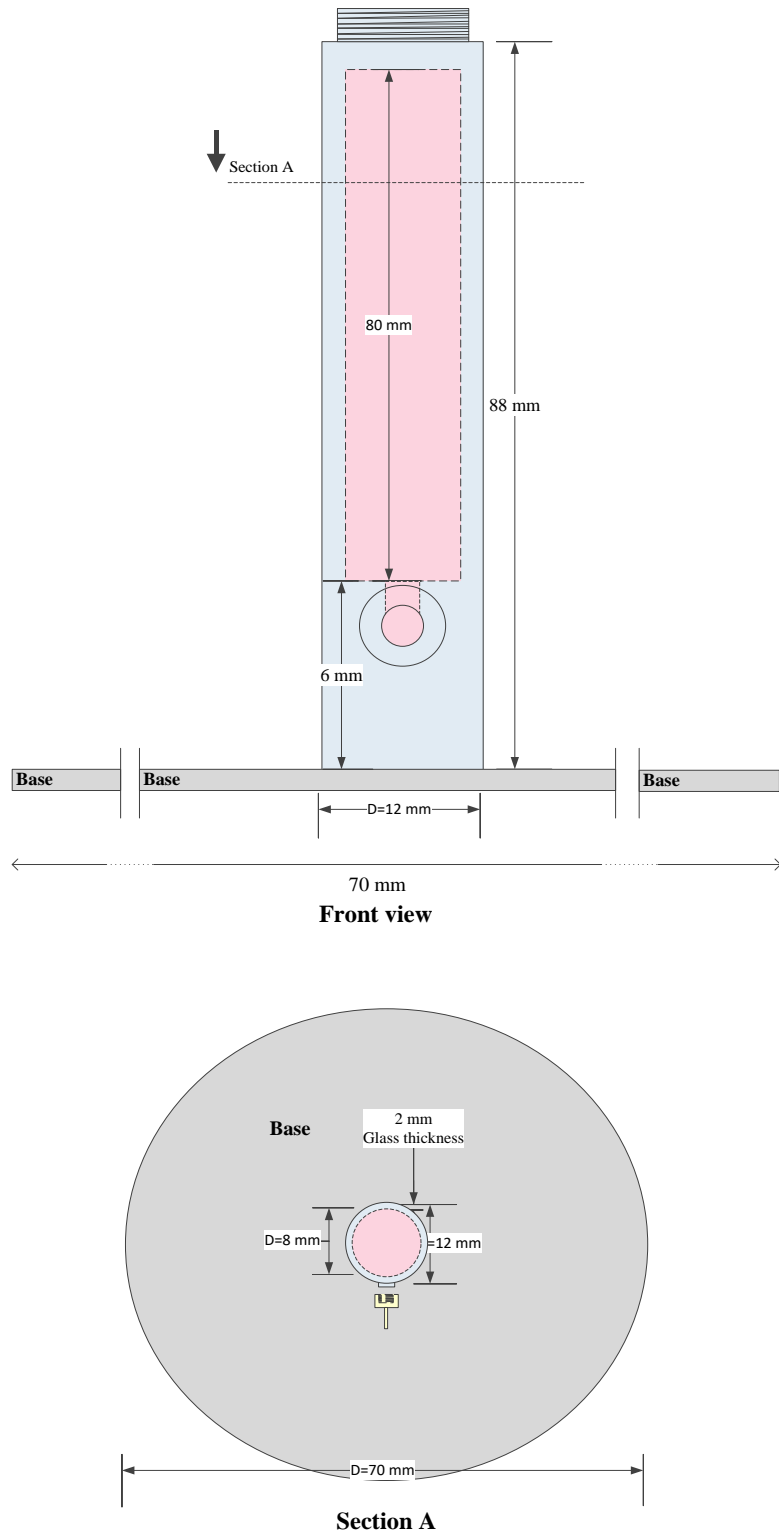


Fig 36. Sketch of the capillary level tank (front and top view).



Fig 37. Capillary level tank.

Fig 37 shows the actual capillary-tank manufactured by Microglass in Naples, Italy.

6.2.2 Level sensor (contactless capacitive CLC)

Electrical capacitance level sensors allow a contact-free measurement of liquid level and can be easily mounted on the outside of a container or vessel. *Fig 38a* shows the Sensortech[®] CLC level sensor as it appears in operation monitoring the height of a liquid interface. The sensor supply voltage is 5.5 to 15 DC volt and its output voltage range is 0-5 V. It has the capability of being used in a different range of temperature (-20 to 85 °C). The measuring range of the sensor is 0 to 100 mm with a resolution of 6 bit. CLC sensor has a 5 pin connector that is V_s , Analog out, 1-wire digital out, Teach-in and

ground (GND) respectively. The spec sheet of the sensor is attached in Appendix C at the end of the thesis but sensor calibration is explained below:

The Teach-In (TI) mode allows for a permanent storage of both low and high-level values of the measurement range. This range is determined by the sensor pad. The TI_{LOW} mode stores the value for the empty or low level container and adapts to the corresponding application conditions. The TI_{HIGH} mode stores the value of the container filled to the desired max level. By factory default, the sensor is 'formatted' and needs to be taught to provide an output signal. The sensor must first be taught Low to adapt to the ambient conditions, then high. For TI_{LOW} mode voltage between 0 and 0.5 V for at least 500 ms at the Teach-In pin is applied. After 1 sec. the value is stored and for TI_{HIGH} mode voltage between 4.5 and 5 V for at least 500 ms at the Teach-In, the pin is applied. After 1 sec. the value is stored. Under normal conditions, the TI-Pin delivers 2.5 V. For all of this procedure electronic switches are prepared that would be discussed later in DAQ box section.

Due to the sensor working mechanism, a number of parameters such as container wall thickness, air gap, and GND connection could influence on measuring resolution. A significant noise was observed in initial tests with water, mostly due to the low amount of liquid in the tank. As the sensor is capacitive, the amount of liquid has a significant effect on the measurement. By a communication with the company that produced the level sensor, the sensor's GND has been connected to a copper foil placed on the opposite side of the container. This results in the electric field going straight through the liquid, disregarding to a large extent the surrounding environment. By creating a fixed reference, the performance is enhanced and the dependence on surrounding conditions greatly reduced. As it can be seen from the *Fig 38b*, a copper foil was designed and installed in front of the level sensor in order to reduce noises in the acquisition of level data.

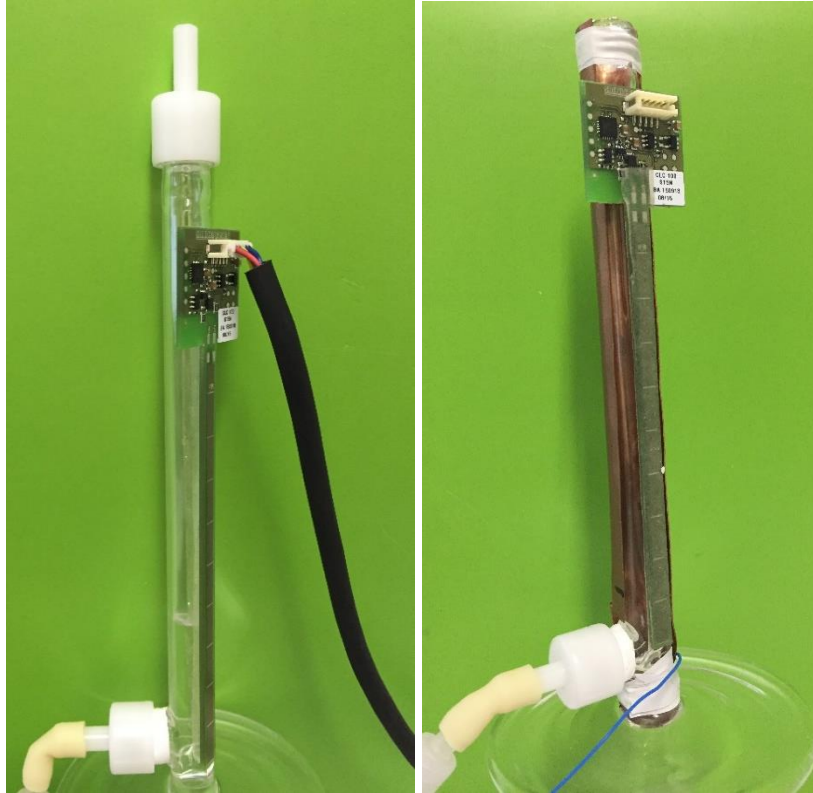


Fig 38. CLC level sensor (a), CLC level sensor with a copper foil (b).

In the *Fig. 39* a comparison between CLC sensor measurement in capillary-tank with and without copper foil is shown. The level was increased 1 cm by 1 cm from 1 to 10 cm (the whole length of capillary-tank). As it is clear from figure there is a significant improvement both in measurement accuracy and oscillation reduction. The result related to tank with copper foil which is plotted by blue color shows a precise measurement. In the other hand, the oscillation is much lower than without copper foil improvement.

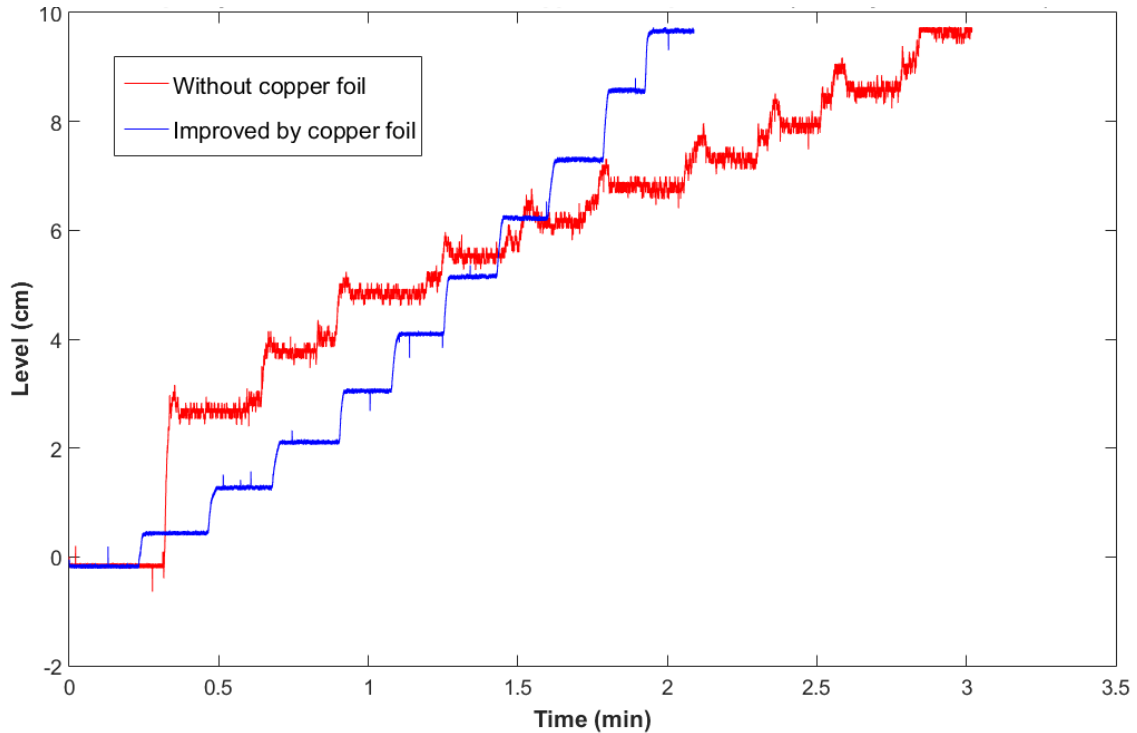


Fig. 39. A comparison of CLC level sensor accuracy measurement with and without copper foil

6.2.3 Liquid flow meter

A liquid flow meter is necessary in order to measure the actual liquid flowrate in the tubings. Monitoring the actual flowrate will also serve to ensure that actuation on the pumps by changing the rotational shaft speed will actually change the inlet (or outlet) flow to (from) the bioreactor. The SENSIRION SLI 2000 Liquid Flow Meter enables fast, non-invasive measurements of very low liquid flow in the ml-range. Excellent chemical resistance and bio-compatibility are ensured.

SLI Liquid Flow Meter is used as a sensor to observe actual inlet or outlet flowrate and improve the accuracy of liquid level control of the extra-capillary space in the MBR. A picture of the SLI flow meter sensor is shown in *Fig 40*. SLI sensor has both Digital (RS485-bus and USB cable) and Analog (Voltage output and additional operational

mode). The output Analog voltage is 0 to 10 V and it can measure up to 5.5 ml/min. 40 ms flow detection is its response time. The flowmeter accuracy is reasonable and for H₂O at 23 °C is 5% of measured value. The SLI Liquid Flow Meter hold calibrations for two liquids, one for water (H₂O) and one for isopropyl alcohol (IPA). Each calibration is stored in a separate calibration field. The fully detailed specification sheet of the sensor was attached at the end of the thesis in Appendix D.



Fig 40. SENSIRION SLI 2000 flow meter.

6.2.4 Peristaltic pumps

As it was shown in *Fig 33* in the previous set-up in the ITM-CNR only one pump (ISMATEC, Germany) was used in order to medium circulation and the flowrate was controlled by manual valve on the other hand, in new experimental set-up with full automatic control system two pumps were used for inlet and outlet flowrate controlling and manipulating, respectively. The ISMATEC pump with 8 rollers is shown below in *Fig. 41*. The rotational speed of this pump is from 2 to 100 rpm and the flowrate is 0.003 to 35 ml/min. The operational voltage of the pump is 115 to 230 V with a max. 20 W power.



Fig. 41. ISMATEC Peristaltic pump

In order to manage the pumps with the control system, the pumps were connected to the computer and their rotational speed was automatically monitored and controlled by a computer with using an Analog interface existing at the behind of the pump. The details related to the Analog interface of the pump is mentioned in *Fig. 42*. As it can be seen with pins number 1, 2 and 3 the pump will change from manual to automatic condition (Digital value). Pin number 5 which set the rotational speed by sending a signal (0-5 V_{DC} / 0-10 V_{DC}) is very important (Analog value). More details were mentioned at the end of the thesis in Appendix E.

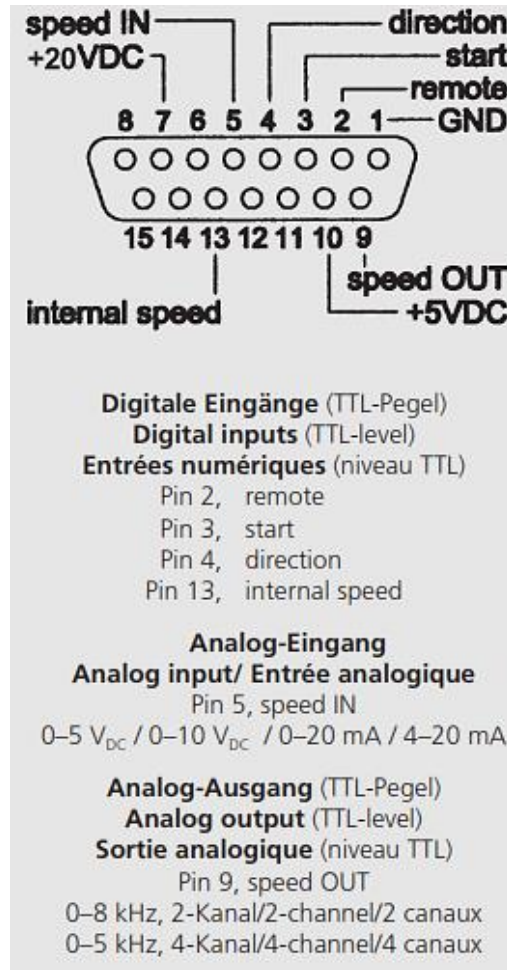


Fig. 42. ISMATEC pump Analog interface details.

6.2.5 Data acquisition board

The data acquisition board (DAQ) is used as a connection to handle communication between the computer with control software and the sensors and actuators. The NI USB-6001 provides basic DAQ functionality for applications such as simple data logging, portable measurements, and academic lab experiments. *Fig 43* shows DAQ 6001. The DAQ provides eight Analog input channels with 14 bits of resolution and a 20 kS/s sampling rate, 13 digital I/O lines, one basic counter for edge counting, and two Analog output channels. It features a lightweight mechanical enclosure and is USB

bus-powered for portability. The NI USB-6001 is fully compatible with the MATLAB Data Acquisition Toolbox. The specification data sheet was attached in Appendix F.



Fig 43. DAQ NI 6001.

6.2.6 DAQ Box

A box was designed and manufactured in order to manage all the connections and switches between sensors, actuators, Computer and DAQ. A sketch of the electrical circuit of DAQ box is shown in *Fig 44*. The figure shows the whole wiring related to power supply, flowmeter, level sensor, pumps and the computer. The wires were connected with appropriate cable with minimum noise to/from DAQ to the instruments. They were connected to the related Analog and Digital input/output by a screw to the DAQ.

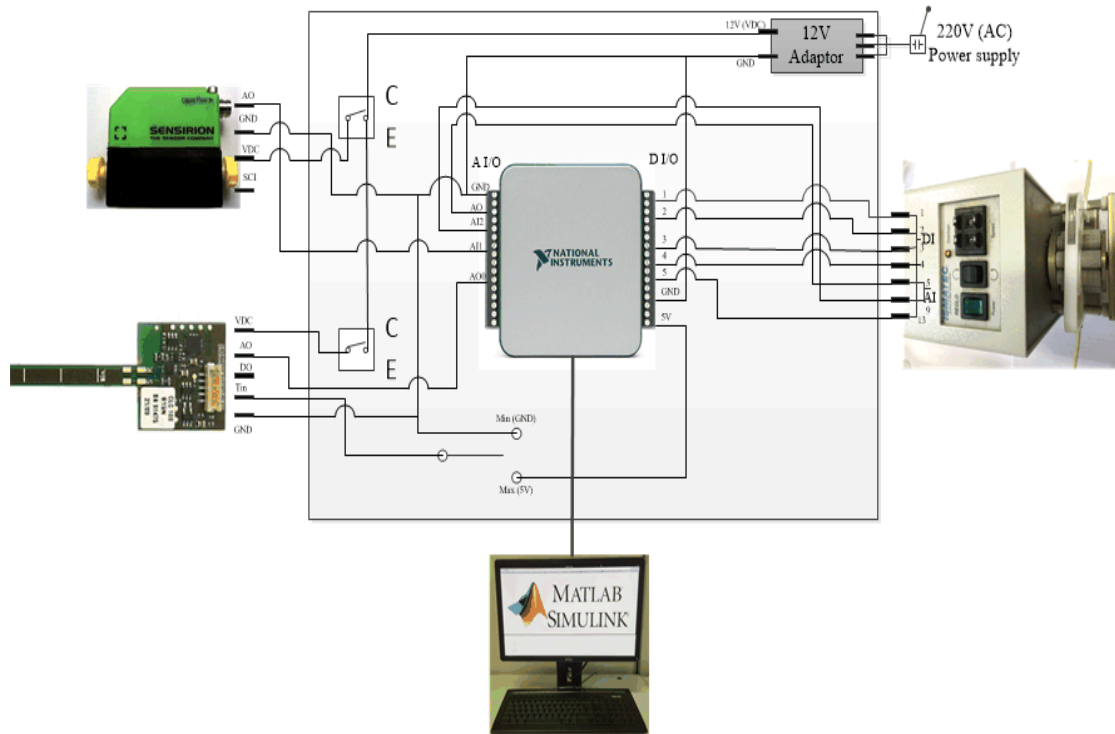


Fig 44. DAQ box electrical circuit scheme.

The picture of DAQ box is shown in Fig 45. As it can be seen from the figure the DAQ was situated in the center of the box and the 12 V adaptor was fixed at the left side of the box. In the down left side of the box, a port was prepared for 220 V power supply and also pumps and sensors cables. At the right side of the box, three switches that are a three-phase switch and two on/off switches in order to turn sensors on or off and also level sensor calibration were situated. The box protects the DAQ and the wiring during the experiments. A sketch of manual and wiring of DAQ box was attached in Appendix B.

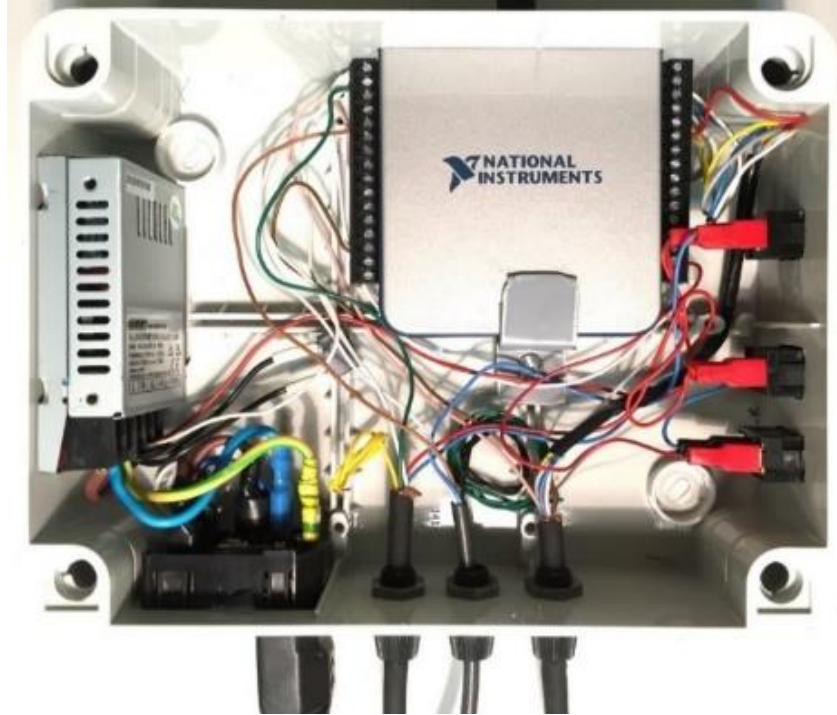


Fig 45. Actual connections of the DAQ box.

6.3 Software (MATLAB)

A MATLAB program was developed in order to monitor the hydrodynamics and implement the control system by means of data acquisition from measuring elements (level and flowrate sensors), computation of the control signal variables and manipulation of the actuators (pumps). The procedure is explained in next sections step by step and an algorithm was drawn below in *Fig. 46*.

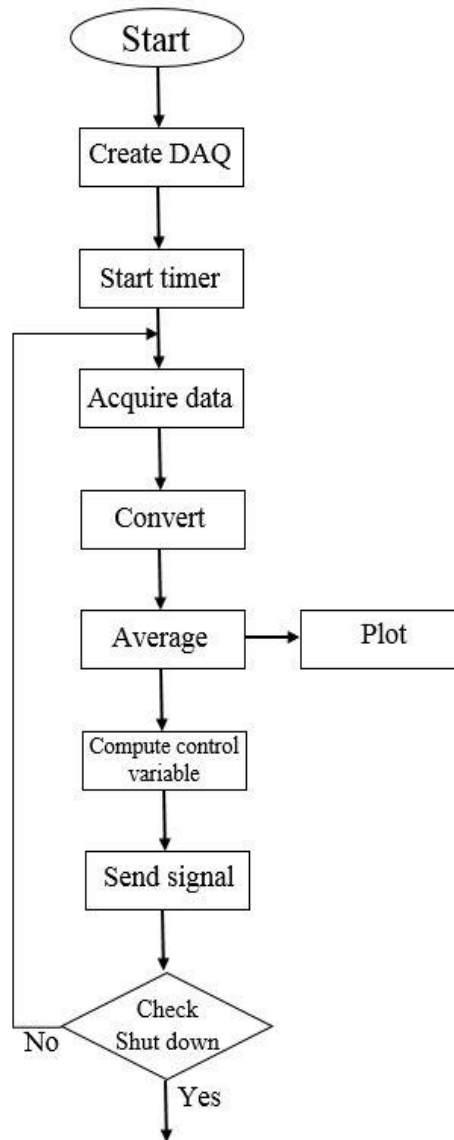


Fig. 46. MATLAB software algorithm

6.3.1 Create DAQ session

Data Acquisition Toolbox supports the use of two interfaces. The legacy interface and the session-based interface. The session-based interface is chosen in order to communicate with DAQ because it is more appropriate for our application. After this an m-file was developed to use DAQ based on steps below:

- 1- The supported devices was discovered by *daq.getDevices*.
- 2- The session was created by *daq.createSession*.
- 3- The analog (input/output) and digital (I/O) channels were added by *addAnalogInput/OutputChannel* and *addDigitalChannel* respectively. The analog channels used as input channels to acquire data from level and flowmeter sensor. As the same way, two analog output channels and two digital I/O channels were added for manipulating and control the pumps functions.
- 4- Run the session by *timer* object.

6.3.1.1 Convert raw data

In the previous sections, the method to collect/send raw data from/to sensors and pumps was explained. The raw data acquired from level sensor and flowmeter and the signal sent to pumps are in voltage unit. So they are converted to level (mm) and flowrate (ml/min) unit based on the conversion formula:

$$u = \frac{R - V_{min}}{V_{max} - V_{min}} \times (D_{max} - D_{min}) + D_{min} \quad (8)$$

where u is the converted data such as level (mm) and flowrate (ml/min), R is raw data, V_{min} and V_{max} are the minimum and the maximum of the instrument voltage range, D_{min} and D_{max} are the minimum and the maximum of the instrument measurement limit.

Table 8 lists all these variables used in the m-file.

Table 8. Instrument and DAQ variables in order to convert voltage to actual units

Variables	Level sensor	Flowmeter	Pump
V_{min}	0.5 (v)	0 (v)	0 (v)
V_{max}	4.5 (v)	10 (v)	0.7 (v)
D_{min}	30 (mm)	-5.5 (ml/min)	0 (ml/min)
D_{max}	90 (mm)	5.5 (ml/min)	3.1 (ml/min)

6.3.1.2 Average of raw data

In the present application, the raw data exhibit significant noise because of the characteristic properties of the level sensor and flowrate while a slowly changing signal is necessary in order to have a stable and optimal control system. For this purpose, the raw data is filtered by moving average (MA) which is a signal processing technique applied in the time domain, intended to increase the strength of a signal relative to noise that is obscuring it. An example of a simple moving average for an n-second sample of level data is the mean of the previous n seconds' level data. If those data are $L_M, L_{M-1}, \dots, L_{M-(n-1)}$ then the formula is:

$$MA = \frac{L_M + L_{M-1} + \dots + L_{M-(n-1)}}{n} = \frac{1}{n} \sum_{i=0}^{n-1} L_{M-i} \quad (9)$$

When calculating successive values, a new value comes into the sum and an old value drops out, meaning a full summation each time is unnecessary for this simple case:

$$MA_{current} = MA_{prev} + \frac{L_M}{n} - \frac{L_{M-n}}{n} \quad (10)$$

The Fig 47 shows a comparison between raw data and filtered one. For the level signal, a time averaging of 6 seconds was used.

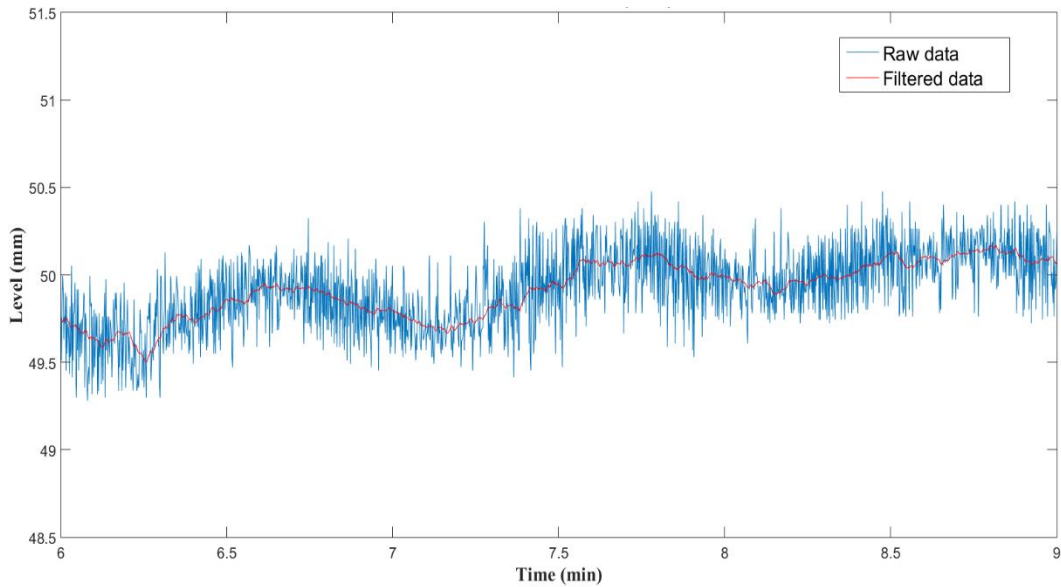


Fig 47. Raw data vs. filtered data (Level).

The same data processing was done in flowrate measurement. The flowrate data has a significant noise because of oscillated flow produced by the peristaltic pump. In *Fig. 48* a comparison between raw data and averaged data in 6 seconds averaging time is shown.

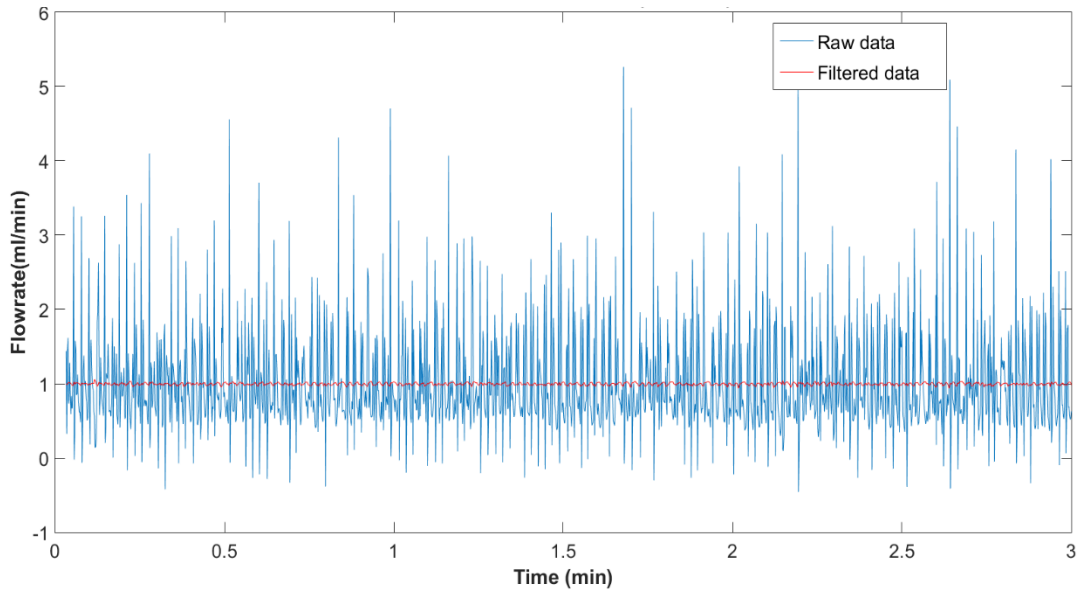


Fig. 48. Raw data vs. filtered data (Flowrate).

6.3.1.3 Digital control

In order to control the level of the bioreactor, a proportional–integral–derivative (PID) control system that is explained in details in the further section is used. The input–output relation of the digital PID controller which is used in the software in velocity form is expressed as:

$$\Delta u(k) = K_c \left[\left(1 + \frac{\Delta t}{\tau_I} + \frac{\tau_D}{\Delta t} \right) \varepsilon(k) - \left(\frac{2\tau_D}{\Delta t} + 1 \right) \varepsilon(k-1) + \frac{\tau_D}{\Delta t} \varepsilon(k-2) \right] \quad (11)$$

where u is the control signal, $\varepsilon = y_{sp} - y_m$ is the error signal (y_{sp} and y_m are set-point and measured variable), and K_c , τ_I and τ_D denote the proportional gain, the integral time and derivative time, respectively [102].

6.3.2 MATLAB interface

An interface for real-time acquiring, monitoring and plotting level sensor and flowmeter signals was developed in MATLAB. *Fig 49* show an example of this interface.

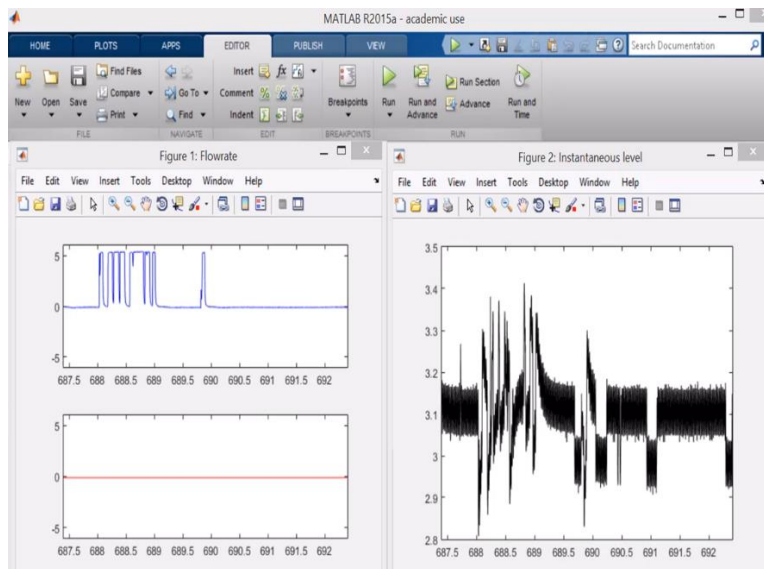


Fig 49. MATLAB interface.

6.3.3 Signal sending to the pumps

As it was discussed the pumps work as actuators to control medium level and flowrate in the bioreactor. An automatic adjustment of pumps rotational speed is necessary to automatically control level and flow rate, so the control system was run with sending a signal to pumps trough the DAQ box. The connection between the DAQ box

and the pumps by Analog interface was investigated in the section 6.2.4 related to pumps properties. The digital values for GND, remote, start, direction and internal speed were sent to the related pins as well as the analog value that was sent to the pump for rotational speed adjustment (*Fig. 42*).

6.4 Hydrodynamic and control experiment setup

The bioreactor was installed in an experimental setup with water in order to carry out the fluid dynamics characterization under operating conditions. The bioreactor was connected to the perfusion system consisting of a glass medium reservoir, tubing, two micro-peristaltic pumps, capillary-tank and flow and a level sensor that were connected to data acquisition board and computer for monitoring and acquiring data. The level sensor was calibrated carefully before filling the bioreactor.

In order to fill the bioreactor, the water enters from the reservoir into the membrane bioreactor by pump 1 with a fully controlled flowrate that was set on the desired set-point. Water was perfused in single-pass and the stream leaving the bioreactor by pump 2, recycled in the medium reservoir. The flowmeter was installed in order to measure and control the liquid flowrate in the inlet stream. The manual option of the pumps was deactivated and automatic mode was activated by sending signals through DAQ box in order to control pumps rotational speed. *Fig 50* shows a scheme of the experimental setup.

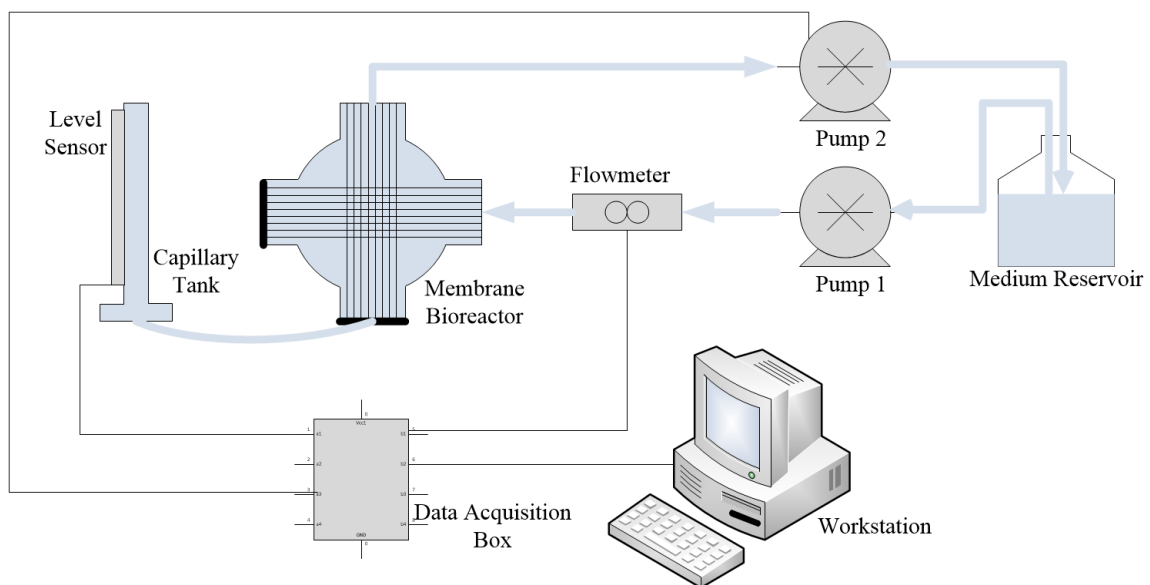


Fig 50. Experimental setup scheme.

Chapter 7

Modeling and control system development

7. Modeling and control system development

In this Chapter, a three-compartment model of the HFMBR bioreactor is presented in an original non-linear form as well as a linearized version. Both will be validated against simple filling experiments in the real bioreactor, as discussed in the next Chapter. Numerical solution of the models is carried out through Simulink block models so that the subsequent synthesis of the multiple feedback loops is facilitated. Control laws are devised for the loops of interest and the controller tuning procedure is described.

7.1 Three-compartment dynamic modeling of bioreactor hydrodynamics

In modelling the membrane bioreactor for control purposes the essential aspects of the process have to be taken into account, rather than microscopic (i.e. finite element) description. Therefore, with respect to the actual bioreactor configuration, various simplifying assumptions were considered to keep the mathematical derivation and real time solution simple. The physical system is composed of two hollow fiber membrane bundles in crossed configuration contained in a spherical glass enclosure that serves as the extra-capillary space (see Fig. 32 in Chap. 6). As discussed earlier, one fiber bundle is used for feeding the inlet stream containing oxygen and nutrients and the other one for extracting the effluent stream, both being in dead end configuration, i.e. with no retentate stream. To a first approximation, the flow paths inside the bioreactor can be considered to be represented as uniformly distributed from the inside of the feed bundle to the extra capillary space and then again uniformly out through the effluent membrane bundle. So, a lumped parameter compartment model appears appropriate to describe the hydrodynamics and species transport through the bioreactor. It was assumed based on De Bartolo et al. [6] study about residence time distribution (RTD). RTD was investigated through the introduction of tracer (step input) at the entrance of fibers and recording it in time at the exit of the fibers. The tracer, consisting in a solution of Williams' medium E, was sent to the bioreactor with flow rate of 1.5 ml/min and continuously monitored by online spectrophotometer (UV Cord Pharmacia, Uppsala, Sweden). After this fluid dynamics characterization, the bioreactor can be considered well mixed in the central part of its body, where hepatocytes are cultured in the extra-lumen side of crossing fibers.

In particular, the bioreactor system is modeled as composed of three distinct zones (see Fig. 1), assumed to interact as lumped parameter compartments separated by the hollow fiber surfaces, as follows:

1. A feed zone composed of a dead-end hollow-fiber membrane bundle (FB) (e.g. made by polyethersulphone, PES) providing oxygenated medium/serum feeds;
2. An intermediate space occupying the reactor inside shell surrounding the two membrane bundles, similar to the extra-capillary space (named ECS), which contains the cell culture;
3. The second bundle of dead-end hollow-fiber membranes in crossed configuration for the effluent stream (EB) (also made by PES in the present application).

A schematic representation of the hollow-fiber membrane bioreactor is shown in Fig 5/a. The corresponding three-compartment model is shown in Fig 5/b, where each compartment will be assumed as perfectly mixed. It should be noted that, as the configuration suggests, the dead-end membrane bundles are represented as closed volumes whilst the ECS is a variable liquid volume, as in operation the upper opening of the bioreactor enclosure is connected to an overflow line to avoid pressure build-up in case of reactor overfilling.

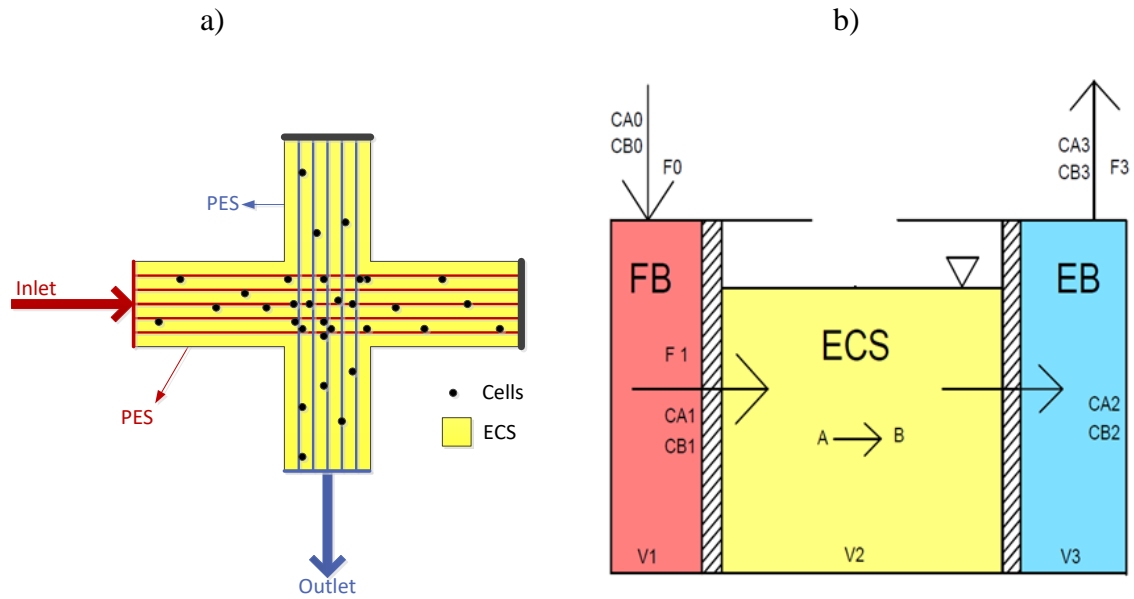


Fig 51. Hollow-fiber membrane bioreactor scheme (a) showing the feed bundle (FB) zone through polyethersulphone, PES, membranes in red, the cell culture environment (extra capillary space, ECS) in yellow and the effluent bundle (EB) zone through the second, crossed set of membranes (also PES) in blue; the corresponding simplified three-compartment model of the bioreactor is also represented (b), also showing the model variable names for flowrates (F), volumes (V) and concentrations of species like oxygen (CA) and urea (CB).

7.1.1 Mass balances

In the three-compartment representation of the membrane bioreactor, model hypotheses also include (i) uniform and constant density (the transport occurs into a large amount of medium), (ii) uniform and constant temperature, as guaranteed by operation within a fully controlled incubator, (iii) simplified biochemical kinetics with constant number of cells, as established for progenitor hepatic cell cultures, and (iv) geometrical relationship between the liquid volume and level height for the ECS (see below). Input variables are inlet concentrations C_{A0} , C_{B0} (concentration of oxygen required for the cell

metabolism (A) and urea as representative metabolism product (B)), and ECS inlet and outlet volumetric flowrates (F_1 , F_2). Due to the closed volume (and constant density) of the feed and effluent bundle conditions, all total flowrates upstream the ECS are equal; similarly, they are also equal downstream the ECS. As introduced in Chapter 6 and discussed below, F_1 and F_2 will be used as manipulated variables in the control system. State variables are all other (6) concentrations and the variable liquid volume in the ECS V_2 . The considerations which led to the design of the capillary tank (small liquid volume and filtered connection with the bioreactor) ensure that its presence does not affect the ECS liquid volume and concentrations if not marginally, so it is neglected in the model.

Constraints are the mass balances across the compartments, both overall and for individual species, including biochemical conversion of A (as a reactant) and B (as a product).

The set of non-linear model equations is:

$$\frac{dC_{A1}}{dt} = \frac{F_1}{V_1} (C_{A0} - C_{A1}) \quad (12)$$

$$\frac{dC_{B1}}{dt} = \frac{F_1}{V_1} (C_{B0} - C_{B1}) \quad (13)$$

$$\frac{dC_{A2}}{dt} = \frac{F_1}{V_2} (C_{A1} - C_{A2}) - \frac{V1_{max}C_{A2}}{K1_m + C_{A2}} \quad (14)$$

$$\frac{dC_{B2}}{dt} = \frac{F_1}{V_2} (C_{B1} - C_{B2}) + \frac{V2_{max}C_{A2}}{K2_m + C_{A2}} \quad (15)$$

$$\frac{dC_{A3}}{dt} = \frac{F_3}{V_3} (C_{A2} - C_{A3}) \quad (16)$$

$$\frac{dC_{B3}}{dt} = \frac{F_3}{V_3} (C_{B2} - C_{B3}) \quad (17)$$

$$\frac{dV_2}{dt} = F_1 - F_2 \quad (18)$$

where Eq. (12-17) are the component balances across the three compartments regarding conservation of oxygen (A) and urea (B) and Eq. (18) is the overall mass balance in the ECS. The latter was used in the previous ones to make the ODE be expressed explicitly in terms of concentration change with time. As shown in Eq. (14) and (15), Michaelis-Menten biochemical kinetics is assumed to be valid as overall kinetic rate term for both oxygen and urea [103]. $V1_{max}$ and $V2_{max}$ represent the maximum rate achieved by the system at maximum concentrations and $K1_{max}$ and $K2_{max}$ are the species concentration at which the reaction rate is half of $V1_{max}$ and $V2_{max}$ respectively.

A four-input/seven-state model of the bioreactor arises, with inlet concentrations, C_{A0} and C_{B0} , and inlet and outlet flowrates, F_1 and F_2 , as 4 input variables and the six concentrations and liquid volume in the ECS, V_2 , as 7 states. To solve the model and investigate control strategies for the bioreactor key variables, it is implemented within the MATLAB/Simulink[®] environment as a block diagram scheme (*Fig 57*). Dynamic simulations of the uncontrolled and controlled bioreactor will be discussed in Chapter 8.

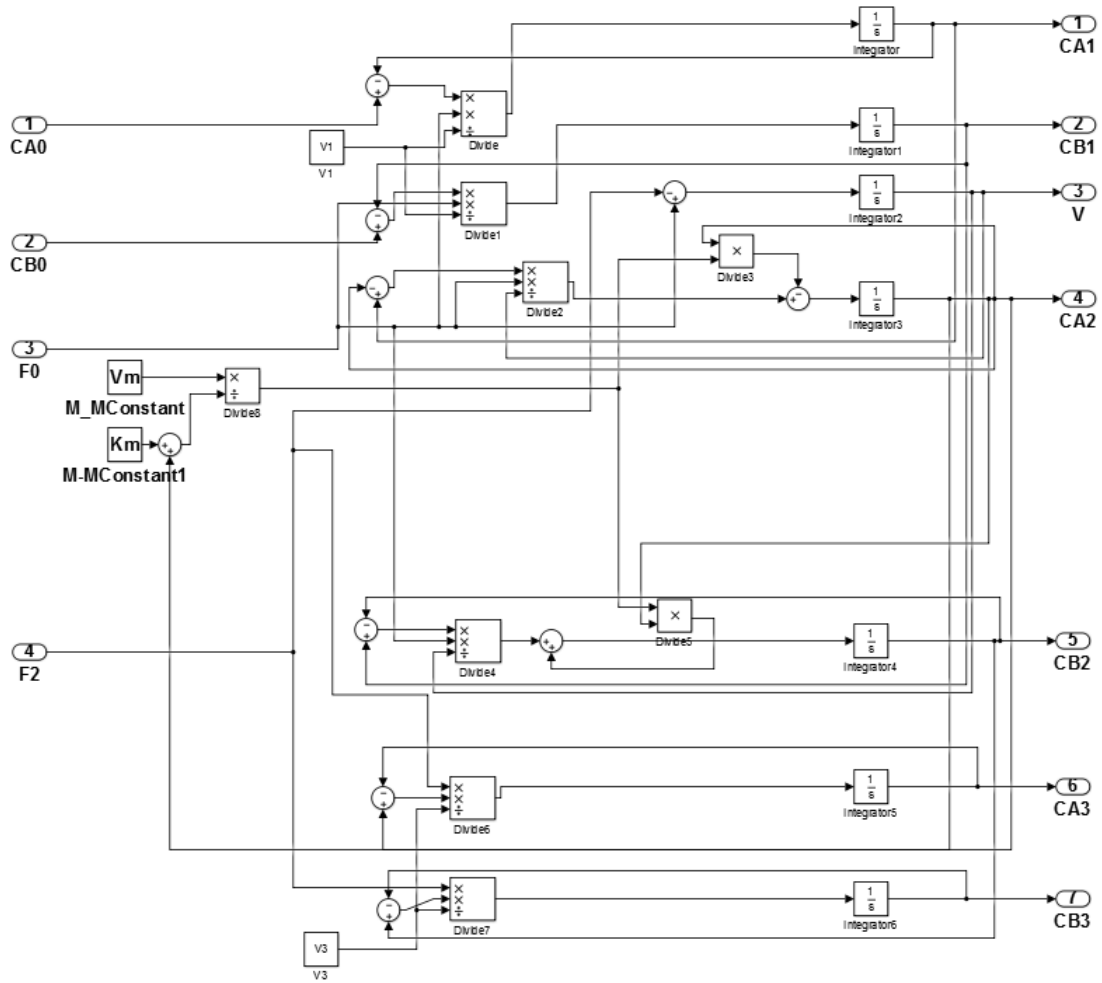


Fig 52. A Simulink block diagram of the three-compartment non-linear model.

The dynamic model is still incomplete, as the volume dynamics has to be converted into a liquid level to allow for its control. Since the geometry of the bioreactor enclosure is complex such relationship requires some simplifying assumption, as discussed in the following paragraph.

7.1.2 Geometrical description of the volume/height relationship

As shown in Fig 32, the shape of the cell culturing environment, i.e. the zone of the bioreactor hosting the (variable-level) ECS liquid, is geometrically complex. This affects the cross-sectional area at different heights, leading to a different sensitivity of the height (controlled variable) to changes in the volumetric flowrates (manipulated variables). According to the design, it is based on an external, approximately spherical shell with six relatively large connection ports, one for each side. Four of these (the lateral ones) are used for the membrane bundles. The top and bottom ones serve for overflow and sampling, respectively, and are considered inactive during regular operation. In addition, it shall be considered that deformation from the external spherical shape due to the lateral connections is very limited after membrane bundle assembling (Fig 32b) as the volume around the bundles is filled with glue.

The dependence of the liquid volume on height can be obtained by fitting expressions (e.g. polynomial) to experimental measurements during bioreactor filling. However, it is proposed to describe the required dependence by means of geometrical considerations, as this allows the model to be adapted to changes in the relative size of the bioreactor shape elements (sphere, connections, etc.). Therefore, a reasonable representation of the volume/height relationship in the cell culturing environment is by a spherical enclosure (with a central part of the volume occupied by the membrane bundles) plus two cylinders at the top and bottom (see Fig 53).

Formulation of the geometrical relation between the liquid volume and height is considered in five zones, which correspond to: the lower cylinder (Eq. 19), the spherical

cap below the fibre bundles (Eq. 20), the central region of the bioreactor through the bundles (Eq. 21), the upper spherical cap above the bundles (Eq. 22) and the upper cylinder (Eq. 23). As a reasonable approximation, the volume occupied by the fibres is subtracted linearly from the spherical volume as the liquid height increases, thus neglecting the cylindrical shape of the fibres and any liquid capillary rise. In general, the measured height \bar{h} can be compared with the modelled value h by subtracting the height of the bioreactor base h_0 , i.e. by comparing h and $\bar{h} - h_0$.

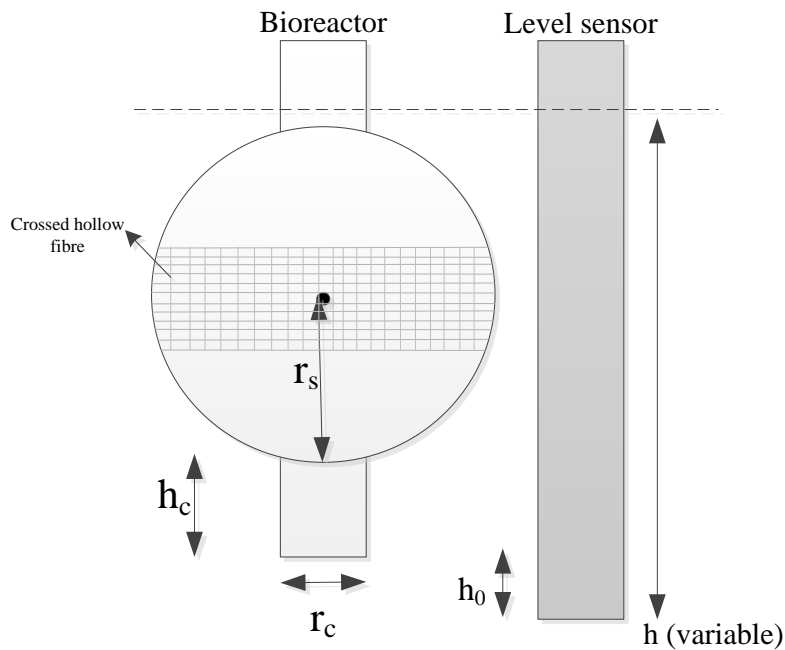


Fig 53. Assumed geometrical shape of the cell culturing environment with a variable liquid level within the bioreactor and level sensor range on the side.

The set of equations defined over the corresponding height intervals are reported below (see Table 9 for the variable definitions):

$$V = \pi r_c^2 h \quad (19)$$

for $0 \leq h \leq h_c$

$$V = \left(\pi r_c^2 h_c - V_{cap} + \frac{1}{3} \pi (h - h_c)^2 (3r_s + h_c - h) \right) \quad (20)$$

for $h_c < h \leq h_c + \left(r_s - \frac{H_{vlt}}{2} \right)$

$$V = \pi r_c^2 h_c - V_{cap} + \frac{1}{3} \pi (h - h_c)^2 (3r_s + h_c - h) - N_{row} V_{fib} \frac{N_{vlt}}{H_{vlt}} \left(h - h_c - \left(r_s - \frac{H_{vlt}}{2} \right) \right) \quad (21)$$

for $h_c + \left(r_s - \frac{H_{vlt}}{2} \right) < h \leq h_c + \left(r_s + \frac{H_{vlt}}{2} \right)$

$$V = \pi r_c^2 h_c - V_{cap} + \frac{1}{3} \pi (h - h_c)^2 (3r_s + h_c - h) - V_{fibt} \quad (22)$$

for $h_c + \left(r_s + \frac{H_{vlt}}{2} \right) < h \leq h_c + 2r_s - h_{cap}$

$$V = V_s - 2V_{cap} + \pi r_c^2 h_c + \pi r_c^2 (h - h_c - 2r_s) - V_{fibt} \quad (23)$$

for $h_c + 2r_s - h_{cap} < h \leq 2h_c + 2r_s$

Table 9. Parameter definitions for the geometrical description of the height change with liquid volume

Parameter	Definition
r_s	Radius of the sphere
h_c	Height of the cylinder
h_0	Height of the bioreactor base (as measured by the level sensor)
r_c	Radius of the cylinder
V_s	Volume of the sphere
N_{row}	Number of fiber rows
L_{fib}	Length of a fiber
r_{fib}	Radius of a fiber
V_{fib}	Volume of a fiber
H_{vlt}	Height of vertical layer total
N_{vlt}	Number of vertical layer total
V_{fibt}	Total volume of fiber
h_{cap}	Height of the small cap at the sphere/cylinder interface
V_{cap}	Volume of the small cap at the sphere/cylinder interface

Comparison of the analytical and experimental dependence of the liquid level on the volume for an actual filling operation of the bioreactor used is described in Chapter 8.

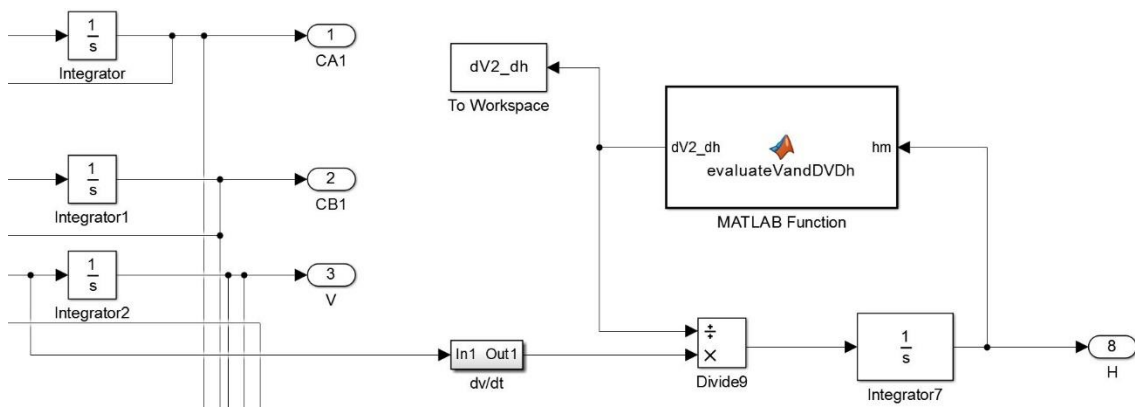


Fig. 54. Volume to height conversion in Simulink

As mentioned before the volume dynamics has to be converted into a liquid level to allow for its control and Fig. 54 shows the implementation of the height/volume relationship in Simulink. The volume was converted by the help of a MATLAB function with the name of *evaluateVandDVDh* that was pointed in Appendix A.

7.1.3 Linearization

The set of ODEs composed by Eq. (12-18) is non-linear in the model variables. The volume/height geometrical relationship adds some more non-linear terms. To make use of advanced control strategies like adaptive control or feedforward schemes, it is useful to derive an analytical linearized version of the three-compartment model, which could be later utilized to build a gain scheduling table (e.g. evaluating optimal gains for

models linearized around different operating points) for adaptive control or to estimate lead-lag units for a feed-forward complement to traditional feedback loop.

The linearized model is obtained by using the first-order Taylor series truncation of the non-linear terms expanded around the steady-state values of the variables. The procedure is conceptually simple but mathematically long and tedious. The full set of linearized equations corresponded to Eq. (12-18) is reported in the Appendix G. A representative linearized equation is shown below, e.g. for Eq. (12):

$$\frac{dC_{A1}}{dt} = \frac{F_{1ss}}{V_1} C_{A0} + \left(-\frac{F_{1ss}}{V_1}\right) C_{A1} + \frac{C_{A0ss} - C_{A1ss}}{V_1} F_1 \quad (24)$$

where the subscript *ss* denotes variable values at the steady-state.

According to the standard procedure, the linearized model allows building the **A**, **B**, **C** and **D** matrices of coefficients that can be used to derive the process transfer function matrix. Starting from the canonical form of the linear model in the state-space:

$$\begin{cases} \frac{dx}{dt} = \mathbf{A} \cdot \mathbf{x} + \mathbf{B} \cdot \mathbf{u} \\ \mathbf{y} = \mathbf{C} \cdot \mathbf{x} + \mathbf{D} \cdot \mathbf{u} \end{cases} \quad (25)$$

where

$$\mathbf{x} = \begin{bmatrix} C_{A1} \\ C_{B1} \\ h \\ C_{A2} \\ C_{B2} \\ C_{A3} \\ C_{B3} \end{bmatrix}; \quad \mathbf{u} = \begin{bmatrix} C_{A0} \\ C_{B0} \\ F_1 \\ F_2 \end{bmatrix}; \quad \mathbf{y} = \mathbf{x} \quad (26)$$

which leads to a transfer function matrix of the form

$$y = Gp \cdot u \quad \text{with} \quad Gp = \begin{bmatrix} G_{11} & \cdots & G_{14} \\ \vdots & \ddots & \vdots \\ G_{71} & \cdots & G_{74} \end{bmatrix} \quad (27)$$

The numerical elements (e.g. numerators and denominators) of the transfer function matrix can be easily derived based on the above-defined A , B , C and D matrices in the state-space domain.

A Simulink block diagram of the linear model is shown in Fig 55. In the block diagram scheme, each transfer function is analytically linked to the linearized form of the original equations and the steady-state conditions assumed at the beginning. Therefore, by changing the initial values of the variables the linearized block diagram version in Simulink is automatically updated.

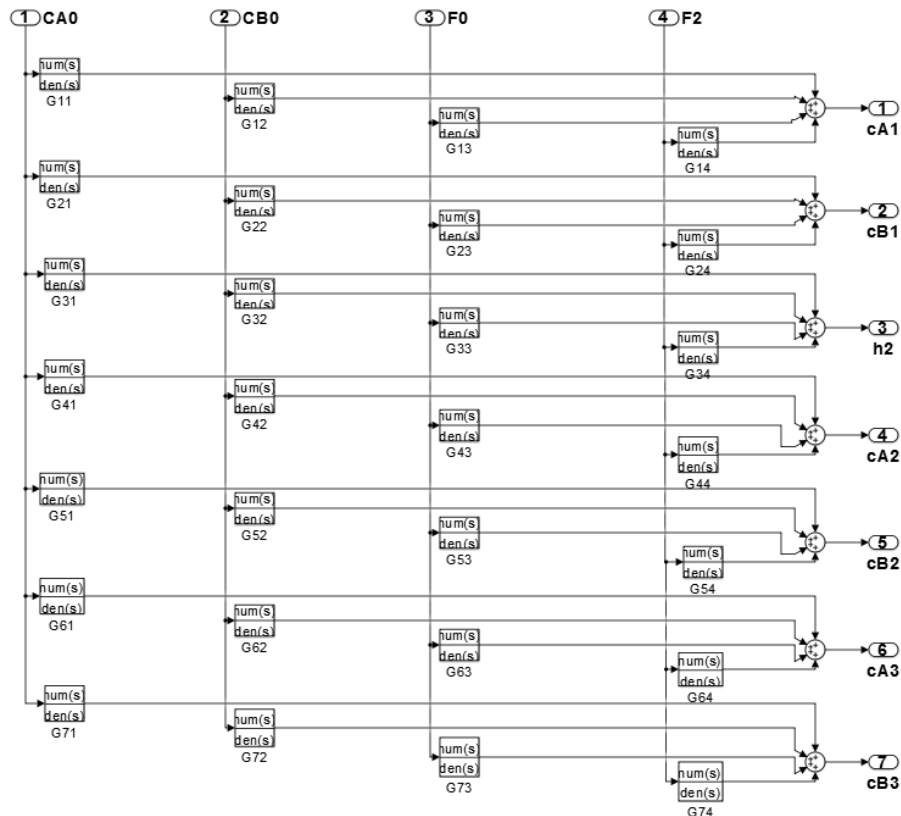


Fig 55. A Simulink block diagram of the linear model.

7.1 Control system development

7.1.1 Scheme for controlled variables

The availability of a process model allows developing and testing control systems for the cell culturing hydrodynamics and transport in the bioreactor. For the purpose of this work, liquid level height in the ECS and oxygen concentration (consumption) are the most important variable to control as measured output. Also, the possibility to set accurately the flowrates through the bioreactor would turn out convenient, as the volumetric pumps utilized to provide a quickly alternating flowrate whose average is difficult to keep at the desired value. A multi-SISO strategy for control of the above variables will be tested, as this may prove sufficient for the intended purposes. According to the experience and characteristic times of the system, flowrate can be set or varied through the rotational speed of the pump practically immediately, at a rate much higher than the other variables so pump speed/flowrate dynamics will be assumed ideal. Liquid level can be controlled by acting on the flowrate difference between inlet and outlet. The height dynamics can be slow or fast depending on the maximum flowrate difference (there is a maximum shear-rate that the cell can tolerate) and the current cross-section area. Species (e.g. oxygen or urea) transport at the typical bioreactor conditions requires a significant time to exhibit variations. So, overall, the system appears clearly decoupled thanks to the different time scale of the processes involved in the control system. Therefore, a set of conventional industrial regulators will be tested using mostly feedback

loops; in the case of level control, a feedforward addition can, in principle, improve the control speed of response and overall effectiveness.

7.1.2 Feedback multi-loop strategy with PID controllers

Process automation based on proportional-integral-derivative (PID) controllers is widely adopted in industrial operations. A PID control law is based on an error function $\varepsilon(t)$ intended as the difference between the desired *set-point* of the controlled variable and its currently measured value. It then determines a corrective action on the manipulated variable based on proportional, integral and derivative terms. The controller operates in the direction to minimize the error over time by adjustment of the manipulated variable $u(t)$, such as the position of a control valve, a damper, or the power supplied to a heating element to a new value determined by a weighted sum:

$$u(t) = K_c \varepsilon(t) + \frac{K_c}{\tau_I} \int_0^t \varepsilon(\tau) d\tau + K_c \tau_D \frac{d\varepsilon(t)}{dt} \quad (28)$$

The controller gain K_c acts as modulation parameter of the intensity of all actions, with the integral and derivative times, τ_I and τ_D , as parameters for the corresponding controller actions. By tuning the three parameters of the model, a PID controller can deal with specific process requirements. As compared to more advanced controllers (i.e. model-based), the use of feedback PID controllers does not guarantee optimal control of the system or even its stability [102]. However, it is robustness to model uncertainty and resilience to any possible disturbance.

Due to the appreciable amount of noise on the level signal (see Fig. 39) observed experimentally, the derivative action is not used to avoid continuous changes on the control signal to the pumps. So, multiple feedback loops, as generically represented in Fig 56 in terms of block diagram [104] will be utilized. In the model, sensors will be

assumed ideal dynamical elements. In analogy with the experiments, the actuators, in the present case variable speed pumps, will also be neglected in the simulations. Indeed, in the actual control experiments, it was possible to calculate the control action directly in terms of flowrate and then convert to electric signal via pump calibration curve before signal sending.

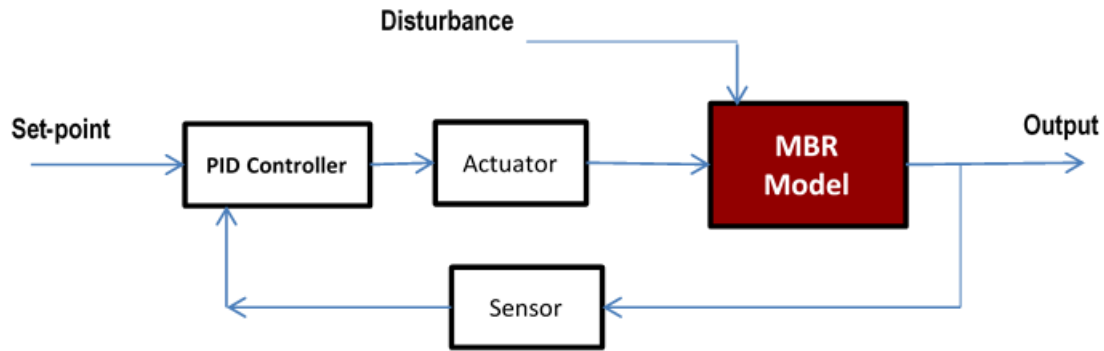


Fig 56. Block diagram of PID control system.

7.1.3 Input-output variable pairing and controller tuning

Input variables for control are the two flowrates (F_1 and F_2) and the inlet concentration of oxygen (C_{A0}). They will be used to control the nominal flowrate across the bioreactor (it could be either F_1 or F_2), the liquid level in the ECS (h) and the oxygen concentration in the ECS (C_{A2}) or output (C_{A3}). Note that in the experimental section concentration control was not considered due to the lack of availability of reliable, on-line measurements of the oxygen concentration in the ECS or output in the bioreactor. That is typically carried out off-line. However, since the inlet oxygen concentration could be available as manipulation variable owing to an oxygenation system dependent on the oxygen concentration in the incubator (that can be regulated), such an important addition is still kept in the simulation part of this work.

The availability of a process model enables the possibility to carry out systematic analysis of steady-state interaction between the loops, with the aim to select the best input-

output variable pairing (e.g. Relative Gain Array, RGA analysis). However, in the present case (intuition and) simple examination of the model equations show that the inlet concentration cannot affect the liquid level or flowrates, so it will be necessarily paired with the output oxygen concentration. Model equations and RGA would also show that either flowrate can be equivalently used for the level and flowrate control. So, the final choice was eventually dictated by experimental evidence that showed slightly smaller level oscillation when the manipulated variable was the outlet flowrate as compared to the inlet one.

The Simulink model with feedback loops is shown in *Fig 57*. As anticipated, the measurement elements' and actuators' dynamics were not considered. The process sub-model can be the non-linear or the linearized versions interchangeably.

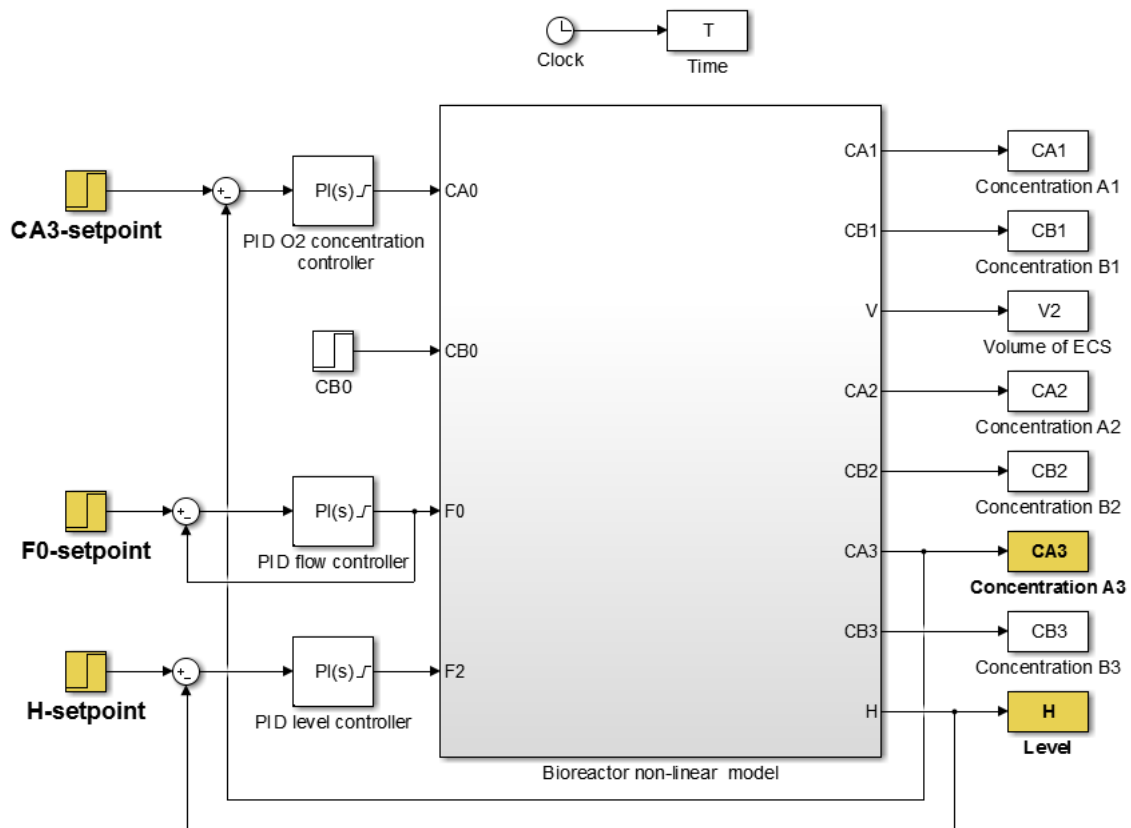


Fig 57. A Simulink simulation block diagram of the controlled MBR.

Finally, individual tuning has been carried out separately for each loop. As mentioned earlier, this is likely to be the final tuning (i.e. no detuning will be required) thanks to the time-scale decoupling typical of the present system.

A preliminary controller tuning was performed using the Simulink PID tuning system. The PID gains were tuned by Simulink PID tuner to achieve a good balance between performance and robustness. By default, the algorithm chooses a crossover frequency (loop bandwidth) based on the plant dynamics and designs for a target phase margin of 60° . When you interactively change the response time, bandwidth, transient response, or phase margin using the PID Tuner interface, the algorithm computes new PID gains. [104]. Subsequent comparison with experiments allowed a check in actual bioreactor conditions, as discussed in Chapter 8.

Chapter 8

Results and discussion

8. Results and discussion

In this chapter, the results of experimental tests and applications of the three-compartment model in the non-linear and linearized versions are illustrated and discussed. Using water as perfusion medium (without cells) verification of the geometrical relationship is proposed first. Typical simulated step responses in the relevant variables are presented, showing the difference between the non-linear and linear models. Application of control to the level and flowrate are then discussed, with some detail on tuning and discussion of the impact of signal noise. Experimental observations of the bioreactor level change and flowrate change under feedback control (i.e. set-point changes) are presented in order to examine the capabilities of the controller to monitor and keep the cell culturing conditions under control. In some case, one-way loop interaction is observed in the responses, but the overall behaviour remains well under control. Results of the dynamic simulations are also shown in the plots for comparison. Finally the results for level control in a fully operating membrane bioreactor in which hepatic cells were cultivated shows the improvements achievable thanks (also) to the PC-controlled operations.

8.1 Geometrical volume model validation

The variable cross-section of the bioreactor at different heights has a marked influence on the level dependence on volumetric flowrate changes. Therefore, the geometric description of the space inside the bioreactor enclosure (i.e. the cell cultivation environment as extracapillary space, ECS) needs an appropriate account. Design data were used to estimate the volumes involved around the membrane bundles, see *Table 10* for all parameter values.

Table 10. Geometrical Model validation parameter values

Experiment data		
F_{0s}	Inlet flowrate (ss*)	1.5 ml/min
F_{2s}	Outlet flowrate (ss)	0 ml/min
V_1	Volume of FB	0.003 ml
V_3	Volume of EB	0.003 ml
r_s	Radius of the sphere	19 mm
h_c	Height of the cylinder	15 mm
h_0	Height of the bioreactor base (as measured by the level sensor)	10 mm
r_c	Radius of the cylinder	7 mm
V_s	Volume of the sphere	28.52 ml
N_{row}	Number of fiber rows	10
L_{fib}	Length of a fiber	40 mm
r_{fib}	Radius of a fiber	0.25 mm
V_{fib}	Volume of a fiber	7.85 mm ³
H_{vlt}	Height of vertical layer total	10 mm
N_{vlt}	Number of vertical layer total	20
V_{fibt}	Total volume of fiber	1.57 ml
h_{cap}	Height of the small cap at the sphere/cylinder interface	1.33 mm
V_{cap}	Volume of the small cap at the sphere/cylinder interface	104.11 mm ³
*ss = steady-state		

A comparison between the geometrical model of the bioreactor volume (height vs. time) and the corresponding experimental values is presented below for a constant flowrate bioreactor filling procedure (*Fig 58*). As it is shown in the figure, the model predictions and experimental observations at the top and bottom of the bioreactor are very close together. The reason lays in the volume vs. height linear relationship in the cylindrical parts of the bioreactor. In the central part of the bioreactor, some difference can be observed, mostly due to the presence of the hollow fibers, which cause some local fluctuations due to the complex shape of the free volume of the fibers and the likely occurrence of capillarity. Overall, the accuracy of the representation of the liquid volume vs. height can be judged adequate for the requirements of the control, particularly because it is expected that the liquid level will be kept above the fibers under regular operation.

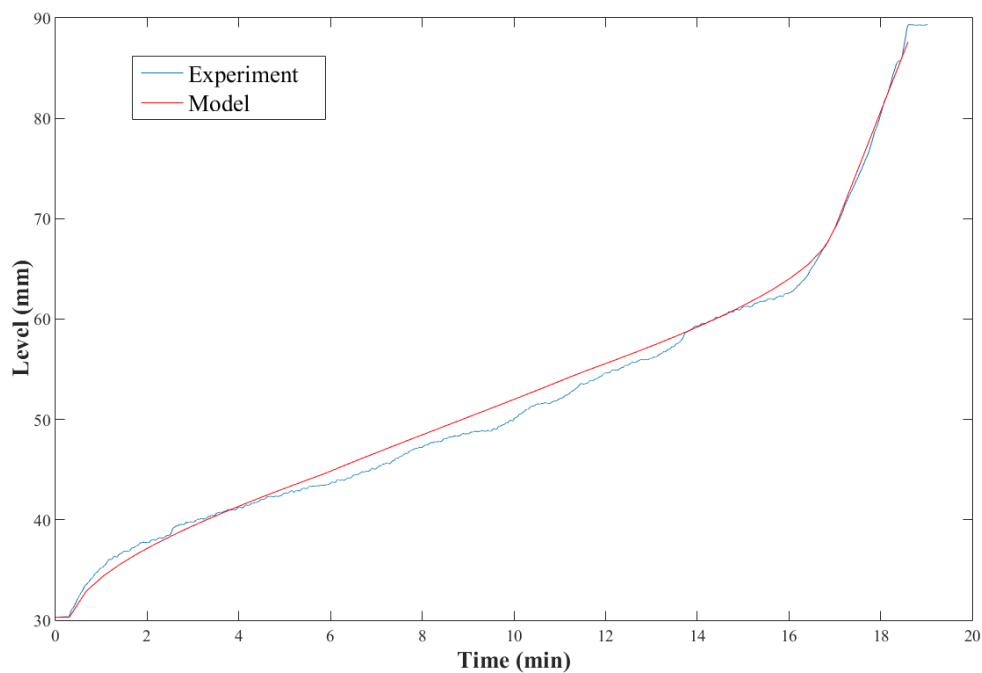


Fig 58. Comparison between the measured height and the model predictions during bioreactor filling at constant flowrate.

8.2 Level dynamics – comparison of the linear and non-linear model results with experiments

Using water as ideal medium experiments have been conducted to study the level dynamics in the bioreactor as occurring during actual operation. Starting from an initial level height of about 42 mm and a steady state (both inlet and outlet) flowrate of 1.03 ml/min, a decrease in the outlet flowrate to 0.73 ml/min has been set and height evolution registered. The about 30% flowrate decrease was obtained by manually changing suddenly the rotational speed of the pump. *Fig 59* shows the corresponding signal as measured by the flowrate sensor, mounted on the outflow line for this test. The straight line represents the corresponding ideal change used in the simulation. The noise in the flowrate signal is due to the particular oscillating flow produced by the peristaltic pump, which the high-speed acquisition sensor can detect rather accurately. The corresponding level evolution is shown in *Fig 60*, where the experimental value is compared with the predictions of the non-linear and linearized models. It can be seen that the non-linear model follows the experimental evolution closely for all the height range, as already shown in Section 8.1. The linearized model exhibits a very similar initial increase, which makes the predicted response highly accurate. At longer times, or at larger deviations, however, the evolution of the height obtained with the linearized model continues indefinitely as a linear increase (the system is a linear integrator), deviating from the actual observation. As with any linearization, the goodness of the approximation is somewhat proportional to the closeness of the current values to the initial value (i.e. the linearization point). The both inlet and outlet flowrate were adjusted and changed manually with manual interface existing on top of the pumps.

The comparison in *Fig 60* shows that the ECS level changed from 42 mm to 65 mm after about 42 min. A few minutes later, the bioreactor volume is completely filled, which is the condition when liquid overflow from the bioreactor start to happen. This time compared with the time needed to perform cell culture experiments (1 month) is very low and this reflects the importance of the control system to the bioreactor.

Finally, although it is more complex than the linearized one, the non-linear model turns out to be a very good choice for model-based control. Results of the control design and tuning are discussed in the next Section.

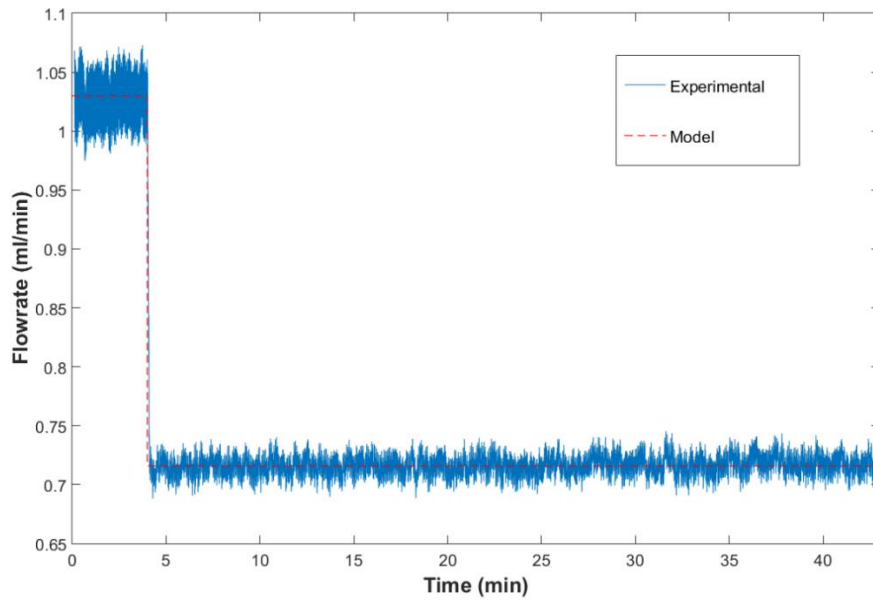


Fig 59. Step change from 1.03 to 0.73 ml/min in the outlet flowrate.

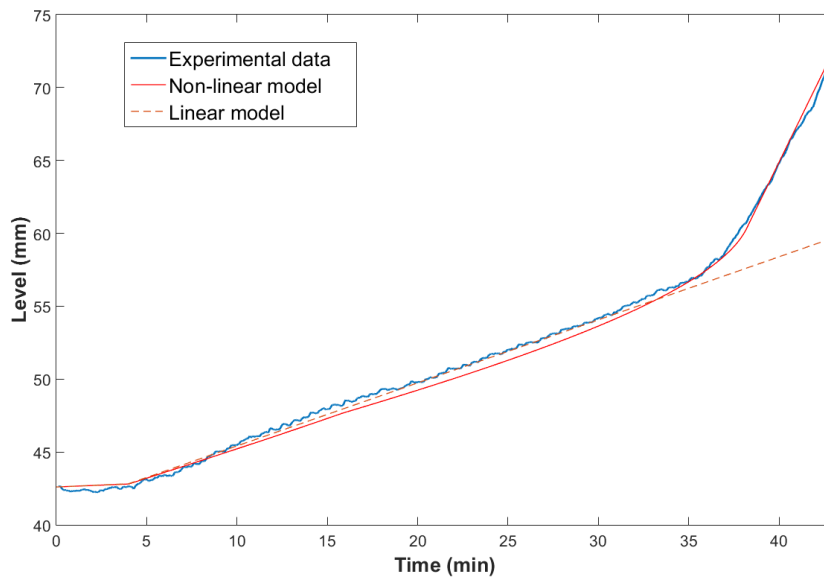


Fig 60. The response in the level height of the linear, Linear, and experimental data to a step change in outlet flowrate.

8.3 System response to step change in input variables – non-linear and linearized models

Implementation of the three-compartment model within the MATLAB environment (control system toolbox) and the Simulink environment allows straightforward computing of output responses to the (e.g step) changes of the input variables. The dynamic analysis of the model can be carried out both in terms of the non-linear and linearized versions, as described in Chapter 7. Output responses to selected input step changes are reported in Fig. 61, Fig. 62 and Fig. 63. To maintain realistically finite stimuli, step amplitudes of the input variables are selected to be the 50% of the corresponding initial value.

Similar to the non-linear model results, not all changes in the inputs alter the values of all the outputs. Typically, the level does not exhibit dependence on e.g. inlet concentrations. On the other hand, changes in the flowrates produce significant modifications of the amount of material in the reactor (V_2) as well as modification of the concentration of feed/product compounds. The latter effect results at least from a “dilution” (or concentration) effect as well as interaction with the conversion by means of the residence time in the reaction zone. The integrating effect of the system as a result of a change in only one flowrate (either inflow or outflow) is also quite evident from Fig. 61, Fig. 62 and Fig. 63. The effect on the accumulated volume V_2 is evident, but also the concentrations of A and B eventually show a theoretically indefinite increase or decrease.

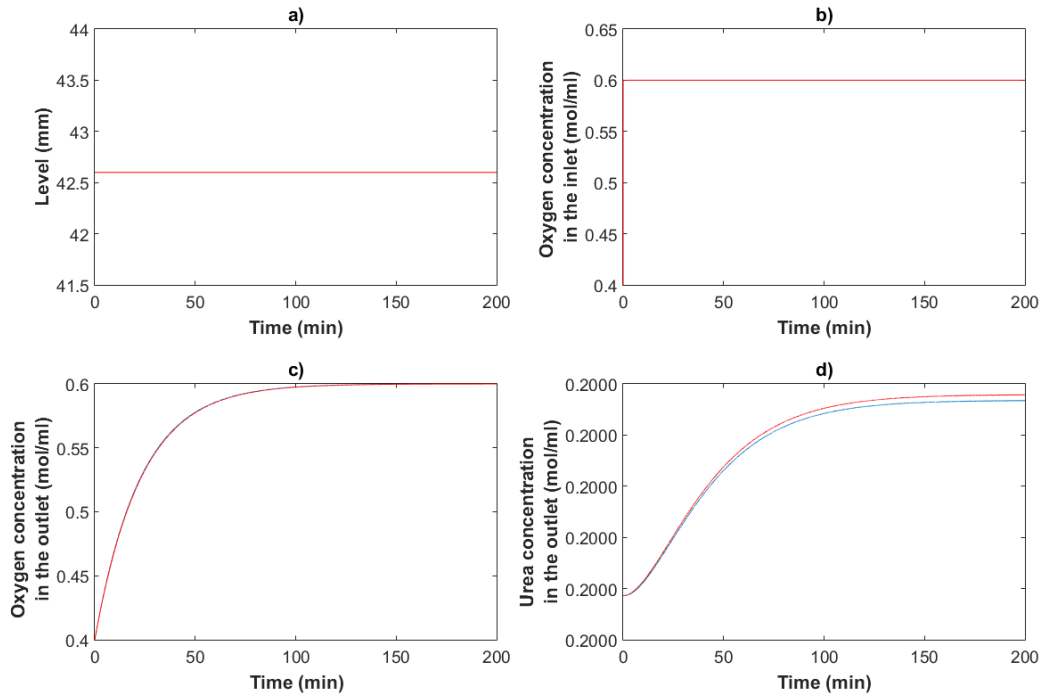


Fig. 61. Response of 4 variables: **a)** Level, **b)** Oxygen concentration in the inlet, **c)** Oxygen concentration in the outlet and **d)** Urea concentration in the outlet for an input step change (increasing 50% of Oxygen concentration in inlet)

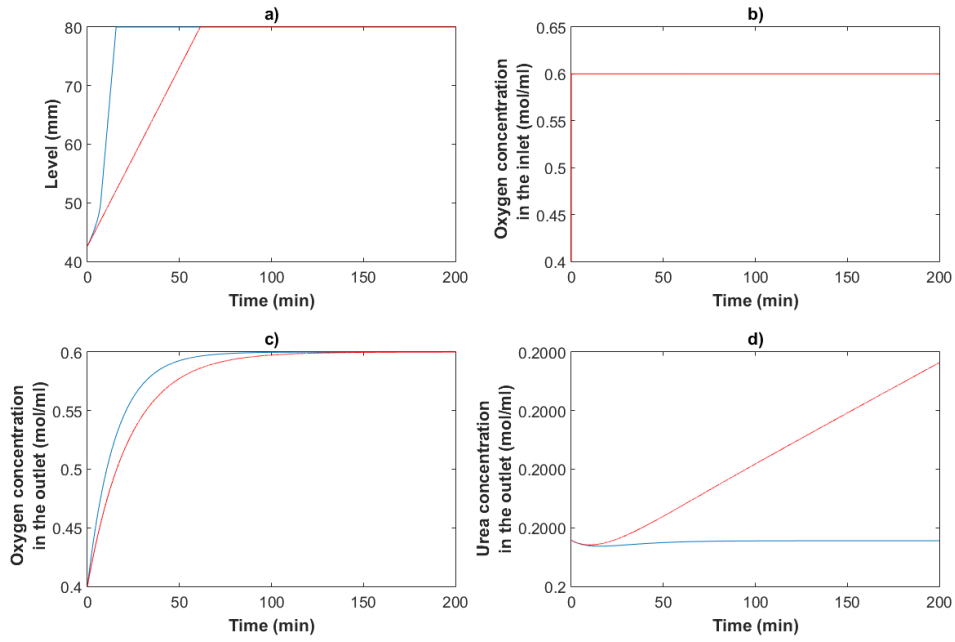


Fig. 62. Response of 4 variables: a) Level, b) Oxygen concentration in the inlet, c) Oxygen concentration in the outlet and d) Oxygen concentration in the outlet for an input step change (decreasing 50% of Oxygen concentration in inlet and increasing 50% of inlet flowrate)

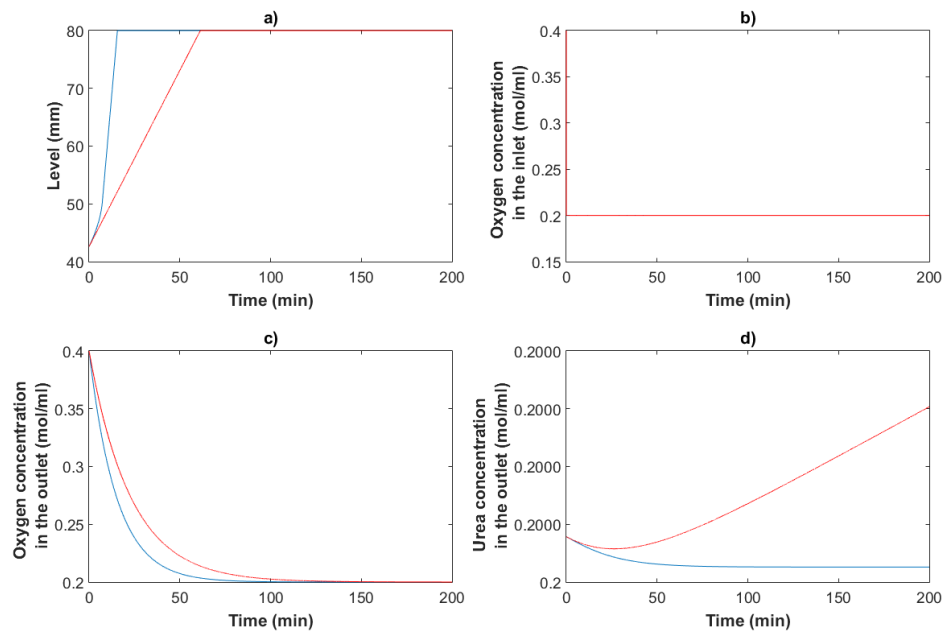


Fig. 63. Response of 4 variables: a) Level, b) Oxygen concentration in the inlet, c) Oxygen concentration in the outlet and d) Oxygen concentration in the outlet for an input step change (increasing 50% of Oxygen concentration in inlet and inlet flowrate)

8.4 Control system and controller tuning

In this part of the thesis, the benefits of the control system are discussed. As described in the previous section, the control system has many advantages, especially in the bioreactor performance. To improve the understanding of issues in actual operation and explore strategies to mitigate their effect on the controlled variables, changes are applied to the inputs one-by-one.

As can be seen in Fig 64, by increasing the outlet flowrate, the bioreactor reacts quickly and the height of the liquid begins to decrease very fast. In the case of no adjustment, this goes on until the bioreactor is completely empty, and this would happen in less than 25 minutes. It is clear that even a small difference between the inlet and outlet flowrates in manual operation can cause bioreactor flooding (bioreactor fill-up) or empty. Such issues are particularly annoying when they occur during cell culture, during overtime of the working days or across the weekend, as typically the cells die and the experiment has to be completely repeated.

On the other hand, by creating and installing a control system (possibly based on an appropriate model, as discussed in the previous sections), the performance and the efficiency of the bioreactor system can greatly improve. After a typical increase of the 10% increase of the outlet flowrate, the ECS level has a sharp decrease in the system without a controller. On the other hand, in the system with PI controller the level will return to the level set point in few minutes by the controller. A comparison between the response of the system to change in the outlet flowrate (disturbance) with and without controller are shown in Fig 64.

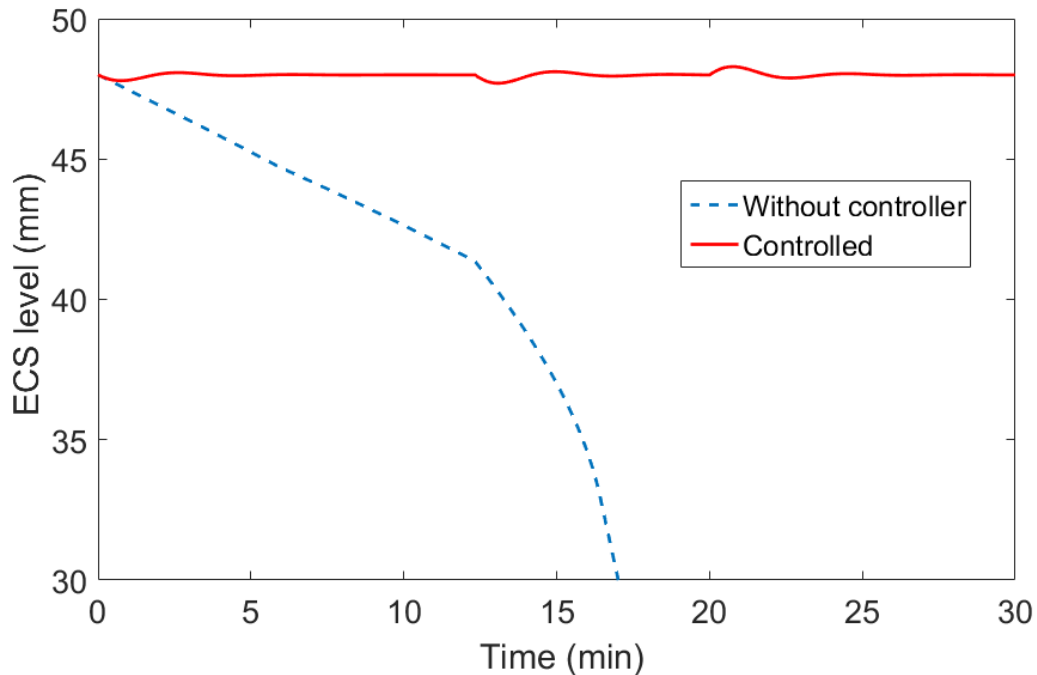


Fig 64. A comparison of the simulated MBR model response with and without controller (response of ECS level to 10% increase of outlet flowrate).

Level controller tuning was performed by using the PID Tuner tool of the Simulink PID Controller. It provides a fast and widely applicable single-loop PID tuning method for the blocks. With this method, the PID controller parameters were tuned to achieve a robust design with the desired response time. A typical design workflow with the PID Tuner involves the following tasks:

- Launch the PID Tuner. When launching, the software automatically computes a linear plant model from the Simulink model and designs an initial controller.
- Tune the controller in the PID Tuner by manually adjusting design criteria in two design modes. The tuner computes PID parameters that robustly stabilize the system.
- Export the parameters of the designed controller back to the PID Controller block and verify controller performance in Simulink. Table 11 shows a comparison between without tuning and tuned controller.

Table 11. Without tuning and tuned controller parameters

Controller parameters		
	Initial setup	With tuning
K_c	-0.1	-1
τ_I	-0.1	-3
τ_D	0	0
Rise time	2.97 s	0.531 s
Settling time	90.6 s	6.73 s
Overshoot	71.7 %	44.6 %

As it is shown in *Fig 65*, a comparison in step response of each loop in order to compare the system with and without tuning was done independently. As expected, the tuned controller works much faster with significantly fewer oscillations both in control variable which is bioreactor level (*Fig 65a*) and manipulated a variable that is outlet flowrate (*Fig 65b*).

In this part, the importunacy and effect of controller tuning were mentioned by comparing the system in two different conditions (with and without tuning) and it is obvious that the default parameters of the Simulink controller are generally not correct for a specific case.

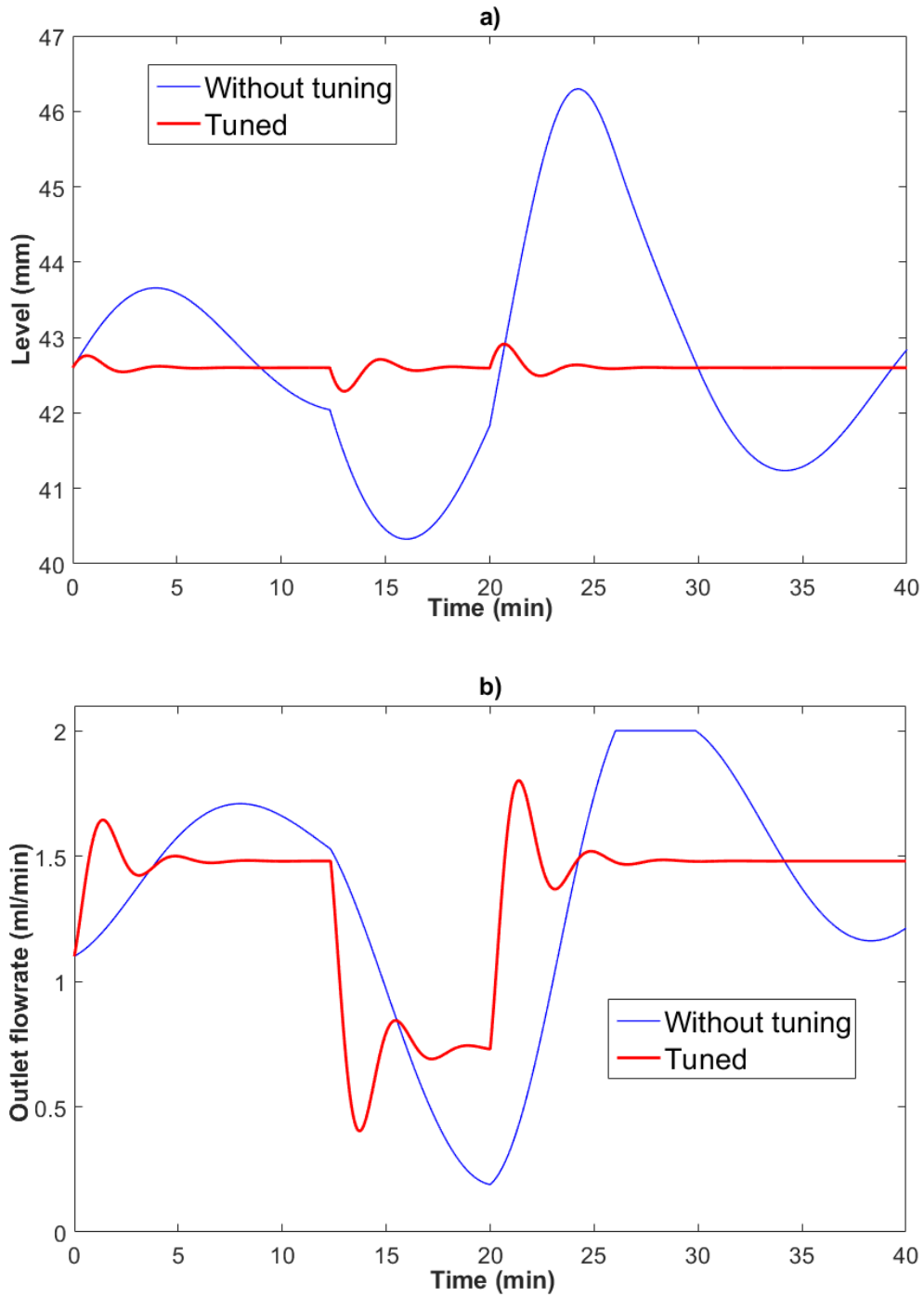


Fig 65. Comparison of the system with and without tuning. a) Liquid level, b) Outlet flowrate (manipulated variable)

8.5 Level control

8.5.1 Level setpoint step-change

Initial tests on the hydrodynamics were carried out using water as recirculating medium. The level control system is tested first under servo-mode and when subjected to potential disturbances. Starting from a steady-state condition, level set-point changes are applied to check the speed and quality of the response and control performance. Table 12 lists the parameter values for this set of experiments.

Table 12. Level control parameter values

Experiment data		
F_{0s}	Inlet flowrate (ss*)	1.1 ml/min
F_{2s}	Outlet flowrate (ss)	1.1 ml/min
$acqrate$	Acquisition rate	10 frames/s
$acqtime$	Acquisition time	1/10 s
$avgtime$	Averaging time	6 s
K_c	Controller gain	-1 ml/min/mm
t_I	Integral time	20 s
t_D	Derivative time	0 s
Q_{min}	Minimum flowrate for anti-reset windup	0 ml/min
Q_{max}	Maximum flowrate for anti-reset windup	2 ml/min
*ss = steady-state		

The control system behaviour and the comparison with experimental data are discussed below. The plot in Fig 67 shows the level control system in action. The experiments are carried out with a 10 by 10 mm step-change in the level setpoint from 80 to 50 mm. The Fig 66 and Fig 67 illustrate a comparison between the dynamic model and experimental data in terms of flowrate and level change. It can clearly be seen that there is a large increase in the (manipulated) outlet flowrate at the time instants of decreasing the level set-point in order to adjust the level. The plots for the experimental data and the

model show a similar trend. The typical characteristic time of the response to increases in the flow rate is different from test to test. This is due to the non-linearity induced by the geometrical shape of the bioreactor, which is evident for the level changes between 60 and 50 mm.

As it can be seen, at times where setpoint changes occur the control system takes corrective actions by increasing the outlet flowrate to the maximum allowed, in an attempt to adjust the liquid level towards the desired value. Indeed, Fig 66 also shows saturation conditions for the flowrate (0 as minimum and 2 ml/min as maximum) as set by stress sensitivity constraints, occasionally hit by the actual flowrate during manipulation. The cut off is imposed in the implemented control algorithm through a limitation of the signal sent to the pump. Care has been paid to ensure anti-reset wind-up through a velocity formulation of the digital control law (see Chapter 7).

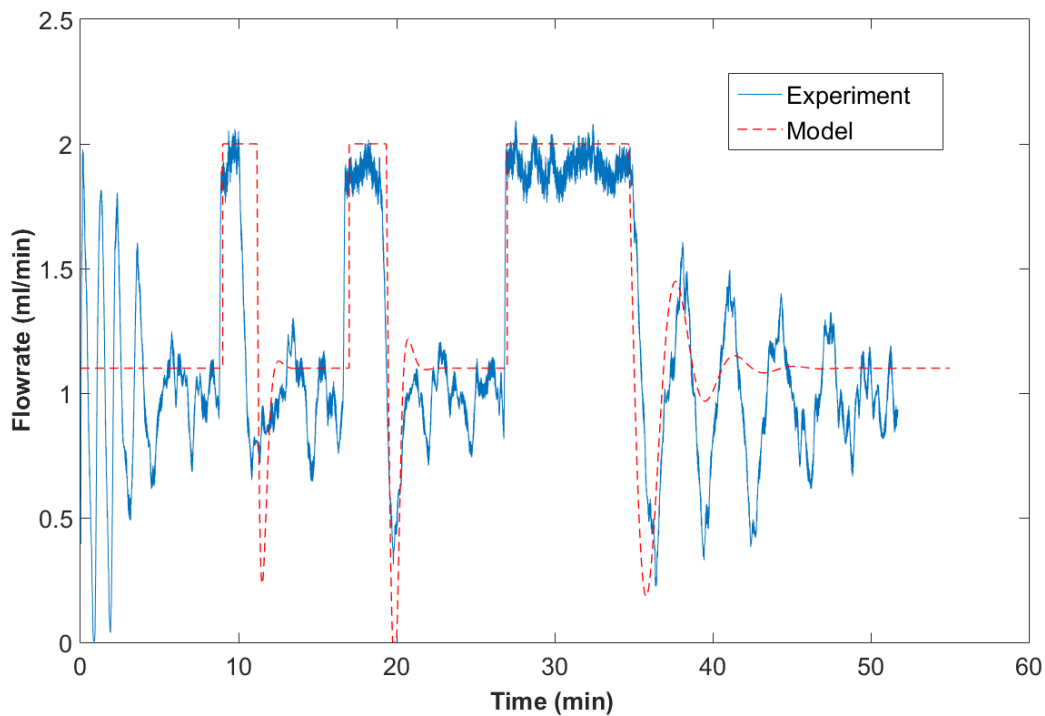


Fig 66. Measured flowrate variation (manipulated variable in the level control loop) as a result of step-changes in the level set-point in 10-by-10 mm steps from 80 to 50 mm.

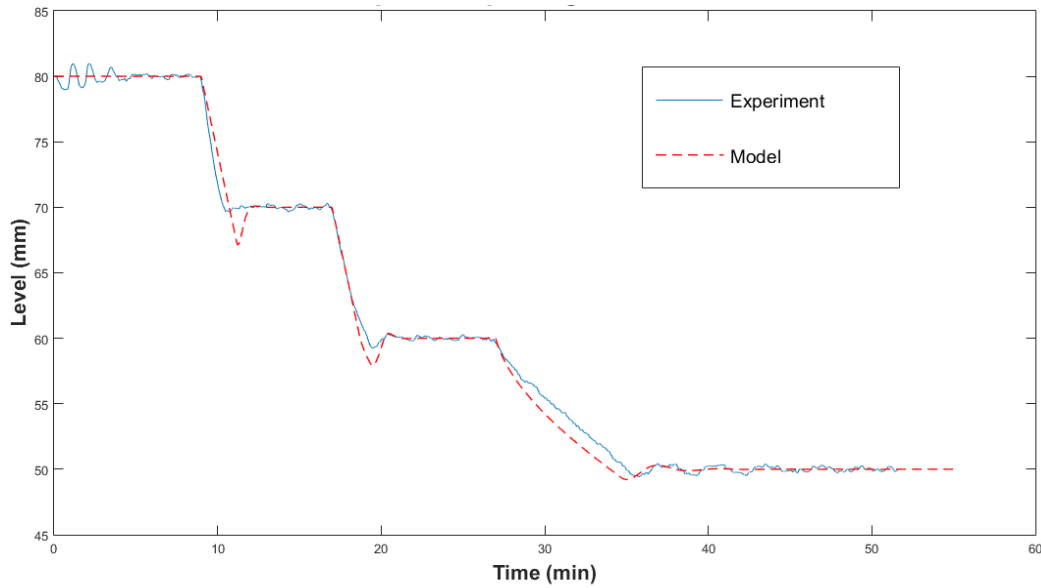


Fig 67. Measured level evolution (controlled variable) as a result of step-changes in the level set-point in 10-by-10 mm steps from 80 to 50 mm.

It can be noticed that whenever the height reached the steady-state desired values, the manipulated flowrate corresponded to the inlet (constant) flowrate. As compared to the simulations, obviously, irregular oscillations in the real system are clearly visible. The reasons for this phenomenon are not constant flowrate produced by the pumps, level sensor sensitivity and other possible sources of noise.

Similar experiments were carried out in the reverse direction, increasing the level setpoint from 50 to 80 mm, in 10-by-10 mm steps. As shown in *Fig 68*, the flowrate decreases suddenly when setpoint increases are imposed (*Fig 69*). In this case, the lower saturation conditions are hit, i.e. zero flowrate due to zero pump speed. In this case, the accuracy of the model at the largest cross-sectional area conditions (50 to 60 mm set-point change) appears somewhat smaller.

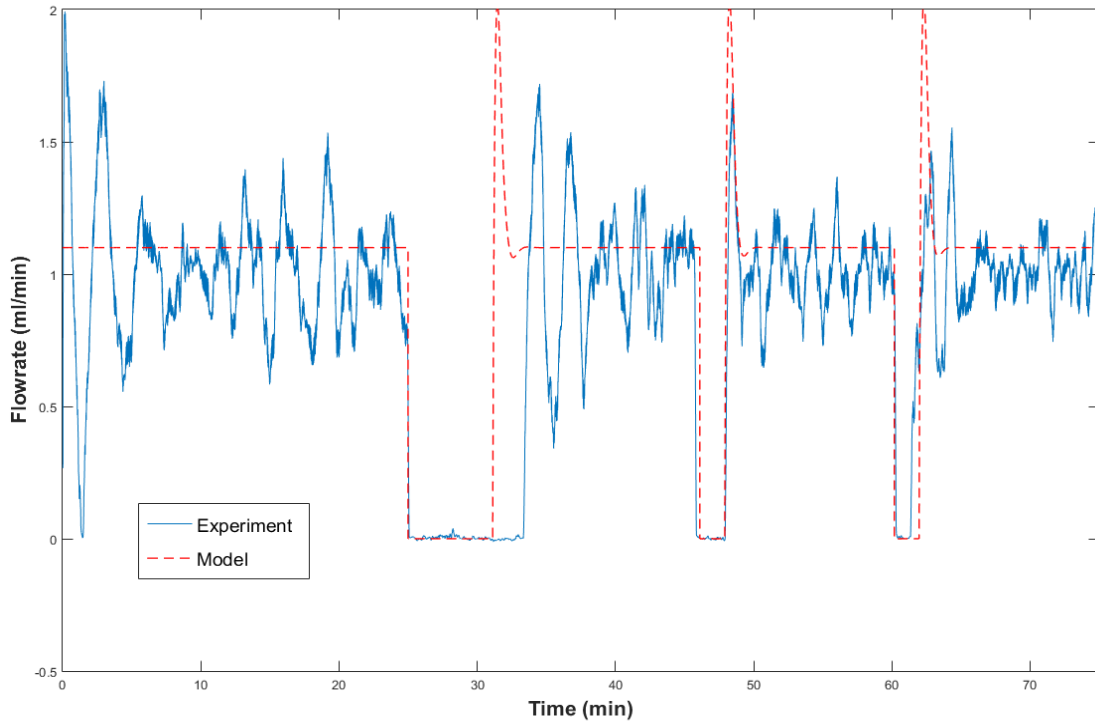


Fig 68. Measured flowrate variation (manipulated variable in the level control loop) as a result of step-changes in the level set-point in 10-by-10 mm steps from 50 to 80 mm.

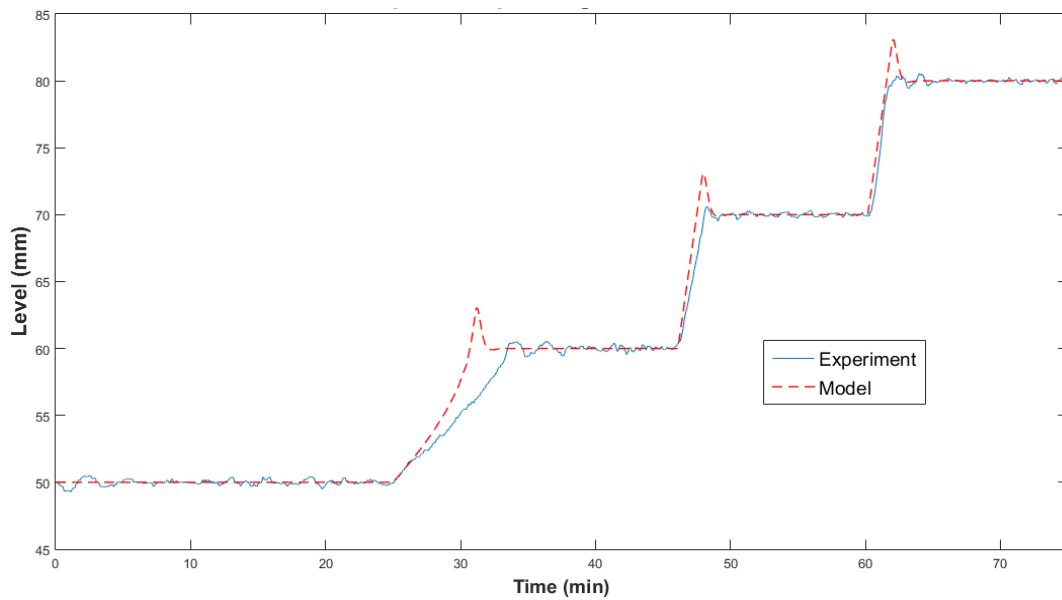


Fig 69. Measured level evolution (controlled variable) as a result of step-changes in the level set-point in 10-by-10 mm steps from 50 to 80 mm.

8.5.2 Inlet flowrate step-change

In the real system for cell culture, there are several possible causes of external disturbances and a well-designed control system against these disturbances is very important to the success of prolonged, continuous operation of the bioreactor. As already mentioned, the flowrate and consequently the medium level can change as a result of phenomena like membrane fouling and resistance build-up in the hollow fiber membrane, which cause pressure increase upstream. So it is vital to investigate also the capability of the level control system to deal with inlet flowrate (i.e. disturbance) changes, under the hypothesis that the inlet flowrate will not (yet) be controlled.

Fig 70 shows the instantaneous values of the outlet flowrate (manipulated variable) as measured by the flowrate sensor and calculated by simulation using the non-linear model when the level is to be kept at a set-point of 60 mm. The input change was in the inlet flowrate from 1.48 to 0.73 ml/min at minute 12.3 and the reverse at minute 20, respectively. As shown in *Fig 70*, the outlet flowrate was adjusted by the controller based on new inlet flowrate in order to keep the level constant. It experienced a sharp drop at minute 12.3 and a corresponding jump at minute 20.

As the *Fig 71* illustrates, the level dropped and peaked, respectively, as soon as the disturbance were applied to the system. However, the control system was able to change the level back to the set-point in 1 minute or so. Model results are also plotted together with the experimental records. Despite the experimental trends show significant irregular variations, the model results agree reasonably with them.

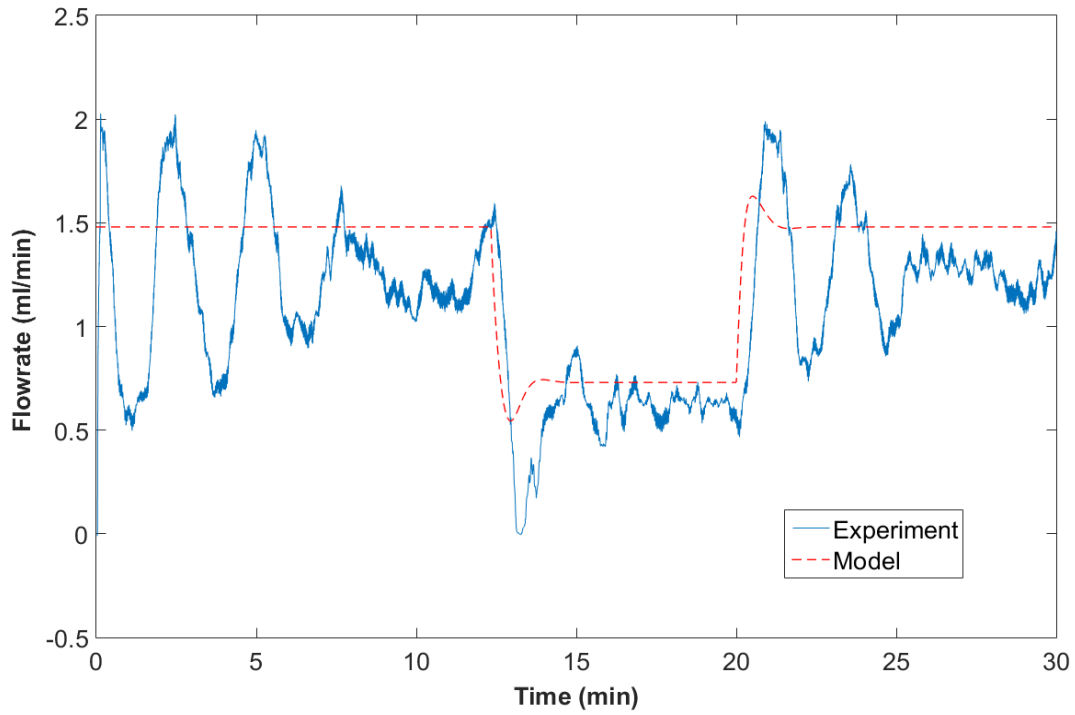


Fig 70. Measured outlet flowrate variation (manipulated variable in the level control loop) as a result of two (visible) step-changes in the inlet flowrate from 1.48 to 0.73 ml/min.

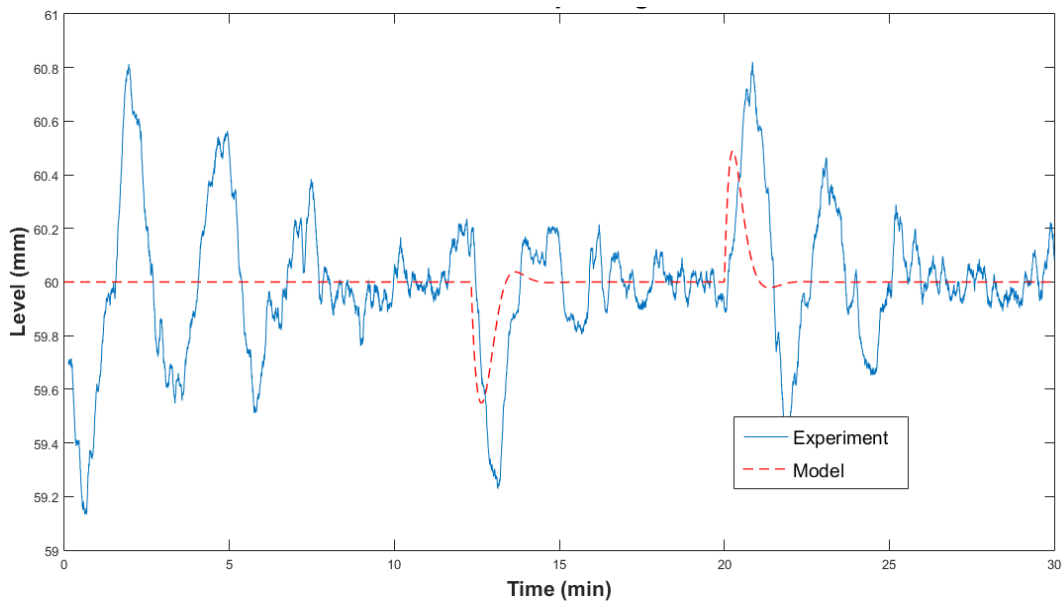


Fig 71. Measured level evolution (controlled variable) as a result of two (visible) step-changes in the inlet flowrate from 1.48 to 0.73 ml/min.

It is clear from *Fig 71* that the level control system, despite an appreciable level of noise and a variable flowrate, the performance of the control system is well suited for the control requirements of the bioreactor. The maximum deviations are within 0.8 mm of maximum discrepancy, which is negligible for the intended applications. In addition, the action of the controller appears quite rapid, with characteristic times appropriate for the slow dynamics of the culturing environment.

8.6 Flowrate control (full hydrodynamics control)

As it is well understood, the level control introduced until now does not ensure any particular value of the operating flowrate across the bioreactor. It only acts to keep inlet and outlet flowrates to be equal, no matter to what value. Indeed, if by accident the disturbance flowrate becomes zero, the level control system will shut the system down by setting to zero also the manipulated flowrate. The level set-point condition would be satisfied and no indication of error would be given to the operator. To control the full bioreactor hydrodynamics, a flowrate loop is also necessary, by making use of the other flowrate available for manipulation (through the second pump). By multiple simultaneous connections to the pumps through the Daq control box, such a system was synthesized via PC-control and put in action in parallel to the level control system.

In this section, experimental tests similar to the level control tests were carried out in order to check the ability of the flowrate control system to act promptly and to investigate possible interactions with the level loop. Full hydrodynamics control parameters and variables are listed in *Table 13*.

Table 13. Full hydrodynamics control parameters and variables

Experiment data		
F_{0s}	Inlet flowrate (ss*)	1.1 ml/min
F_{2s}	Outlet flowrate (ss)	1.1 ml/min
$acqrate$	Acquisition rate	10 frames/s
$acqtime$	Acquisition time	1/10 s
$avgtime$	Averaging time	6 s
K_c	Controller gain (level controller)	-1 ml/min/mm
t_I	Integral time (level controller)	20 s
t_D	Derivative time (level controller)	0 s
Q_{min}	Minimum flowrate for anti-reset windup (level controller)	0 ml/min
Q_{max}	Maximum flowrate for anti-reset windup (level controller)	2 ml/min
K_{cfr}	Controller gain (flowrate controller)	2 ml/min/mm
t_{Ifr}	Integral time (flowrate controller)	0.01 s
t_{Dfr}	Derivative time (flowrate controller)	0 s
Q_{min}	Minimum flowrate for anti-reset windup (flowrate controller)	0 ml/min
Q_{max}	Maximum flowrate for anti-reset windup (flowrate controller)	2 and 3 ml/min
*ss = steady-state		

8.6.1 Inlet flowrate step-change

In the first set of experimental tests, inlet flowrate set-point changes were investigated. The desired inlet flowrate was increased from 0.5 to 1,5 ml/min in steps of amplitude 0.25 ml/min. *Fig. 72* shows the result related to the first experiment. The figure is divided into 4 plots: inlet flowrate evolution (a), voltage signal sent to the pump 1 (flowrate controller) (b), bioreactor liquid level (c) and voltage sent to the pump 2 (level controller) (d).

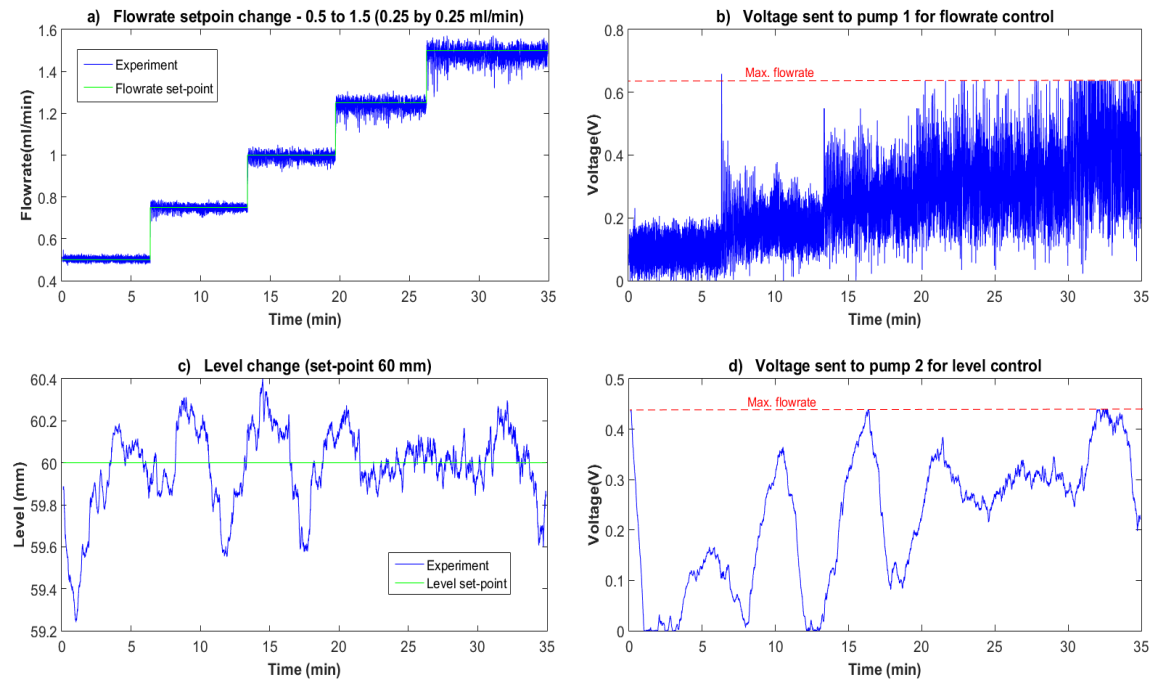


Fig. 72. Inlet flowrate set-point change (0.5 to 1.5 ml/min- by 0.25 ml/min step changes) - inlet flowrate (a), voltage sent to the pump 1 (flowrate controller) (b), bioreactor liquid level (c) and voltage sent to the pump 2 (level controller) (d).

In the plot, *a* the experimental data (step changes of the flowrate set-point) and the actual setpoint are shown by blue and green colors, respectively. The maximum allowed flowrate which was defined in the control system software is shown by dash red color in plots *b* (3 ml/min) and *d* (2 ml/min). As it can be seen from *Fig. 72* in part *b* the voltage proportionate of the flowrate was sent to pump 1 in order to adjust and control the flowrate in its set-point. The change can be seen clearly, especially in step time (6, 14, 20 and 27 min).

In this experiment, the level setpoint was set to 60 mm as it is shown in plot *c* by the green line. The oscillation around the set-point, produced by control system can be seen from the *Fig. 72* in plot *c*, but the effect of flowrate control system is not significant to identify. In the other hand, the loop interaction and the effect of flow control system

on the level and consequently on the voltage sent to pump 2 by the level control system is clear especially in the step time point (6, 14, 20 and 27 min) and part *d* shows it.

Fig. 73 presents an experiment similar to the previous one, with an inlet flowrate set-point change, changed in reverse mode by increasing the flowrate step by step. The figure confirms the results discussed before. The plots *b* and *d* show an expected decreasing trend in voltage both in pumps 1 and 2. The data show a reasonable fixed medium level by the level controller in plot *c*.

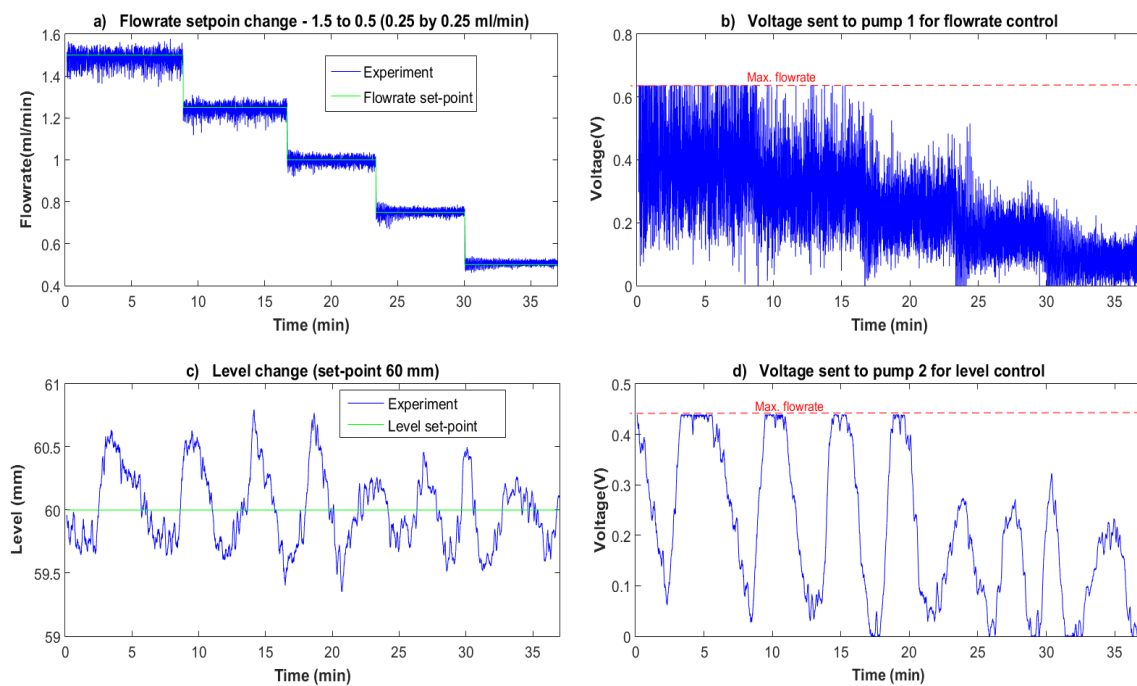


Fig. 73. Inlet flowrate set-point change (1.5 to 0.5 ml/min- by 0.25 ml/min step changes) - inlet flowrate (a), voltage sent to the pump 1 (flowrate controller) (b), bioreactor liquid level (c) and voltage sent to the pump 2 (level controller) (d).

In this part, an inlet flowrate set-point change was imposed on the controls system. The inlet flowrate was increased and decreased from 0.5 to 1.5 ml/min suddenly at minutes 7.5 and 14.5 respectively. Fig. 74 shows the result similar to the first experiment.

The differences of this test with first one, are the prompt changes of the inlet flowrate and a comparison of the experimental data with the model. As it can be seen from the figure the model, highlighted by dashed red color in plots *a* and *b* are in a good agreement with the experimental data in both level and flowrate control system. In addition, the effects of flowrate change and the interaction of the flowrate loop with the level control loop is shown in plots *c* and *d* at the moment of inlet flowrate change (minutes 7.5 and 14.5)

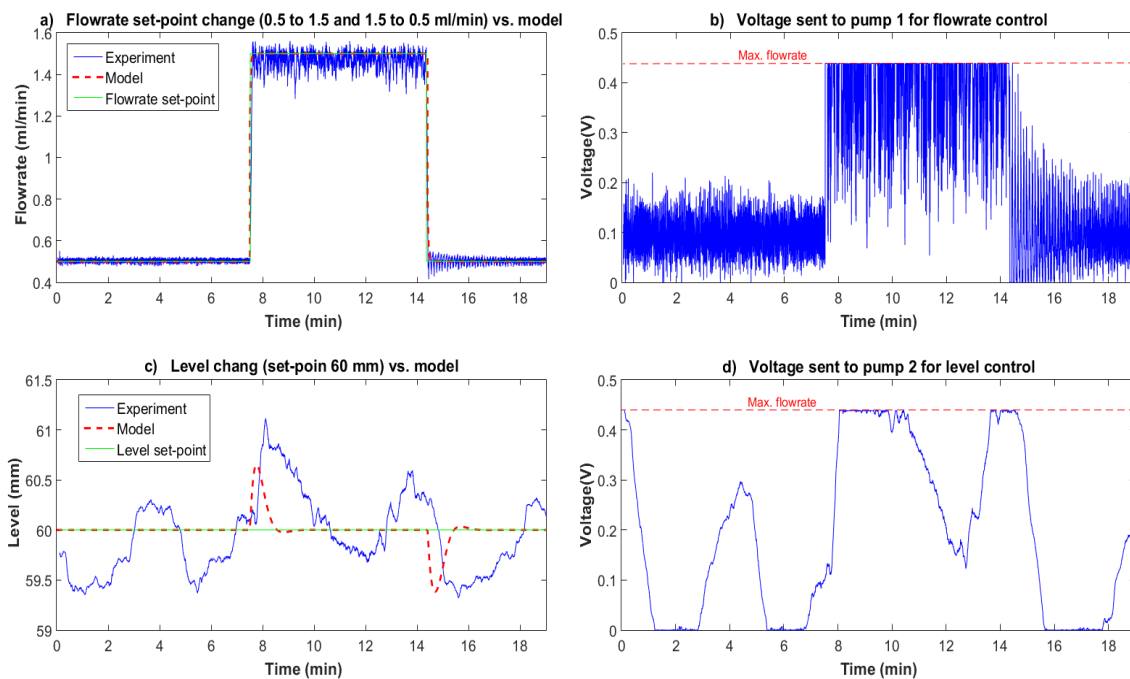


Fig. 74. Inlet flowrate set-point change (0.5 to 1.5 and 1.5 to 0.5 ml/min) - inlet flowrate (a), voltage sent to the pump 1 (flowrate controller) (b), bioreactor liquid level (c) and voltage sent to the pump 2 (level controller) (d)

8.6.2 Automatic to manual switch (flowrate control disturbance)

Inlet flowrate as manipulated and control variable is fully under automatic control as it was discussed before. It was changed from automatic mode to manual mode to carry out an investigation about the effect of disturbance on flowrate control system. *Fig. 75*

illustrates the effect of disturbance on controls system. As the figure (plot *a*) shows at minutes around 8 and 13 the flowrate was changed to manual from automatic control and vice versa respectively. In this period (between 8 to 13 min), the voltage was not sent to the pump 1 due to flow control system disconnection (plot *b*) and the inlet flowrate was a change from 0.5 to around 1.5 ml/min (the exact value is not available due to manual mode).

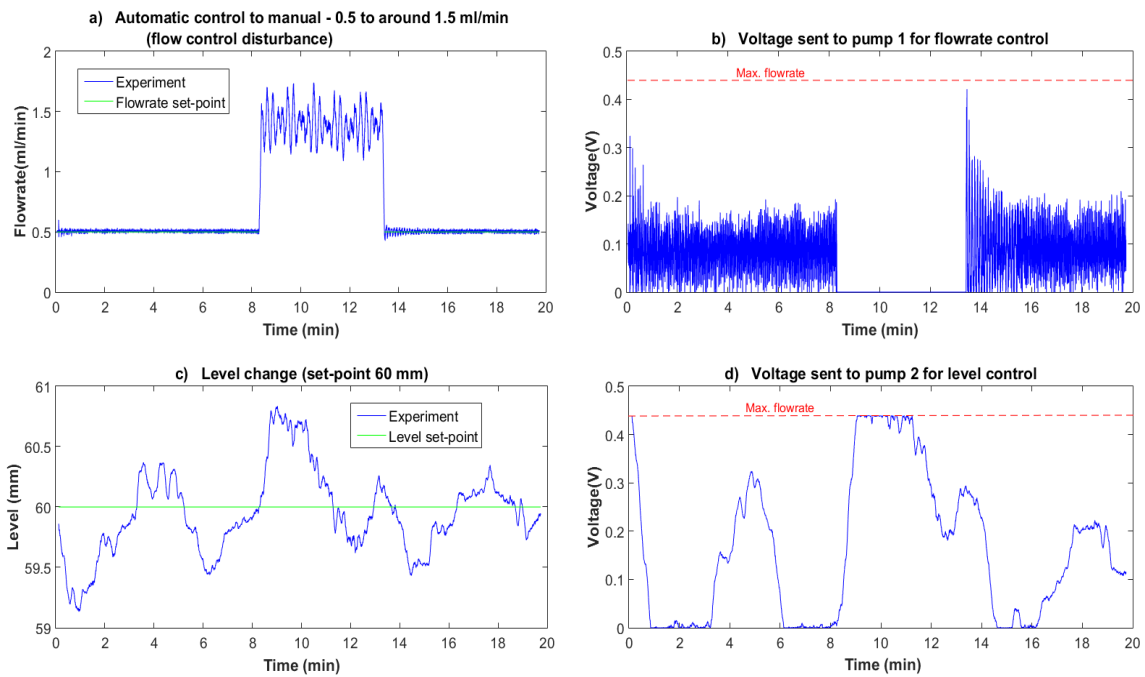


Fig. 75. Automatic control to manual as a flowrate control disturbance (0.5 to around 1.5 ml/min) - (a), voltage sent to the pump 1 (flowrate controller) (b), bioreactor liquid level (c) and voltage sent to the pump 2 (level controller) (d)

The only significant change in bioreactor level results from the increase of inlet flowrate in the mentioned period of manual mode. It can be seen from plot b that the level was increased exactly at the time of automatic to manual mode switch and started to decrease at the time of switching back to automatic mode (decrease inlet flowrate). It can

be concluded from *Fig. 75* that the disturbance has no significant effect on the flowrate and level controller from the control system point of view.

Below is *Fig. 76* which shows another experiment results regarding the effect of flowrate disturbance on the bioreactor control system. In this part, a set of experiment was carried out in reverse mode with respect to the previous one. In this case, the flowrate was changed from 1.5 to around 0.5 by changing the automatic mode to manual. In all of 4 plots, the effect of decreasing the flowrate is clearly visible especially at minutes from 5 to 10.

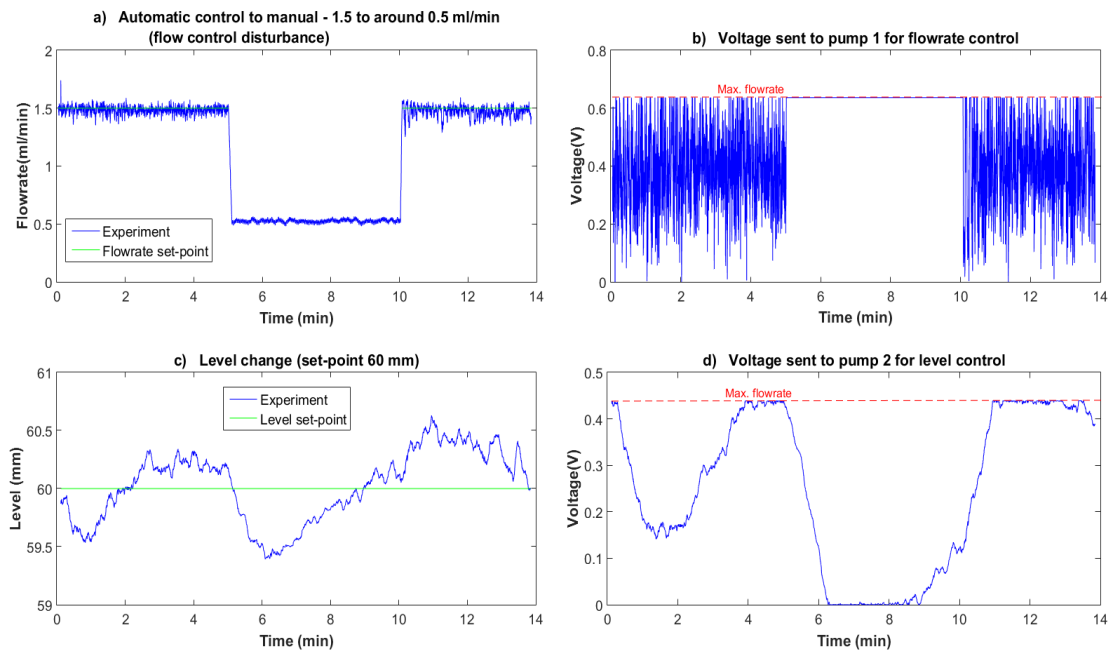


Fig. 76. Automatic control to manual as a flowrate control disturbance (1.5 to around 0.5 ml/min) - (a), voltage sent to the pump 1 (flowrate controller) (b), bioreactor liquid level (c) and voltage sent to the pump 2 (level controller) (d)

8.6.3 Level setpoint step-change

A level set-point change from 50 to 80 and 80 to 50 was tested here and the difference is that this time flowrate control was investigated too. The results regarding level control were discussed before in *Fig 69* and *Fig 67*. It can be seen from *Fig. 77* and *Fig. 78* there is no interaction between level set-point change and inlet flowrate. The inlet flowrate was set to 1 ml/min at the beginning of the experiment and it was not changed until the end. Successfully, it was kept constant by the flowrate controller during the whole experiment time. Overall, the hydrodynamic features of the bioreactors, i.e. its liquid level at constant pressure and the feed flowrate, turned out smoothly controllable with sufficient confidence. Some doubts remain on the quality of the signals arriving at the controller, in particular concerning the liquid level.

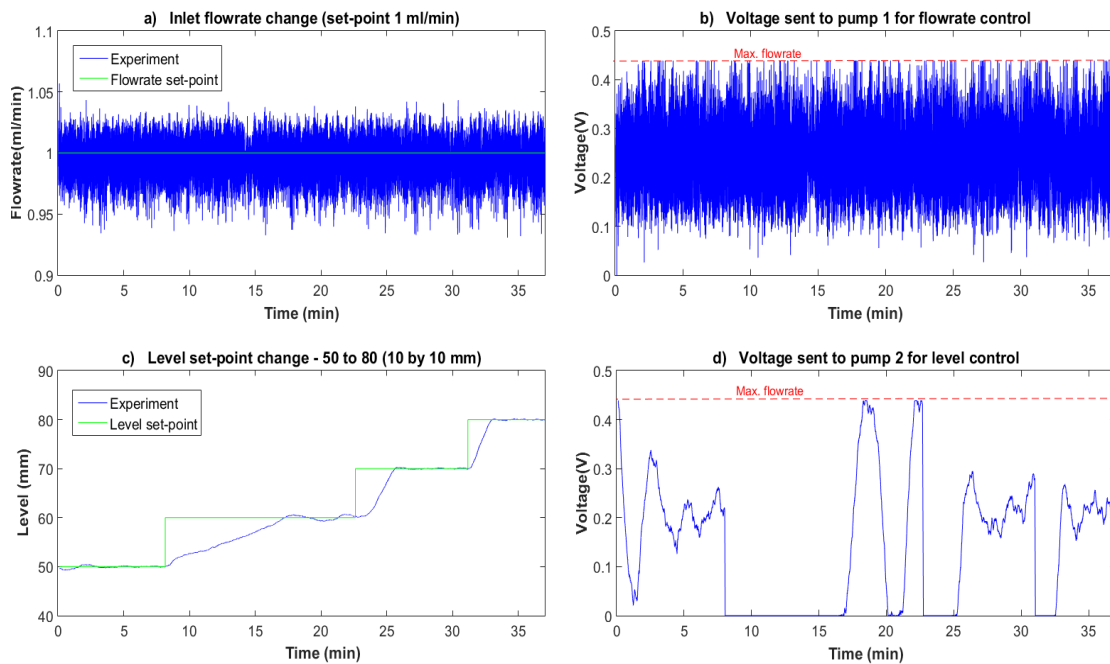


Fig. 77. Level set-point change from 50 to 80 mm (10 by 10 mm) - - (a), voltage sent to the pump 1 (flowrate controller) (b), bioreactor liquid level (c) and voltage sent to the pump 2 (level controller) (d).

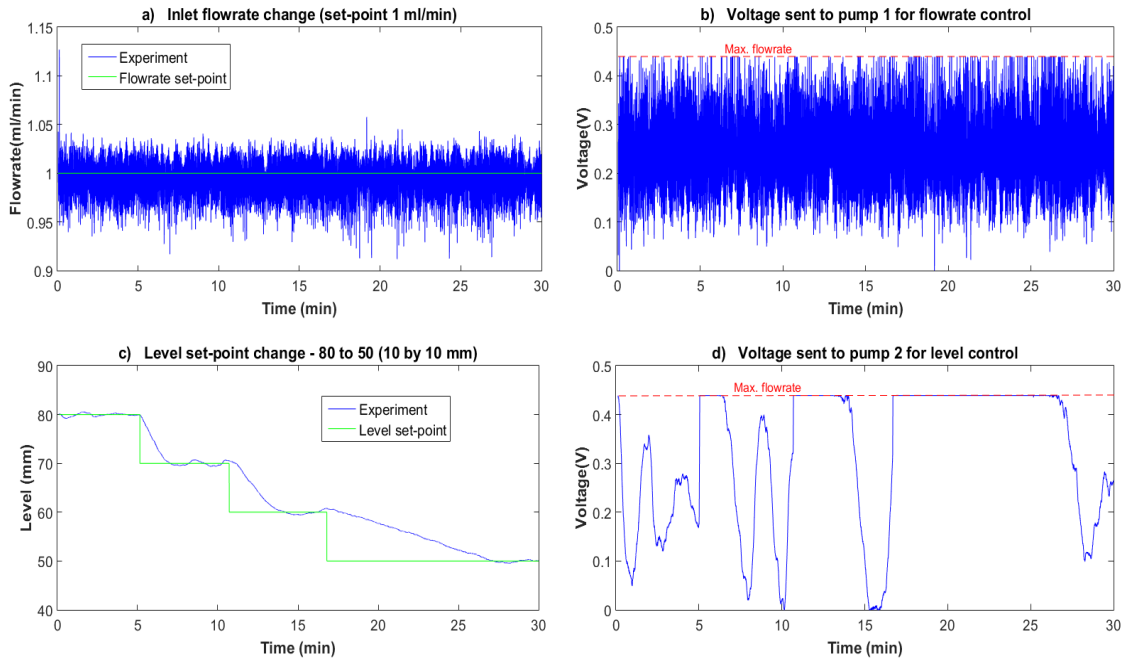


Fig. 78. Level set-point change from 80 to 50 mm (10 by 10 mm) - inlet flowrate (a), voltage sent to pump 1 by flowrate controller (b), bioreactor medium level (c) and voltage sent to pump 2 by a level controller (d).

8.7 Level control of bioreactor in actual cell culturing

Application of the control system for bioreactor hydrodynamics was tested under three-cell system co-culture conditions as described in Section “Cell culturing”. Human primary hepatocytes were over-seeded at a density of 105 cells/cm² into the co-culture membrane bioreactor system in a medium composed of a mixture of human sinusoidal endothelial cells (Sciencell, California, United States) and human stellate liver cells (Sciencell, California, US). Controlled temperature and atmosphere, including sterile conditions, were maintained constant by an incubator containing the whole bioreactor set-up (37°C in 5% CO₂; 20% O₂ atmosphere (v/v) with 95% relative humidity for the first 7 days and then O₂ was increased to 25% until day 9 then further increased to 30% for

the rest of the experiment). The nominal flowrates (set-point for the inlet) were set to 1 ml/min. The pump regulating the outlet flow was used as an actuator and its rotational speed manipulated by the level controller.

During typical batch experiments without control, operations were often affected by even the smallest difference between the inlet and outlet flowrates. Many factors affected such operating parameters, like membrane permeability variations over time (e.g. fouling), tube differences in the multi-tube pump or slow pressure buildups. Indeed, even the slightest detail could generate appreciable differences between inflow and outflow over long period of time (e.g. hours) and in various cases costly experiments have been found to fail due to bioreactor dry-up or flooding. By using the hydrodynamics control system developed, a much smoother operation was achieved, including fully automatic handling overnight and during the weekends, as recorded by log files. As exemplary results over time, *Fig 79* shows the bioreactor level during 24 hours of tests together with the oxygen consumption rate of the three-cell system at day 18 of the culturing operation. As reported in *Fig 79*, the level set-point was set to 41 mm, in this set-up also corresponding to above the fiber bundles (the 0-mm quote depends on the height of the capillary tank relative to the bioreactor). As a functional parameter of the cells the oxygen consumption rate was assessed with the aim to evaluate the efficiency of the control system connected to the membrane bioreactor. Cell viability and functionality was demonstrated for a duration of 27 days by the evaluation of metabolic rates. *Fig 79* shows a steady level except for two initial sharp drops due to testing of the height measuring system, which was performed at each start of the day. The oxygen consumption rate was relatively scattered but always within the range proving full viability and functionality of the cell culture.

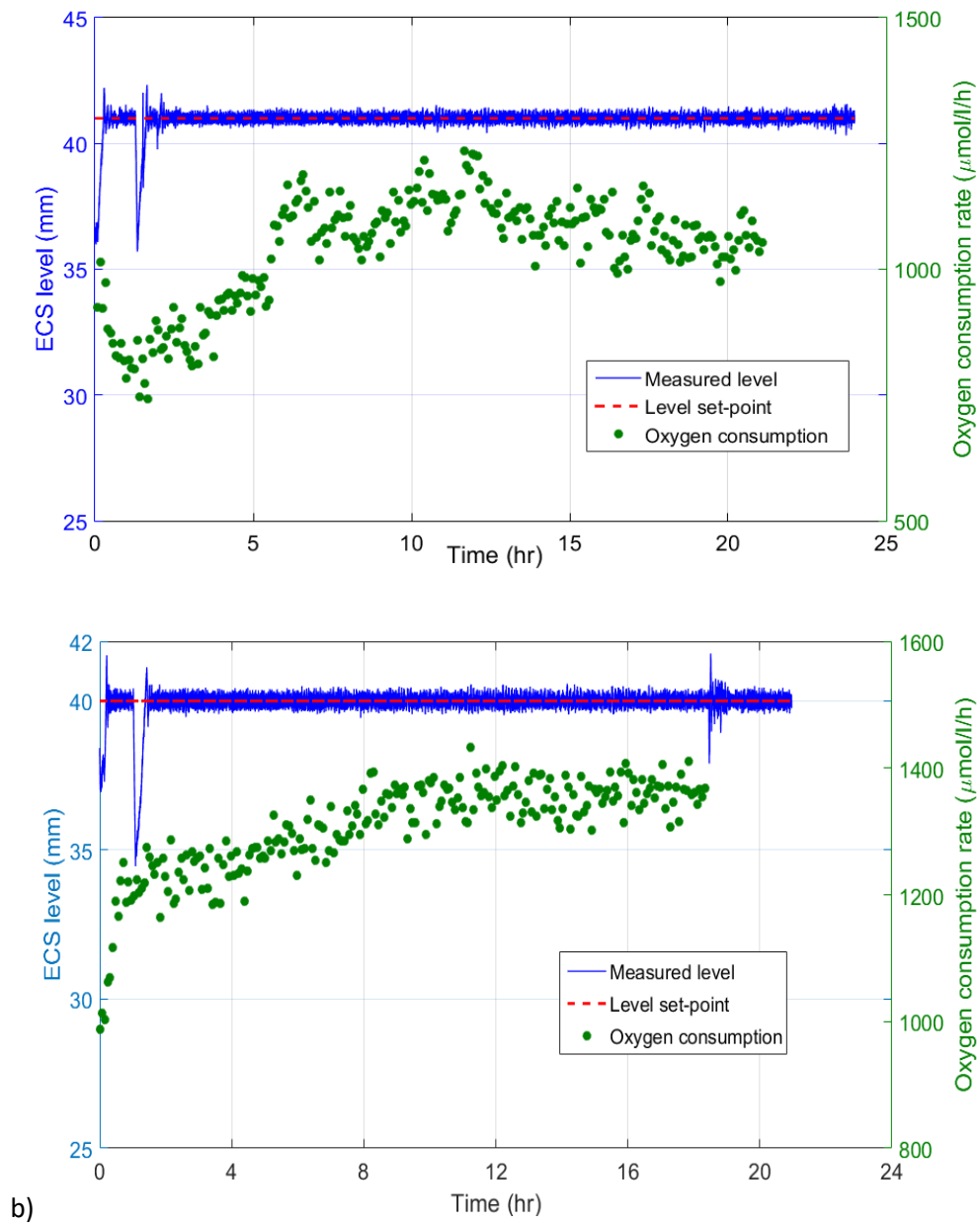


Fig 79. 24-hour bioreactor level control results during cell culturing at day 18 (a) and evaluation of oxygen consumption rate of cells cultured into the bioreactor at day 27 (b).

In this section, the benefits of the control systems have been investigated. There was always a lot of changes in the bioreactor medium level, because the output and input

flowrate were not fully equal, even if the flowrate was provided by just one pump. The reasons for this phenomenon could be a different application of the fibers in the inlet and outlet, as well as the insignificant difference in the type of the tubes and also the oxygenation system at the input flow.

As the bioreactor system must work continuously and for long-term (e.g. during day and night time) even the smallest differences in the input and output flowrate, inappreciable in a few minutes, can cause significant changes in the liquid height when left for few hours. If not properly addressed, this may easily lead to cell death. In previous open loop experiments (without the control system), it happened several times that the experiment was lost.

While both level and flowrate appear to be stably controlled under appropriate conditions, we should also emphasize that the capacitance sensor applied to the capillary tank exhibits a still significant level of noise, which could affect the operation in other applications should the requirements on performances be stricter. In those cases, probably feedforward prediction could be added to the level control system to increase the speed of response. The flexible PC-based control proposed could be readily adapted to this situation. The derivative action in the controller logic could also increase the robustness provided a cleaner measured signal is obtained, e.g. by increasing the amount of liquid in the auxiliary tank (to increase its absolute electrical capacity) or by selecting a sensor based on a different principle (e.g. ultrasound). As a final further optimization, the pump rotation reversal feature could be utilized to increase the range of flowrate difference (e.g. including negative flowrates) if required.

Based on the experimental results achieved, after the appropriate equipment installation, as well as using a full control system, all variables such as the liquid level and input flowrate, are adjustable and controllable. The bioreactor level is quite stable at desired set-point during the working time as well as the inlet flowrate. The control system devices, such as capillary-tank and level sensor introduced some limitation during the experiments, especially inside the incubator that should be resolved by selecting different instruments in the future.

After a detailed review of all the presented results, it can be concluded that the controlled bioreactor system works well. All issues related to operation both at overnight and in the weekends, as well as maintenance, medium substitution and break down of the plant, are quickly and accurately dealt with by the control system. In the case of flowrate and level, the control system is fully autonomous. All these tests had been carried out to assess the capability of the control system to exhibit the right behaviour during the operations and this also has been experienced in practice during tests which then lead to the final result.

On the other hand, there are still some problems such as viability and also noise in the level sensor that should be improved. As it was mentioned in the previous chapter the level measurement must be contactless because of contamination problem and despite many practical solutions used, a final amount of noise remained, eventually causing some residual pump rotation even at zero flowrates. There is still some oscillation especially at higher flowrates in comparison with lower flowrates that eventually do not affect too much the quality of the control system, but still are something that should be improved.

Overall, thanks to controlled operations, bioreactor operations for providing all ingredients to a successful culture, i.e. anchorage, effective and reliable nutrient and oxygen feed, low level of pressure/shear stress and appropriate temperature, have benefitted from an environment maintained constant, which eventually allowed reaching almost one month of successful cell culturing. The implications of such result appear particularly attractive for a more wide-spread, stable and reliable use of such biotechnological device as bioartificial liver system.

8.8 Conclusion and outlook

The research in this part was focussed on improving an HFMBR as bioartificial liver by means of modeling, online monitoring, synthesis and manufacturing of a control system. For this purpose, a detailed transient model was prepared and a model-based

control strategy was studied and conceptually tested. In order to carry out this goal, a four-input/seven-state model of the bioreactor has been developed. From the original non-linear model, a linearized version has been derived. Responses produced by the linearized model and the non-linear model were compared for a step change in selected inputs. As can be seen from the results, with a comparison of non-linear model and experimental results, it is understood that this model is very close to reality and this model can be used to control the system. Selecting appropriate sensors for on-line monitoring of relevant properties as well as the manipulated variables for control was carried out. Different control schemes were tested by making use of specific control system software packages (MATLAB/Simulink).

For practical validation of the control schemes, instruments were connected to the MBR in actual cell culturing operation. Based on the results, apart from very low changes in the bioreactor level, it has remained stable throughout all testing and finally, for about one month which is pretty considerable, the cell culture was successfully done.

Ultimately, the present work allows improving the understanding of the behaviour of HFMBR for biomedical application under transient conditions, as well as gaining the ability to proactively increase the performances (both during operations and in terms of cell culture durability) by means of specific automation and control techniques.

For future work plan, efforts will be devoted to set-up an expanded dynamic model of the process able to contemplate all the key aspects determining a successful cell culturing process (transport of nutrients, catabolites, control of oxygen flow, temperature and pH levels etc.) and a professional control system.

References

- [1] J. C. Gerlach, K. Zeilinger, and J. F. Patzer II, "Bioartificial liver systems: why, what, whither?," 2008.
- [2] C.-F. Mandenius, *Bioreactors: design, operation and novel applications*: John Wiley & Sons, 2016.
- [3] O. SRTR, "OPTN & SRTR Annual Data Report 2010," *Am J Transplant*, vol. 12, p. 9, 2012.
- [4] C. Legallais, B. David, and E. Dore, "Bioartificial livers (BAL): current technological aspects and future developments," *Journal of Membrane Science*, vol. 181, pp. 81-95, 2001.
- [5] L. De Bartolo, A. Leindlein, D. Hofmann, A. Bader, A. de Grey, E. Curcio, *et al.*, "Bio-hybrid organs and tissues for patient therapy: A future vision for 2030," *Chemical Engineering and Processing: Process Intensification*, vol. 51, pp. 79-87, 2012.
- [6] L. De Bartolo, S. Salerno, E. Curcio, A. Piscioneri, M. Rende, S. Morelli, *et al.*, "Human hepatocyte functions in a crossed hollow fiber membrane bioreactor," *Biomaterials*, vol. 30, pp. 2531-2543, 2009.
- [7] H. Ijima, Y. Takeya, T. Yokonuma, Y.-T. Hou, and T. Takei, "Composition of culture medium is more important than co-culture with hepatic non-parenchymal cells in albumin production activity of primary rat hepatocytes, and the effect was enhanced by hepatocytes spheroid culture in collagen gel," *Biochemical Engineering Journal*, vol. 45, pp. 226-231, 2009.
- [8] V. Dixit and G. Gitnick, "Artificial liver support: state of the art," *Scandinavian Journal of Gastroenterology*, vol. 31, pp. 101-114, 1996.
- [9] J. W. Allen, T. Hassanein, and S. N. Bhatia, "Advances in bioartificial liver devices," *Hepatology*, vol. 34, pp. 447-455, 2001.
- [10] A. Pauwels, N. Mostefa-Kara, C. Florent, and V. G. Lévy, "Emergency liver transplantation for acute liver failure: evaluation of London and Clichy criteria," *Journal of hepatology*, vol. 17, pp. 124-127, 1993.
- [11] A. C. Anand, P. Nightingale, and J. M. Neuberger, "Early indicators of prognosis in fulminant hepatic failure: an assessment of the King's criteria," *Journal of hepatology*, vol. 26, pp. 62-68, 1997.
- [12] M. Grompe, "Therapeutic liver repopulation for the treatment of metabolic liver diseases," *Human cell*, vol. 12, pp. 171-180, 1999.
- [13] S. Strom, R. Fisher, W. Rubinstein, J. Barranger, R. Towbin, M. Charron, *et al.*, "Transplantation of human hepatocytes," in *Transplantation proceedings*, 1997, pp. 2103-2106.

References

- [14] S. Kaihara and J. P. Vacanti, "Tissue engineering: toward new solutions for transplantation and reconstructive surgery," *Archives of surgery*, vol. 134, pp. 1184-1188, 1999.
- [15] K. Overturf, M. Al-Dhalimy, M. Finegold, and M. Grompe, "Serial transplantation reveals stem cell like regenerative potential in parenchymal mouse hepatocytes," *FASEB Journal*, vol. 11, 1997.
- [16] J. P. Vacanti, M. A. Morse, W. M. Saltzman, A. J. Domb, A. Perez-Atayde, and R. Langer, "Selective cell transplantation using bioabsorbable artificial polymers as matrices," *Journal of pediatric surgery*, vol. 23, pp. 3-9, 1988.
- [17] A. Park, B. Wu, and L. G. Griffith, "Integration of surface modification and 3D fabrication techniques to prepare patterned poly (L-lactide) substrates allowing regionally selective cell adhesion," *Journal of Biomaterials Science, Polymer Edition*, vol. 9, pp. 89-110, 1998.
- [18] D. Mooney, P. Kaufmann, K. Sano, K. McNamara, J. Vacanti, and R. Langer, "Transplantation of hepatocytes using porous, biodegradable sponges," in *Transplantation proceedings*, 1994, pp. 3425-3426.
- [19] V. Dixit, M. Arthur, R. Reinhardt, and G. Gitnick, "Improved function of microencapsulated hepatocytes in a hybrid bioartificial liver support system," *Artificial organs*, vol. 16, pp. 336-341, 1992.
- [20] A. A. Demetriou, S. M. Levenson, P. M. Novikoff, A. B. Novikoff, N. R. Chowdhury, J. Whiting, *et al.*, "Survival, organization, and function of microcarrier-attached hepatocytes transplanted in rats," *Proceedings of the National Academy of Sciences*, vol. 83, pp. 7475-7479, 1986.
- [21] C. COSTA, L. ZHAO, W. V. BURTON, K. R. BONDIOLI, B. L. WILLIAMS, T. A. HOAGLAND, *et al.*, "Expression of the human $\alpha 1, 2$ -fucosyltransferase in transgenic pigs modifies the cell surface carbohydrate phenotype and confers resistance to human serum-mediated cytolysis," *The FASEB journal*, vol. 13, pp. 1762-1773, 1999.
- [22] M. Matsushita and Y. Nosé, "Artificial liver," *Artificial organs*, vol. 10, pp. 378-384, 1986.
- [23] E. S. Tzanakakis, D. J. Hess, T. D. Sielaff, and W.-S. Hu, "Extracorporeal tissue engineered liver-assist devices," *Annual review of biomedical engineering*, vol. 2, pp. 607-632, 2000.
- [24] A. J. Ellis, R. D. Hughes, J. A. Wendon, J. Dunne, P. G. Langley, J. H. Kelly, *et al.*, "Pilot-controlled trial of the extracorporeal liver assist device in acute liver failure," *Hepatology*, vol. 24, pp. 1446-1451, 1996.
- [25] J. M. Millis, D. C. Cronin, R. Johnson, H. Conjeevaram, C. Conlin, S. Trevino, *et al.*, "Initial experience with the modified extracorporeal liver-assist device for

References

- patients with fulminant hepatic failure: system modifications and clinical impact," *Transplantation*, vol. 74, pp. 1735-1746, 2002.
- [26] G. V. Mazariegos, D. J. Kramer, R. C. Lopez, A. O. Shakil, A. J. Rosenbloom, M. DeVera, *et al.*, "Safety observations in phase I clinical evaluation of the Excorp Medical Bioartificial Liver Support System after the first four patients," *Asaio Journal*, vol. 47, pp. 471-475, 2001.
- [27] G. V. Mazariegos, J. F. Patzer, R. C. Lopez, M. Giraldo, M. E. DeVera, T. A. Grogan, *et al.*, "First clinical use of a novel bioartificial liver support system (BLSS)," *American Journal of Transplantation*, vol. 2, pp. 260-266, 2002.
- [28] A. A. Demetriou, R. S. Brown Jr, R. W. Busuttil, J. Fair, B. M. McGuire, P. Rosenthal, *et al.*, "Prospective, randomized, multicenter, controlled trial of a bioartificial liver in treating acute liver failure," *Annals of surgery*, vol. 239, pp. 660-670, 2004.
- [29] M. Van de Kerkhove, E. Di Florio, V. Scuderi, A. Mancini, A. Belli, A. Bracco, *et al.*, "Phase I clinical trial with the AMC-bioartificial liver," *International journal of artificial organs*, vol. 25, pp. 950-959, 2002.
- [30] E. Morsiani, P. Pazzi, A. Puviani, M. Brogli, L. Valieri, P. Gorini, *et al.*, "Early experiences with a porcine hepatocyte-based bioartificial liver in acute hepatic failure patients," *The International journal of artificial organs*, vol. 25, pp. 192-202, 2002.
- [31] J. Gerlach, M. Botsch, D. Kardassis, P. Lemmens, M. Schön, J. Janke, *et al.*, "Experimental evaluation of a cell module for hybrid liver support," *The International journal of artificial organs*, vol. 24, pp. 793-798, 2001.
- [32] I. M. Sauer, K. Zeilinger, G. Pless, D. Kardassis, T. Theruvath, A. Pascher, *et al.*, "Extracorporeal liver support based on primary human liver cells and albumin dialysis—treatment of a patient with primary graft non-function," *Journal of hepatology*, vol. 39, pp. 649-653, 2003.
- [33] H. C. Fiegel, P. M. Kaufmann, H. Bruns, D. Kluth, R. E. Horch, J. P. Vacanti, *et al.*, "Hepatic tissue engineering: From transplantation to customized cell-based liver directed therapies from the laboratory," *Journal of cellular and molecular medicine*, vol. 12, pp. 56-66, 2008.
- [34] R. Bañares, M.-V. Catalina, and J. Vaquero, "Liver support systems: will they ever reach prime time?," *Current gastroenterology reports*, vol. 15, p. 312, 2013.
- [35] J. Uchino, T. Tsuburaya, F. Kumagai, T. Hase, T. Hamada, T. Komai, *et al.*, "A hybrid bioartificial liver composed of multiplated hepatocyte monolayers," *ASAIO transactions/American Society for Artificial Internal Organs*, vol. 34, pp. 972-977, 1987.

References

- [36] V. Roger, P. Ballardur, J. Honiger, M. Baudrimont, R. Delelo, A. Robert, *et al.*, "Internal bioartificial liver with xenogeneic hepatocytes prevents death from acute liver failure: an experimental study," *Annals of surgery*, vol. 228, p. 1, 1998.
- [37] E. Curcio, S. Salerno, G. Barbieri, L. De Bartolo, E. Drioli, and A. Bader, "Mass transfer and metabolic reactions in hepatocyte spheroids cultured in rotating wall gas-permeable membrane system," *Biomaterials*, vol. 28, pp. 5487-5497, 2007.
- [38] E. Curcio, P. Macchiarini, and L. De Bartolo, "Oxygen mass transfer in a human tissue-engineered trachea," *Biomaterials*, vol. 31, pp. 5131-5136, 2010.
- [39] H. Klinkmann and J. Vienken, "Membranes for dialysis," *Nephrology Dialysis Transplantation*, vol. 10, pp. 39-45, 1995.
- [40] S. Qiang, Y. Yaoting, L. Hongyin, and H. Klinkmann, "Comparative evaluation of different membranes for the construction of an artificial liver support system," *The International journal of artificial organs*, vol. 20, pp. 119-124, 1997.
- [41] A. Jóźwiak, W. Karlik, M. Wiechetek, and A. Weryński, "Attachment and metabolic activity of hepatocytes cultivated on selected polymeric membranes," *The International journal of artificial organs*, vol. 21, pp. 460-466, 1998.
- [42] J. Gerlach, P. Stoll, N. Schnoy, and E. Bücherl, "Membranes as substrates for hepatocyte adhesion in liver support bioreactors," *The International journal of artificial organs*, vol. 13, pp. 436-441, 1990.
- [43] J. Gerlach, N. Schnoy, J. Vienken, M. Smith, and P. Neuhaus, "Comparison of hollow fibre membranes for hepatocyte immobilisation in bioreactors," *The International journal of artificial organs*, vol. 19, pp. 610-616, 1996.
- [44] G. Catapano, M. Di Lorenzo, C. D. Volpe, L. De Bartolo, and C. Migliaresi, "Polymeric membranes for hybrid liver support devices: the effect of membrane surface wettability on hepatocyte viability and functions," *Journal of Biomaterials Science, Polymer Edition*, vol. 7, pp. 1017-1027, 1996.
- [45] L. De Bartolo, G. Catapano, C. D. Volpe, and E. Drioli, "The effect of surface roughness of microporous membranes on the kinetics of oxygen consumption and ammonia elimination by adherent hepatocytes," *Journal of Biomaterials Science, Polymer Edition*, vol. 10, pp. 641-655, 1999.
- [46] G. Biagini, S. Stefoni, R. Solmi, C. Castaldini, R. Buttazzi, A. Rossetti, *et al.*, "Fibroblast proliferation over dialysis membrane: an experimental model for" tissue" biocompatibility evaluation," *The International journal of artificial organs*, vol. 17, pp. 620-628, 1994.
- [47] A. Kamlot, J. Rozga, F. D. Watanabe, and A. A. Demetriou, "Review: Artificial liver support systems," *Biotechnology and bioengineering*, vol. 50, pp. 382-391, 1996.

References

- [48] Y. Kino, M. Sawa, S. Kasai, and M. Mito, "Multiporous cellulose microcarrier for the development of a hybrid artificial liver using isolated hepatocytes," *Journal of Surgical Research*, vol. 79, pp. 71-76, 1998.
- [49] S. L. Nyberg, R. A. Shatford, M. V. Peshwa, J. G. White, F. B. Cerra, and W. S. Hu, "Evaluation of a hepatocyte-entrapment hollow fiber bioreactor: A potential bioartificial liver," *Biotechnology and bioengineering*, vol. 41, pp. 194-203, 1993.
- [50] H. Shiraha, N. Koide, H. Hada, K. Ujike, M. Nakamura, T. Shinji, *et al.*, "Improvement of serum amino acid profile in hepatic failure with the bioartificial liver using multicellular hepatocyte spheroids," *Biotechnology and bioengineering*, vol. 50, pp. 416-421, 1996.
- [51] J. Gerlach, J. Encke, O. Hole, C. Müller, J. Courtney, and P. Neuhaus, "Hepatocyte culture between three dimensionally arranged biomatrix-coated independent artificial capillary systems and sinusoidal endothelial cell co-culture compartments," *The International journal of artificial organs*, vol. 17, p. 301, 1994.
- [52] M. Gleissner, R. Bornemann, R. Stemerowicz, M. Meissler, P. Neuhaus, and J. Gerlach, "Immunoisolation of hybrid liver support systems by semipermeable membranes," *The International journal of artificial organs*, vol. 20, pp. 644-649, 1997.
- [53] S. L. Nyberg and S. P. Misra, "Hepatocyte liver-assist systems—a clinical update," in *Mayo Clinic Proceedings*, 1998, pp. 765-771.
- [54] C. Mullan, "Bioartificial organs may help reduce risk of zoonosis in xenotransplantation," *Artificial organs*, vol. 23, pp. 366-367, 1999.
- [55] G. Catapano, "Mass transfer limitations to the performance of membrane bioartificial liver support devices," *The International journal of artificial organs*, vol. 19, pp. 18-35, 1996.
- [56] A. L. Zydney and C. K. Colton, "Augmented solute transport in the shear flow of a concentrated suspension," *Physicochemical hydrodynamics*, vol. 10, pp. 77-96, 1988.
- [57] A. Demetriou, J. Rozga, L. Podesta, E. Lepage, E. Morsiani, A. Moscioni, *et al.*, "Early clinical experience with a hybrid bioartificial liver," *Scandinavian Journal of Gastroenterology*, 2009.
- [58] J. Gerlach, "Development of a hybrid liver support system: a review," *The International journal of artificial organs*, vol. 19, pp. 645-654, 1996.
- [59] H. Iwata, T. Sajiki, H. Maeda, Y. G. Park, B. Zhu, S. SAIOH, *et al.*, "In vitro evaluation of metabolic functions of a bioartificial liver," *ASAIO journal*, vol. 45, pp. 299-306, 1999.

References

- [60] T. D. Giorgio, A. D. Moscioni, J. Rozga, and A. A. Demetriou, "Mass transfer in a hollow fiber device used as a bioartificial liver," *ASAIO journal*, vol. 39, pp. 886-892, 1993.
- [61] L. M. Flendrig, A. A. t. Velde, and R. A. Chamuleau, "Semipermeable hollow fiber membranes in hepatocyte bioreactors: a prerequisite for a successful bioartificial liver?," *Artificial organs*, vol. 21, pp. 1177-1181, 1997.
- [62] L. M. Flendrig, J. W. la Soe, G. G. Jörning, A. Steenbeek, O. T. Karlsen, W. M. Bovée, *et al.*, "In vitro evaluation of a novel bioreactor based on an integral oxygenator and a spirally wound nonwoven polyester matrix for hepatocyte culture as small aggregates," *Journal of hepatology*, vol. 26, pp. 1379-1392, 1997.
- [63] N. Ohshima, K. Yanagi, and H. Miyoshi, "Packed-Bed Type Reactor to Attain High Density Culture of Hepatocytes for Use as a Bioartificial Liver," *Artificial organs*, vol. 21, pp. 1169-1176, 1997.
- [64] D. Fassnacht, S. Rossing, J. Stange, and R. Portner, "Long-term cultivation of immortalised mouse hepatocytes in a high cell density, fixed-bed reactor," *Biotechnology techniques*, vol. 12, pp. 25-30, 1998.
- [65] A. Bader, E. Knop, K. Böker, N. Frühauf, W. Schüttler, K. Oldhafer, *et al.*, "A novel bioreactor design for in vitro reconstruction of in vivo liver characteristics," *Artificial organs*, vol. 19, pp. 368-374, 1995.
- [66] K. Taguchi, M. Matsushita, M. Takahashi, and J. Uchino, "Development of a Bioartificial Liver with Sandwiched-Cultured Hepatocytes Between Two Collagen Gel Layers," *Artificial organs*, vol. 20, pp. 178-185, 1996.
- [67] T. M. Chang, "Semipermeable microcapsules," *Science*, vol. 146, pp. 524-525, 1964.
- [68] R. G. Tompkins, E. A. Carter, J. D. Carlson, and M. L. Yarmush, "Enzymatic function of alginate immobilized rat hepatocytes," *Biotechnology and bioengineering*, vol. 31, pp. 11-18, 1988.
- [69] Y. Miura, T. Akimoto, N. Yoshikawa, and K. Yagi, "Characterization of immobilized hepatocytes as liver support," *Biomaterials, Artificial Cells and Artificial Organs*, vol. 18, pp. 549-554, 1990.
- [70] J. Stange and S. Mitzner, "Hepatocyte encapsulation--initial intentions and new aspects for its use in bioartificial liver support," *The International journal of artificial organs*, vol. 19, pp. 45-48, 1996.
- [71] G. Wells, M. Fisher, and M. Sefton, "Microencapsulation of viable hepatocytes in HEMA-MMA microcapsules: a preliminary study," *Biomaterials*, vol. 14, pp. 615-620, 1993.
- [72] H. W. MATTHEW, S. O. SALLEY, J. WARD D PETERSON, D. R. DESHMUKH, A. MUKHOPADHYAY, and M. D. KLEIN, "Microencapsulated

References

- hepatocytes: prospects for extracorporeal liver support," *ASAIO Journal*, vol. 37, pp. M328-M329, 1991.
- [73] B. Fremond, A. Joly, M. Desille, J. Desjardins, J. Champion, and B. Clement, "Cell-based therapy of acute liver failure: the extracorporeal bioartificial liver," *Cell biology and Toxicology*, vol. 12, pp. 325-329, 1996.
- [74] C. A. Sardonini and D. Dibiasio, "An investigation of the diffusion-limited growth of animal cells around single hollow fibers," *Biotechnology and bioengineering*, vol. 40, pp. 1233-1242, 1992.
- [75] E. Dore and C. Legallais, "A new concept of bioartificial liver based on a fluidized bed bioreactor," *Therapeutic Apheresis*, vol. 3, pp. 264-267, 1999.
- [76] D. Kunii and O. Levenspiel, *Fluidization engineering*: Elsevier, 2013.
- [77] F. Federici, M. Petruccioli, and M. W. Miller, "Enhancement and stabilization of the production of glucoamylase by immobilized cells of *Aureobasidium pullulans* in a fluidized-bed reactor," *Applied microbiology and biotechnology*, vol. 33, pp. 407-409, 1990.
- [78] A. Joly, J.-F. Desjardins, B. Fremond, M. Desille, J.-P. Champion, Y. Malledant, *et al.*, "SURVIVAL, PROLIFERATION, AND FUNCTIONS OF PORCINE HEPATOCYTES ENCAPSULATED IN COATED ALGINATE BEADS: A STEP TOWARD A RELIABLE BIOARTIFICIAL LIVER1," *Transplantation*, vol. 63, pp. 795-803, 1997.
- [79] C. Legallais, E. Dore, and P. Paullier, "Design of a fluidized bed bioartificial liver," *Artificial organs*, vol. 24, pp. 519-525, 2000.
- [80] S. Figaro, U. Pereira, H. Rada, N. Semenzato, D. Pouchoulin, and C. Legallais, "Development and validation of a bioartificial liver device with fluidized bed bioreactors hosting alginate-encapsulated hepatocyte spheroids," in *Engineering in Medicine and Biology Society (EMBC), 2015 37th Annual International Conference of the IEEE*, 2015, pp. 1335-1338.
- [81] A. Gautier, B. Carpentier, M. Dufresne, Q. Vu Dinh, P. Paullier, and C. Legallais, "Impact of alginate type and bead diameter on mass transfers and the metabolic activities of encapsulated C3A cells in bioartificial liver applications," *Eur Cell Mater*, vol. 21, pp. 94-106, 2011.
- [82] S. M. Coward, C. Legallais, B. David, M. Thomas, Y. Foo, D. Mavri-Damelin, *et al.*, "Alginate-encapsulated HepG2 Cells in a Fluidized Bed Bioreactor Maintain Function in Human Liver Failure Plasma," *Artificial organs*, vol. 33, pp. 1117-1126, 2009.
- [83] L. De Bartolo, S. Salerno, S. Morelli, L. Giorno, M. Rende, B. Memoli, *et al.*, "Long-term maintenance of human hepatocytes in oxygen-permeable membrane bioreactor," *Biomaterials*, vol. 27, pp. 4794-4803, 2006.

References

- [84] S. F. DE AZEVEDO, R. OLIVEIRA, and B. SONNLEITNER, "CHAPTER THREE NEW METHODOLOGIES FOR MULTIPHASE BIOREACTORS 3: DATA ACQUISITION, MODELLING AND CONTROL," *Multiphase bioreactor design*, p. 57, 2001.
- [85] J. M. Cabral, M. Mota, and J. Tramper, *Multiphase bioreactor design*: CRC Press, 2003.
- [86] R. Di Felice, "Hydrodynamics of liquid fluidisation," *Chemical Engineering Science*, vol. 50, pp. 1213-1245, 1995.
- [87] N. Epstein, "Teetering," *Powder Technology*, vol. 151, pp. 2-14, 2005.
- [88] R. C. Dean Jr, P. V. Grela, S. B. Karkare, and P. W. Runstadler Jr, "Fluidized cell cultivation process," 1990.
- [89] P. Foscolo, L. Gibilaro, and S. Waldram, "A unified model for particulate expansion of fluidised beds and flow in fixed porous media," *Chemical Engineering Science*, vol. 38, pp. 1251-1260, 1983.
- [90] J. Richardson and W. Zaki, "The sedimentation of a suspension of uniform spheres under conditions of viscous flow," *Chemical Engineering Science*, vol. 3, pp. 65-73, 1954.
- [91] A. Hirata and F. B. Bulos, "Predicting bed voidage in solid-liquid fluidization," *Journal of Chemical Engineering of Japan*, vol. 23, pp. 599-604, 1990.
- [92] U. Ganguly, "Direct method for the prediction of expanded bed height in liquid-solid fluidization," *The Canadian Journal of Chemical Engineering*, vol. 58, pp. 559-563, 1980.
- [93] A. Kinasiewicz, A. Gautier, D. Lewinska, J. Bukowski, C. Legallais, and A. Weryński, "Culture of C3A cells in alginate beads for fluidized bed bioartificial liver," in *Transplantation proceedings*, 2007, pp. 2911-2913.
- [94] N. Epstein, "Liquid-Solids Fluidization, Chapter 26," in *Handbook of fluidization and fluid-particle systems*
W. C. Yang, Ed., ed: CRC press, 2003.
- [95] A. Khan and J. Richardson, "Fluid-particle interactions and flow characteristics of fluidized beds and settling suspensions of spherical particles," *Chemical Engineering Communications*, vol. 78, pp. 111-130, 1989.
- [96] R. Turton and N. Clark, "An explicit relationship to predict spherical particle terminal velocity," *Powder technology*, vol. 53, pp. 127-129, 1987.
- [97] P. O. Seglen, "Preparation of isolated rat liver cells," *Methods in cell biology*, vol. 13, pp. 29-83, 1976.
- [98] R. Di Felice and E. Parodi, "Wall effects on the sedimentation velocity of suspensions in viscous flow," *AIChE journal*, vol. 42, pp. 927-931, 1996.

References

- [99] S. Morelli, S. Salerno, M. Rende, L. C. Lopez, P. Favia, A. Procino, *et al.*, "Human hepatocyte functions in a galactosylated membrane bioreactor," *Journal of Membrane Science*, vol. 302, pp. 27-35, 2007.
- [100] E. Curcio, L. De Bartolo, G. Barbieri, M. Rende, L. Giorno, S. Morelli, *et al.*, "Diffusive and convective transport through hollow fiber membranes for liver cell culture," *Journal of biotechnology*, vol. 117, pp. 309-321, 2005.
- [101] G. K. Batchelor, *An introduction to fluid dynamics*: Cambridge university press, 2000.
- [102] B. A. Ogunnaike and W. H. Ray, *Process dynamics, modeling, and control* vol. 1: Oxford University Press New York, 1994.
- [103] P. Hay, A. Veitch, M. Smith, R. Cousins, and J. Gaylor, "Oxygen Transfer in a Diffusion-Limited Hollow Fiber Bioartificial Liver," *Artificial organs*, vol. 24, pp. 278-288, 2000.
- [104] A. O'Dwyer, *Handbook of PI and PID controller tuning rules* vol. 57: World Scientific, 2009.

Appendix A - MATLAB Scripts

Membrane bioreactor model

Evaluate V from H (evaluateVfromh)

```
function [V2,dV2_dh]=evaluateVfromh(hm)

% Command for generate the relation of V2 vs. H (after this
launchglobal_MBR.m and MBRmodel_v3.m)
% h=0+h_0:0.2:h_sphf+h_c+h_0;for i=1:length(h),
[V2(i),dV2_dh(i)]=evaluateVfromh(h(i)); if
i>=2,intdV2(i)=trapz(h(1:i),dV2_dh(1:i));end,
end,figure(2),plot(h,V2,h,intdV2),xlabel('h_m, [mm]'),ylabel(' V2,
[ml]')

global H_s r_s h_c h_0 r_c h_vlt N_row N_vlt r_fib L_fib
h_cap V_cap V_sph V_cyl V_fib V_fibt h_sph0 h_fib0 h_fibf
h_sphf

% hm height measured from the sensor zero (i.e. not from the reactor
zero)
% h_0 height of the bioreactor zero with respect to the sensor zero
% V2 liquid volume in the reactor (measured from the reactor zero).

% h height from the reactor zero
h = hm - h_0;

if h < 0
    error(' Invalid height: lower than minimum. ');
elseif 0 <= h && h < h_sph0
    V2 = pi*r_c^2*h; % mm^3
```


Appendixes

```
dV2_dh = pi*r_c^2;           % mm^3/mm (to convert to ml/mm by
dividing by 1000)

elseif h < h_sphf
    h_cs = h+h_cap-h_c;
    V2 = V_cyl-V_cap+1/3*pi*h_cs^2*(3*r_s-h_cs)-
N_row*V_fib*N_vlt/h_vlt*(h-h_fib0)*(h>=h_fib0)*(h<h_fibf)-
V_fibt*(h>=h_fibf);
    dV2_dh = 1/3*pi*2*h_cs*(3*r_s-h_cs)-1/3*pi*h_cs^2-
N_row*V_fib*N_vlt/h_vlt*(h>h_fib0)*(h<h_fibf);

else %if h <= h_sphf+h_c
    V2 = V_cyl+V_sph-V_fibt+pi*r_c^2*(h-h_sphf);
    dV2_dh = pi*r_c^2;

% else
% error(' Invalid height: higher than maximum. ');
end

V2=V2/1000;           % mm^3 to ml
dV2_dh=dV2_dh/1000; % mm^3/mm to ml/mm

end
```

Launch global MBR (launchglobal_MBR.m)

```
global F0_s V1 CA0_s CB0_s CA1_s CB1_s CA2_s CB2_s CA3_s CB3_s
V2_s F2_s DF2 V3 k Vm Km Gp Gd H_s r_s h_c h_0 r_c h_vlt
N_row N_vlt r_fib L_fib h_cap V_cap V_sph V_cyl V_fib V_fibt
h_sph0 h_fib0 h_fibf h_sphf LC
```

Membrane bioreactor model (MBRmodel_v3.m)

```
function MBRmodel_v3()

launchglobal_MBR;
%Parameters
F0_s=1.48;    % ml/min
F2_s=0;      % ml/min
DF2 =-0.305*F2_s; % ml/min
V1=0.003;    % ml
% V2_s evaluated below from h_s;    % V2_s=13.3158;    % ml
H_s=60;      %10.1    % mm (steady-state measured height)
V3=0.003;    % ml
% k=3e-1;    % 1/s    (** 1/min?? **)
Vm=6e-6;     % mol/ml.min
Km=7e2;      % mol/ml

%Geometrical data of the bioreactor
r_s=19;      % mm radius of sphere
h_c=15;      % mm height of cylinder
h_0=10;      % mm bioreactor zero measured with respect to the sensor
zero
r_c=7;       % mm radius of cylinder
L_fib=40;    % mm length of fiber
r_fib=0.25;  % mm radius of fiber
N_row=10;    % number of fibers in a horizontal row
N_vlt=20;    % number of vertical layer total
h_vlt=10;    % mm height of vertical layer total

V_fib = pi*r_fib^2*L_fib;    % mm^3 volume of one fiber
V_fibt = V_fib*N_row*N_vlt; % mm^3 total volume of the
fibers
h_cap = r_s-sqrt(r_s^2-r_c^2); % mm height of the small cap
at sphere/cylinder interface
```

Appendixes

```
V_cap = 1/3*pi*h_cap^2*(3*r_s-h_cap); % mm volume of the small cap
at sphere/cylinder interface
V_sph = 4/3*pi*r_s^3-2*V_cap; % mm^3 volume of sphere minus
two small caps
V_cyl = pi*r_c^2*h_c; % mm^3 volume of one reactor
volume cylinder

h_sph0 = h_c; % height of the beginning of
the sphere
h_fib0 = h_c+r_s-h_cap-h_vlt/2; % height of the beginning of
the fibers
h_fibf = h_c+r_s-h_cap+h_vlt/2; % height of the end of the
fibers
h_sphf = h_c+2*(r_s-h_cap); % height of the end of the
sphere

% V2_s based on related equation of H_s

[V2_s,dV2_dh_s] = evaluateVfromh(H_s)

CA0_s=0.4 %mol/ml
CB0_s=0.2 %mol/ml
CA1_s=CA0_s %mol/ml
CB1_s=CB0_s %mol/ml
aa=F0_s/V2_s; bb=-((F0_s*CA1_s-F0_s*Km)/V2_s-Vm);
cc=- (F0_s*CA1_s*Km/V2_s);
DD=bb^2-4*aa*cc;
CA2_s=(-bb+sqrt(DD))/(2*aa) %mol/ml
0 = F0_s/V2_s*(CA1_s-CA2_s)-(Vm*CA2_s)/(Km+CA2_s)
CB2_s=CB1_s+(V2_s*(Vm*CA2_s)/(F0_s*(Km+CA2_s))) %mol/ml
0 = F0_s/V2_s*(CB1_s-CB2_s)+(Vm*CA2_s)/(Km+CA2_s)
CA3_s=CA2_s %mol/ml
CB3_s=CB2_s %mol/ml

%LC=Level coefficient for linearization
```

Appendixes

```
if H_s<h_sph0
    LC=1000/(pi*r_c^2);
elseif H_s<h_fib0
    LC=1000/((1/3)*pi*(H_s-h_c)*(6*r_s+3*h_c-3*H_s));
elseif H_s<h_fibf
    LC=1000/((1/3)*pi*(H_s-h_c)*(6*r_s+3*h_c-3*H_s)-
(N_row*V_fib*N_vlt/h_vlt));
elseif H_s<h_sphf
    LC=1000/((1/3)*pi*(H_s-h_c)*(6*r_s+3*h_c-3*H_s));
else
    LC=1000/(pi*r_c^2);
end
```

% A, Bu, Bd, C, Du, Dd matrix coefficients for the linearized model

```
A=[-F0_s/V1  0  0  0  0  0
    0  -F0_s/V1  0  0  0  0
    0  0  0  0  0  0
    F0_s/V2_s  0  ((F0_s*CA2_s)-(F0_s*CA1_s))/(V2_s^2)
    (-F0_s/V2_s)-(Vm*Km/((Km+CA2_s)^2))  0  0
    0  F0_s/V2_s  ((F0_s*CB2_s)-(F0_s*CB1_s))/(V2_s^2)
    Vm*Km/(Km+CA2_s)^2  -F0_s/V2_s  0
    0  0  0  F2_s/V3  0  -F2_s/V3
    0  0  0  0  0  F2_s/V3  0  -F2_s/V3];
```

```
Bu=[F0_s/V1  0  (CA0_s-CA1_s)/V1
    0  F0_s/V1  (CB0_s-CB1_s)/V1
    0  0  1
    0  0  (CA1_s-CA2_s)/V2_s
    0  0  (CB1_s-CB2_s)/V2_s
    0  0  0  (CA2_s-CA3_s)/V3;
    0  0  0  (CB2_s-CB3_s)/V3];
```

```
Bd=[0;
    0;
    0;
    0;
    0;
```

Appendixes

```
0;
0];

C=[1    0    0                                0    0    0    0;
   0    1    0                                0    0    0    0;
   0    0    LC                               0    0    0    0;
   0    0    0                                1    0    0    0;
   0    0    0                                0    1    0    0;
   0    0    0                                0    0    1    0;
   0    0    0                                0    0    0    1];

Du=0;
Dd=0;

%Gp and Gd transfer function matrices
sysP=ss(A,Bu,C,Du);
Gp=tf(sysP);
sysD=ss(A,Bd,C,Dd);
Gd=tf(sysD);

Gp.InputName={'C_', 'C_{B0}', 'F_0', 'F_2'};
Gp.OutputName={'C_{A1}', 'C_{B1}', 'h', 'C_{A2}', 'C_{B2}', 'C_{A3}',
'C_{B3}'};

%Plot all input unit step responses in all outputs
figure(1), step(Gp, 5)

%Open-loop stability
eigenvalues=eig(A)

%Controllability analysis
condition_number=cond(A)
```

Control system

Main-timer

```
global s time0 time_rec dt insfr_rec avgfr_rec inslv_rec avglv_rec
acqframes avgtimelv avgtimefr ...
    avgframeslv avgframesfr haif haaf hail get_flow get_level
set_pump Qold outprint ...
    fid_lv fid_fr use_flow_in_lvcontrol QoutVlv outputData fSP
use_flow_in_frcontrol Qoldfr QoutVfr dt_fr

% Flags
get_flow = 1;           % acquire flow measurements from SLI flow
                        sensor (Analog Input "ai1") (required if set_pump=1)
get_level = 1;         % acquire level measurements from CLC
                        sensor (Analog Input "ai0")
set_pump = 1;         % adjust Ismatec Reglo pump speed
use_flow_in_lvcontrol = 0; % use measurement of flow as Qold for
                        level control
use_flow_in_frcontrol = 1; % use measurement of flow as Qoldfr for
                        flow control
Qold = 1;             % previous value for pump speed (needed
                        for velocity form of PID controller)
outprint = 1;

% Parameters
acqrate = 10;         % frames/seconds
acqtime = 1/acqrate; % seconds
disptime = 50;       % seconds
avgtimelv = 6;       % seconds
avgtimefr = 6;       % seconds

acqframes = acqtime*acqrate;
```

Appendixes

```
ndispacqs = disptime*acqrate+1;
avgframeslv = avgtime1v*acqrate+1;
avgframesfr = avgtimefr*acqrate+1;
dt = 1/acqrate;
dt_fr = 1/acqrate;
% Vector initialization
time_rec = zeros(1,ndispacqs*acqframes);
insfr_rec = zeros(1,ndispacqs*acqframes);
avgfr_rec = zeros(1,ndispacqs*acqframes);
inslv_rec = zeros(1,ndispacqs*acqframes);
avglv_rec = zeros(1,ndispacqs*acqframes);

time0=now; % base time for counting seconds (see
postprocessdata)

% Create DAQ session and open appropriate I/O channels
daq.getDevices;
s = daq.createSession('ni');
if get_level
    s.addAnalogInputChannel('Dev1','ai0','Voltage');
end
if get_flow
    s.addAnalogInputChannel('Dev1','ai1','Voltage');
end
if set_pump
    chDigP1=addDigitalChannel(
s,'Dev1','Port0/Line1:5','OutputOnly'); % Pump 1
    chAnlP1=addAnalogOutputChannel(s,'Dev1','ao0','Voltage');
% Pump 1
    chDigP2=addDigitalChannel(s,'Dev1','Port0/Line6'
,'OutputOnly'); % Pump 2
    chDigP2=addDigitalChannel(
s,'Dev1','Port1/Line0:3','OutputOnly'); % Pump 2
    chAnlP2=addAnalogOutputChannel(s,'Dev1','ao1','Voltage');
% Pump 2
end
```

Appendixes

```
% Create figure for flowrate
if isempty(haaf) && get_flow
    hfif=figure('Name','Flowrate','Position',[50 460 500 300]);
    haaf=axes;
elseif get_flow
    axes(haaf);
end

% Create figure for level
if isempty(hail) && get_level
    hfil=figure('Name','Instantaneous level','Position',[610 460 500
300]);
    hail=axes;
elseif get_level
    axes(hail);
end

% Create output text file for flowrate
if outprint && get_flow
    filename_fr = strcat('flow_data_',datestr(now,'yyyymmdd-
HHMMSS'),' .txt');
    fid_fr = fopen(filename_fr,'wt');
end

% Create output text file for level
if outprint && get_level
    filename_lv = strcat('level_data_',datestr(now,'yyyymmdd-
HHMMSS'),' .txt');
    fid_lv = fopen(filename_lv,'wt');
end

% Create timer object with properties and start it
t = timer;
t.StartFcn = @(src,event) disp([event.Type ' executed '...
datestr(event.Data.time,'dd-mmm-yyyy HH:MM:SS.FFF')]);
```


Appendixes

```
t.TimerFcn      = @(src,event) postprocessdata_timer(src,event);
t.StopFcn       = @(src,event) disp([event.Type ' executed '...
    datestr(event.Data.time, 'dd-mmm-yyyy HH:MM:SS.FFF')]);
t.Period        = 1/acqrate;
t.TasksToExecute = inf;
t.ExecutionMode = 'fixedRate';

start(t)        % use stop(t) to manually stop execution of the timer
```

Postprocessdata

```
function postprocessdata_timer( src,event )
global s time0 time_rec dt insfr_rec avgfr_rec inslv_rec avglv_rec
acqframes avgtimelev avgtimefr ...
    avgframeslv avgframesfr haif haaf hail get_flow get_level
set_pump Qold outprint ...
    fid_lv fid_fr htxt use_flow_in_lvcontrol QoutVlv outputData fSP
use_flow_in_frcontrol Qoldfr QoutVfr dt_fr

format compact
[data,timestamps]=inputSingleScan(s);

n      = length(insfr_rec);
nraw  = length(timestamps);

% Read raw data
times  = (timestamps'-time0)*86400;          % seconds from the start
of the test
```

Appendixes

```
if get_level
    rawdata_lv = data(:,1)';
    if get_flow
        rawdata_fr = data(:,2)';
    end
elseif get_flow
    rawdata_fr = data(:,1)';
end

% Shift previous time back and append new ones (for live plot)
time_rec=append_data(time_rec,times,n,acqframes);

if get_flow
    % Convert flowrate readings
    insfr_acq=convertflowrate(rawdata_fr);

    % Shift previous measurements back and append new ones (for live
    plot)
    insfr_rec=append_data(insfr_rec,insfr_acq,n,acqframes);

    % Calculate new set of nraw average flowrates across averaging
    time and
    % update average flowrate record
    avgfr_rec =
    compute_update_average(avgfr_rec,time_rec,insfr_rec,nraw,n,avgframesfr
    ,avgtimefr);

    plot(haaf,time_rec,avgfr_rec,'r', time_rec,insfr_rec,'b')
    %   haaf_title=sprintf('Average flowrate over the last %4.2f
    s',avgtimefr);
    set(haaf,'ylim',[0 2],'xlim',[time_rec(1),time_rec(n)]);
    %,'title',haaf_title);
    text(time_rec(n)+1,avgfr_rec(n),num2str(avgfr_rec(n),'%6.3f'))
    %   value=num2str(avgfr_rec(n));
```

Appendixes

```
%
text('Units','normalized','Position',[1.02,0.6],'FontSize',9,'String',
value)

end

if get_level
    % Convert level readings
    inslv_acq=convertheight(rawdata_lv);

    % Shift previous measurements back and append new ones (for live
    plot)
    inslv_rec=append_data(inslv_rec,inslv_acq,n,acqframes);

    % Calculate new set of nraw average levels across averaging time
    and
    % update average level record
    avglv_rec =
compute_update_average(avglv_rec,time_rec,inslv_rec,nraw,n,avgframeslv
,avgtimelv);

    plot(hail,time_rec,avglv_rec,'r',time_rec,inslv_rec,'b');
    h_min=30; h_max=90;
    % set(hail,'xlim',[time_rec(1),time_rec(n)],'ylim',[h_min,h_max]);
    %,'title','Instantaneous level');
    set(hail,'xlim',[time_rec(1),time_rec(n)],'ylim',[45,85]);
    %,'title','Instantaneous level');
    % value=num2str(inslv_rec(n));
    %
htxt=text('Units','normalized','Position',[1.02,0.6],'FontSize',9,'Str
ing',value)
    text(time_rec(n)+1,avglv_rec(n),num2str(avglv_rec(n),'%6.3f'))

% ***** Section for (digital) level control *****
if set_pump
    hSP(1:n) = 60; % set-point height (mm)
```

Appendixes

```
eps1      = hSP-avglv_rec;    % error to the controller
eps1(n-3:n)          % print last three error values

% ***** CONTROLLER PARAMETERS *****
Kc = -1;              % controller gain (ml/min/mm)
tI =20;              % integral time (s)
tD = 0*dt;           % derivative time (s)

Qmin = 0;            % (ml/min) for anti-reset windup
Qmax = 2;            % (ml/min) for anti-reset windup

DQ      = Kc*((1+dt/tI+tD/dt)*eps1(n) - (2*tD/dt+1)*eps1(n-
1)+tD/dt*eps1(n-2))    %Digital PID control (velocity form, p.962 O&R)

if use_flow_in_lvcontrol && get_flow
    Qold = avgfr_rec(:,n);          % if using
flowrate measurement take the last MEASURED (averaged) flowrate
end

% Controller output (in flowrate units)
Qnew = min(max(Qold + DQ,Qmin),Qmax)    % min/max for
anti-reset windup

if ~use_flow_in_lvcontrol || ~get_flow
    Qold = Qnew;                    % if not using
measurement, store current COMPUTED Qnew as Qold
end

% convert u to Volt
QoutVlv = convertspeed(Qnew);

% Manipulation through actuation of pump
ctrlpump='P2';                    % Flag for pump selection
```

Appendixes

```
% ***** Section for (digital) flow control *****
fSP(1:n) = 1.5;           % set-point flowrate (ml/min)
epsfr    = fSP-avgfr_rec; % error to the controller
epsfr(n-3:n)           % print last three error values

% ***** CONTROLLER PARAMETERS *****
Kc_fr = 2;               % controller gain (ml/min/mm)
tI_fr = 0.01;           % integral time (s)
tD_fr = 0*dt_fr;       % derivative time (s)

Qmin = 0;               % (ml/min) for anti-reset windup
Qmax = 2;               % (ml/min) for anti-reset windup

DQfr = Kc_fr*((1+dt_fr/tI_fr+tD_fr/dt_fr)*epsfr(n)-
(2*tD_fr/dt_fr+1)*epsfr(n-1)+tD_fr/dt_fr*epsfr(n-2)) %Digital PID
control (velocity form, p.962 O&R)

if use_flow_in_frcontrol && get_flow
    Qoldfr = avgfr_rec(:,n);           % if using
flowrate measurement take the last MEASURED (averaged) flowrate
end

% Controller output (in flowrate units)
Qnewfr = min(max(Qoldfr + DQfr,Qmin),Qmax) % min/max
for anti-reset windup

% convert u to Volt
QoutVfr = convertspeed(Qnewfr);

% Manipulation through actuation of pump
ctrlpump='P1';           % Flag for pump selection

% PUMP settings definition and signal send

if ctrlpump=='P1'
```

Appendixes

```
iStartP1 = 0;          % On?
speedP1  = QoutVfr;   %
iStartP2 = 0;          % Off?
speedP2  = QoutVlv;   %
elseif ctrlpump=='P2'
    iStartP1 = 0;      % Off?
    speedP1  = QoutVfr; %
    iStartP2 = 0;      % On?
    speedP2  = QoutVlv; %
end

% PUMP 1          -- 0 = On -- 1 = Off
iGrnd  = 0;          iAnInp = 0;          iStart = iStartP1;
iDirec = 1;          iPanel  = 1;          zSpeed = speedP1;
vP1=[iGrnd, iAnInp, iStart, iDirec, iPanel, zSpeed];

% PUMP 2          -- 0 = On -- 1 = Off
iGrnd  = 0;          iAnInp = 0;          iStart = iStartP2;
iDirec = 1;          iPanel  = 1;          zSpeed = speedP2;
vP2=[iGrnd, iAnInp, iStart, iDirec, iPanel, zSpeed];
% send signals
outputSingleScan(s, [vP1,vP2]);
end
end
if outprint
    printstep=ceil(nraw/2);
    if printstep>1
        Mfr_out=[times(1:printstep:nraw) '
insfr_acq(1:printstep:nraw) ' avgfr_rec((end-nraw+1):printstep:end)'];
    else
        Mfr_out=[times' insfr_acq' avgfr_rec(end) ' QoutVfr'];
    end
    fprintf(fid_fr, '%12.4E %12.4E %12.4E %12.4E\n',Mfr_out');
end
if outprint
    printstep=ceil(nraw/2);
    if printstep>1
```

Appendixes

```
        Mlv_out=[times(1:printstep:nraw) '
inslv_acq(1:printstep:nraw) ' avglv_rec((end-nraw+1):printstep:end)'];
    else
        Mlv_out=[times' inslv_acq' avglv_rec(end) ' QoutVlv'];
    end
    fprintf(fid_lv, '%12.4E %12.4E %12.4E %12.4E\n', Mlv_out');
end
end

function vect_rec = append_data(vect_rec, newdata, n, nnewdata)

vect_rec = circshift(vect_rec, -nnewdata, 2);
vect_rec((n-nnewdata+1):n) = newdata;

end

function avg_rec =
compute_update_average(avg_rec_old, time_rec, ins_rec, nraw, n, avgframes, a
vgtime)

% computes last nraw averages
avg_last = zeros(1, nraw);

% averages based on algebraic mean of last avgframes steps
for i=1:nraw
    avg_last(i) = trapz(time_rec((n-avgframes+1-nraw+i):(n-
nraw+i)), ins_rec((n-avgframes+1-nraw+i):(n-nraw+i)))/(time_rec(n-
nraw+i)-time_rec(n-avgframes+1-nraw+i));    %avgtime;    %avgtime;
end

% shift previous averages back and append new ones (for live plot)
avg_rec=circshift(avg_rec_old, -nraw, 2);
avg_rec((n-nraw+1):n)=avg_last;

end
```

Appendixes

```
function height = convertheight(rawdata)
% convert level readings
v_min=0.5; v_max=4.5;
h_min=30; h_max=90; % minimum height (teach-in
low); maximum height (teach-in high)
height=(rawdata-v_min)/(v_max-v_min)*(h_max-h_min)+h_min; %
Conversion from rawdata (0.5/4.5 V to hmin/hmax)
end
```

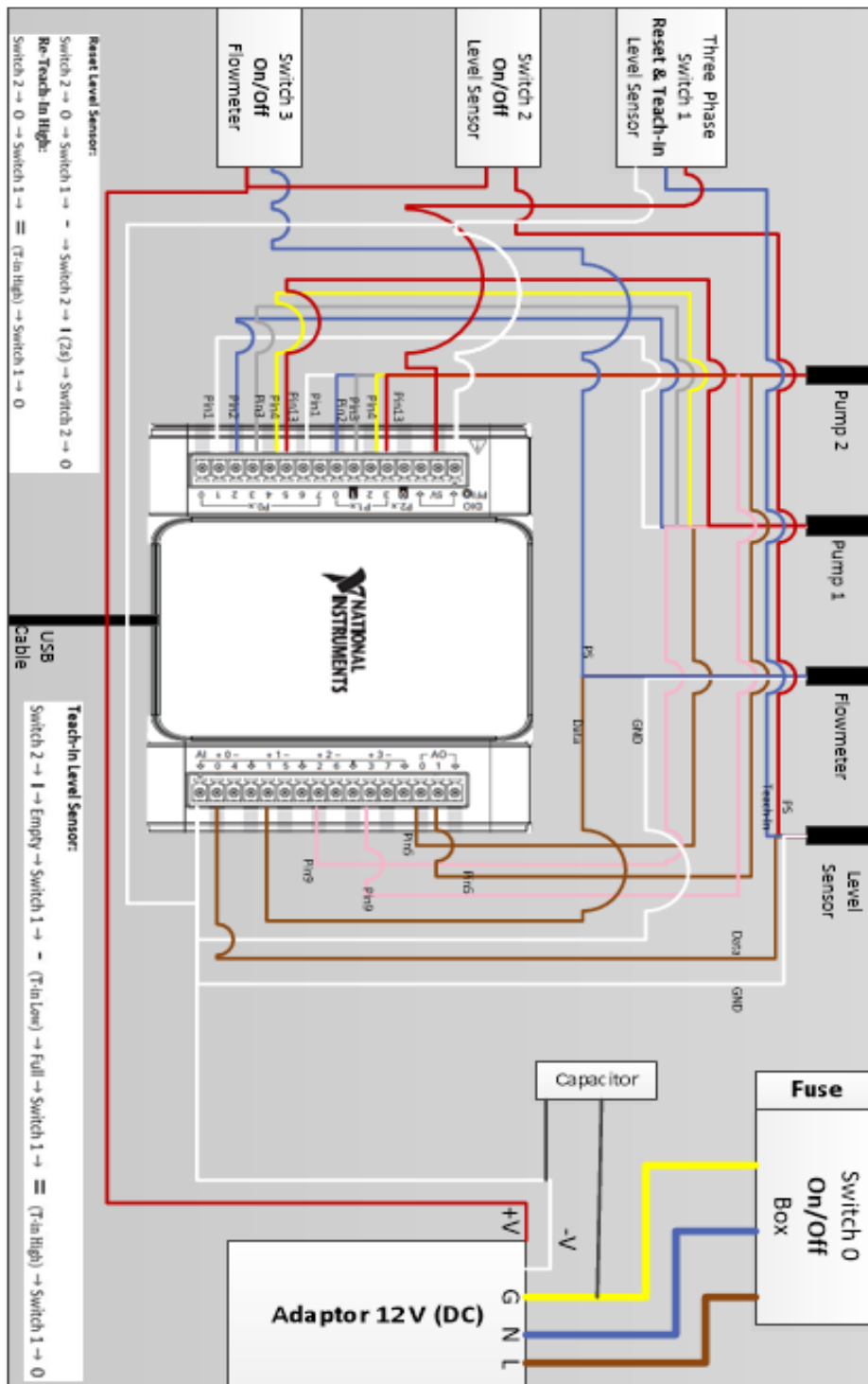
```
function flowrate = convertflowrate(rawdata)
% convert flowrate readings
v_min=0; v_max=10;
fr_min=-5.5; fr_max=5.5; % minimum flowrate;
maximum flowrate
flowrate=(rawdata-v_min)/(v_max-v_min)*(fr_max-fr_min)+fr_min; %
Conversion from rawdata (0/10 V to -5.5/5.5 ml/min)
end
```

```
function signal2pump = convertspeed(Q)
%convert flowrate to volt for the pump
Vmin = 0; Vmax = 0.7;
QminP = 0; QmaxP = 3.19; % Check maximum flowrate of the pump
signal2pump = max([min([(Q - QminP)/(QmaxP - QminP)*(Vmax - Vmin)+Vmin
, Vmax]), Vmin]);
end
```

Shutup

```
s.stop;
s.stop;
% s2.stop;
fclose('all');
```


Appendix B – DAQ box manual



Appendix C – CLC level sensor manual

CLC Series Miniature capacitive continuous liquid level sensors

FEATURES

- Contact-free measurement of continuous liquid level
- Measurement of both metallic and non-metallic substances
- Measurement of granular or pulverised materials
- Positioning/proximity sensor
- Displacement sensor
- Easy mounting
- RoHS compliant
- Quality Management System according to ISO 13485:2003 and ISO 9001:2008

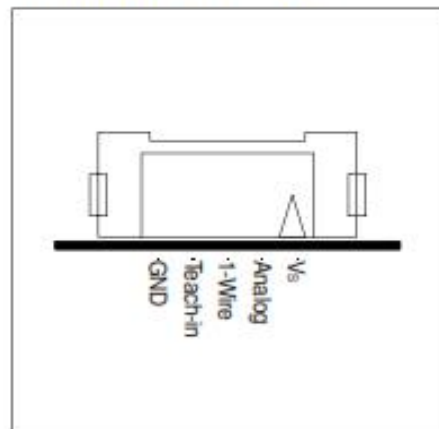


SPECIFICATIONS

Maximum ratings

Supply voltage (V_{CC})	5.5...15 V _{DC}
Output voltage ($R_L=1\text{ k}\Omega$)	5 V
Temperature ranges	
Operating	-20 ... 85 °C
Compensated	±20 °C
	relative to calibration temperature

ELECTRICAL CONNECTION



CLC Series

Miniature capacitive continuous liquid level sensors

PERFORMANCE CHARACTERISTICS

Characteristic	Min.	Typ.	Max.	Unit
Measuring range (vertical)	0		100	mm
Resolution ¹		6		bit
Response time	10	50	1000	ms

Note:

- At 3 mm distance between sensor and medium.

OUTPUT SIGNAL

The sensor calculates an actual measurement value between the Teach-In points 'LOW' and 'HIGH'. LOW corresponds to 0 % and HIGH equals 100 %.

Output	0 %	25 %	50 %	100 %
RS232	0x01	0x3F	0x80	0xFE
Analog	0.5 V	1.5 V	2.5 V	4.5 V

ELECTRICAL CHARACTERISTICS

Pin	Pin name	Explanation	Min.	Typ.	Max.	Unit
1	V _S ⁴	Supply pin ²	5.5	9	15	V
		Current draw of sensor	7	8.5	10	mA
2	Analog ⁵	Analog output (R _L =1 kΩ)	0.5		4.5	V
3	1-wire ⁵	RS232 Out, 9600, 8N1				
		Output voltage (R _L =1 kΩ)	0		5	V
4	TI	Teach-in ³	-0.25		5.25	
		Current draw			1	mA
5	GND	Ground				

Note:

- Length of power supply cable must not exceed 2.5 m.
- Only for Teach-In, do not connect during operation. (T_{Teach}=4.5...5.25 V, T_{Low}=-0.25...0.5 V)
- The quality of the supply voltage (with regards to ripple or other disturbances) may have an impact on the accuracy of the measurement.
- No protection against electrical surge (e.g. with inductive load)

ELECTRICAL CONNECTION (cont.)



CLC Series

Miniature capacitive continuous liquid level sensors

TEACH-IN

The Teach-In (TI) mode allows for a permanent storage (EEPROM) of both low and high level values of the measurement range. This range is determined by the sensor pad. The TI_{LOW} mode stores the value for the empty or low level container and adapts to the corresponding application conditions. The TI_{HIGH} mode stores the value of the container filled to the desired max. level. By factory default the sensor is 'formatted' and needs to be taught to provide an output signal.

Preconditions for successful Teach-In

- **Do not touch** the sensor or container during the Teach-In or measuring process.
- The sensor must be in original mounting position.
- After connecting to V_S the sensor must level off for 2 sec.
- **Important:** The sensor must **first be taught LOW** to adapt to the ambient conditions, **then HIGH**.
- The TI_{HIGH} value must not be lower than the TI_{LOW} value.
- Best results will be achieved when GND is connected to earth potential (see GROUND REFERENCE).

Note: The maximum tolerable voltage range for the TI pin is -0.25...+5.25 V.

TI_{LOW} mode:

Apply voltage between 0 and 0.5 V for at least 500 ms at the Teach-in pin.
After 1 sec. the value is stored in the EEPROM.

TI_{HIGH} mode:

Apply voltage between 4.5 and 5 V for at least 500 ms at the Teach-in pin.
After 1 sec. the value is stored in the EEPROM.

Under normal conditions, the TI-Pin delivers 2.5 V.

It is possible to re-teach the HIGH level only (in case, the LOW level remains the same). A re-teaching is only possible after having disconnected the supply voltage. However, if the LOW level needs to be changed, the sensor first has to be formatted (see Reset).

Reset

The sensor can be reset to factory default ('format') as follows:

1. Disconnect the sensor from V_S .
2. Connect the TI-Pin (pin 4) to GND.
3. Connect the sensor to V_S for at least 2 sec.
4. Disconnect the sensor from V_S and formatting is completed.

Appendix D – Flowmeter manual



SLI Liquid Flow Meter Series

Media Isolated Microfluidic Flow Meter

- Liquid flow rates up to 10 ml/min
- Non-invasive measurement
- Different interface options
- 40 ms flow detection response time



Product Summary

The SLI Liquid Flow Meter enables fast, non-invasive measurements of very low liquid flow in the $\mu\text{l}/\text{min}$ - to ml/min -range. Excellent chemical resistance is ensured: The flow path of the SLI Liquid Flow Meter is formed by a simple, straight glass capillary. The fourth generation MEMS sensors combine a thermal high precision sensor element with amplification circuits and digital intelligence for linearization and temperature compensation on one single microchip – the product's core element.

Interface Options

Digital

- I²C-Bus
- RS485-Bus
- USB Cable

Analog

- Voltage Output (0-10 V)
- Additional operation modes

For more information on communication, please refer to page 2 of this document.

1 Sensing Performance

Table 1: Model specific performance of SLI (all data for medium H₂O, 23°C)

Parameter	SLI-0430	SLI-1000	SLI-2000	Unit
H ₂ O Full scale flow rate	80	1000	5000	$\mu\text{l}/\text{min}$
H ₂ O Sensor output limit ^a	120	1100	5500 ^b	$\mu\text{l}/\text{min}$
Accuracy below full scale (whichever error is larger)	5.0 0.15	5.0 0.2	5.0 0.2	% of m.v. ^c % of full scale
Repeatability below full scale (whichever error is larger)	0.5 0.01	0.5 0.02	0.5 0.02	% of m.v. % of full scale
Temperature coefficient (additional error / °C; whichever is larger)	0.13 0.003	0.1 0.004	0.1 0.004	% m.v. / °C % full scale / °C
Mounting orientation sensitivity ^d	<0.4	1.0	1.5	% of full scale
Flow detection response time τ_{95}	40			ms
Response time on power-up	120			ms
Operating temperature	+10...+50			°C
Ambient storage temperature ^e	-10...+60			°C
Maximum recommended operating pressure	50	15	15	bar
Burst pressure	150	30	30	bar

^a Flow rate at which the sensor output saturates. See section 2 for performance between full scale and saturation point

^b Extended range up to 10500 $\mu\text{l}/\text{min}$, see section 2 for performance specifications

^c Measured value

^d Maximum additional offset when mounted vertically

^e Non-condensing, flow path empty

Table 2: Model specific performance of SLI (all data for medium IPA, 23°C)

Parameter	SLI-0430	SLI-1000	SLI-2000	Unit
IPA full scale flow rate	500	10'000		µl/min
			80	ml/min
Sensor output limit ^a	600	11'000		µl/min
			90	ml/min
Accuracy below full scale (whichever error is larger)	20	20	10	% of m.v. ^b
	1	1	0.5	% of full scale
Repeatability below full scale (whichever error is larger)	1	1	1.5	% of m.v.
	0.05	0.05	0.03	% of full scale
Temperature coefficient (additional error / °C; whichever is larger)	0.5	0.4	0.35	% m.v. / °C
	0.025	0.02	0.02	% full scale / °C

^aFlow rate at which the sensor output saturates^bMeasured value

1.1 Calibration Field Information

The SLI Liquid Flow Meters hold calibrations for two liquids, one for water (H₂O) and one for isopropyl alcohol (IPA). Each calibration is stored on a separate calibration field (CF):

- Calibration field 0: H₂O (factory default)
- Calibration field 1: IPA
- Calibration field 2 (SLI-2000 only, starting from SN 1627-00000): H₂O extended range

The default calibration field (i.e. the active calibration field at power up) can be permanently changed via I²C or RS485 commands. Alternatively, the default calibration field can be changed using the USB-RS485 Sensor Viewer which is part of the Liquid Flow Meter Kit and also available in the download center on the Sensirion liquid flow webpage. www.sensirion.com/liquidflow-download

3 Communication with the Sensor

The SLI flow meter shows bidirectional, linear transfer characteristics. The product comes fully calibrated for water and IPA.

Digital Sampling Time, 16 bit	74 ms
Digital Sampling Time, 9 bit	1 ms

3.1 Electrical Specifications

Table 3: DC Characteristics

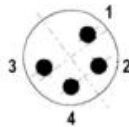
Parameter	Conditions	Min.	Typ.	Max.	Units
Power Supply DC, VDD	Sensor only	4	5	6	V
	RS485 cable	4	5	6	V
	Analog cable	12	24	36	V
Operating Current	VDD = 4-6 V, no load	5	5.5	6	mA
	RS485 cable		20	70	mA
	Analog cable		4.3		mA

3.2 Electrical Connector and Pinout

The flow meter is equipped with a male connector type M8, 4-pin, threaded lock according to IEC 61076-2-101 (Ed. 1)/ IEC 60947-5-2, and is compatible with Sensirion's SCC1 interface cables.

Table 3: Electrical pinout

Pin	
1	SDA (data)
2	GND
3	VDD
4	SCL (clock)



3.3 Communication via USB cable

The Sensirion USB Sensor Cable provides an easy to use USB Interface for laboratory and desktop use.

For further information please see the SCC1-USB Sensor Cable datasheet, available on www.sensirion.com/liquidflow-download.

3.4 Digital Communication via RS485-Bus

The SCC1-RS485 Sensor Cable for flow sensors allows the communication via RS485 interface for use in a demanding industrial automation environment. In addition to the standard commands available in the I²C interface of the sensor, the incorporated microcontroller of the cable provides more complex logic such as a dispense volume totalizer, automatic dispense detection, automatic heater control and data buffer for asynchronous read-out.

For further information please see the SCC1-RS485 Sensor Cable datasheet, available on www.sensirion.com/liquidflow-download.

3.5 Analog Communication

The SCC1-ANALOG Sensor Cable allows simple and quick readout of Sensirion's liquid flow meters by converting the digital sensor reading to a 0...10.5 V analog voltage output. Additionally, a digital (high/low) output with two different modes of operation is available (Flow Switch / Volume Counter)

For further information please see the SCC1-USB Sensor Cable datasheet, available on www.sensirion.com/liquidflow-download.

3.6 Digital Communication via I²C-Bus

Digital communication between a master and the SLI sensor runs via the standard I²C-interface. The physical interface consists of two bus lines, a data line (SDA) and a clock line (SCL) which need to be connected via pull-up resistors to the bus voltage of the system.

These lines can be used on 3.3V or 5.0V level with a clock frequency of 100 kHz. For the detailed specifications of this I²C communication, please refer to specific I²C Application Notes from Sensirion.

Important Notices

Warning, personal injury

Do not use this product as safety or emergency stop devices or in any other application where failure of the product could result in personal injury (including death). Do not use this product for applications other than its intended and authorized use. Before installing, handling, using or servicing this product, please consult the datasheet and application notes. Failure to comply with these instructions could result in death or serious injury.

If the Buyer shall purchase or use SENSIRION products for any unintended or unauthorized application, Buyer shall defend, indemnify and hold harmless SENSIRION and its officers, employees, subsidiaries, affiliates and distributors against all claims, costs, damages and expenses, and reasonable attorney fees arising out of, directly or indirectly, any claim of personal injury or death associated with such unintended or unauthorized use, even if SENSIRION shall be allegedly negligent with respect to the design or the manufacture of the product.

ESD Precautions

The inherent design of this component causes it to be sensitive to electrostatic discharge (ESD). To prevent ESD-induced damage and/or degradation, take customary and statutory ESD precautions when handling this product.

Warranty

SENSIRION warrants solely to the original purchaser of this product for a period of 12 months (one year) from the date of delivery that this product shall be of the quality, material and workmanship defined in SENSIRION's published specifications of the product. Within such period, if proven to be defective, SENSIRION shall repair and/or replace this product, in SENSIRION's discretion, free of charge to the Buyer, provided that:

- notice in writing describing the defects shall be given to SENSIRION within fourteen (14) days after their appearance;
- such defects shall be found, to SENSIRION's reasonable satisfaction, to have arisen from SENSIRION's faulty design, material, or workmanship;
- the defective product shall be returned to SENSIRION's factory at the Buyer's expense; and
- the warranty period for any repaired or replaced product shall be limited to the unexpired portion of the original period.

This warranty does not apply to any equipment which has not been installed and used within the specifications recommended by SENSIRION for the intended and proper use of the equipment. EXCEPT FOR THE

WARRANTIES EXPRESSLY SET FORTH HEREIN, SENSIRION MAKES NO WARRANTIES, EITHER EXPRESS OR IMPLIED, WITH RESPECT TO THE PRODUCT. ANY AND ALL WARRANTIES, INCLUDING WITHOUT LIMITATION, WARRANTIES OF MERCHANTABILITY OR FITNESS FOR A PARTICULAR PURPOSE, ARE EXPRESSLY EXCLUDED AND DECLINED.

SENSIRION is only liable for defects of this product arising under the conditions of operation provided for in the datasheet and proper use of the goods. SENSIRION explicitly disclaims all warranties, express or implied, for any period during which the goods are operated or stored not in accordance with the technical specifications.

SENSIRION does not assume any liability arising out of any application or use of any product or circuit and specifically disclaims any and all liability, including without limitation consequential or incidental damages. All operating parameters, including without limitation recommended parameters, must be validated for each customer's applications by customer's technical experts. Recommended parameters can and do vary in different applications.

SENSIRION reserves the right, without further notice, (i) to change the product specifications and/or the information in this document and (ii) to improve reliability, functions and design of this product.

Copyright © 2001-2016, SENSIRION.

CMOSens® is a trademark of Sensirion

All rights reserved

CE, RoHS, REACH and WEEE Statement

The flow meters of the SLI series comply with requirements of the following directives and regulations:



- The device fully complies with norm EN 50081-2 (Emission Test Series), EN 50082-2 (Immunity Test Series) and ESD protection when used in combination with the SCC1-RS485 or SCC1-ANALOG Sensor Cables.
- EU Directive 1907/2006/EC concerning Registration, Evaluation, Authorization and Restriction of Chemicals (REACH)
- EU Directive 2002/96/EC on waste electrical and electronic equipment (WEEE), OJ13.02.2003; esp. its Article 6 (1) with Annex II.
- EU Directive 2002/95/EC on the restriction of certain hazardous substances in electric and electronic equipment (RoHS), OJ01.01.2011

Headquarters and Subsidiaries

SENSIRION AG
Laubisruetistr. 50
CH-8712 Staefa ZH
Switzerland

phone: +41 44 306 40 00
fax: +41 44 306 40 30
info@sensirion.com
www.sensirion.com

Sensirion Taiwan Co. Ltd.
info@sensirion.com
www.sensirion.com

Sensirion Inc., USA
phone: +1 805 409 4900
info-us@sensirion.com
www.sensirion.com

Sensirion Japan Co. Ltd.
phone: +81 3 3444 4940
info-jp@sensirion.com
www.sensirion.co.jp



Sensirion Korea Co. Ltd.
phone: +82 31 337 7700-3
info-kr@sensirion.com
www.sensirion.co.kr

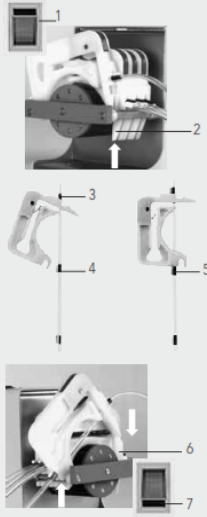
Sensirion China Co. Ltd.
phone: +86 755 8252 1501
info-cn@sensirion.com
www.sensirion.com.cn

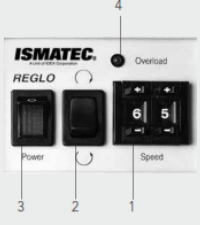
To find your local representative, please visit www.sensirion.com/contact

Appendix E – Pump manual

	Betriebsanleitung	Operating Manual	Mode d'emploi
	<p>Schlauchpumpe REGLO Analog</p> <p>2 Kanäle ISM830 6 Rollen ISM829 8 Rollen ISM795 12 Rollen</p> <p>4 Kanäle ISM828 6 Rollen ISM827 8 Rollen ISM796 12 Rollen</p>	<p>Tubing pump REGLO Analog</p> <p>2 channels ISM830 6 rollers ISM829 8 rollers ISM795 12 rollers</p> <p>4 channels ISM828 6 rollers ISM827 8 rollers ISM796 12 rollers</p>	<p>Pompe péristaltique REGLO Analog</p> <p>2 canaux ISM830 6 galets ISM829 8 galets ISM795 12 galets</p> <p>4 canaux ISM828 6 galets ISM827 8 galets ISM796 12 galets</p>
	DEUTSCH	ENGLISH	FRANÇAIS

	Geräterückwand	Rear panel	Panneau arrière												
 <p>Fenster für Spannungswahlanzeige Window for voltage setting Fenêtre de réglage de la tension</p> <p>REGLO ANALOG, 14-026, REV. C</p>	<ol style="list-style-type: none"> 1. Anlogschnittstelle 2. Netzbuchse 3. Sicherungshalter mit Spannungswähler 115/230V <table border="1"> <thead> <tr> <th>Netzanschluss</th> <th>Sicherung</th> </tr> </thead> <tbody> <tr> <td>220-240 V_{AC} 110-120 V_{AC}</td> <td>2 x T500mA/250V 2 x T500mA/250V</td> </tr> </tbody> </table> <p>⚠ Steckdose/Netz kabel Verwenden Sie ausschließlich das mitgelieferte Originalkabel. Die Steckdose muss geerdet sein. (Schutzleiterkontakt).</p> <p>⚠ Vor der Inbetriebnahme Prüfen Sie, ob die Spannungswahl-anzeige im Fenster des Sicherungshalters der Netzspannung Ihres Landes entspricht. Wenn nötig, muss die Einstellung geändert und die 2 Sicherungen müssen ausgetauscht werden.</p>	Netzanschluss	Sicherung	220-240 V _{AC} 110-120 V _{AC}	2 x T500mA/250V 2 x T500mA/250V	<ol style="list-style-type: none"> 1. Analog Interface 2. Mains Socket 3. Fuse-Holder with Voltage Selector 115/230V <table border="1"> <thead> <tr> <th>Mains voltage</th> <th>Fuse rating</th> </tr> </thead> <tbody> <tr> <td>220-240 V_{AC} 110-120 V_{AC}</td> <td>2 x T500mA/250V 2 x T500mA/250V</td> </tr> </tbody> </table> <p>⚠ Socket/Power cord Use exclusively the originally supplied power cord. The socket must be connected to earth ground.</p> <p>⚠ Before starting-up Check that the voltage setting visible in the window of the fuse-holder complies with the local mains voltage. If necessary, the voltage setting must be changed and the 2 fuses must be replaced.</p>	Mains voltage	Fuse rating	220-240 V _{AC} 110-120 V _{AC}	2 x T500mA/250V 2 x T500mA/250V	<ol style="list-style-type: none"> 1. Interface analogique 2. Prise d'alimentation 3. Porte-fusibles avec sélecteur de tension 115/230V <table border="1"> <thead> <tr> <th>Tension d'alimentation</th> <th>Fusibles de sécurité</th> </tr> </thead> <tbody> <tr> <td>220-240 V_{CA} 110-120 V_{CA}</td> <td>2 x T500mA/250V 2 x T500mA/250V</td> </tr> </tbody> </table> <p>⚠ Prise/câble d'alimentation N'employer que le câble d'alimentation d'origine. La prise doit être raccordée à la terre (contact conducteur de protection).</p> <p>⚠ Avant la mise en service Contrôlez si la tension indiquée dans la fenêtre du porte-fusibles correspond à la tension de votre réseau local. Si nécessaire, modifiez la tension et remplacez les deux fusibles correspondants.</p>	Tension d'alimentation	Fusibles de sécurité	220-240 V _{CA} 110-120 V _{CA}	2 x T500mA/250V 2 x T500mA/250V
Netzanschluss	Sicherung														
220-240 V _{AC} 110-120 V _{AC}	2 x T500mA/250V 2 x T500mA/250V														
Mains voltage	Fuse rating														
220-240 V _{AC} 110-120 V _{AC}	2 x T500mA/250V 2 x T500mA/250V														
Tension d'alimentation	Fusibles de sécurité														
220-240 V _{CA} 110-120 V _{CA}	2 x T500mA/250V 2 x T500mA/250V														

	Schläuche einlegen	Inserting the tubing	Insertion des tubes
 <p>REGLO ANALOG, 14-026, REV. C</p>	<ol style="list-style-type: none"> ➡ Pumpe ausschalten Fixierlasche leicht eindrücken, Kasette gleichzeitig nach oben stoßen und herausnehmen Pumpenschlauch (3 Color Code Stopper) mit einem Reiter in Kasette einsetzen Schlauch hängen lassen (darf nicht verdreht sein) Schlauch mit zweitem Reiter am anderen Ende der Kasette einsetzen Kasette auf Rollenkopf zurücksetzen und einklinken ➡ Pumpe einschalten <p>➡ Bei längerem Stillstand Kassetten an der Fixierlasche (2) ausklinken.</p> <p>Ersatz-Kassetten MS/CA Click'n'go Bestell-Nr. IS3510A</p>	<ol style="list-style-type: none"> ➡ Switch the pump OFF Remove the cassette by slightly pressing the fixing-tongue and lifting it simultaneously Insert the 3-stop color-coded tubing with one collar into the cassette Let the tubing hang down (prevent it from being twisted) Insert the second collar of the tube at the other end of the cassette Reinsert the cassette into the roller-head ➡ Switch the pump ON <p>➡ When the pump is idle, release all cassettes at the fixing-tongue (2).</p> <p>Spare-cassettes MS/CA Click'n'go Order-No. IS3510A</p>	<ol style="list-style-type: none"> ➡ Mettre la pompe hors service Extraire la cassette en pressant légèrement la languette de fixation et en la soulevant simultanément. Insérer le tube à 3 manifolds avec un manifold dans la cassette. Laisser pendre le tube au-dessous (il ne doit pas être tordu) Insérer le tube avec le deuxième cavalier à l'autre bout de la cassette. Remettre la cassette sur la tête à galets et l'y fixer ➡ Remettre la pompe en service <p>➡ Lorsque la pompe n'est pas utilisée pendant un certain temps, libérer les cassettes de la languette de fixation (2).</p> <p>Cassettes suppl. MS/CA Click'n'go No de commande IS3510A</p>

	Inbetriebnahme	Starting the pump	Mise en service
 <p>REGLO ANALOG, 14-026, REV. C</p>	<ol style="list-style-type: none"> Am Digipot die gewünschte Drehzahl einstellen. 99 = 100 min⁻¹ bzw. 160 min⁻¹ (max. Drehzahl) ➡ Die Drehzahl kann auch bei laufender Pumpe verändert werden. Drehrichtung wählen Netzschalter ein = Start/Stopp-Funktion Überlastanzeige (rote LED) 	<ol style="list-style-type: none"> Set the required speed on the 2-digit speed selector. 99 = 100 rpm or 160 rpm (max. revolution) ➡ The rotation speed can be adjusted while the pump is running. Choose the rotation direction Start the pump with the mains switch = run/stop function Overload indicator (red LED) 	<ol style="list-style-type: none"> Régler le nombre de tours souhaité sur le Digipot 99 = 100, resp. 160 t/min (tours max.) ➡ Le nombre de tours peut également être modifié en cours d'exploitation. Sens de rotation Interrupteur de réseau en service = fonction marche et arrêt Indicateur de surcharge (LED rouge)

	Analogschnittstelle	Analog interface	Interface analogique
<p>Digitale Eingänge (TTL-Pegel) Digital inputs (TTL-level) Entrées numériques (niveau TTL) Pin 2, remote Pin 3, start Pin 4, direction Pin 13, internal speed</p> <p>Analog-Eingang / Analog input / Entrée analogique Pin 5, speed IN $0-5 V_{cc} / 0-10 V_{cc} / 0-20 \text{ mA} / 4-20 \text{ mA}$</p> <p>Analog-Ausgang (TTL-Pegel) Analog output (TTL-level) Sortie analogique (niveau TTL) Pin 9, speed OUT $0-8 \text{ kHz, 2-Kanal/2-channel/2 canaux}$ $0-5 \text{ kHz, 4-Kanal/4-channel/4 canaux}$</p> <p>REGLO ANALOG, 14-026, REV. C</p>	<p>Pin 1, GND (Masse) Bezugspotential für alle anderen Eingänge.</p> <p>Pin 2, remote Für Umschaltung zwischen manueller Bedienung und der Analogschnittstelle. Zur Aktivierung der Analog-Schnittstelle muss Pin 2 mit Pin 1 (GND) verbunden werden.</p> <p>Pin 3, start Im Remote-Betrieb (Pin 2 auf GND) startet die Pumpe bei Verbindung mit Pin 1 (GND).</p> <p>Pin 4, direction Wenn offen, dreht die Pumpe im Gegenuhrzeigersinn; wenn mit Pin 1 (GND) verbunden, dreht sie im Uhrzeigersinn.</p>	<p>Pin 1, GND (ground) Reference potential for all other inputs.</p> <p>Pin 2, remote For changing between manual control and analog interface. For activating the analog interface, Pin 2 must be connected with Pin 1 (GND).</p> <p>Pin 3, start In remote operation (Pin 2 to GND) the pump starts when connected to Pin 1 (GND).</p> <p>Pin 4, direction In the open position, the pump turns counter-clockwise; when connected to Pin 1 (GND) it turns clockwise.</p>	<p>Pin 1, GND (masse) Potentiel de référence pour toutes les autres entrées.</p> <p>Pin 2, remote Pour commuter du service manuel à l'interface analogique. Pour activer l'interface analogique, le Pin 2 doit être connecté au Pin 1 (GND).</p> <p>Pin 3, start En exploitation à distance (Pin 2 sur GND), la pompe se met en route dès qu'elle est connectée au Pin 1 (GND).</p> <p>Pin 4, direction Si ouvert, le sens de rotation de la pompe est celui contraire des aiguilles d'une montre; si relié avec le Pin 1 (GND), elle tourne dans le sens des aiguilles d'une montre.</p> <p>19 of 32</p>

	Analogschnittstelle	Analog interface	Interface analogique																																				
<p>Digitale Eingänge (TTL-Pegel) Digital inputs (TTL-level) Entrées numériques (niveau TTL) Pin 2, remote Pin 3, start Pin 4, direction Pin 13, internal speed</p> <p>Analog-Eingang / Analog input / Entrée analogique Pin 5, speed IN $0-5 V_{cc} / 0-10 V_{cc} / 0-20 \text{ mA} / 4-20 \text{ mA}$</p> <p>Analog-Ausgang (TTL-Pegel) Analog output (TTL-level) Sortie analogique (niveau TTL) Pin 9, speed OUT $0-8 \text{ kHz, 2-Kanal/2-channel/2 canaux}$ $0-5 \text{ kHz, 4-Kanal/4-channel/4 canaux}$</p> <p>REGLO ANALOG, 14-026, REV. C</p>	<p>Pin 5, speed IN Externe Drehzahlsteuerung $(0-5V_{cc}, 0-10V_{cc}, 0-20\text{mA}, 4-20\text{mA})$ Eingangsimpedanz und Wahlmöglichkeiten mittels DIP-Switch im Geräteinnern (siehe Seite 22).</p> <p>Eingangsimpedanzen</p> <table border="1"> <tr> <td>0-5</td> <td>V</td> <td>18 kΩ</td> </tr> <tr> <td>0-10</td> <td>V</td> <td>38 kΩ</td> </tr> <tr> <td>0-20</td> <td>mA</td> <td>270 Ω</td> </tr> <tr> <td>4-20</td> <td>mA</td> <td>270 Ω</td> </tr> </table> <p>Pin 7, +20V_{cc} Es stehen ca. +20 V_{cc} zur Verfügung (max. Strom 0.2 A).</p> <p>Pin 9, speed OUT Frequenz proportional zur Drehzahl: 2 Kanal: 0-8 kHz, 3.2-160 min⁻¹ 4 Kanal: 0-5 kHz, 2.0-100 min⁻¹</p>	0-5	V	18 k Ω	0-10	V	38 k Ω	0-20	mA	270 Ω	4-20	mA	270 Ω	<p>Pin 5, speed IN External speed control $(0-5V_{cc}, 0-10V_{cc}, 0-20\text{mA}, 4-20\text{mA})$ Input impedance and input range can be selected via a dip-switch inside the pump (see P. 22).</p> <p>Input impedance</p> <table border="1"> <tr> <td>0-5</td> <td>V</td> <td>18 kΩ</td> </tr> <tr> <td>0-10</td> <td>V</td> <td>38 kΩ</td> </tr> <tr> <td>0-20</td> <td>mA</td> <td>270 Ω</td> </tr> <tr> <td>4-20</td> <td>mA</td> <td>270 Ω</td> </tr> </table> <p>Pin 7, +20V_{cc} About +20 V_{cc} are available (max. current 0.2 A).</p> <p>Pin 9, speed OUT Frequency proportional to the rotation speed: 2 channels: 0-8 kHz, 3.2-160 rpm 4 channels: 0-5 kHz, 2.0-100 rpm</p>	0-5	V	18 k Ω	0-10	V	38 k Ω	0-20	mA	270 Ω	4-20	mA	270 Ω	<p>Pin 5, speed IN Réglage externe du nombre de tours $(0-5V_{cc}, 0-10V_{cc}, 0-20\text{mA}, 4-20\text{mA})$ Impédance d'entrée et réglage de zone au moyen de l'interrupteur DIP à l'intérieur de l'appareil (voir P. 22).</p> <p>Impédance d'entrée</p> <table border="1"> <tr> <td>0-5</td> <td>V</td> <td>18 kΩ</td> </tr> <tr> <td>0-10</td> <td>V</td> <td>38 kΩ</td> </tr> <tr> <td>0-20</td> <td>mA</td> <td>270 Ω</td> </tr> <tr> <td>4-20</td> <td>mA</td> <td>270 Ω</td> </tr> </table> <p>Pin 7, +20V_{cc} Environ +20 V_{cc} sont à disposition (courant maximal 0.2 A).</p> <p>Pin 9, speed OUT Fréquence proportionnelle au nombre de tours: 2 canaux: 0-8 kHz, 3.2-160 t/min 4 canaux: 0-5 kHz, 2.0-100 t/min</p> <p>20 of 32</p>	0-5	V	18 k Ω	0-10	V	38 k Ω	0-20	mA	270 Ω	4-20	mA	270 Ω
0-5	V	18 k Ω																																					
0-10	V	38 k Ω																																					
0-20	mA	270 Ω																																					
4-20	mA	270 Ω																																					
0-5	V	18 k Ω																																					
0-10	V	38 k Ω																																					
0-20	mA	270 Ω																																					
4-20	mA	270 Ω																																					
0-5	V	18 k Ω																																					
0-10	V	38 k Ω																																					
0-20	mA	270 Ω																																					
4-20	mA	270 Ω																																					

	Anlogschnittstelle	Analog interface	Interface analogique
<p>Digitale Eingänge (TTL-Pegel) Digital inputs (TTL-level) Entrées numériques (niveau TTL) Pin 2, remote Pin 3, start Pin 4, direction Pin 13, internal speed</p> <p>Analog-Eingang / Analog input / Entrée analogique Pin 5, speed IN 0-5 V_{cc} / 0-10 V_{cc} / 0-20 mA / 4-20 mA</p> <p>Analog-Ausgang (TTL-Pegel) Analog output (TTL-level) Sortie analogique (niveau TTL) Pin 9, speed OUT 0-8 kHz, 2-Kanal/2-channel/2 canaux 0-5 kHz, 4-Kanal/4-channel/4 canaux</p> <p>REGLO ANALOG, 14-026, REV. C</p>	<p>Pin 10, +5V_{cc} Es stehen ca. +5 V_{cc} zur Verfügung (max. Strom 0.1 A).</p> <p>Pin 13, internal speed Anlogschnittstelle aktiviert (Pin 2 auf GND)</p> <ul style="list-style-type: none"> - Pin 13 offen: Die Drehzahl wird über Pin 5 (speed IN) vorgegeben. - Pin 13 auf GND: Die Drehzahl kann am Bedienungspanel der Pumpe eingestellt werden. 	<p>Pin 10, +5V_{cc} About +5 V_{cc} are available (max. current 0.1 A).</p> <p>Pin 13, internal speed Analog interface activated (Pin 2 on GND)</p> <ul style="list-style-type: none"> - Pin 13 open: The rotation speed is adjusted via Pin 5 (speed IN). - Pin 13 on GND: The rotation speed can be adjusted by the speed selector on the control panel of the pump. 	<p>Pin 10, +5V_{cc} Environ +5 V_{cc} sont à disposition (courant maximal 0.1 A).</p> <p>Pin 13, internal speed Interface analogique activée (Pin 2 sur GND)</p> <ul style="list-style-type: none"> - Pin 13 ouvert: La vitesse de rotation doit être ajustée par le Pin 5 (speed IN). - Pin 13 sur GND: La vitesse de rotation peut être ajustée par le sélecteur de vitesse sur le tableau de commande de la pompe. <p>21 of 32</p>

	Zubehör	Accessories	Accessoires																																																
<p>MS/CA Click'n'go Mit Feder aus rostfreiem Chromstahl With stainless steel pressure spring Avec ressort en acier inoxydable</p> <p>MS/CA Anpresshebel MS/CA pressure lever MS/CA levier de pression</p> <p>REGLO ANALOG, 14-026, REV. C</p>	<p>Ersatz-Kassetten</p> <table border="0"> <tr> <td>Kassette</td> <td>MS/CA Click'n'go Material</td> </tr> <tr> <td>Bestell-Nr.</td> <td>POM IS3510A</td> </tr> <tr> <td>Kassette</td> <td>MS/CA Anpresshebel</td> </tr> <tr> <td>Material</td> <td>POM</td> </tr> <tr> <td>Bestell-Nr.</td> <td>IS0649A</td> </tr> <tr> <td>Kassette</td> <td>MS/CA Anpresshebel</td> </tr> <tr> <td>Material</td> <td>PVDF</td> </tr> <tr> <td>Bestell-Nr.</td> <td>IS3629A</td> </tr> </table> <ul style="list-style-type: none"> ➡ Die Kassetten mit Anpresshebel sind als Option lieferbar. Für den Schlauch Tygon MH oder bei höherem Differenzdruck können sie geeigneter sein. ➡ Unterschiedliche Schlauchabmessungen und Schlauchmaterialien sind gleichzeitig einsetzbar. 	Kassette	MS/CA Click'n'go Material	Bestell-Nr.	POM IS3510A	Kassette	MS/CA Anpresshebel	Material	POM	Bestell-Nr.	IS0649A	Kassette	MS/CA Anpresshebel	Material	PVDF	Bestell-Nr.	IS3629A	<p>Spare-cassettes</p> <table border="0"> <tr> <td>Cassette</td> <td>MS/CA Click'n'go Material</td> </tr> <tr> <td>Order No.</td> <td>POM IS3510A</td> </tr> <tr> <td>Cassette</td> <td>MS/CA pressure lever</td> </tr> <tr> <td>Material</td> <td>POM</td> </tr> <tr> <td>Order No.</td> <td>IS0649A</td> </tr> <tr> <td>Cassette</td> <td>MS/CA pressure lever</td> </tr> <tr> <td>Material</td> <td>PVDF</td> </tr> <tr> <td>Order No.</td> <td>IS3629A</td> </tr> </table> <ul style="list-style-type: none"> ➡ Pressure lever cassettes are available on request. This type of cassette may provide better results when using the Tygon MH tubing and at elevated differential pressure conditions. ➡ The cassettes allow the user to insert tubes with different diameters and materials on the same roller-head. 	Cassette	MS/CA Click'n'go Material	Order No.	POM IS3510A	Cassette	MS/CA pressure lever	Material	POM	Order No.	IS0649A	Cassette	MS/CA pressure lever	Material	PVDF	Order No.	IS3629A	<p>Cassettes de rechange</p> <table border="0"> <tr> <td>Cassette</td> <td>MS/CA Click'n'go Matériau</td> </tr> <tr> <td>No de commande</td> <td>POM IS3510A</td> </tr> <tr> <td>Cassette</td> <td>MS/CA levier de pression</td> </tr> <tr> <td>Matériau</td> <td>POM</td> </tr> <tr> <td>No de commande</td> <td>IS0649A</td> </tr> <tr> <td>Cassette</td> <td>MS/CA levier de pression</td> </tr> <tr> <td>Matériau</td> <td>PVDF</td> </tr> <tr> <td>No de commande</td> <td>IS3629A</td> </tr> </table> <ul style="list-style-type: none"> ➡ Les cassettes avec levier de pression sont disponibles sur demande. Ce type de cassette peut produire de meilleurs résultats avec les tubes Tygon MH ou sous des conditions de pression différentielle supérieure. ➡ Différents types de tubes ou matériaux de tubes sont utilisables simultanément. <p>24 of 32</p>	Cassette	MS/CA Click'n'go Matériau	No de commande	POM IS3510A	Cassette	MS/CA levier de pression	Matériau	POM	No de commande	IS0649A	Cassette	MS/CA levier de pression	Matériau	PVDF	No de commande	IS3629A
Kassette	MS/CA Click'n'go Material																																																		
Bestell-Nr.	POM IS3510A																																																		
Kassette	MS/CA Anpresshebel																																																		
Material	POM																																																		
Bestell-Nr.	IS0649A																																																		
Kassette	MS/CA Anpresshebel																																																		
Material	PVDF																																																		
Bestell-Nr.	IS3629A																																																		
Cassette	MS/CA Click'n'go Material																																																		
Order No.	POM IS3510A																																																		
Cassette	MS/CA pressure lever																																																		
Material	POM																																																		
Order No.	IS0649A																																																		
Cassette	MS/CA pressure lever																																																		
Material	PVDF																																																		
Order No.	IS3629A																																																		
Cassette	MS/CA Click'n'go Matériau																																																		
No de commande	POM IS3510A																																																		
Cassette	MS/CA levier de pression																																																		
Matériau	POM																																																		
No de commande	IS0649A																																																		
Cassette	MS/CA levier de pression																																																		
Matériau	PVDF																																																		
No de commande	IS3629A																																																		

Appendix F – DAQ manual

SPECIFICATIONS

NI USB-6001

Low-Cost DAQ USB Device

The following specifications are typical at 25 °C, unless otherwise noted. For more information about the NI USB-6001, refer to the *NI USB-6001/6002/6003 User Guide* available at ni.com/manuals.

Analog Input

Number of channels	
Differential.....	4
Single-ended.....	8
ADC resolution.....	14-bit
Maximum sample rate (aggregate).....	20 kS/s
Converter type.....	Successive approximation
AI FIFO.....	2,047 samples
Trigger sources.....	Software, PFI 0, PFI 1



Input range.....	±10 V
Working voltage.....	±10 V
Overvoltage protection	
Powered-on.....	±30 V
Powered-off.....	±20 V
Input impedance.....	>1 GΩ
Input bias current.....	±200 pA
Absolute accuracy	
Typical at full scale.....	6 mV
Maximum over temperature,.....	26 mV
full scale	
System noise.....	0.7 mVrms
DNL.....	14-bit, no missing codes
INL.....	±0.5 LSB
CMRR.....	56 dB (DC to 5 kHz)
Bandwidth.....	300 kHz

Analog Output

Analog outputs.....	2
DAC resolution.....	14-bit
Output range.....	±10 V
Maximum update rate.....	5 kS/s simultaneous per channel, hardware-timed
AO FIFO.....	2,047 samples
Trigger sources.....	Software, PFI 0, PFI 1
Output current drive.....	±5 mA
Short circuit current.....	±11 mA
Slew rate.....	3 V/μs
Output impedance.....	0.2 Ω

Absolute accuracy (no load)	
Typical at full scale.....	9.1 mV
Maximum over temperature, full scale.....	34 mV
DNL.....	14-bit, no missing codes
INL.....	±1 LSB
Power-on state.....	0 V
Startup glitch.....	-7 V for 10 µs

Timebase



Note The following specifications apply to the sampling accuracy for hardware-timed analog input and analog output.

Timebase frequency.....	80 MHz
Timebase accuracy.....	±100 ppm
Timing resolution.....	12.5 ns

Digital I/O

13 digital lines

Port 0.....	8 lines
Port 1.....	4 lines
Port 2.....	1 lines

Function

P0.<0..7>.....	Static digital input/output
P1.0.....	Static digital input/output
P1.1/PFI 1.....	Static digital input/output, counter source or digital trigger

P1.<2..3>.....	Static digital input/output
P2.0/PFI 0.....	Static digital input/output, counter source or digital trigger
Direction control.....	Each channel individually programmable as input or output
Output driver type.....	Each channel individually programmable as open collector or active drive
Absolute maximum voltage range.....	-0.3 V to 5.5 V with respect to D GND
Pull-down resistor.....	47.5 kΩ to D GND
Power-on state.....	Input

Digital Input

Input voltage range (powered on).....	0 to 5 V
Input voltage range (powered off).....	0 to 3.3 V
Input voltage protection.....	±20 V on two lines per port (maximum of five lines for all ports) for up to 24 hours



Caution Do not leave a voltage above 3.3 V connected on any DIO line for extended periods of time when the device is powered off. This may lead to long term reliability issues.

Minimum V_{IH}	2.3 V
Maximum V_{IL}	0.8 V
Maximum input leakage current	
At 3.3 V.....	0.8 mA
At 5 V.....	4.5 mA

Digital Output (Active Drive)

Maximum V_{OL} (4 mA).....	0.7 V
Maximum V_{OL} (1 mA).....	0.2 V
Minimum V_{OH} (4 mA).....	2.1 V
Minimum V_{OH} (1 mA).....	2.8 V
Maximum V_{OH}	3.6 V
Maximum output current per line.....	±4 mA

Digital Output (Open Collector)

Maximum V_{OL} (4 mA).....0.8 V

Maximum V_{OL} (1 mA).....0.2 V



Note Minimum V_{OH} dependent on user-provided pull-up resistor and voltage source. Recommended pull-up resistor is 1 k Ω .

Using a 1 k Ω pull-up resistor and 5 V voltage source:

Minimum V_{OH}3.5 V

Typical V_{OH}4.5 V

Maximum output (sinking) current per line.....-4 mA

Maximum pull-up voltage.....5 V

Maximum leakage current

At 3.3 V.....0.8 mA

At 5 V.....4.5 mA

Counter

Number of counters.....1

Resolution.....32-bit

Counter measurements.....Edge counting, rising or falling

Counter direction.....Count up

Counter source.....PFI 0 or PFI 1

Maximum input frequency.....5 MHz

Minimum high pulse width.....100 ns

Minimum low pulse width.....100 ns

+5 V Power Source

Output voltage.....	+5 V, $\pm 3\%$
Maximum current.....	150 mA
Overcurrent protection.....	200 mA
Short circuit current.....	50 mA
Overvoltage protection.....	± 20 V

Bus Interface

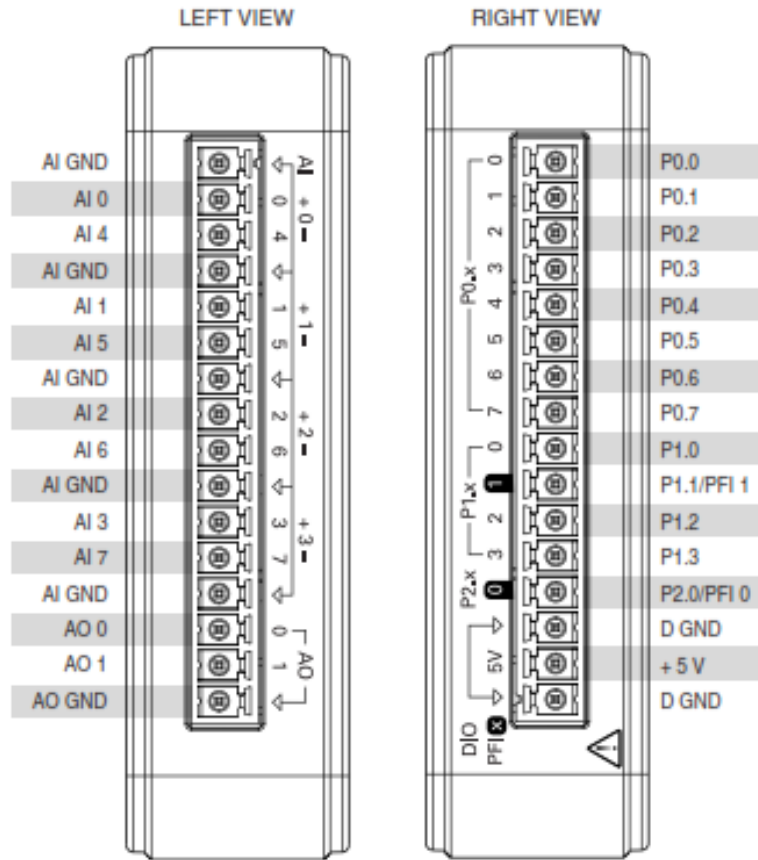
USB specification.....	USB Full Speed
USB bus speed.....	12 Mb/s

Physical Characteristics

Dimensions

Without screw terminal connector plugs....	75.4 mm \times 86.2 mm \times 23.6 mm, (2.97 in. \times 3.40 in. \times 0.93 in.)
With screw terminal connector plugs.....	93.2 mm \times 86.2 mm \times 23.6 mm, (3.67 in. \times 3.40 in. \times 0.93 in.)

Device Pinout



Refer to the *NI Trademarks and Logo Guidelines* at ni.com/trademarks for information on National Instruments trademarks. Other product and company names mentioned herein are trademarks or trade names of their respective companies. For patents covering National Instruments products/technology, refer to the appropriate location: **Help>Patents** in your software, the `patents.txt` file on your media, or the *National Instruments Patent Notice* at ni.com/patents. You can find information about end-user license agreements (EULAs) and third-party legal notices in the readme file for your NI product. Refer to the *Export Compliance Information* at ni.com/legal/export-compliance for the National Instruments global trade compliance policy and how to obtain relevant HTS codes, ECCNs, and other import/export data. NI MAKES NO EXPRESS OR IMPLIED WARRANTIES AS TO THE ACCURACY OF THE INFORMATION CONTAINED HEREIN AND SHALL NOT BE LIABLE FOR ANY ERRORS. U.S. Government Customers: The data contained in this manual was developed at private expense and is subject to the applicable limited rights and restricted data rights as set forth in FAR 52.227-14, DFAR 252.227-7014, and DFAR 252.227-7015.

© 2014 National Instruments. All rights reserved.

374369A-01 May14

Appendix G – Linearized version of the three-compartment model

$$\frac{dC_{A1}}{dt} = \frac{F_{1ss}}{V_1} C_{A0} + \left(-\frac{F_{1ss}}{V_1}\right) C_{A1} + \frac{C_{A0ss} - C_{A1ss}}{V_1} F_1 \quad (29)$$

$$\frac{dC_{B1}}{dt} = \frac{F_{0ss}}{V_1} C_{B0} + \left(-\frac{F_{0ss}}{V_1}\right) C_{B1} + \frac{C_{B0ss} - C_{B1ss}}{V_1} F_0 \quad (30)$$

$$\begin{aligned} \frac{dC_{A2}}{dt} = & \frac{F_{0ss}}{V_{2ss}} C_{A1} + \left(\frac{C_{A1ss} - C_{A2ss}}{V_{2ss}}\right) F_0 + \left(\frac{F_{0ss} C_{A2ss} - F_{0ss} C_{A1ss}}{V_{2ss}^2}\right) V_2 + \left(\frac{-F_{0ss}}{V_{2ss}} - \right. \\ & \left. \frac{V_1 m k_1 m}{(k_1 m + C_{A2ss})^2}\right) C_{A2} \end{aligned} \quad (31)$$

$$\begin{aligned} \frac{dC_{B2}}{dt} = & \frac{F_{0ss}}{V_{2ss}} C_{B1} + \left(\frac{C_{B1ss} - C_{B2ss}}{V_{2ss}}\right) F_0 + \left(\frac{F_{0ss} C_{B2ss} - F_{0ss} C_{B1ss}}{V_{2ss}^2}\right) V_2 + \left(\frac{-F_{0ss}}{V_{2ss}}\right) C_{B2} + \\ & \frac{V_2 m k_2 m}{(k_2 m + C_{A2ss})^2} C_{A2} \end{aligned} \quad (32)$$

$$\frac{dC_{A1}}{dt} = \frac{F_2}{V_3} (C_{A2} - C_{A3}) \sim \frac{F_{2ss}}{V_3} C_{A2} + \left(-\frac{F_{2ss}}{V_3}\right) C_{A3} + \frac{C_{A2ss} - C_{A3ss}}{V_3} F_2 \quad (33)$$

$$\frac{dC_{A1}}{dt} = \frac{F_2}{V_3} (C_{B2} - C_{B3}) \sim \frac{F_{2ss}}{V_3} C_{B2} + \left(-\frac{F_{2ss}}{V_3}\right) C_{B3} + \frac{C_{B2ss} - C_{B3ss}}{V_3} F_2 \quad (34)$$

$$\frac{dV_2}{dt} = F_1 - F_2 \quad (35)$$

linearization of the geometrical relation between the height and liquid volume is considered in five zones that show in Eq. (39).

$$h_2 = \begin{cases} \frac{1}{\pi r_c^2} \times V_2 & \text{if } 0 \leq h \leq h_c \\ \frac{3}{\pi(h_{ss}-h_c)(6r_s+3h_c-3h_{ss})} \times V_2 & \text{if } h_c < h \leq h_c + (r_s - \frac{H_{vlt}}{2}) \\ \frac{1}{\left[\left(\frac{\pi}{3}\right)(h_{ss}-h_c)(6r_s+3h_c-3h_{ss}) - N_{row} v_{fib} \frac{N_{vlt}}{H_{vlt}}\right]} \times V_2 & \text{if } h_c + (r_s - \frac{H_{vlt}}{2}) < h \leq h_c + (r_s + \frac{H_{vlt}}{2}) \\ \frac{3}{\pi(h_{ss}-h_c)(6r_s+3h_c-3h_{ss})} \times V_2 & \text{if } h_c + (r_s + \frac{H_{vlt}}{2}) < h \leq h_c + 2r_s - h_{cap} \\ \frac{1}{\pi r_c^2} \times V_2 & \text{if } h_c + 2r_s - h_{cap} < h \leq 2h_c + 2r_s \end{cases} \quad (36)$$